CONSTITUTIVE MODELLING OF THE BEHAVIOUR OF CLAYS UNDER CYCLIC LOADING

by

E.J. SELLERS
BSc (Eng) in Civil Engineering,
University of Cape Town

A thesis submitted to the University of Cape Town in partial fulfilment of the requirements for the degree of Master of Science in Engineering

Department of Civil Engineering
University of Cape Town

October 1989

DECLARATION

I, Ewan James Sellers, hereby declare that this thesis is my own work and that it has not been submitted for a degree at any other university.

Signed by candidate

E J SELLERS
October 1989

SYNOPSIS

This research work involved the implementation of a constitutive model based on plasticity theory to model the behaviour of a clay under cyclic loading.

The modelling must be based on an understanding of the soil response and the critical state theory provides a description of the soil response which then be formulated in terms of plasticity theory.

A literature review showed that there is a shortage of information on the behaviour of soils under cyclic loading. Constitutive models for cyclic loading are discussed to compare the predictions and thus select a model.

A model for clay under cyclic loading was developed which can model the resulting accumulation of plastic strain and degradation in strength. The single additional cyclic parameter can be evaluated from a cyclic triaxial test although such apparatus is uncommon in South Africa at present.Two alternative yield surfaces (Cam-clay and Modified Cam-clay) were applied, and the model was implemented in CRISP, a commercially available finite element package for geotechnical engineering.

The program was modified to employ a combined stiffness algorithm. A pre-processing program was developed to facilitate data input and a post-processing program was written to provide graphical output of the critical state parameters.

The model was used to back predict cyclic triaxial tests which showed that it is most appropriate for one-way stress controlled, and two-way strain controlled loading.

A series of laboratory tests were performed on a local Kaolin, to determine the parameters and to gain further understanding of the soil behaviour under cyclic loading. The trends in the response of

the clay corresponded to those observed in the literature. No further research can continue until the testing system is modified to include independant deformation measurement and more frequent data logging.

This research work has shown that the results of sophisticated analyses and test procedures are entirely dependent on the assumptions inherent in the models and the computer programs which must therefore be used with caution and understanding. On such a basis, the model provides predictions of the behaviour of clays under cyclic loading.

To achieve the ultimate aim of a generalised constitutive model for clays under cyclic loading, a substantial effort is required to test clay of different types, under various confining pressures and loadings.

ACKNOWLEDGEMENTS

I would like to express my gratitude to my thesis supervisor, Dr F. Scheele for his help, guidance and encouragement during this thesis period.

I would also like to thank Mr D. Wright and the Directors of Ninham Shand Inc. for allowing me to use their laboratory, and in particular, the cyclic triaxial test device.

My thanks are also due to Mr R. Clayton and the laboratory staff of the Ninham Shand laboratory, especially Mr R Fortuin.

I would also like to express my thanks to the staff of the Department of Civil Engineering for general assistance throughout the two years of the study.

TABLE OF CONTENTS

NOMENCLATURE

Matrix and tensor notation are used to simplify calculation and presentation of sets of equations. In the literature a wide variety of conventions are used in writing matrices and tensors. The convention used in this thesis is as follows:

matrix notation
scalar a vector $\underset{\sim}{a}$ Matrix $\underset{\approx}{A}$

tensor notation
zero order a , first order a_i , second order a_{ij},
fourth order $a_{ijk\ell}$.

The Kronecker delta (δ_{ij}) is defined by:

$$\delta_{ij} = 1 , \quad i = j ,$$

$$\delta_{ij} = 0 , \quad i \neq j \quad .$$

The co-ordinate system used in applied mechanics is a right handed system with axes x_1 , x_2 , x_3 which are equivalent to x, y, z . The indices (i, j, k, ℓ) of the tensors run from 1 to 3.

Since the mechanics of the response are derived from the behaviour of single phase materials, the effective stress is often denoted by σ rather than the σ' from soil mechanics. Compression is taken as positive because soil is generally loaded in compression. Strain and volumetric strain are considered to be positive for a reduction.

The following symbols are given in alphabetical order in the chapter of first occurrence.

Chapter 2

a_{ij}	yield surface position tensor
c'	cohesion in terms of effective stress
$C_{ijk\ell}$	constitutive matrix
$D^{e}_{ijk\ell}$, $D^{ep}_{ijk\ell}$	tangent constitutive matrix (elastic, elastic-plastic)
E, E', E'_t	Young's Modulus (total, effective, tangent)
E_{ij}	deviatoric strain tensor
f_i	body force vector
F	yield surface

G, G', G'_e	shear modulus (total, effective, tangent)
$h_\alpha (\alpha=1,..n)$	hardening parameters
I_1, I_2, I_3	invariants of strain tensor (first, second, third)
I_{2D}, I_{3D}	invariants of deviatoric strain tensor(second, third)
J_1, J_2, J_3	invariants of stress tensor (first, second, third)
J_{2D}, J_{3D}	invariants of deviatoric stress tensor (second, third)
k	material parameter for von Mises yield criterion
K, K', K'_t	bulk modulus (total, effective, tangent)
p	mean stress
Q	flow potential
S_{ij}	deviatoric stress tensor
t	time
u_i	displacement vector
W	strain energy density function
x_i	coordinate system
α	material parameter for Drucker Prager yield criterion
$E_{ij}, E^e_{ij}, E^p_{ij}$	strain tensor (total, elastic plastic)
ϵ_{kk}	volumetric strain
θ	Lode angle
λ	Lamé's constant
ν, ν', ν'_t	Poisson's ratio (total, effective, tangent)
σ_{ij}, $\underset{\approx}{\sigma}$	stress (tensor, matrix)
ρ	density
ϕ'	angle of internal friction in terms of effective stress
Ω	complementary energy density function

Chapter 3

C_c	consolidation coefficient
Δ, δ, d	incremental quantities
dE, dU, dW	energy (total, recoverable, dissipated
dv, dv^e, dv^p	specific volume (total, elastic, plastic)
$d\epsilon$, $d\epsilon^e, d\epsilon^p$	shear strain (total, elastic, plastic)
D	specific volume of swelling line at unit p'
e	void ratio

G_s	specific gravity of solids
K_o	coefficient of lateral stress
M	slope of projection of critical state line
M_s, M_w	mass (solids, water)
NCL	normal consolidation line
N	specific volume of NCL at unit p'
P	mean normal total stress
P'	mean normal effective stress
P_c'	preconsolidation pressure/hardening parameter
q	deviatoric stress
SSBS	stable state boundary surface
s,t	MIT stress parameters
u	pore pressure
v	specific volume
V_s, V_v	volume (solids, voids)
V_o	initial specific volume
V_k	specific volume of k line at unit p'
V_λ	specific volume of λ-line at unit p'
Γ	specific volume of critical state line at unit p'
η	stress ratio (q/p')
κ	slope of swelling line in v-ln p' plane
ψ	slope of yield surface
σ_a, σ_a'	axial stress (total, effective)
$\sigma_r, \sigma_r', \sigma_{ro}$	radial stress (total, effective, initial)

Chapter 4

$a^{(i)}$	isotropic hardening functions for yield surfaces R_i
a	amplitude
c_u	undrained shear strength
CLRL	critical level of repeated loading
f_i	nest of yield surfaces
f_o, f_k	yield surface (initial, k-th)
F_c	consolidation surface
F_1	intermediate yield surface
K	hardening modulus
$K_{(k)}$	hardening modulus for yield surface f_k

K_o	coefficient of lateral stress
N	number of cycles to failure
P_i	conjugate points
q_c	cyclic deviatoric stress
q_f	static failure stress
q_i	initial deviatoric stress
T	period (= 1/frequency)
$\underset{\approx}{d}^{(i)}$	position tensors of yield surfaces, f_i
G_u	accumulated plastic deviatoric strain
G_{ij}	viscoplastic strain tensor
Θ	degradation parameter

Chapter 5

$\underset{\sim}{a}^{(e)}, \underset{\sim}{a}^{n}, \Delta\underset{\sim}{a}, {}^{i+1}\Delta\underset{\sim}{a}$	nodal displacements (element, nth, change, i+1th change)
$\underset{\approx}{B}^{(e)}$	strain matrix
$\underset{\approx}{D}_c^{(e)}, \underset{\approx}{D}_{ep}^{(e)}$	constitutive matrix (elastic, elastic plastic)
(e)	(superscript) element
$\underset{\sim}{f}^{(e)}$	body force vector (element)
$\underset{\approx}{k}', \underset{\approx}{k}_t$	stiffness matrix (global, tangent)
$\underset{\approx}{K}_1, \underset{\approx}{K}_2$	penalty function stiffness matrixes
K', K_u	bulk modulus (effective, undrained)
$\underset{\approx}{N}^{(e)}, \underset{\approx}{N}^{(e)T}$	shape function matrix (element, transpose)
$\underset{\sim}{P}, \underset{\sim}{P}^n, \Delta\underset{\sim}{P}$	load vector (global, n-th, change)
$\underset{\sim}{Q}$	internal forces vector
$\underset{\sim}{R}^n, \underset{\sim}{R}^{n+1}, {}^i\underset{\sim}{R}^{n+1}$	residual forces vector (nth, n+1th, ith of n+1th)
$\underset{\sim}{s}^{(e)}$	initial stress vector (element)
u	pore pressure
$\underset{\sim}{u}$	displacement vector
$\underset{\sim}{t}^{(e)}$	initial stress vector (element)
α	penalty number

LIST OF ILLUSTRATIONS

Tables

Plate

CHAPTER 1

INTRODUCTION AND OBJECTIVES

An understanding of the mechanical behaviour of an engineering material under load is a fundamental prerequisite for any civil engineering design. Simplistic approaches for the quantification of material behaviour can be obtained either from elastic or plastic idealisations. Soil is a particulate material consisting of solids, voids containing fluid (water) and gas (air) and its response to loading is not only influenced by the interaction of these three phases, but also by the stress history and, the current state of stress in the whole mass. The stress-strain response to load results in a nonlinear and increasing, deformation as the permanent strain increases while the soil material approaches failure.

Geotechnical Engineers, faced with the a wide range of soil types and behaviour, have, in general, relied on elastic theory and limit state analysis techniques, based on simple conceptual models such as the Mohr-Coulomb failure criterion. These methods are usually only applied to static loading situations of small deformations or failure, respectively. The wide range of soil response, ie. the deformation that occcurs as the soil progresses to failure is not accounted for by the conventional techniques. The analysis of a problem for an entire loading process becomes especially important when the soil is subject to variable loading, where excessive deformation, and ultimately failure, can occur at lower stress levels than predicted from limit analysis of the static loading.

A load that repeatedly causes variations in the state of stress or strain in the soil, however, without introducing inertial effects, is termed cyclic loading. This classification thus includes natural loads, particularly those due to wind, waves and earthquakes, traffic loads, and other activities such as blasting and pile driving. The loading can be transmitted either directly

to the soil, or indirectly, through the interaction with structures such as foundations, quays, silos, piles and anchors.

Laboratory experiments can provide information about the soil response to cyclic loading, but even the most sophisticated testing apparatus is restricted to very specific loading conditions. Additionally, the stress and strain fields occurring within the sample, cannot be defined because of the limitations of the measuring devices. Expressing the data in terms of standard soil mechanics properties and conventions can, however, aid in the interpretation of the test results.

To predict the soil behaviour under cyclic loading, the relationships between the stress and strain are formulated in a constitutive model. Plasticity theory , originally developed to describe the behaviour of metals, was modified to determine the response of soils to static loads. The extension of the theory to cyclic loading conditions has recently received attention and a variety of models have been proposed, but the accurate prediction of the soil behaviour for a generalised stress path is still a formidable task.

The application of the constitutive model to design problems requires the solution of a set of equations which can only be achieved with advanced numerical techniques such as the finite element method. The development of these solution techniques has far exceeded the present knowledge of the behaviour of soil and the constitutive representation.

At this stage, finite element programs available commercially do not contain models appropriate to cyclic loading of soils and a specific model required for design or research purposes, must be formulated and implemented by the analyst. Implementation of a model covers a wide range of disciplines, including applied mechanics and numerical analysis, many of which are outside the experience of practicing engineers. In this research work, however, basic knowledge of applied mechanics and the finite element method are assumed.

The development of a constitutive law specifically for cyclic loading cannot proceed without an understanding of the material response. The aim of this thesis is to gain insight into the problems involved in the formulation of constitutive relations for soils, by focusing on the modelling of the response of clays to cyclic loading using plasticity theory.

The main objective of this research is to review existing constitutive laws based on plasticity theory and thus find a model specifically for cyclic loading that can represent the soil behaviour. The model should have parameters that can be determined from available laboratory tests, and having been selected, must then be implemented in a commercial finite element package.

A second objective is therefore to study the reponse of clay to cyclic loading, by considering laboratory experiments in the context of established conceptual models such as the critical state theory.

The third objective is the evaluation of the model predictions by backpredicting the results of triaxial tests on a local clay material. The model parameters must be determined from laboratory tests, which will also provide additional information about the soil response to cyclic loading.

This study will then enable further research into constitutive models for soils under cyclic loading to proceed on the basis of a sound knowledge of the modelling techiques and the material behaviour.

CHAPTER 2

THE MECHANICS OF MODELLING CYCLIC LOADING OF SOIL

2.1 REVIEW OF FUNDAMENTAL PRINCIPLES OF MECHANICS

To analyse a situation where a soil mass is affected by cyclic changes in loading, the physical situation must be transformed into a mathematical model. In the formulation of this model or "boundary value problem", four requirements must be satisfied. These are the kinematics, kinetics, thermodynamics and the imposed boundary conditions. The three requirements of kinematics, kinetics and thermodynamics can be formulated in a set of partial differential equations. The solution then depends on the imposed boundary conditions and is achieved using numerical techniques. The solution technique used in this thesis will be the finite element method because it is suitable for the solution of engineering problems. The method of solution will be considered in Chapter 5.

The kinematics relate the strain field ϵ_{ij} within the body to the displacement field u_i acting on the body. In this thesis, only small strain theory will be considered, in which case

$$\epsilon_{ij} = \frac{1}{2}\left(\frac{\partial u_i}{\partial x_j} + \frac{\partial u_j}{\partial x_i} \right) \qquad (2.1.1)$$

where u_i is the displacement in the x_i direction. The derivation is given in textbooks of continuum mechanics and will not be repeated.

The kinetics relate the internal forces in the body to the externally applied loads. The relationship can be obtained from the principles of conservation of linear momentum and of conservation of mass resulting in the equation of motion (Reddy, 1984) and is expressed as

$$\frac{\partial \sigma_{ij}}{\partial x_j} + f_i = \rho \frac{\partial^2 u_i}{\partial t^2} \qquad (2.1.2)$$

where σ_{ij} is the Cauchy stress tensor, f_i is the vector of body forces per unit volume, ρ the density and $\partial/\partial t$ the partial time derivative with respect to time. The term $\rho \frac{\partial^2 u_i}{\partial t^2}$ represents the contribution of inertial effects and is zero for a static problem. The equation of motion is then called the equation of equilibrium.

Cyclic loading is defined as any repeated load (stress) or displacement (strain) that is applied in such a manner that the inertial effects are negligible. The problem is then be considered as static, with a varying set of loads. The assumption that inertial effects are negligible depends on the material response and the load frequency. This effect has not been extensively investigated. Procter and Khaffef (1984) found that behaviour of a remoulded clay was independent of frequency below 1/5 Hz and Wong et al (1975) showed that gravelly sand experienced negligible frequency effects below 1.3 Hz. Wood (1982) discusses this at length and concludes that the effect of frequency is greater for more plastic soils. It is also noted that the results of time effects such as creep must be distinguished from those due to cyclic loading to achieve rate independence.

Once the kinematic and kinetic formulations have been established, it is then necessary to relate the stress field to the strain field, making use of thermodynamics. This relation is the constitutive law. Jain (1980) considers that the constitutive law "signifies the functional correspondence between the causes and effects of the physical processes occurring within the material".

The constitutive relations must not depend on the frame of reference and therefore a set of variables that are independent of rigid motions must be defined for all states of stress and strain. (Jain, 1980; Chen and Baladi, 1985).

These invariant quantities should correspond to material parameters which can be determined from laboratory tests. A successful application of constitutive model will depend on the ease with which the parameters can be obtained and the availability of the required test devices. Models that require excessive amounts of sophisticated laboratory testing are unlikely to be used in practice.

The relation of the stress and strain fields must hold for every point in the body and hence all further considerations of the stress-strain relationship will be for a single point.

The stress at a point is defined by six independent variables and expressed as a stress tensor σ_{ij} . The stress tensor can be transformed by solving the characteristic equation to give three principal stresses σ_1 , σ_2 , σ_3 in three principal directions $\underset{\sim}{n}_1$, $\underset{\sim}{n}_2$, $\underset{\sim}{n}_3$ which are not affected by the rotation of the stress tensor.

The characteristic equation can be written as

$$\underset{\approx}{\sigma}^3 - J_1 \underset{\approx}{\sigma}^2 + J_2 \underset{\approx}{\sigma} - J_3 = 0 \qquad (2.1.3)$$

where the stress invariants J_1 , J_2 , J_3
are : $J_1 = \text{trace } (\underset{\approx}{\sigma}) = \sigma_{11} + \sigma_{22} + \sigma_{33}$

$$J_2 = \frac{1}{2} \text{trace } (\underset{\approx}{\sigma})^2 = \frac{1}{2} (\sigma_{ij} \sigma_{ji})$$

$$J_3 = \frac{1}{3} \text{trace } (\underset{\approx}{\sigma})^3 = \frac{1}{3} (\sigma_{ik} \sigma_{km} \sigma_{mi}).$$

(Desai and Siriwardane, 1984)

The stress tensor can be decomposed into deviatoric and hydrostatic components such that

$$\sigma_{ij} = \left(S_{ij} + \frac{1}{3} \sigma_{kk} \delta_{ij}\right) = \left(S_{ij} + p\delta_{ij}\right) , \qquad (2.1.4)$$

where S_{ij} is the deviatoric stress tensor

and p is the mean stress, $p = \frac{1}{3} (\sigma_{11} + \sigma_{22} + \sigma_{33})$.

The hydrostatic tensor has the same first invariant J_1 as the stress tensor which is equal to three times the mean stress

$$J_1 = 3 \sigma_{kk} = 3p .$$

The first invariant of the deviatoric stress tensor S_{ij} is zero, but the second invariant known as J_{2D} is equal to $\frac{1}{2}\left(S_{ij}\ S_{ij}\right)$ and represents the shear behaviour of the material.

A function of invariants is also an invariant and it is therefore possible to choose a stress space in which the axis components are functions of invariants. The invariant functions used in continuum mechanics are the normal octahedral stress σ_{oct} and the octahedral shear stress τ_{oct}. In terms of principal stresses, these are

$$\sigma_{oct} = \frac{1}{3}(\sigma_1 + \sigma_2 + \sigma_3) = \frac{1}{3} J_1 .$$

$$\tau_{oct} = \frac{1}{3}[(\sigma_1-\sigma_2)^2 + (\sigma_2-\sigma_3)^2+(\sigma_3-\sigma_1)^2]^{\frac{1}{2}} = \sqrt{\frac{2}{3} J_{2D}}. \qquad (2.1.5)$$

The normal octahedral stress hydrostatic stress is the distance of a stress point along the space diagonal, in the stress space where all three principal stresses are equal. The octahedral shear stress is the distance of the point in the octahedral plane, which is perpendicular to the space diagonal. The points in principal stress space can be projected onto an octahedral plane called the π-plane. When viewed from along the space diagonal, the π-plane shows the variation of the points in principal stress space.

These can then be represented in principal stress space as in Figure 2.1.1 .

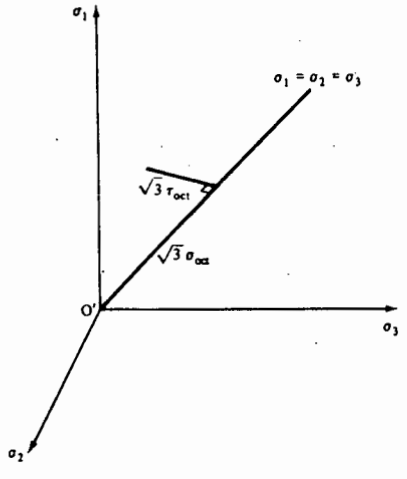

Figure 2.1.1 : Principal stress space.

The strain tensor ϵ_{ij} can be similarly decomposed as

$$\epsilon_{ij} = E_{ij} + \frac{1}{3}\epsilon_{kk}\delta_{ij} \qquad (2.1.6)$$

with invariants of ϵ_{ij} being I_1 , I_2 , I_3 and those of the deviatoric strain tensor E_{ij} being I_{2D} , I_{3D} , whilst I_{1D} vanishes.

The invariant constitutive function is then derived from thermodynamic principles, relating the stress to the strain by considering the energy of the body. The first law of thermodynamics or "balance of energy principle" states that the time rate of change of the sum of the kinetic and internal energy is equal to the sum of the work done by the external forces and the change of heat content (Reddy, 1984). The second law or entropy equation constrains the direction of flow of energy (Jain, 1980).

The application of the energy equations in deriving a relationship between stress and strain, depends on the dissipation of energy within a cycle of load application. Soil is a particulate material and thus will in general experience a dissipation of energy during a cycle of load application and load removal. This causes the unloading path to deviate from the loading path resulting in hysteresis in the stress strain relation. The deviation in the load paths causes permanent deformation. A schematic diagram of stress-strain cycle is given in Figure 2.1.2 which shows the characteristic effects of the change in slope (modulus) at unloading, the different unloading and reloading paths and the resultant accumulation of unrecoverable (plastic) strain. The actual stress-strain response of clay to cyclic loading will be reviewed in Section 4.1 . In some situations, however, it is convenient to consider the soil as elastic, in which case no dissipation occurs during a cycle of load application.

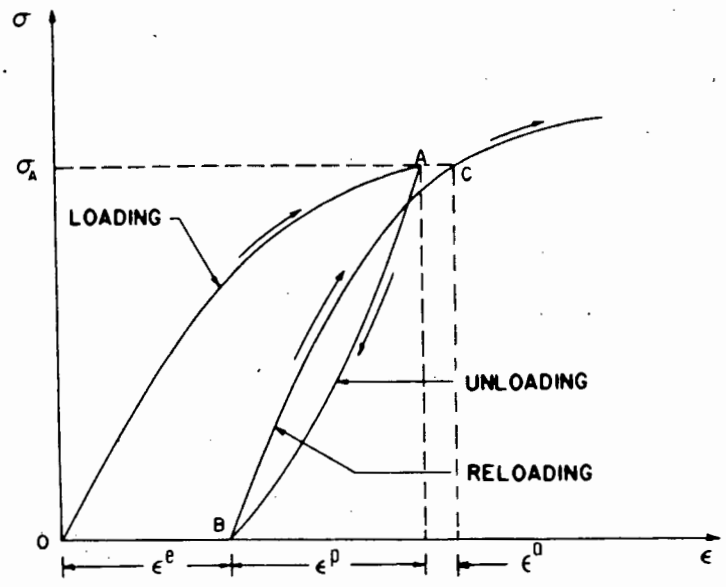

Figure 2.1.2 : Schematic diagram of stress-strain behaviour.
(after Chen and Baladi, 1985)

2.2 ELASTICITY AND QUASI-ELASTICITY FOR SOILS UNDER CYCLIC LOADING

2.2.1 Linear elasticity

The simplest type of constitutive equation considers a linear relationship between the stress and strain fields. This is known as linear elasticity.

For uniaxial behaviour, the constitutive law is Hooke's law and can be written as

$$\sigma = E\,\epsilon$$

where σ is the stress, ϵ the strain in the direction of loading and E the Young's modulus. In three dimensions, assuming the material is isotropic, the relation can be expressed as

$$\sigma_{ij} = \frac{E}{1+\nu}\,\epsilon_{ij} + \frac{\nu E}{(1+\nu)(1-2\nu)}\,\epsilon_{kk}\,\delta_{ij} \quad . \qquad (2.2.1)$$

When describing the behaviour of soil, it is often more convenient to separate out the effects of volumetric and shear behaviour. A bulk modulus, K , is therefore defined to represent the volumetric behaviour and a shear modulus, G , represents the shear behaviour. These moduli are related to the Poisson's ratio ν and Young's modulus as follows :

$$K = E/3(1 - 2\nu)$$
$$G = E/2(1 + \nu) \qquad (2.2.2)$$

Decomposing the stress and strain tensors into hydrostatic and deviatoric parts, the constitutive equations (2.2.1) become:

$$p = \frac{J_1}{3}\delta_{ij} = \frac{E}{3(1-2\nu)}\epsilon_{kk} = K\,\epsilon_{kk} = K\,\epsilon_v \qquad (2.2.3)$$
$$S_{ij} = \frac{E}{1+\nu}E_{ij} = 2G\,E_{ij}$$

where ϵ_v is the volumetric strain. These parameters are defined for the conditions

$$G > 0 \quad , \quad K > 0 \quad , \quad -1 < \nu < \frac{1}{2} \qquad (2.2.4)$$

[Jaunzemis, 1967]. They are also restricted by the physical constraints that the Young's modulus is always greater than zero and Poisson's ratio lies between zero and one half ie:

$$E > 0 \quad , \quad 0 < \nu < \frac{1}{2} \qquad (2.2.5)$$

If Poisson's ratio was negative, the material would expand under compression which is physically impossible. A Poisson's ratio of $\nu = 1/2$ implies that the material is incompressible and experiences no net change in volume under compression. Soil loaded in undrained conditions is considered to be incompressible and the changes in the solid volume are resisted by an increase in the pore pressure. The assumption of $\nu = 1/2$, however, violates the relations of eqn. (2.2.4) and for numerical purposes the Poisson's ratio of undrained soil is taken as 0,49.

The bulk modulus K , will be infinite for undrained loading because the material is incompressible, and thus an effective bulk modulus K' and an effective value of Poisson's ratio, ν' are defined to describe the soil phase behaviour. Water can sustain no shear stress and therefore the shear modulus is unchanged for drained and undrained behaviour i.e. G = G'.

$$K = E/3(1 - 2\nu)$$
$$G = E/2(1 + \nu) \qquad (2.2.2)$$

Decomposing the stress and strain tensors into hydrostatic and deviatoric parts, the constitutive equations (2.2.1) become:

$$p = \frac{J_1}{3}\delta_{ij} = \frac{E}{3(1-2\nu)}\epsilon_{kk} = K\,\epsilon_{kk} = K\,\epsilon_v \qquad (2.2.3)$$
$$S_{ij} = \frac{E}{1+\nu}E_{ij} = 2G\,E_{ij}$$

where ϵ_v is the volumetric strain. These parameters are defined for the conditions

$$G > 0 \quad , \quad K > 0 \quad , - \quad 1 < \nu < \frac{1}{2} \qquad (2.2.4)$$

[Jaunzemis, 1967]. They are also restricted by the physical constraints that the Young's modulus is always greater than zero and Poisson's ratio lies between zero and one half ie:

$$E > 0 \quad , \quad 0 < \nu < \frac{1}{2} \qquad (2.2.5)$$

If Poisson's ratio was negative, the material would expand under compression which is physically impossible. A Poisson's ratio of $\nu = 1/2$ implies that the material is incompressible and experiences no net change in volume under compression. Soil loaded in undrained conditions is considered to be incompressible and the changes in the solid volume are resisted by an increase in the pore pressure. The assumption of $\nu = 1/2$, however, violates the relations of eqn. (2.2.4) and for numerical purposes the Poisson's ratio of undrained soil is taken as 0,49.

The bulk modulus K , will be infinite for undrained loading because the material is incompressible, and thus an effective bulk modulus K' and an effective value of Poisson's ratio, ν' are defined to describe the soil phase behaviour. Water can sustain no shear stress and therefore the shear modulus is unchanged for drained and undrained behaviour i.e. G = G'.

Linear elastic models are used as approximations in static loading situations where small displacements are expected. Soil generally has a nonlinear stress-strain behaviour and exhibits energy losses and permanent deformations under cyclic loading which linear elasticity cannot account for. Linear elastic theory, however, forms the basis of nonlinear elastic and elastic-plastic constitutive theories.

2.2.2 Nonlinear Elasticity

Various types of elasticity have been developed to model the anisotropic and nonlinear stress-strain behaviour of soil. These models are extensively described in Chen and Saleeb, 1982; Chen and Baladi, 1985; Desai and Siriwardane, 1984 amongst many others. A brief review will be given here.

The simplest method of modelling nonlinear behaviour is to define a relation of the form $\sigma_{ij} = C_{ijk\ell}\ \epsilon_{k\ell}$ where the constitutive tensor $C_{ijk\ell}$ is a function of the stress or strain invariants at the point under consideration. The moduli can be either tangent or secant to the stress-strain curve at that point and the material behaviour is therefore piecewise linear (Figure 2.2.1). These Cauchy elastic models can describe the nonlinear stress-strain behaviour of soil, but energy generation can result under certain types of stress cycles. Cauchy elasticity is path independent and thus shows no permanent deformation due to load cycling.

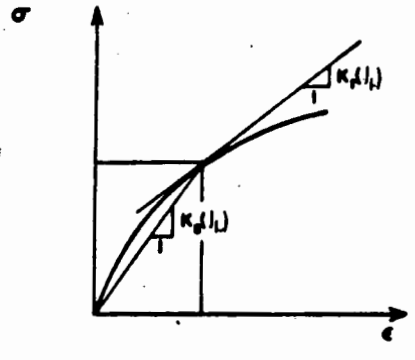

Figure 2.2.1 : Cauchy elastic models

To overcome the possibility of energy generation a strain energy density function W or complementary energy density function Ω is defined so that

$$\sigma_{ij} = \frac{\partial W}{\partial \epsilon_{ij}} = C_{ijk\ell}\, \epsilon_{k\ell} \qquad (2.2.6)$$

or in inverse form:

$$\epsilon_{ij} = \frac{\partial \Omega}{\partial \sigma_{ij}} = B_{ijk\ell}\, \sigma_{k\ell} \quad . \qquad (2.2.7)$$

Elastic equations derived from internal energy considerations are called Hyperelastic or Green elastic models. These can model anisotropic behaviour, but are reversible and show no plastic deformation (Figure 2.2.2a). Hyperelastic models require large numbers of parameters depending on the order of the strain tensor used in the strain energy function. The first order Green elastic model, being the same as Hooke's law of elasticity requires two material constants. The third order model requires nine constants and a fifth order model requires fourteen constants (Chen and Baladi, 1985).

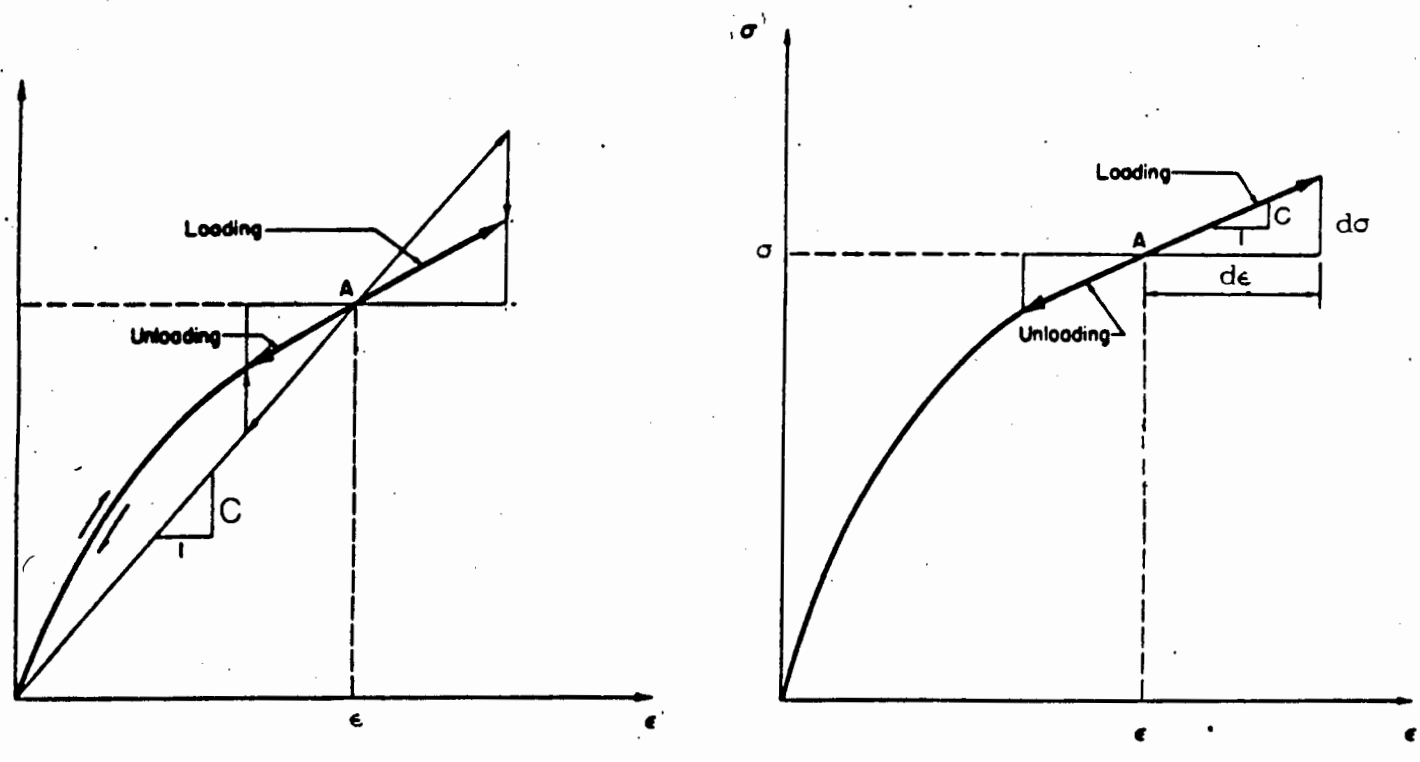

Figure 2.2.2 : Nonlinear elastic models (a) hyperelastic
(b) hypoelastic
(after Chen and Baladi, 1985)

A hypoelastic model was developed to introduce path dependent behaviour and relates the increment of stress to the increment of strain as shown in Figure (2.2.2b) with moduli that are functions of the stress state (σ_{mn}). The hypoelastic constitutive equation is then

$$d\sigma_{ij} = C_{ijk\ell}(\sigma_{mn})d\epsilon_{k\ell} \qquad (2.2.8)$$

where d means an incremental quantity.

These models work well under uniaxial conditions though in general multiaxial conditions they exhibit stress induced anisotropy requiring the specification of 21 load path dependent parameters resulting in an extensive amount of laboratory testing (Chen and Baladi, 1985).

Chen and Saleeb [1982] show that the resulting tangent stiffness matrix is asymmetric. This causes computational problems requiring increased storage and slower solution algorithms. Hypoelastic models have been successfully applied by Duncan (1970) and Kondner (1963), but because of the need to specify unloading and reloading criteria, Chen and Baladi (1985) recommend that their use be confined to monotonic conditions.

2.2.3 Quasi-Elastic Models

Elastic material models are reversible and the stress-strain response follows the same path in loading as in unloading. A variation of the linear elastic model was developed to model nonlinear behaviour and hysteresis whilst retaining the computational efficiency of a linear model. Linear elastic behaviour is assumed to apply over an increment of load, but with one or more of the elastic parameters E, ν, K, G being functions of the state of stress or strain.

These quasi-elastic models exist in two forms depending on how the parameters are specified. In a variable parameter model, the stress strain relation is described by a nonlinear function fitted to test data. The expression for the effective tangent moduli E_t' and ν_t' or G_t' and K_t' are obtained by differentiating these functions. Some widely

used functions include the hyperbolic (Duncan and Chang, 1970) and the spline functions (Desai and Siriwardane, 1971) as well as the Ramberg Osgood model (Richard and Abbot, 1975).

The second form are variable moduli models. They are obtained by expressing the bulk modulus as a function of the mean stress, and the shear modulus as a function of the deviatoric stress invariant J_{2D}. An application of these models is described by Nelson (1977) who used $K' = K'(p)$ and $G = G(p, J_{2D})$ to model the behaviour of sand and rock under blast loading.

Nelson (1977) discovered that the major problem was the lack of continuity in neutral loading in shear (J_{2D} = constant) which implied that different numerical techniques and computers produced different results.

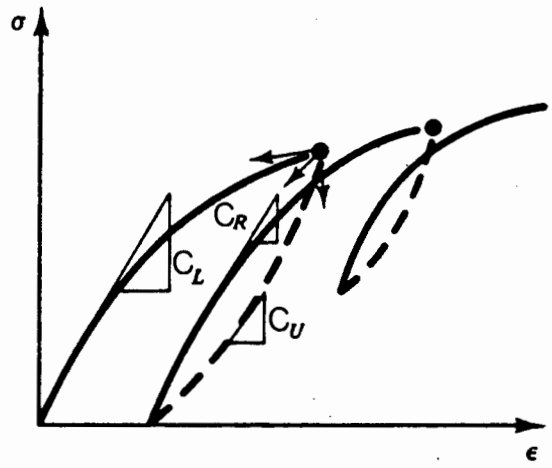

Figure 2.2.3 : Variable moduli model. [Desai and Siriwardane, 1984]

Zytynski et al [1978] discuss some problems with variable moduli models. Experimental evidence showed that for soil the bulk modulus of soil K' varies with mean pressure p and therefore only one of the other parameters E' , ν' and G' may be chosen, the others being related through the elastic relations (2.2.2). The choice of a constant Poisson's ratio then implies that a loading cycle leads to permanent shear deformation, but loading in the opposite direction leads to an

energy gain and hence unconservative behaviour. The alternative of choosing G' as a constant, leads to negative values of Poisson's ratio which violate the constraints expressed in equation (2.2.5).

Britto and Gunn (1985) suggest that since experimental evidence shows that G' is also a function of mean pressure p the choice of a constant ν' is more reasonable.

A disadvantage of these models when applied to cyclic loading is the need to specify separate loading, unloading and reloading parameters for the model (Figure 2.2.3). A further problem is that these models have no clearly defined unloading criteria which must be specified on the basis of a distinct change in stress level or principal stress magnitude (Pyke, 1986). The choice of the unloading criteria will determine the response of the model to cyclic loading and this combined with the uncoupled volumetric and shear behaviour implies that it is possible for the model to load in one mode and unload in another. The term uncoupled means independent volumetric and shear responses to hydrostatic deviatoric stress.

2.3 PLASTICITY THEORY

The consistent treatment of the effect of multiaxial stress paths, including cyclic loading and unloading, on materials that experience plastic deformation requires the use of plasticity theory which allows the modelling of stress path dependence, dilatancy and dependence on the intermediate principal stress. The specification of unloading and reloading is an integral part of the plasticity formulation which is a significant advantage for modelling cyclic loading situations.

In a uniaxial tensile test on a metal specimen it is apparent that there is some stress beyond which plastic or permanent strain occurs. At stress levels lower than the yield stress, the strain is recoverable and the behaviour is therefore elastic. Soil is generally subjected to multiaxial stress paths and there exists a hypersurface (yield surface) in stress space which separates elastic and plastic regions. Stress points below this yield surface experience only elastic behaviour, and plastic deformation occurs for stress paths directed on or outside the

surface. The theory of plasticity and derivation of the equations is given by Hill (1950) and Martin (1975), amongst others. Reviews on its application to soils are given by Scott (1985) and Mroz and Norris (1982), amongst others.

The following brief description of plasticity theory is based on the referred literature and forms the basis of the constitutive equations that will be used for modelling soil under cyclic loading in this research work.

The yield surface is expressed as a function of the stress tensor σ_{ij} and described as :

$$F(\sigma_{ij}) = 0 \qquad (2.3.1)$$

when the material is in a plastic state.

Prager (1949) formulated four conditions for the relationship between stress and plastic strain to ensure an appropriate description of the physical processes involved in plastic deformation. These conditions are :

continuity
consistency
uniqueness
and irreversibility.

The condition of continuity requires that the plastic strain increment $d\epsilon^p$ is entirely dependent on the component of the stress increment which is normal to the yield surface.

The consistency requirement states that any stress increment directed outside of the yield surface should produce plastic strains only. This implies that the strain tensor must be decomposed into elastic and plastic parts so that

$$d\epsilon_{ij} = d\epsilon_{ij}^{e} + d\epsilon_{ij}^{p} \qquad (2.3.2)$$

Since plastic deformation is a form of flow, the direction of the increment of plastic strain is defined by a flow potential Q to which the strain increment vectors are orthogonal. The plastic strain increment is given by :

$$d\epsilon_{ij}^{p} = \lambda \frac{\partial Q}{\partial \sigma_{ij}} \quad . \tag{2.3.3}$$

where λ is an arbitrary non-negative scalar.

If the yield surface is assumed to be the same as the flow potential then

$$d\epsilon_{ij}^{p} = \lambda \frac{\partial F}{\partial \sigma_{ij}} \quad . \tag{2.3.4}$$

The conditions of uniqueness and irreversibility are accounted for by Drucker's stability postulate. This postulate states that if a load is slowly applied and removed then the external agency applying the load must do positive work and thus $d\sigma_{ij}\ d\epsilon_{ij}^{p} \geq 0$. Furthermore, the complementary work performed over the stress cycle must be non-positive i.e.

$$\oint \epsilon_{ij}\, d\sigma_{ij} \leq 0 \tag{2.3.5}$$

The material may therefore not yield on reloading before the previous yield surface has been reached. The consequences of the stability postulate are that the yield surface $F(\sigma_{ij})$ must be convex in σ_{ij}-space and that the direction of plastic strain must be normal to the yield surface at the stress point σ_{ij} .

$$d\epsilon_{ij}^{p} = \lambda \frac{\partial F}{\partial \sigma_{ij}}\bigg|_{\sigma_{ij}} \qquad \lambda \geq 0 \tag{2.3.6}$$

and therefore the yield function and flow potential are equivalent $F(\sigma_{ij}) \equiv Q(\sigma_{ij})$. The flow is associated and the relation (2.3.4) is termed the normality rule.

The concept of normality are derived from Drucker's stability postulate which depends on energy considerations for a homogeneous body. Soil, however, is a particulate material and consideration must be given to whether these are alternatives or whether normality is a reasonable assumption for soil.

The alternative to normality is non-associative flow for which the yield function F is not the same as the plastic potential Q . A non-associated flow rule is not stable. This does not imply collapse of the material, but rather that a unique solution cannot be guaranteed. Prevost and Höeg (1975) question the appropriateness of Drucker's stability postulate and conclude that frictional materials can be stable.The constitutive equations for non-associated flow are not symmetric which means that conventional solution techniques cannot be employed. The algorithms for the solution on non-symmetric equations are more complex and therefore more expensive in terms of solution time.

Jain (1980) discusses the application of the normality rule to clays and concludes that the soil tends toward associative behaviour as the stress state tends toward failure. When the soil is in a virtually unstressed state, the strain increment is parallel to the stress increment, but tends to become parallel to the total value of stress direction (associated) near failure. Jain (1980) proposes two modifying factors to correct for non-associated behaviour. Most models are derived with associated flow rules.

For many materials, the size and position of the yield surface in stress space is affected by the plastic deformation. The yield surface in equation (2.3.1) is then written as: $F(\sigma_{ij},h_{\alpha}) = 0$ where h_{α} are hardening parameters ($\alpha = 0,1 , \ldots n$). The hardening parameters are usually functions of the plastic strain and two types of hardening can be described.

Isotropic hardening involves the uniform expansion of the yield surface with each plastic strain increment without any change in position and orientation in stress space. This is shown schematically in Figure 2.3.1(a). The yield surface is a function of both the stress state and the plastic strain.

$$F = F(\sigma_{ij}, \epsilon^{p}_{ij}) = 0 \qquad (2.3.7)$$

Kinematic hardening implies the translation of the yield surface in stress space without any change of size. A stress induced anisotropy develops as the stress state moves away from the initial conditions as shown Figure 2.3.1(b). The yield function for kinematic hardening can be written as

$$F = F(\sigma_{ij} - a_{ij}) = 0 \qquad (2.3.8)$$

where a_{ij} is a measure of the translation of the yield surface.

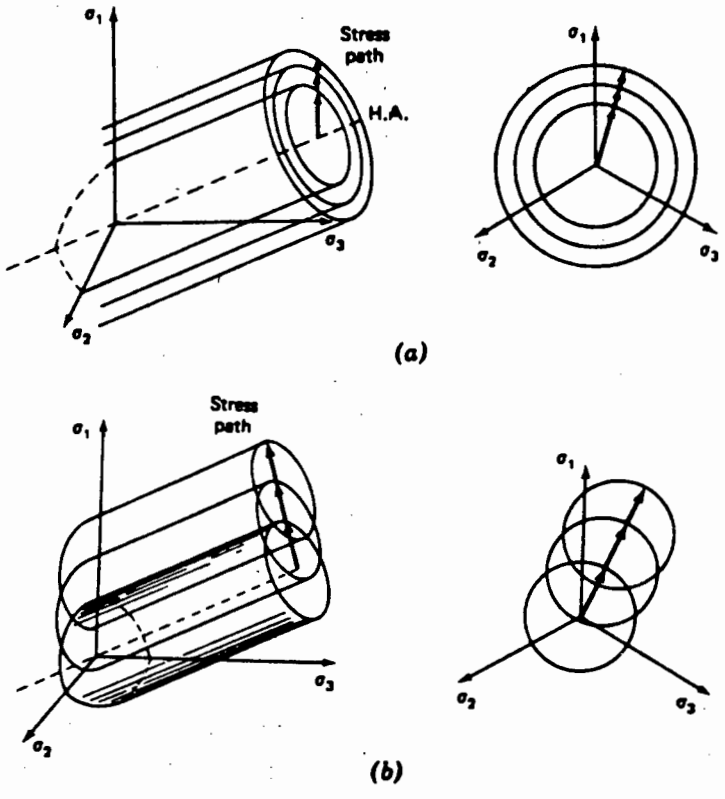

Figure 2.3.1 : Hardening models (a) isotropic (b) kinematic

The yield function can combine both isotropic and kinematic hardening and will then be :

$$F = (\sigma_{ij} - a_{ij}, \epsilon^{p}_{ij}) = 0 \quad . \qquad (2.3.9)$$

Some materials, such as highly overconsolidated clays, experience a reduction in stress, with increasing strain after yield. This is strain - softening behaviour and is unstable in the sense of Drucker's stability postulate, but will not be considered in this thesis.

The constitutive behaviour can now be described for the elastic response and loading and unloading from the yield surface.

For elastic behaviour :

$$F < 0 \quad \text{and} \quad d\epsilon^{p}_{ij} = 0$$

$$\text{therefore} \quad d\epsilon_{ij} = d\epsilon^{e}_{ij} = C_{ijk\ell}\, d\sigma_{k\ell} \tag{2.3.10}$$

where $C_{ijk\ell}$ is the elastic constitutive matrix.

At the point of unloading from the yield surface :

$$F = 0 \quad \text{and} \quad \frac{\partial F}{\partial \sigma_{ij}} d\sigma_{ij} < 0 \tag{2.3.11}$$

and

$$d\epsilon_{ij} = d\epsilon^{e}_{ij} = C_{ijk\ell}\, d\sigma_{k\ell} \quad .$$

For plastic loading :

there is no change in the yield surface, therefore :

$$F = 0 \ , \quad \frac{\partial F}{\partial \sigma_{ij}} d\sigma_{ij} + \frac{\partial F}{\partial h_{\alpha}} = 0 \quad . \tag{2.3.12}$$

For hardening, $\frac{\partial F}{\partial \sigma_{ij}} d\sigma_{ij} \geq 0$ and therefore $\frac{\partial F}{\partial h_{\alpha}} < 0$.

Solving for Λ in eqn. (2.3.6) under conditions (2.3.12) gives

$$d\epsilon^{p}_{ij} = B_{ijk\ell}\, d\sigma_{k\ell} \tag{2.3.13}$$

with B_{ijkl} the plastic constitutive matrix.

The constitutive equation for the plastic loading is thus

$$d\epsilon_{ij} = C_{ijkl}\, d\sigma_{kl} + B_{ijkl}\, d\sigma_{kl} \quad . \tag{2.3.14}$$

For rate independent deformation plasticity the strain increment is specified and the stress increment must be determined using the constitutive equation. The constitutive equation in the form of eqn. (2.3.14) can be inverted by a standard manipulation (Zienkiewicz, 1977) to give :

$$d\sigma_{ij} = D^{ep}_{ijkl}\, d\epsilon_{kl} \tag{2.3.15}$$

where D^{ep}_{ijkl} is the elastic-plastic constitutive tensor.

$$D^{ep}_{ijkl} = \left[D^{e}_{ijrs} - \frac{D^{e}_{ijkl}\, A_{kl}\, B_{mn}\, D^{e}_{mnrs}}{B_{mn}\, D^{e}_{mnrs} - H\, A_{ii}} \right] \tag{2.3.16}$$

$$A_{ij} = \frac{\partial Q}{\partial \sigma_{ij}}$$

$$B_{ij} = \frac{\partial F}{\partial \sigma_{ij}}$$

$$H = \frac{\partial h_{\alpha}}{\partial \epsilon^{p}_{ii}}$$

and D^{e}_{ijkl} is the elastic matrix such that

$$d\sigma^{e}_{ij} = D^{e}_{ijkl}\, d\epsilon^{e}_{kl} \tag{2.3.17}$$

In the previous formulation of the constitutive equations of plasticity theory the actual form of the yield surface was not specified. The following discussion presents some simple yield surfaces based on metal plasticity and subsequent modifications to account for the behaviour of

soils. These models were not necessarily developed to model loading and reloading behaviours and if so only one or two load cycles could be handled. Models developed solely for cyclic loading of soils will be discussed in Chapter 4.

Classical plasticity was developed for metals where the shape of the yield surface is independent of the mean pressure. The yield surface can be written in terms of deviatoric stress tensor only. The von Mises yield criteron states that yielding will occur when J_{2D} reaches a specific value. This implies that the yielding occurs at a maximum shear strain energy. The von Mises yield criteria has the form

$$F = J_{2D} - k^2 \qquad (2.3.18)$$

This forms a cylinder in principal stress space which is circular in cross-section when projected onto the π-plane. The other common yield criteria for metal is the Tresca criterion for which yield occurs when the maximum value of shear stress is reached. The Tresca yield surface is a hexagonal prism in principal stress space (see Figure 2.3.3), bounded by the von Mises yield surface.

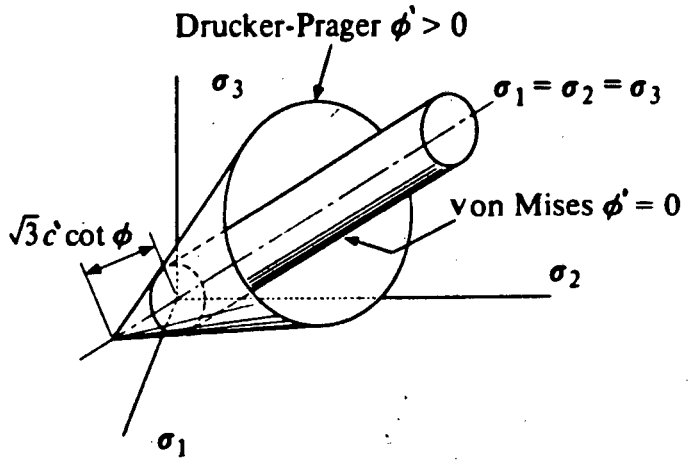

Figure 2.3.2 : Drucker-Prager and von Mises yield criteria in principal stress space. (after Zienkiewicz, 1977)

Soil, however, is not independent of the mean stress and the Mohr-Coulomb yield criterion $\tau = c' + \sigma \tan \phi'$ can be generalised for multi-axial states of stress as :

$$F = \sqrt{J_{2D}} - \alpha J_1 - k = 0 \qquad (2.3.21)$$

The material coefficients α and k are related to the internal angle of friction ϕ' and cohesion c'. Their derivation is to be seen in the context of the type of analysis to be undertaken. For instance an axisymmetric problem requires the constants for triaxial compression or triaxial extension as follows :

$$\alpha = \frac{2 \sin \phi'}{\sqrt{3}\,(3 \mp \sin\phi')}$$

$$k = \frac{6c \cos \phi'}{\sqrt{3}\,(3 \mp \sin\phi')} \qquad (2.3.22)$$

When normality is applied to a Mohr-Coulomb or Drucker-Prager yield surface, a constant increment of negative volumetric strain during shear is implied. Using equations (2.3.6) and (2.3.14), the plastic strain $d\epsilon^P_{ij}$ is

$$d\epsilon^P_{ij} = \lambda \left(\frac{S_{ij}}{2\sqrt{J_{2D}}} - \alpha \delta_{ij} \right) \qquad (2.3.23)$$

from which the plastic volumetric strain increment $d\epsilon^P_{ii}$ can be found by applying a tensor contraction. Thus

$$d\epsilon^P_{ii} = 3\alpha \lambda \qquad \alpha > 0 \,, \quad \lambda > 0 \,. \qquad (2.3.24)$$

The material therefore exhibits a continuous increase in dilation during shear. A dense granular material, such as sand, sheared under a low confining pressure will show an increase in volume, but the volume increase will tend to a limiting value. Loose sand, cohesive soils and dense sand under high confining pressures tend to contract during shear Bishop (1975). The yield criteria are therefore not generally applicable, though the volumetric dilation can be reduced using a non-associated flow rule with the corresponding problems of the asymmetric constitutive tensor and the violation of the stability postulate.

Soil under hydrostatic compression experiences a permanent deformation due to the rearrangement of the particles and a recoverable deformation due to the elastic deformation of the particles. Soil can therefore yield under pure hydrostatic compression. To account for this, Drucker et al (1955) proposed a spherical work hardening "cap" yield surface connecting the perfectly plastic Drucker-Prager surface to the hydrostatic axis (as shown in Figure 2.3.4).

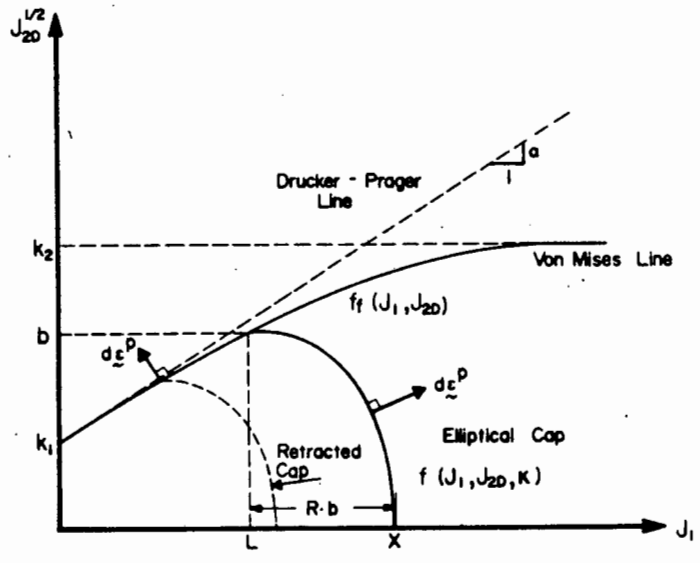

Figure 2.3.4 : Cap Model. (after Ko and Sture, 1981)

Drucker et al (1955) concluded that their spherical cap was not the correct shape, but should be more precisely defined from experimental evidence.

Sandler et al (1976) introduced a hypo-elastic formulation as an improvement for modelling hysteresis in the unloading-reloading behaviour. The model required 29 parameters of which 14 were for the hypoelastic model and was criticised by Pender (1977) for requiring too much test data for general application.

Nelson (1977) discusses the development of the cap model for the simulation of ground shock effects of nuclear and large conventional explosions where the typical loading is small amplitude cycles of short

duration under extremely high mean pressures (1 to 10 MPa). A perfectly plastic yield surface consisting of a Drucker-Prager surface with a transition to a von Mises surface at high mean stresses was used. Di Maggio and Sandler (1971) introduced an elliptical moving cap which hardens or softens depending on the stress path. The discontinuity between the cap and the yield surface was accounted for by constraining the flow vector depending on the stress path directions.

Resende and Martin (1985) criticised the cap models because of the discontinuity at the intersection of the two yield surfaces and proposed a parabolic cap.

Nelson (1977) concludes that the cap models give a good prediction of vertical ground motion due to the blast loading, but are not as successful for horizontal motion and seismic loading because of the predominance of shear behaviour in those load situations. The shear behaviour of the cap model depends entirely on the form of elasticity that is used. At the high stresses of 1-10 MPa the hysteresis effect is unimportant and the models are therefore sufficiently accurate.

Chen and Baladi (1985) discuss improvements for total stress, strain softening, elastic-viscoplastic, transverse isotropic and effective stress behaviour, but do not consider cyclic loading. The cap models each require between 17 to 30 parameters which implies a significant amount of testing.

An alternative approach to modelling the behaviour of saturated clays was taken at Cambridge University where the Critical State Theory was developed to help understand the soil behaviour observed in an extensive series of triaxial tests. The theory made it possible to predict the behaviour of a soil from the initial state and the applied load path. The evaluation of the soil response is simplified by fitting the soil state into a principal stress - volumetric strain space.

The critical state concept was developed into a plasticity model after a suggestion by Calladine (1963), but such models are generally more complex than those of classical plasticity because of the nature of the yield surfaces and the dependance on volumetric rather than shear strain. The cyclic models discussed in Chapter 4 are all based on critical state concepts and the theory of critical state soil mechanics is briefly presented in Chapter 3.

CHAPTER 3

THE CRITICAL STATE THEORY AS A FRAMEWORK FOR SOIL BEHAVIOUR

3.1 CRITICAL STATE THEORY

A conceptual framework for the description of soil behaviour is provided by the Critical State Theory. The concept of a critical state which a soil will ultimately reach upon continued shear deformation was first proposed for sand by Casagrande in 1936 (Holtz and Kovacs, 1981). In a series of direct shear tests he discovered that although loose and dense sand show different stress-strain characteristics, both eventually reach a distinct state where shearing occurs with constant strength and at constant volume. Casagrande found that for sands the density at the critical state was independent of the confining pressure.

Roscoe and coworkers (1963) studied the results of triaxial tests on clay. They found that clay also tended to a critical state, but that this state was a function of the mean confining pressure though was independant of the initial state and the test path. This section provides an overview of the concepts relevant to critical state soil mechanics. Detailed descriptions and derivations can be found in Schofield and Wroth (1968), Roscoe and Burland (1968), Atkinson and Bransby (1978). Further information is presented in Atkinson (1981), Jain (1980) Britto and Gunn (1987) and Naylor et al (1981).

3.1.1 Parameters used in critical state soil mechanics

As stated earlier the constitutive variables should be related to stress and strain invariants and thus be independent of the spatial frame of reference.

Many different stress parameters have been defined for soils and have been used in derivations of the critical state equations. The

parameters used in this thesis are p' and q and correspond to the "Cambridge" notation. The two stress parameters are

(i) the mean normal effective stress

$$p' = 1/3\ (\sigma'_{11} + \sigma'_{22} + \sigma'_{33}) \qquad (3.1.1)$$

$$= 1/3\ (\sigma'_a + 2\ \sigma'_r) \text{ in triaxial (axisymmetric) conditions}$$

where σ'_a is the effective axial stress and σ'_r the effective radial stress.

(ii) the deviator stress

$$q = \frac{1}{\sqrt{2}} \left[(\sigma_{11} - \sigma_{22})^2 + (\sigma_{22} - \sigma_{33})^2 + (\sigma_{33} - \sigma_{11})^2 + 6\ \sigma_{12}^2 + 6\ \sigma_{23}^2 + 6\ \sigma_{31}^2 \right] \qquad (3.1.2)$$

$$= \sigma_a - \sigma_r = \sigma'_a - \sigma'_r \text{ in the triaxial plane.}$$

The mean normal total stress p is given by

$$p = 1/3\ (\sigma_{11} + \sigma_{22} + \sigma_{33}) = 1/3\ (\sigma_a + 2\ \sigma_r)\ . \qquad (3.1.3)$$

The deviator stress q is the same for effective and total stresses. The use of p and p' to denote total and effective stress conditions differs from the original Cambridge notation which only considers effective stresses which are denoted by p. The question of the most appropriate stress parameters and notation is discussed by Wood (1984) who deals mainly with the difference between the Cambridge (p', q) stress field and the Massachusetts Institute of Technology (MIT) stress parameters originally also (p, q), but now generally called s and t.

Wood (1984) considers that the Cambridge p',q are most suitable for triaxial conditions though they can be used for plane strain analysis as well. The MIT parameters

$$s = 1/2\ (\sigma'_1 + \sigma'_3) \qquad (3.1.4)$$

$$t = 1/2\ (\sigma_1 - \sigma_3) \qquad (3.1.5)$$

will be advantageous in plane strain considerations since they are independant of the intermediate principal stress acting out of the plane. They should, however, not be used in triaxial conditions.

The measure of volumetric strain most commonly used is the specific volume v which is the volume of soil containing a unit volume of solids.

$$v = \frac{V_s + V_v}{V_s} = 1 + \frac{V_v}{V_s} = 1 + e \qquad (3.1.6)$$

where V_s & V_v are the volumes of solids and voids respectively and e is the voids ratio. If the soil is fully saturated the specific volume can be expressed in terms of the specific gravity of solids G_s and the moisture content w as :

$$v = 1 + G_s.w \qquad (3.1.7)$$

where w = mass of water/mass of dry solids = M_w/M_s .

The critical state theory is derived for an axisymmetric soil "element" and the strain invariants for axial symmetry related to the stress invariants were defined as :

increment of volumetric strain :

$$\delta v = -\frac{\delta v}{v} = -\frac{\delta e}{1+e} = \delta\epsilon_1 + 2\,\delta\epsilon_3 \qquad (3.1.8)$$

increment of deviatoric strain :

$$\delta\epsilon = \frac{2}{3}(\delta\epsilon_1 - \delta\epsilon_3) = (\delta\epsilon_1 - \frac{\delta v}{3}) \qquad (3.1.9)$$

3.1.2 The effect of the mean normal effective stress (p')

If a saturated (remoulded) clay is subject to an isotropic increase of

mean normal effective stress p' under drained conditions, the specific volume will decrease and the soil will follow a line in $v - p'$ space. This line is known as the isotropic normal consolidation line (NCL). If the pressure is reduced from p'_1 at point x (in Figure 3.1.1) to p'_2, the sample will swell to point y. The sample will then have a specific volume v_y which is greater than v_x, the specific volume at x. The clay is now overconsolidated with an overconsolidation ratio (OCR) equal to p'_1/p'_2.

If the pressure is increased to p'_3, the sample follows the swelling line to x, then once again follows the NCL. A successive reduction in pressure to p'_2 will result in swelling to point z. The specific volume v_z is now less than v_y and a non-recoverable change in specific volume $(v_y - v_z)$ has occurred.

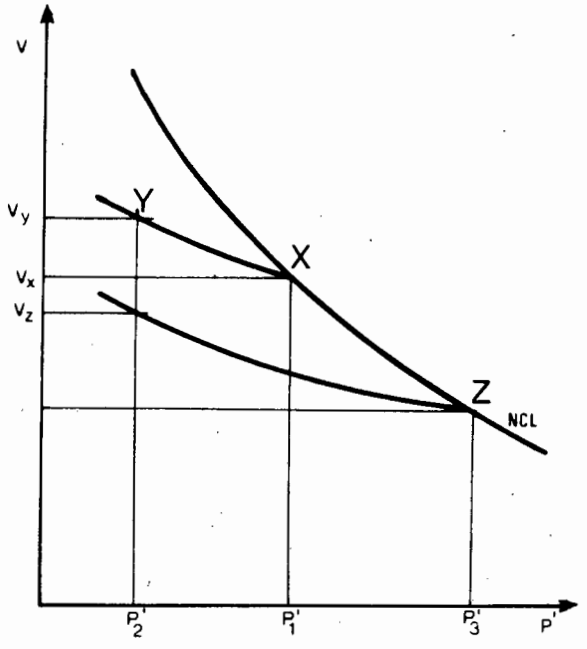

Figure 3.1.1 : Schematic representation of drained consolidation of clay in $v - p'$ plane

The critical state concept idealises the NCL and swelling lines as straight lines in $v - \ell n\ p'$ space. The normal consolidation line can be expressed as

$$v = N - \lambda \ell n p' \qquad (3.1.10)$$

where $-\lambda$ is the slope of the NCL.

The swelling line, having a slope of $-\kappa$, is

$$v = D - \kappa \ell n p' \quad . \qquad (3.1.11)$$

where N and D are the specific volumes for the mean normal effective stress $p' = 1$ i.e. $\ell n\, p' = 0$.

Butterfield (1973) suggested an alternative idealisation might be the consideration of a $\ell nv - \ell np'$ space. This thesis only refers to the $v - \ell np'$ space.

The increment of recoverable (elastic) volumetric strain dv^e due to an increment in mean normal effective pressure dp' is thus

$$dv^e = \frac{\kappa}{v} \frac{dp'}{p'} \qquad (3.1.12)$$

Each point in $v - \ell np'$ space is uniquely associated with a swelling line and a line parallel to NCL which have specific volumes at unit mean normal effective pressure of v_κ and v_λ, respectively. The value of v_λ for the normal consolidation curve is therefore N as is shown in Figure 3.1.2.

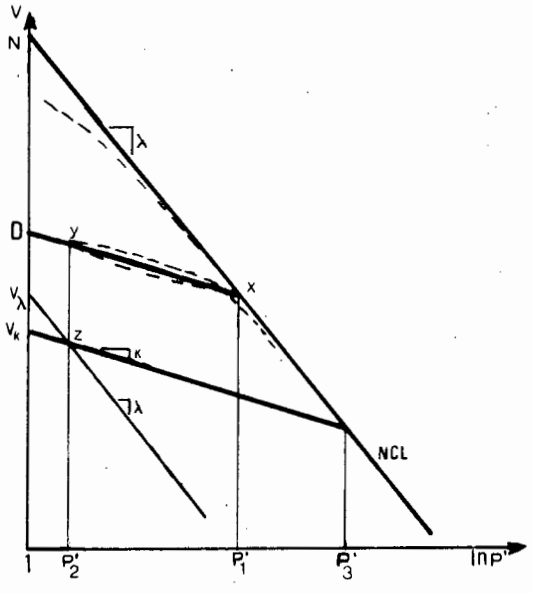

Figure 3.1.2 : Schematic representation of $v - \ell n\, p'$ plane

3.1.3 Effect of deviator stress q

The effect of increasing the deviator stress q can be visualised by considering the results of triaxial tests on saturated clay. The stress paths applied in triaxial compression tests occur on planes in p' - q - v sapce as shown in Figure 3.1.3.

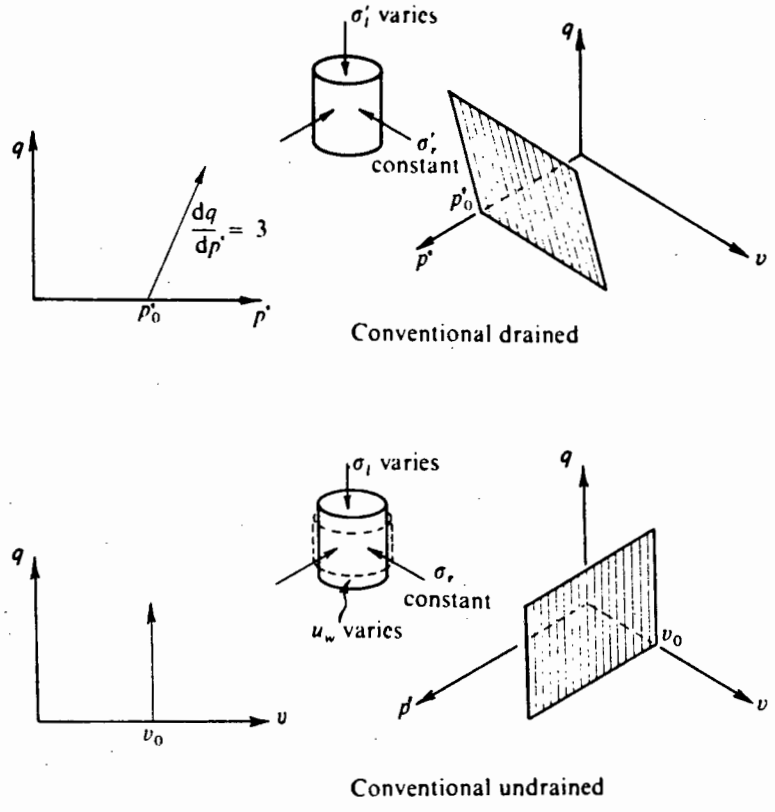

Figure 3.1.3 : Stress paths for triaxial tests (Schofield & Wroth, 1968)

In a drained test, total and effective stresses are the same and starting at a point

$$(p',q) = (p,q) = (p'_0 , o)$$

If an increment of deviator stress, Δq , is applied the stress point moves to the point

$$(((p'_0 + \Delta q) + 2\,\sigma_r)/3,\ \Delta q\ ) = (p'_0 + \Delta q/3,\ \Delta q)$$

in the p - q plane. The slope of the plane containing the stress path is therefore 1:3. The specific volume decreases according to the increment in stress as discussed earlier.

During an undrained test, the total stress plane also has a slope of 1:3, but the constraint of zero volume change causes a change in pore pressure. The effective stress path AB therefore curves away from the total stress path AC as shown in Figure 3.1.4.

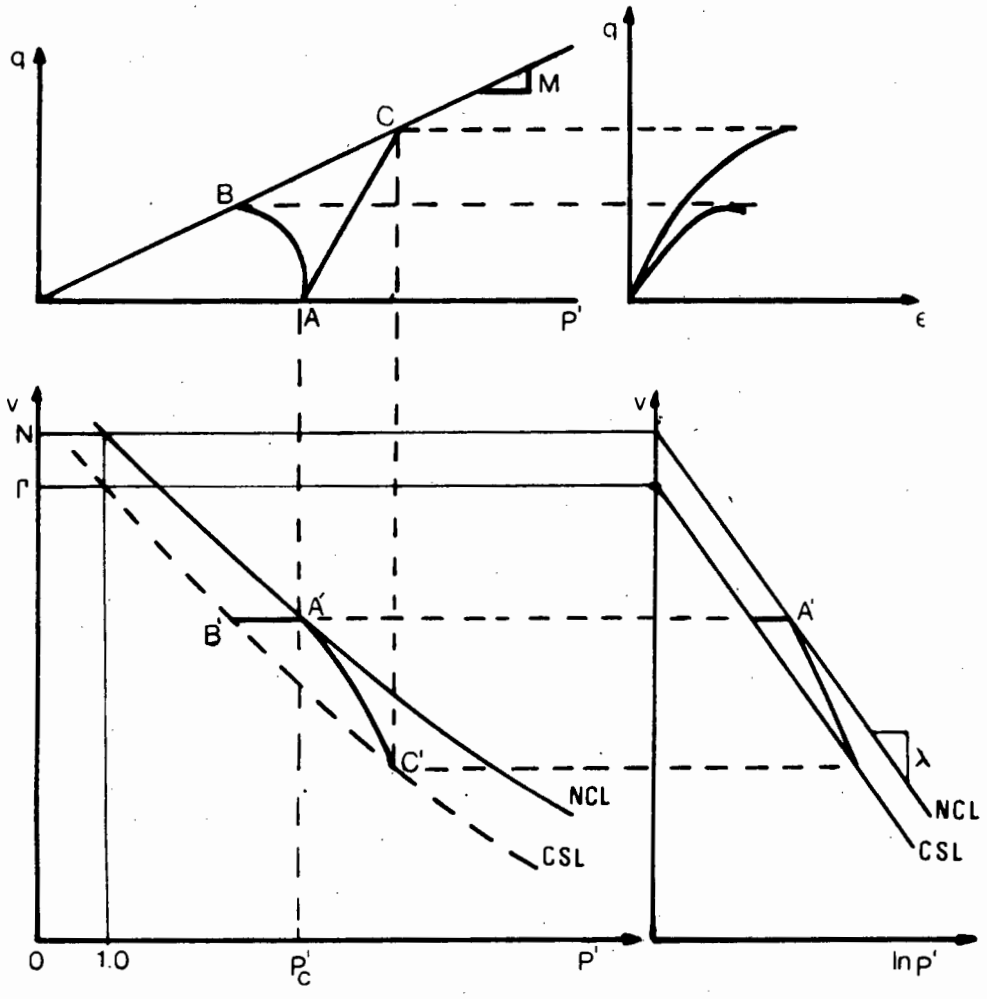

Figure 3.1.4 : Behaviour of normally consolidated clay (after Head, 1986)

If a sample of clay is initially normally consolidated (at A in Figure 3.1.4) and no back-pressure is applied, the total and effective stress paths will start at A. Both the drained effective stress path AC and the undrained effective stress path AB will end when the soil reaches failure on a projection of the critical state line. This

projection which is a straight line of slope M is of the form :

$$q = Mp' \qquad (3.1.13)$$

From the v - p' plane it can be seen that the final points, B',C' are on the same curve which is a straight line in the v - ℓnp' plane. This line is parallel to the NCL and therefore has the same slope of $-\lambda$. This projection of the critical state line can be written as

$$v = \Gamma - \lambda \, \ell np' \qquad (3.1.14)$$

where Γ is the specific volume for a mean normal effective stress p' of one unit.

Considering the drained and undrained stress paths of tests on normally consolidated clay at different specific volumes, it is evident that they form a surface in p' - q - v space culminating at the critical state line as shown in Figure 3.1.5. This surface separates admissible soil states from inadmissible states and is known as the Stable State Boundary Surface (SSBS). Since the surface passes through the NCL, soil states outside of the surface are not admissible. The surface is known as the Roscoe surface.

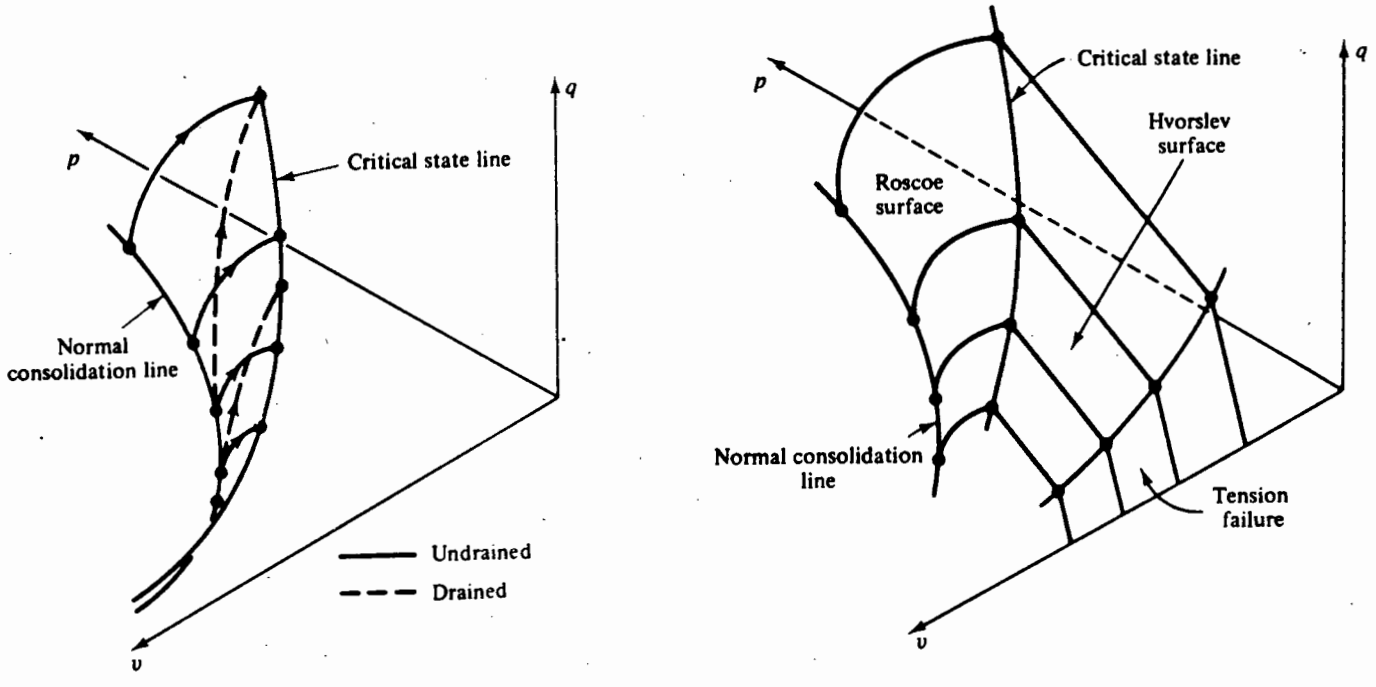

Figure 3.1.5 : Stable state boundary surface (Atkinson & Bransby, 1978)
a) derivation from drained and undrained tests
b) complete surface.

Uniqueness of the surface was proved by Henkel in 1960 by plotting contours of water content to show that points on any test path with the same value of effective stress p', q will have the same specific volume. The surface is thus independent of the drainage conditions in the test.

The behaviour of overconsolidated samples is similar and also tends towards the stable state surface boundary. The overconsolidated sample has been consolidated along the NCL then allowed to swell along a swelling line. When sheared, the soil follows a path in a plane above the swelling line until at some point the state boundary surface is reached and the soil state translates across the surface until failure.

The critical state theory therefore distinguishes between yielding and failure. Yielding occurs as the material translates across the SSBS whereas failure only occurs at the critical state line. The definition of failure is that the material flows as a frictional fluid at constant mean normal effective stress, deviator stress and specific volume. Failure at the critical state therefore implies

$$\frac{dp'}{d\epsilon} = 0 \; ; \quad \frac{dq}{d\epsilon} = 0 \; ; \quad \frac{dv}{d\epsilon} = 0 \qquad (3.1.15)$$

The critical state theory therefore postulates that :

i) below the SSBS only elastic (recoverable) straining can occur

ii) elastic shear strains are zero $d\epsilon^e = 0$

iii) the elastic strain consists of volumetric strain only and occurs along a swelling line

iv) during shear, the soil follows a vertical plane in $p' - q - v$ space, through the κ-line in $p' - v$ space, known as the "elastic wall"

v) plastic straining may only occur when the soil state lies on the stable state boundary surface

vi) failure occurs at the critical state line.

The volumetric straining is dependent on the overconsolidation ratio and two categories of overconsolidation may be determined. A lightly overconsolidated soil is such that the initial state lies between the NCL and the projection of the critical state line in the v - p' plane (denoted as H' in Figure 3.1.6). The soil will either develop a positive pore pressure or compact, in undrained or drained tests, respectively, and is termed "wet of critical".

The stable boundary surface in the region wet of critical is curved in p-q space and assumptions about the shape of the surface will be given in Section 3.2 .

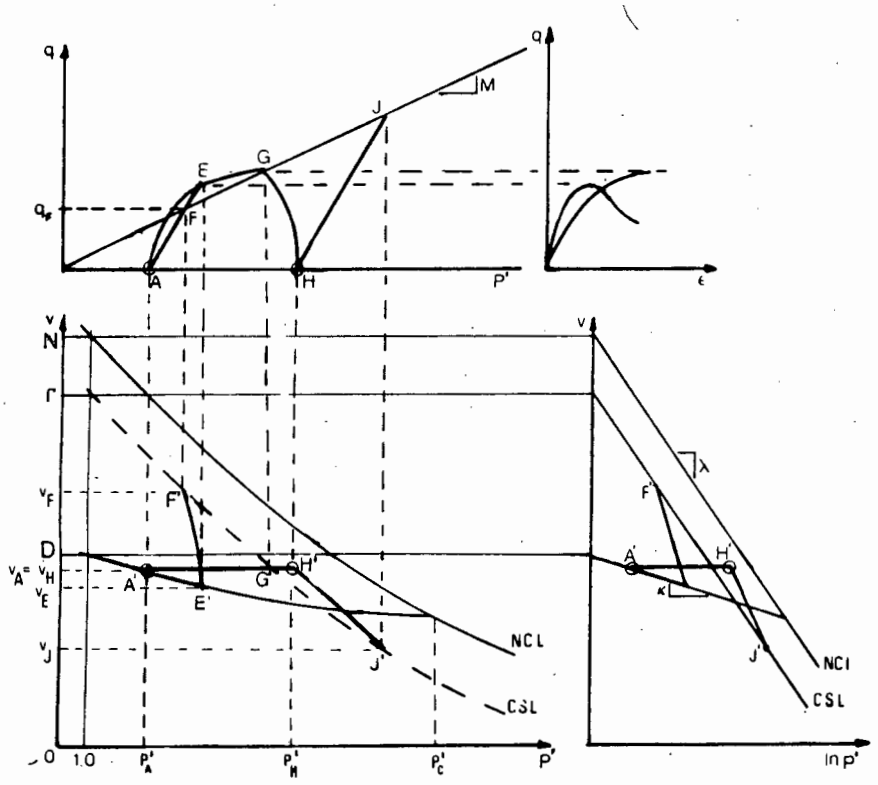

Figure 3.1.6 : Behaviour of overconsolidated clay

In a drained test, the critical state assumptions imply that the soil moves along the elastic wall then climbs the state surface to failure at a value of deviatoric stress q_J. The non-recoverable reduction in specific volume is thus $(v_H - v_J)$. The prevention of volumetric change in undrained loading results in an increase in pore pressure u , as the stress point moves from H (in Figure 3.1.6) toward the critical state and failure at G.

The second category of overconsolidation occurs when highly overconsolidated clay, which has swollen past the projection of the critical state (to A in Figure 3.1.6) and is therefore dry of critical, will expand in a drained test and experience negative pore pressure in an undrained test. The SSBS has a different shape in this region and is generally considered to be a straight line in p-q space. This portion of the state surface is called the Hvorslev surface.

In undrained conditions, the stress state of highly overconsolidated clay moves up the elastic wall (in Figure 3.1.6) from where the stress state tends to the critical state at G. In a drained test, the stress will move up the elastic wall to E with a recoverable decrease in specific volume $(v_A - v_E)$ and then move down the SSBS with increasing specific volume and decreasing deviator stress to point F . The deviator stress at failure (q_F) is lower than the deviator stress at which the soil state first reaches the SSBS (q_E) in contrast to the behaviour of lightly overconsolidated clay. The reduction in deviator stress and volumetric expansion is softening behaviour and is unstable in the sense of Drucker as discussed in Section 2.3.

The concept of a swelling line with a recoverable strain and a state boundary surface on which non-recoverable strains occur leads directly to the theory of plasticity. This suggests that the elastic swelling line is bounded by a yield surface which hardens isotropically (Calladine, 1963). The locus of successive yield surfaces forms the state surface boundary as shown in Figure 3.1.7 .

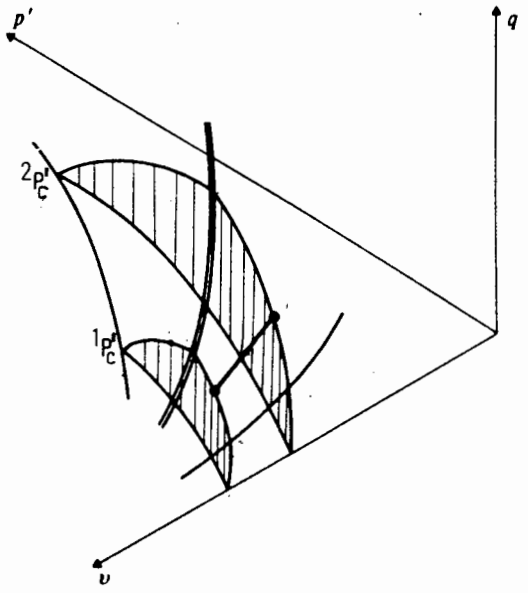

Figure 3.1.7 : Two yield surfaces with hardening parameters $^{i}p_c'$ (after Atkinson and Bransby, 1978)

The hardening is a function of plastic volumetric strain ϵ^p_{ii} and not deviatoric strain ϵ^p_{ij} as used in classical plasticity. The hardening parameter used is p_c', the pre-consolidation pressure, which is the pressure at the intersection of the yield surface and the normal consolidation line in the isotropic plane.

The shape of the yield surface can be determined experimentally.

3.2 APPLICATION OF PLASTICITY THEORY TO THE CRITICAL STATE CONCEPT

The application of normality to the yield surface (Calladine, 1963) implies that the plastic strain increment vector $d\epsilon^p$ is normal to the state surface with the plastic shear strain increment $d\epsilon^p$ component parallel to the q- axis and the volumetric plastic strain increment dv^p component parallel to the p' axis. Then, the gradient of the plastic strain increment vector is :

$$\frac{d\epsilon^p}{dv^p} = -\left(\frac{dp'}{dq}\right) = \frac{1}{\bar{r}} \qquad (3.2.1)$$

where ψ is the slope of a yield surface at a given point (p',q,v) in space. It has been shown (Roscoe & Burland 1968) that the slope is independent of the stress increment and the specific volume and is a function of the stress ratio η only.

where $\eta = q/p'$. (3.2.2)

Setting $q = \eta p'$, then $dq = qdp + pdq$ and equation 3.2.1 becomes

$$\frac{dp'}{p'} + \frac{d\eta}{\psi+\eta} = 0 \qquad (3.2.3)$$

The shape of the yield function can be found by integrating 3.2.3 to obtain

$$\ell np' + \int_o^{\eta} \frac{d\eta}{\psi+\eta} = \ell np'_c \qquad (3.2.4)$$

This can be integrated when ψ is expressed as a function of η . From the principles of constitutive modelling, as described in Chapter 2, this function should be derived from the energy equations.

The increment of energy per unit volume dE transmitted to a soil is the sum of recoverable energy dU and dissipated energy dW .

$$dE = dW + dU \qquad (3.2.5)$$

In critical state theory these are expressed as :

$$\begin{aligned} dE &= p'dv + qd\epsilon \\ dU &= p'dv^e + qd\epsilon^e \\ dW &= p'dv^p + qd\epsilon^p \end{aligned} \qquad (3.2.6)$$

From the assumption of zero recoverable shear strain $d\epsilon^e = 0$ the plastic shear strain increment $d\epsilon^p$ is equal to the total shear strain increment $d\epsilon$. Using equations (3.1.12) amd (3.2.6), the recoverable energy is therefore

$$dU = \frac{\kappa}{v} dp' \qquad (3.2.7)$$

The relationship between Ψ and η is derived from the dissipated energy dW . The shape of the yield function depends on the assumption of the form of the dissipated work.

Roscoe et al,(1963) assumed that

$$dW = Mp' d\epsilon \qquad (3.2.8)$$

where M is defined as in equation (3.1.13).

Therefore equation (3.2.6) can be written as :

$$p'dv^p + qd\epsilon = Mp' d\epsilon \qquad (3.2.9)$$

and thus

$$\frac{1}{\Psi} = \frac{d\epsilon}{dv^p} = \frac{1}{M-\eta} \qquad (3.2.10)$$

The yield surface is a log spiral curve as shown in Figure 3.2.1 of the form as derived from equation (3.2.3)

$$\eta = M \ln(p_c'/p') \qquad (3.2.11)$$

The theoretical elastic-plastic material described using this yield surface is called Cam-clay (Schofield and Wroth, 1968).

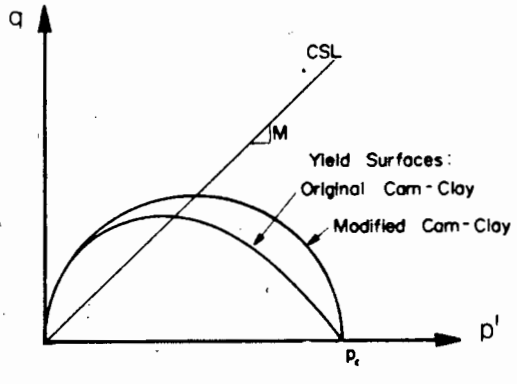

Figure 3.2.1 : Cam-clay and Modified Cam-clay yield surfaces (after Ko and Sture, 1981)

The stable state boundary surface (SSBS) can be shown to have the form

$$v_\lambda = \Gamma + (\lambda - \kappa)\ (1 - \eta/M) \qquad (3.2.12)$$

The surface intersects the v - p' plane along the NCL where q = 0 and $v_\lambda = N$ thus :

$$N = \Gamma + (\lambda - \kappa) \qquad (3.2.13)$$

Roscoe and Burland (1968) studied the expressions for dW and concluded that many hypotheses can be made about the dissipated energy, but all must lie between specific limits to satisfy isotropy, continuity and the assumptions of critical state theory. They assumed the dissipated work to be :

$$dW = p' \{ (dv^p)^2 + M^2 (d\epsilon^p)^2 \}^{\frac{1}{2}} \qquad (3.2.14)$$

The resulting yield locus is an ellipse in the p',q - plane (see Figure 3.2.1) and is known as the Modified Cam-clay surface which has the expression :

$$M^2 (p')^2 - M^2 p'_c p' + q^2 = 0 \qquad (3.2.15)$$

The SSBS has the equation

$$v_\lambda = \Gamma + (\lambda - \kappa)\ \{ \ell n(2) - \ell n\ (1 + (\eta/M)^2 \} \qquad (3.2.16)$$

and $$N = \Gamma + (\lambda - \kappa)\ \ell n(2) \qquad (3.2.17)$$

Both the Cam-clay and Modified Cam-clay yield surfaces are defined for all ranges of overconsolidation ratios, including heavily overconsolidated soils with η greater than M (see also Figure 3.2.1.).

Atkinson and Bransby (1978), Naylor et al (1981) use discontinuous yield surfaces. Both define the Hvorslev surface, where η is greater than M , as a straight line yield surface with a cut-off to define the

limits for no tension in granular materials. This is shown in Figure 3.2.2. Atkinson and Bransby (1978) apply the Cam-clay surface and Naylor et al (1981) use the Modified Cam-clay surface for $\eta < M$. The Hvorslev surface requires a non-associative flow rule and will not be considered in this thesis.

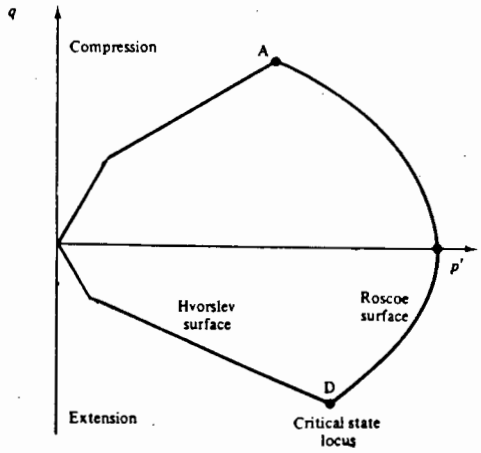

Figure 3.2.2 : Discontinuous yield surfaces for Critical State Theory (after Atkinson and Bransby, 1978)

The definitions of p' and q from (3.1.1) and (3.1.2) imply that the yield surface is a surface of revolution in principle stress space with a section equivalent to that of the Drucker-Prager yield surface for each value of specific volume. The critical state line becomes a cone in principle stress space similar to the Drucker-Prager cone (see Figure 2.3.2), but is a locus of failure points and not a yield surface. Use of the parameters s and t of equations (3.1.4) and (3.1.5) would result in a Mohr-Coulomb section (see Figure 2.3.3), but are not used in this thesis.

3.3 DETERMINATION OF PARAMETERS

Five parameters are required for the critical state models. The dimensions of the surface are fixed by specifying λ, κ and M . The parameter Γ (or N) is required to fix the position of the surface in v-ℓnp' space and the preconsolidation pressure p'_c is required to specify the position of the initial stress state.

The slope of the critical state line in p' q - space, M, can be determined by plotting the results at failure of at least three triaxial tests in p'q space. The best fit slope through the origin

is then M. The value of M can be derived from the internal angle of friction ϕ' from a consideration of the failure criterion in principal stress space. The most common relation, using the Drucker-Prager failure criterion is

$$M = \frac{6 \sin \phi}{3 - \sin \phi'} \qquad (3.3.1)$$

The values of λ and κ can be determined by drained compression tests. These tests should be isotropic ($q = 0$) to give the NCL, but may be conducted at a constant stress ratio. The parameter λ can be found as the slope of the compression curve in a consolidometer test which is a constant stress ratio test. Britto and Gunn (1987) show that the stress ratio changes during swelling so that horizontal stress measurement is necessary for determining κ in a consolidometer.

The results of consolidometer tests are often presented in $e - \log_{10} \sigma'_v$ space. Where e is the voids ratio and σ'_v the effective vertical stress. The slope of the consolidation curve is the compression index C_c and therefore $\lambda = C_c / \ell n(10) \approx C_c / 2.303$. Most soils will not have a straight line relation between v and $\ell np'$ and the most appropriate slope must be chosen.

To define the location of the critical state surface, either Γ or N must be specified. The relationship of the parameters Γ and N depends on the shape of the yield surface and this highlights the difference between Cam-clay and Modified Cam-clay.

If it is assumed that the two critical states coincide, then Γ will be the same for both models and the normal consolidation lines will differ - as shown in Figure 3.3.1. The test path must, however, start at a specific pressure and on the normal consolidation line and so the initial specific volumes will differ. The Modified Cam-clay will predict a lower specific volume v_{mcc} and higher deviatoric stress q_{mcc} than Cam-clay (v_{cc} and q_{cc}, respectively).

If the value of N and hence Γ is determined from an isotropic consolidation test, Modified Cam-clay and Cam-clay will have different values of Γ (compare equations 3.2.13 and 3.2.17). The Modified

Cam-clay will have a higher failure stress q_{mcc} than the Cam-clay but both will have the same specific volume. Britto and Gunn (1987) give the ratio of q_{mcc}/q_{cc} as 1.36 Λ , where

$$\Lambda = 1 - \kappa/\lambda \qquad (3.3.2)$$

The second method, choosing N , is preferable since this assumes the same initial specific volume.

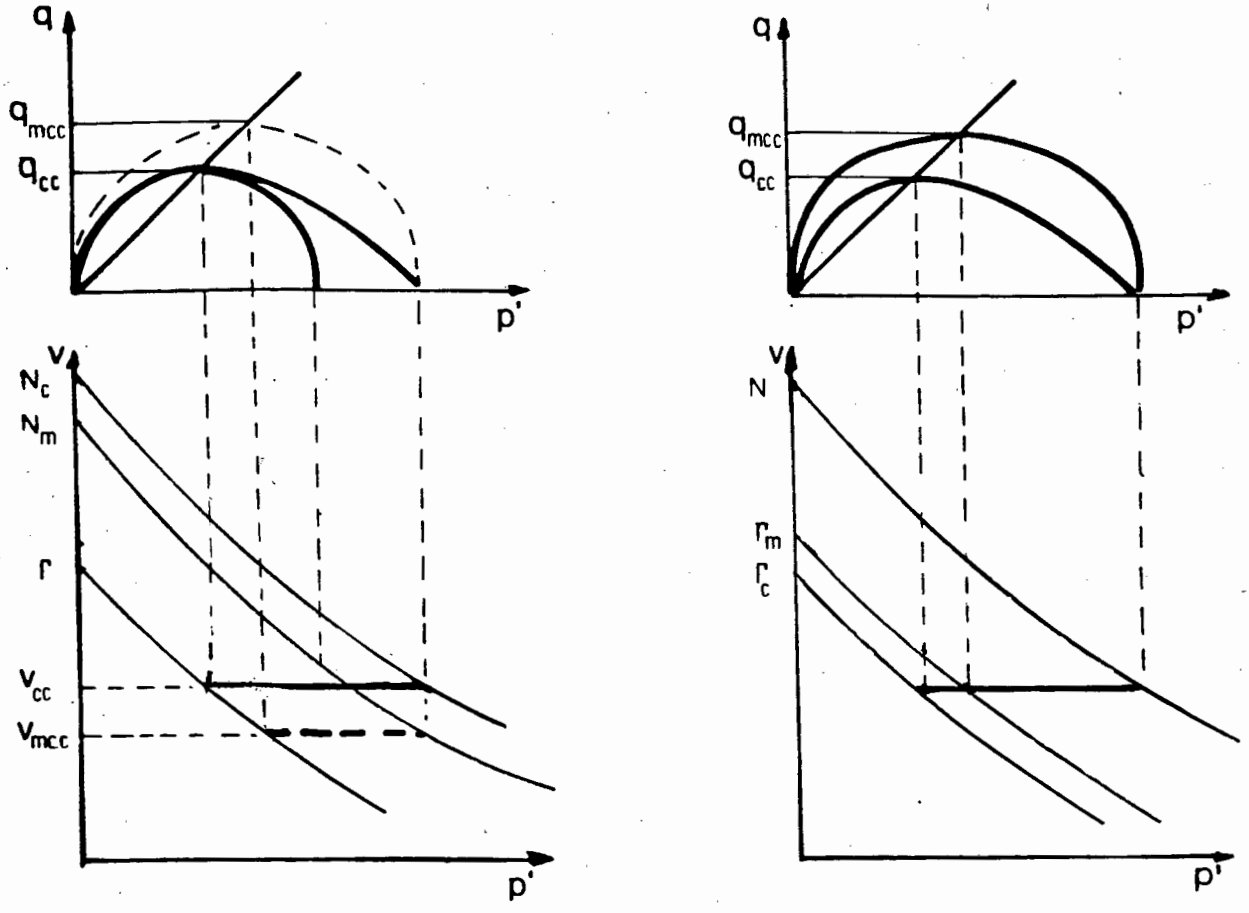

Figure 3.3.1 : Effect of choice of N or Γ in p'-q-v space

An alternative method for finding the parameters N, Γ and M can be found for Cam-clay by plotting

$$v_\lambda = v_o + \ell n p' \qquad (3.3.3)$$

against the stress ratio of η where v_o is the specific volume at the start of the test (Schofield and Wroth 1968). From equation 3.2.12 this gives a straight line of slope $M/(\lambda-\kappa)$ and intercept on the v_λ-axis of $\Gamma + (\lambda-\kappa)$ which is N from equation 3.2.13. When the results are plotted, a deviation is expected at low and high values of η due to variations in stress distribution (Figure 3.3.2). A straight line drawn through the intermediate points gives the parameters :

i) N - from the intersection with the v_λ – axis

ii) Γ - from $\Gamma = N - (\lambda - \kappa)$

iii) M - as the stress ratio at the intersection with the line $v_\lambda = \Gamma$.

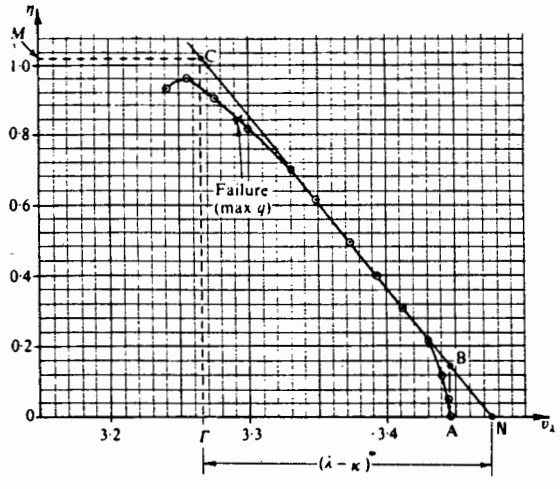

Figure 3.3.2 : $v_\lambda - \eta$ diagram for Cam-clay (Schofield & Wroth, 1968)

3.4 ACCURACY OF THE CRITICAL STATE MODELS

The question of the applicability of the critical state concept to soil has received much discussion. Britto and Gunn (1987) found that some clays do exhibit behaviour that is not predicted by the critical state theory. Soils with a high clay fraction can have residual strengths which are lower than the critical state predictions, some normally consolidated clays fail before the critical state is reached and experiments with high precision strain gauges show that the nonlinear range occurs at much lower strain levels than predicted.

As can be seen in Figure 3.1.1, the $v - \ell np'$ idealization does not model the hysteresis that occurs during swelling and reloading. Soils do not reach the original normal consolidation line on reloading but tend to follow a new λ - line, parallel to the NCL.

Natural sand is, generally, in a state denser than critical and the critical state concept is applied to the behaviour of sand by Atkinson and Bransby (1978). The behaviour is equivalent to that of an overconsolidated clay. The straight line Hvorslev surface provides a better model for soils dry of critical though Britto and Gunn (1987) suggest that since soil behaviour in this range is unstable and varied that Cam-clay or Modified Cam-clay are reasonable assumptions. Luong (1980) shows that the line of zero dilation (characteristic state) and the critical state do not coincide for sand and additional assumptions are necessary to model sand. Vaid and Chern (1985) present state surfaces, with distinct characteristic and critical states, for Tailings and Ottawa sands.

Roscoe and Burland (1968) discuss the differences between Modified Cam-clay, Cam-clay and experiments on kaolin. They conclude that the Cam-clay over-predicts both shear and volumetric strain whereas the Modified Cam-clay under-predicts these strains. This conclusion is supported by van Eekelen and Potts (1978) from tests on Drammen Clay. Both Roscoe and Burland and van Eekelen and Potts present yield surfaces which include the effects of deviatoric plastic strain below the state surface boundary.

A further problem involves the specification of the in situ stresses at the start of an analysis. This requires a value of the coefficient of lateral stress K_o. Both, Cam-clay and Modified Cam-clay over-predict the measured values of K_o (Britto and Gunn, 1987). The Cam-clay model can only predict a value of $K_o = 1$ (Schofield and Wroth, 1968) which was a reason for the development of Modified Cam-clay by Roscoe and Burland (1968). They show that the prediction of K_o by Modified Cam-clay depends on the ratio of κ/λ. An increase in κ/λ results in

a better prediction of K_o , but κ/λ is a function of the soil type. Recommendations for the choice of K_o are discussed in detail in Britto and Gunn (1987).

The critical state theory does, however, provide a unified conceptual framework which can be used to determine soil response to loading based on the initial state of the soil. This is particularly important for cyclic loading where the response of soils in different states seems contradictory, but when placed within the context of critical state theory the behaviour can be easily explained.

The criticisms of critical state theory centre around the behaviour of overconsolidated clays and sands. The theory can be refined to account for this type of behaviour, but with the additional expense of increased computational effort and an increase in the amount and sophistication of laboratory test procedures necessary to fit additional parameters for the soil.

The conventional critical state theory provides a reasonably accurate model for clays and the parameters can be obtained from test equipment that is standard in any commercial soil testing laboratory.

CHAPTER 4

CONSTITUTIVE MODELLING OF CYCLICALLY LOADED CLAYS

4.1 ASPECTS OF THE BEHAVIOUR OF CLAYS UNDER CYCLIC LOADING

4.1.1 Background to the review of laboratory investigations

The aim of developing constitutive models for soils under cyclic loading is to relate stresses and strains within the soil and thereby enable a designer to predict any changes in strength and deformation of a soil mass specifically caused by the cyclic loading as opposed to those from static loads. The nature of such changes in the soil characteristics can be determined in laboratory tests.

The subject of cyclic loading of clays in laboratory tests is extensive and has been reviewed in detail elsewhere (Wood, 1982, Sellers, 1987). The intention of this short review is to present an overview of those aspects of the clay behaviour that will provide a basis for the understanding of the constitutive models that will be examined later in this chapter.

If a model is to apply for a full three dimensional principal stress space, it must be based on laboratory tests carried out on stress paths covering the entire stress space. For historical and practical reasons, most testing is carried out in triaxial testing devices which can only explore the triaxial stress plane, i.e. triaxial compression and extension. More specialised test apparatus such as hollow cylinders, resonant columns (Hardin and Drnevich, 1972) and simple shear devices (Silver and Seed, 1971; Peacock and Seed, 1968) have been developed to explore other stress states (Prater and Studer, 1987; Sellers, 1987; Wood, 1982; Khosla, 1985). However, some researchers question the results from a laboratory test device because of the non uniformity of stress distributions within the samples. This research work concentrates on the results of cyclic triaxial testing of clay

only. Tests required for comparative studies could only be undertaken in a cyclic triaxial apparatus, the only device presently available in South Africa.

There are many situations in nature which result in a varying load being applied to soils, examples of which are shown in Table 4.1.1. (Head, 1986). Natural loading is in general irregular in form. For modelling purposes the loading is idealised in laboratory tests as a regular wave form most commonly of sinuosoidal, trapezoidal, triangular or square shape. The loading of the specimen can be either stress or strain controlled (i.e. the limits of the loading are defined in terms of stress or strain, respectively).

Situation	*Frequency of load application*
Offshore structures:	Tidal effects: usually 2 cycles per day
	Wave effects: several cycles per minute, continuously
Wind loading	0.01–0.1 Hz
Structures in areas susceptible to earthquakes	0.1–10 Hz, infrequently
Sub-bases for roads, railways, airfields	10–100 Hz
Foundation for machinery	Up to 100 Hz

Table 4.1.1 Types of cyclic loading (Head, 1985).

The terminology in the literature on cyclic loading is inconsistent and a wide variety of conventions are used which makes comparison difficult and hinders comprehension of the soil behaviour. The following definitions are given to provide a nomenclature which is consistent with that of the critical state theory previously defined and will be used throughout this work.

Loading is described as one-way if the stress or strain limits have the same sign. The loading is thus entirely in compression or entirely in extension.

A situation when the signs of limiting values of stress or strain differ will be defined as two-way loading. The loading, therefore, acts between compression and extension. If the limit values are of

equal magnitude, but opposite signs, the loading is termed symmetric.

For the purposes of this thesis, the term "repeated" will be used as a synonym to "cyclic" and not necessarily one-way compressive loading.

The wave form can be represented as shown in Figure 4.1.1

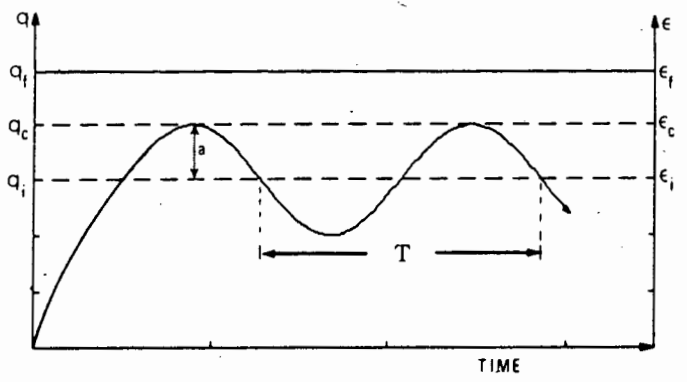

Figure 4.1.1 : Schematic diagram of load waveform

where q_i, ϵ_i is the initial deviatoric stress/strain
q_c, ϵ_c is the maximum cyclic deviatoric stress/strain
q_f, ϵ_f is the static failure stress/strain
a is the amplitude
T period = (1/frequency)

The cyclic stress ratio is defined as q_c/q_f . In undrained conditions, this is equivalent to $q_c/2c_u$, where c_u is the undrained shear strength of the soil.

The low permeability of clay and the high rate of loading prevents drainage during cyclic loading and this thesis will concentrate on undrained conditions.

The cyclic loading is a variation either in the total stress or the strain. The constitutive model should be able to predict the response in terms of effective stress and the resulting changes in strength and the accumulation of deformation, both of which could lead to failure and which are discussed in the following sections.

4.1.2 Effects of cyclic loading on the effective stress path

Cyclic soil behaviour is dependent on the current state of effective stress, the specific volume and on the stress history. The behaviour is therefore a function of the overconsolidation ratio (OCR) (Meimon and Hicher, 1980).

The cyclic change of stress causes a migration in the effective stress state resulting in the clay becoming more overconsolidated. The rate of migration depends on the cyclic stress ratio, the consolidation history and the frequency of the load application. The effective stress path of fast (high frequency) tests tends to move outside the failure envelope defined from slow monotonic tests (Wood, 1982; Anderson et al, 1976; Matsui et al, 1981; Takahashi et al, 1980). In strain controlled loading, Taylor and Bacchus (1969) noted that the effective stress migration was a function of the strain amplitude and the confining pressure.

In undrained loading, the prevention of volumetric change causes a change in pore water pressure. Pore pressure increases for samples with an OCR smaller than 2 and decreases for OCR greater than 2 (Sangrey et al, 1969). The pore pressure tends to cycle in phase with the loading. Sangrey and France (1980) noted the accumulation of pore pressure could be a function of the accumulated strain, but remarked that the mechanism was not understood. In drained conditions, volumetric change takes the place of pore pressure change in undrained conditions (Wood, 1982).

4.1.3 Effect of cyclic loading on the strength and deformation of clay

In the case of static loading of soil, failure can be defined as a loss of strength accompanied by excessive deformation that occurs when a maximum value of deviator stress is exceeded. The same criterion can be applied to cyclic load situations. However, it should be noted that the accumulation of strain due to cyclic loading below failure stress levels can lead to deformations that are excessive and could, for example, result in damage to a structure founded on such a soil mass.

The strength failure criterion can be determined by considering laboratory test results in the context of the critical state theory. The failure due to excessive deformation is dependent on the specific field situation and its prediction is one of the aims of the application of a constitutive model.

A measure of the resistance of the soil to cyclic loading is the number of load cycles N_f which the soil can sustain before failure. In the laboratory, this quantity is highly dependent on the test apparatus and will differ for samples of the same material, and cannot distinguish between sudden and gradual failure.

Sangrey et al (1969) found that for one-way stress controlled loading, there is a critical level of loading which separates two distinct categories of the ultimate cyclic stress state. This critical level of the cyclic deviator stress q_c is termed the critical level of repeated loading (CLRL). If the cyclic deviator stress remains less than the CLRL then the soil tends to a stable state of non-failure equilibrium where there is no further increase in axial strain or pore pressure. When q_c exceeds the CLRL, the effective stress state translates to failure at the same value of stress ratio q/p' at which failure occurs in static tests. The existence of this CLRL has been confirmed by Andersen et al (1976) and Sheu and Chang (1987) for both one-way and two-way stress controlled loading and by Matsui et al (1981), Meimon and Hicher (1980) and Procter and Khaffef (1984) for two-way strain control loading, respectively. The CLRL is a function of the soil and must be determined experimentally for each soil, but could be related to the bulk modulus according to Wood (1982).

Sangrey et al (1969) showed that the static effective stress failure criterion was not affected by one-way cyclic loading. Failure due to subsequent monotonic load increase, however, occurs at a lower deviator stress (Sangrey and France 1980). In the context of the critical state theory, this "cyclic degradation" can be seen as a translation and rotation of the failure line in the p' - v plane whilst remaining constant in p' - q plane (Wood, 1982). If drainage is permitted after cycling, the soil will move along a swelling line until the mean confining pressure is obtained.

The pore pressure increase during undrained cyclic conditions therefore leads to a reduction in strength for normally consolidated clay, but a subsequent period of drainage will cause a higher strength than that prior to cycling (Matsui et al 1981). Andersen et al (1976) confirms this effect, but warns that the strength of overconsolidated clays may reduce after cyclic loading.

4.1.4 Stress, strain and pore pressure behaviour due to cyclic loading

The modelling of the changes in the effective stress state, strength and deformation characteristics due to undrained loading is achieved by formulating the constitutive law to relate the stress, strain and pore pressure variations at a point in the soil.

The stress-strain and pore pressure-strain relationships are dependent on the type of cyclic loading. Wood (1982) comments on the scarcity of good test data. This becomes evident when attempting to assemble sufficient information to establish relationships between the stress, strain and pore pressure response to the various types of loading.

As a further complication, the reliability of test data from fast cyclic tests is in question because global pore pressure measuring devices depend on pore pressure equalizations throughout the sample. A fast test does not allow time for equalization and pore pressure gauges will indicate more or less constant pressures. As an example, Sangrey et al (1969) needed a period of 10 hrs to ensure pore pressure equalization. To reduce the load rate, Takahashi et al (1980) use a pore pressure probe within the sample and cycle for periods ranging from 30 minutes to 480 minutes to achieve pore pressure equalization.

At slower load rates, undrained creep may occur due to viscous flow resulting in an increase in axial strain and hence in the pore pressure (Meimon and Hicher, 1980). Slow tests with long load periods may therefore not be relevant to prototype situations (Table 4.1.1) where the frequency is much higher. A compromise must be sought between the response of the sample, test technique, testing inaccuracies and the possible rate dependence of the soil (Wood, 1982).

The following summary of the stress-strain and pore pressure characteristics has been collected from the available literature as a function of the type of loading and unloading.

One-way stress controlled loading :

The stress-strain behaviour is initially the same as in the static test, but unloading occurs with a much higher modulus which decreases as unloading continues. On reloading the modulus increases then gradually decreases forming an open hysteresis loop (a,b,c in Figure 4.1.2(a)) with a plastic increase in axial strain (a to c in Figure 4.1.2(a)). The hysteresis loops migrate along the strain axis depending on the increase of accumulated axial strain. Above the critical level of repeated loading, CLRL, the accumulated axial strain and the pore pressure increase continually to failure. Below the CLRL, the accumulation of axial strain tends to a limit and the hysteresis loops tend to a closed, stable loop (m,n in Figure 4.1.2(b)). The pore pressure increases to a stable value (Sangrey et al 1969).

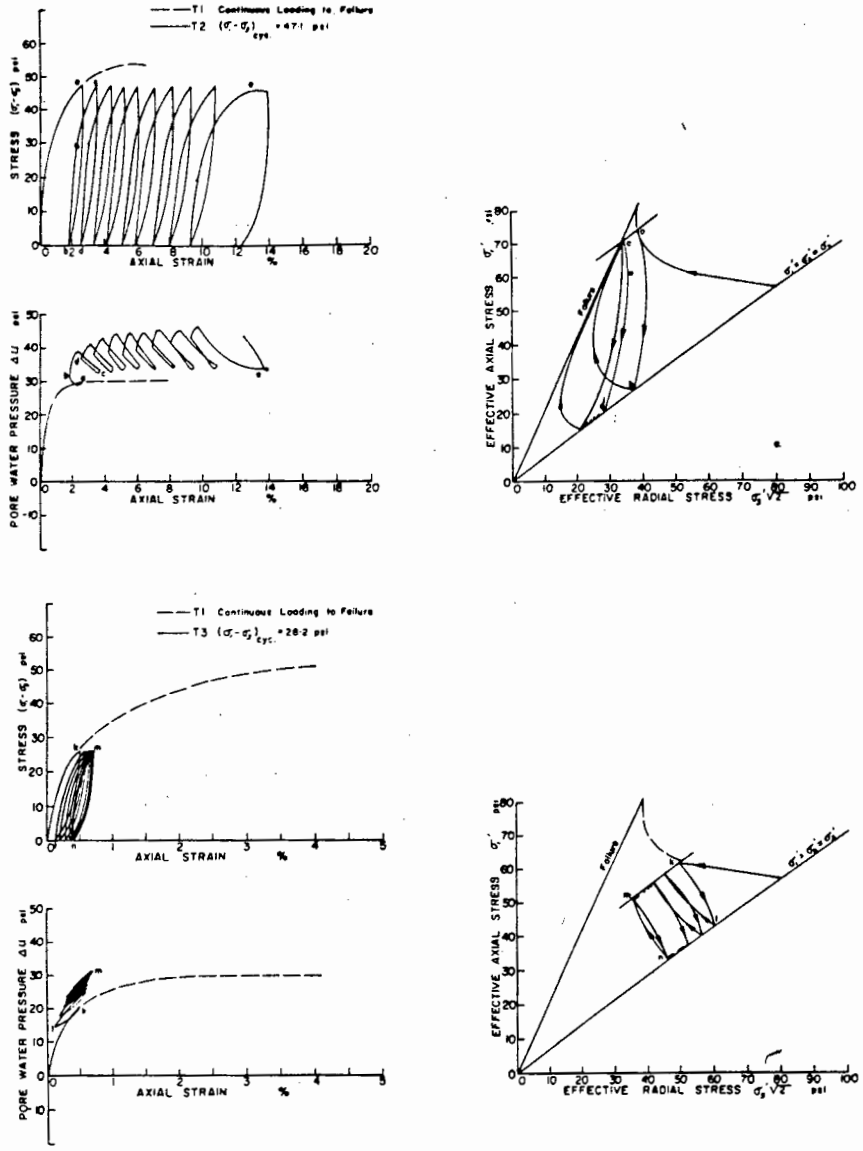

Figure 4.1.2 : One-way stress controlled loading of Newfield Clay (Sangrey et al, 1969)

One-way strain controlled loading :

Literature is lacking on this type of test and no data was available for this research work.

Two-way stress controlled loading :

Takahashi, Hight and Vaughn (1981) observed the stress-strain curves formed hysteresis loops about the origin of the stress-strain diagram for the two way tests. The peak strain in extension was greater than the peak compression strain as shown in Figure 4.1.3. The accumulated strain increased to failure for all tests of a cyclic stress ratio of 0,56 which, they conclude, is greater than the CLRL defined by Sangrey et al (1969).

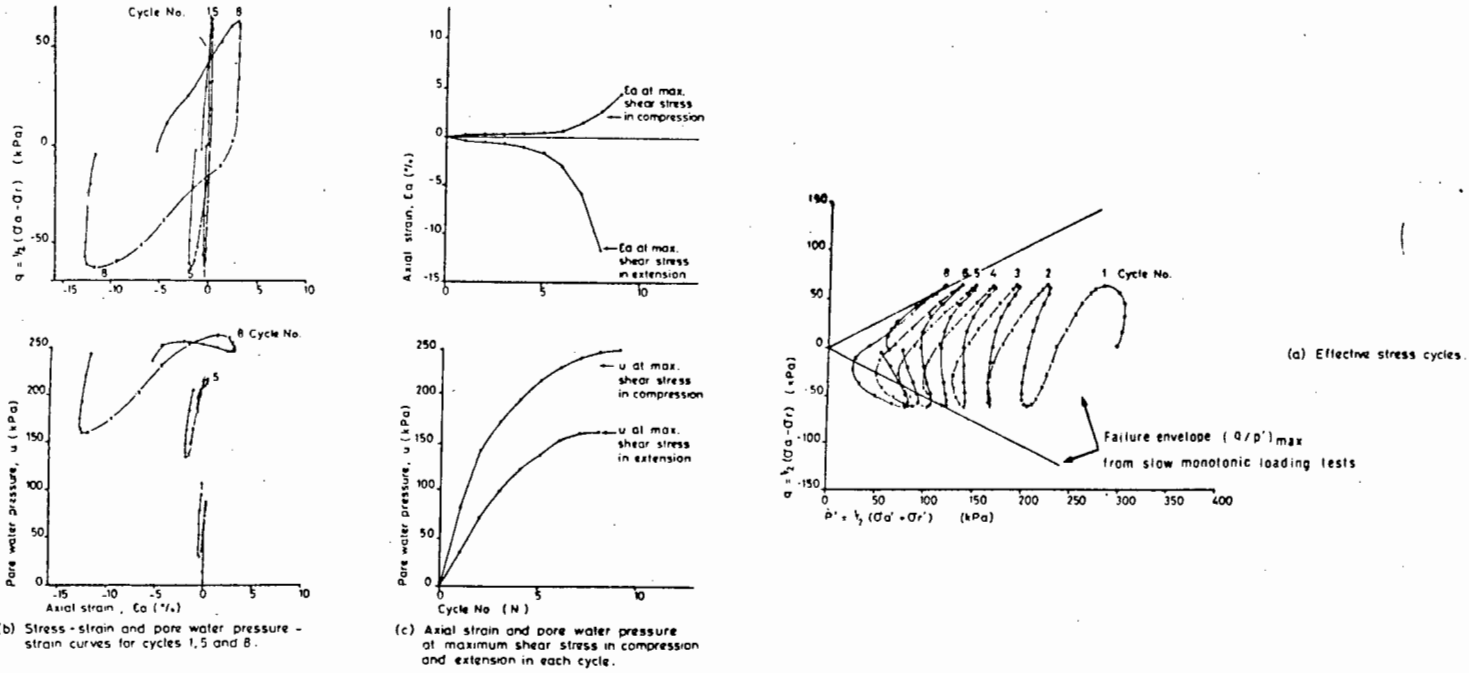

(a) Effective stress cycles.

(b) Stress - strain and pore water pressure - strain curves for cycles 1, 5 and 8.

(c) Axial strain and pore water pressure at maximum shear stress in compression and extension in each cycle.

Figure 4.1.3 : Two-way stress controlled loading of Happisburgh Till (Takahashi, Hight and Vaughn, 1981)

Matsui et al (1981) show that the pore pressure will either stabilize or increase to failure depending on whether the cyclic stress is below or above the CLRL, but provide no stress-strain or pore pressure-strain diagrams.

The apparent shear modulus, $\bar{G}$, is defined in the deviator stress-strain diagram as 1/3 of the slope defined by the two stress reversal points. For two-way stress controlled cycling, $\bar{G}$ reduces with the increasing number of cycles as the amplitude of the strain increases.

Two-way strain controlled loading :

The stress-strain response to cyclic loading in a hysteresis curve about the origin with the migration of the effective stress path causing a decrease in the maximum shear stress attained for each cycle.

The apparent shear modulus $\bar{G}$ therefore reduces as the number of cycles increases (Taylor and Bacchus, 1969). The loops are elliptical for low levels of strain, but tend to become s-shaped for higher strain amplitudes (Figure 4.1.4). Taylor and Bacchus (1969) consider this to be a material property though Pietruszczak and Pooroorshasb (1985) attribute the degeneration in shape to rate effects.

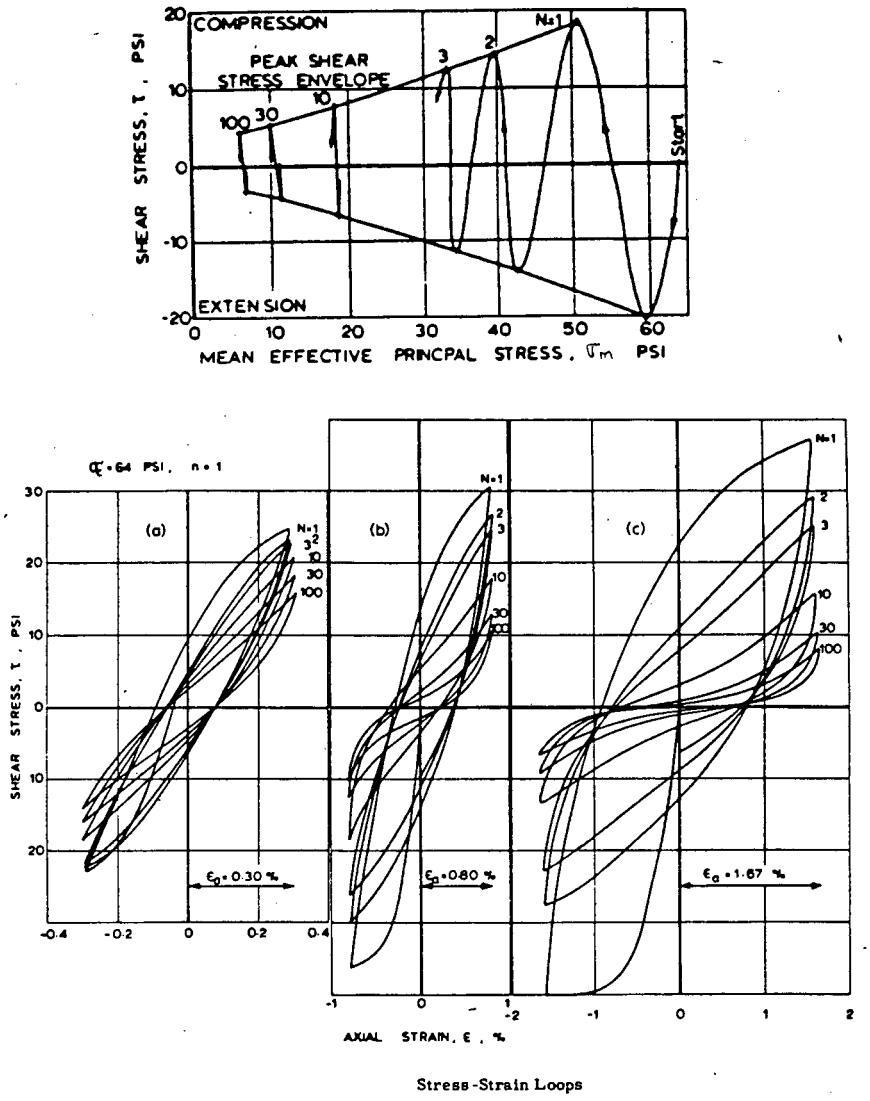

Stress-Strain Loops

Figure 4.1.4 : Two-way strain controlled loading of Halloysite (Taylor and Bacchus, 1969)

Wood (1982) suggests that the range of mineralogical properties and the differences in the plasticity of the clays studied is such that no single model could be expected to model all details of the soil response.

4.2 MODELLING OF CLAYS UNDER CYCLIC LOADING USING PLASTICITY THEORY

Roscoe and Burland (1968) noted that the unloading-reloading of clay caused hysteresis cycles in the stress-strain behaviour, but continued with the Modified Cam-clay model based on the assumption that this was a satisfactory response if the stress was not unloaded below half of the stress prior to unloading.

A "revised Modified Cam-clay" was introduced which included a cut-off yield surface independent of deviatoric stress allowing shear deformation at constant volumetric strain. Reloading cycles would therefore exhibit permanent strain.

This concept was developed for static loading by Potts (1985) and van Eekelen and Potts (1978), but two concepts in modelling emerged (Pande and Pietruzczak 1986), the first group advocating simple model with few parameters whereas the other favour a more general model with a significant number of parameters.

The simpler models either consist of empirical modifications of the static critical state theory or concepts that do not involve plasticity theory such as the fatigue model (van Eekelen and Potts, 1978). Fatigue models make no attempt to model individual cycles, but predict the trends by using functions of a monotonically increasing fatigue parameter and are essentially nonlinear quasi-elastic laws and do not account for accumulation of permanent strain.

More complex models are based on generalizations of monotonic plasticity and viscoplasticity to cyclic loading. The endochronic theory consists of a form of viscoplasticity that is dependent on accumulated strain instead of time. The endochronic models are considered to be outside the scope of this thesis. Most plasticity models for cyclic loading of soils are based on a formulation by Mroz, 1967, and are known as nested yield surface models. These will be briefly reviewed in the next sections, followed by a discussion of the simpler models. The choice of model must be based on criteria that include ease of implementation, predictive capabilities and availability of test systems to evaluate the parameters.

4.3 NESTED YIELD SURFACES

4.3.1 Concept

The conventional elastic-plastic constitutive model with isotropic hardening can model monotonic loading reasonably well, but the large elastic domain does not allow for hysteresis when considering cyclic or time varying loads (Mroz and Norris, 1982). Additionally, a stress induced anisotropy occurs when a soil is not consolidated under isotropic conditions and isotropic hardening models are not able to model this phenomonen.

In order to model these conditions, a concept of "material memory" was postulated. This implies that the soil has a memory of previous stress states which determines the material behaviour. These states are remembered until a state of higher intensity erases the memory. This erasure of less important events means that only a discrete set of prior states need to be remembered which is termed a "discrete memory" (Mroz and Norris, 1982).

This concept is illustrated in Figure 4.3.1 for a uniaxial case. The load intensity function P = P(t) is shown as a series of random cycles of varying intensity. A large intensity load, P_9 , controls the material behaviour during loads P_9 to P_8 , but is erased from memory by the event P_9 . The state of soil under intensity P_9 will determine the behaviour until a larger intensity load removes it from memory.

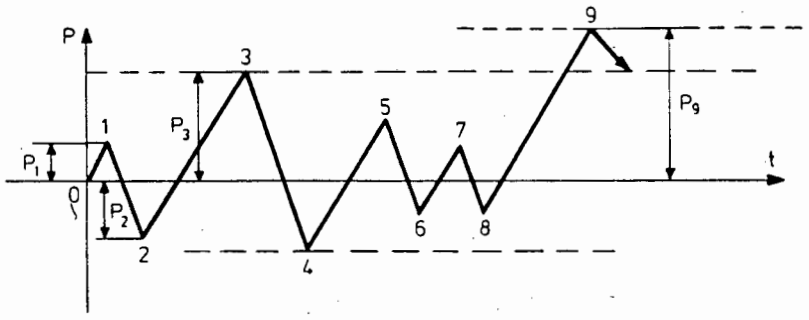

Figure 4.3.1 : Schematic representation of soil memory (Mroz and Norris, 1982)

To model this behaviour in multiaxial conditions requires a yield surface which defines the stress state, a consolidation surface which defines the initial state of the material and some means of describing the translation of the yield surface depending on the memory of previous stress states.

A yield surface, f_o is assumed to enclose an elastic domain, and to harden kinematically and isotropically. Thus

$$f_o \left(\underset{\approx}{\sigma} - \underset{\approx}{\alpha}^{(o)} , e^p \right) = 0 \qquad (4.3.1)$$

where $\underset{\approx}{\alpha}^{(o)}$ defines the translation in stress space of f_o, due to kinematic hardening and the plastic void ratio, e^p , defines the expansion of the surface due to isotropic hardening. The consolidation surface, F_c defined by the initial degree of consolidation can expand or contract isotropically. This surface is equivalent to the original critical state surfaces such as Cam-clay and Modified Cam-clay and can be expressed as

$$F_c = f(\underset{\approx}{\sigma} , e^p) = 0 \quad . \qquad (4.3.2)$$

The incorporation of the concept of memory for the translation rule of the yield surface requires the definition of a hardening modulus K. This hardening modulus depends on the relative distance in stress space between the yield surface and the consolidation surface and determines the evolution of the plastic strains $d\underset{\approx}{\epsilon}^p$. The evolution law can then be written as

$$d\underset{\approx}{\epsilon}^p = \frac{1}{K} \underset{\approx}{n}_f \left(\underset{\approx}{n}_f^T \, d\underset{\approx}{\sigma}\right) \qquad (4.3.3)$$

where $$\underset{\approx}{n}_f = \frac{\partial f/\partial \underset{\approx}{\sigma}}{[(\partial f/\partial \underset{\approx}{\sigma})^T \cdot (\partial f/\partial \underset{\approx}{\sigma})]^{1/2}} \qquad (4.3.4)$$

The evolution law is equivalent to equation (2.3.4) with the associative flow rule applying.

It was found that the hardening modulus had to be specified by a set of n similar yield surfaces f_i within the consolidation surface where :

$$f_i\ [(\underset{\approx}{\sigma}' - \underset{\approx}{\alpha}^{(i)}) - [a^{(i)}(e^p)]^2] = 0 \qquad i = 0,1,2...n \qquad (4.3.5)$$

These surfaces are initially concentric, hence form a "nest" of yield surfaces. For any point, P_o , on surface f_o there are conjugate points, P_i , on each other surface such that the normal vector $\underset{\sim}{n}_f^{(i)}$ has the same direction as shown diagrammatically in Figure 4.3.2. The stress point (after consolidation to P_c) will initially move through the elastic domain, but on reaching P_o will translate toward P_1 employing the hardening modulus $K_{(o)}$. When surface f_o contacts surface f_1 at P_1 , both f_o and f_1 will translate toward P_2 with hardening modulus $K_{(1)}$ defined by f_1 .

On unloading, the stress point will move into the elastic until it again contacts the surface, f_o which will translate in the new direction.

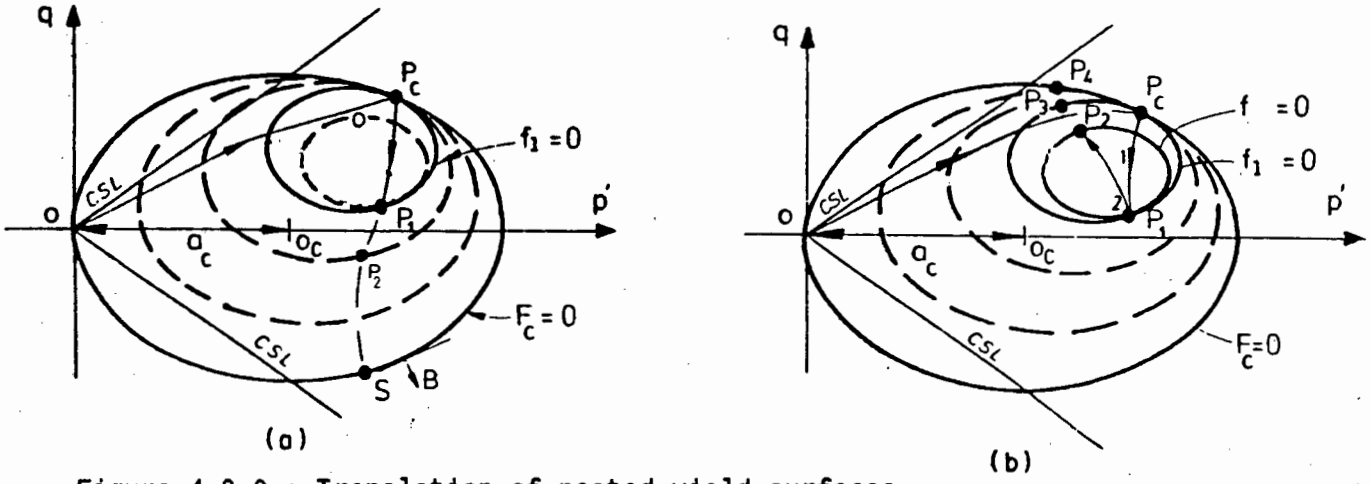

Figure 4.3.2 : Translation of nested yield surfaces.
(after Mroz and Norris, 1982)
a) loading, b) first unloading

Three classifications of nested yield surfaces can be distinguished depending on the way in which the magnitude of the hardening modulus at any point be given in three different ways. This is specified :

- In "multisurface hardening" models, the same function specifies the value of the hardening modulus $K_{(k)}$ for each yield surface f_k .

- In "infinite number of surfaces" (ins) models, the hardening modulus depends on the ratio of the diameter (or major axis) of the instantaneous yield surface to that of the consolidation surface.

- For "two surface" or "bounding surface" models, where only the yield, and consolidation, surfaces are considered, the hardening is a function of the distance of the stress point to its conjugate point P_c on the consolidation surface.

The form of the yield surfaces has varied as researchers sought to improve the predictions of their models. The earliest models were total stress approaches with the von Mises yield criteria. Subsequently, critical static ellipses (Mroz, Norris and Zienkiewicz, 1981), rotated partial ellipses (Mroz and Norris, 1982), and two ellipses combined with hyperbola (Dafalias, 1982) have been used. The main reason for using the more complex shapes is to predict the value of K_o, the coefficient of lateral stress, and the deviatoric strain more accurately. The predictions of K_o have been improved, but the stress strain curves are only realistic for stress paths approximately symmetric about the hydrostatic axis.

The nested yield surface models require a large number of parameters most of which are required to "tune" the models to account for observed soil behaviour, Mroz and Norris (1982) need 10 parameters and a model by Prevost requires about 20 parameters (Pande and Pietruszczak 1986). The advantage of being able to model complex stress paths is counteracted by the large computational effort required.

4.3.2 Application to cyclic loading

The ability of the model to predict cyclic behaviour depends on the way the model allows the translation of the effective stress path. In a

multisurface model, the stress path always moves towards the centre of the consolidation surface and stabilizes below the apex as shown in Figure 4.3.3.

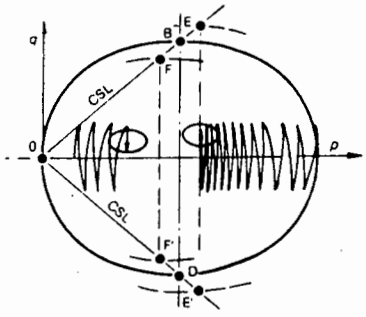

Figure 4.3.3 : Stabilization of effective stress path in multi-surface model. (Mroz, Norris and Zienkiewicz, 1981).

This is in contradiction to the experimental evidence of Sangrey et al (1969) (see Section 4.1) where the effective stress paths stabilized below the CLRL and reached failure for cyclic stress ratios above the CLRL . Mroz, Norris and Zienkiewicz (1981) proposed two solutions which were applied to both, two-surface and ins models.

The first solution is to shrink the consolidation surface as a function of accumulated plastic deviatoric strain ϵ_a where

$$\epsilon_a = \int |d\epsilon^p| . \qquad (4.3.6)$$

Applied to the infinite yield surface model and by "tuning" the function of ϵ_a , predictions similar to the results of Sangrey et al (1969) were obtained, but without any effect of cyclic degradation. The locus of stable states passed through the intersection of the consolidation and bounding surfaces as shown in Figure 4.3.4(a). The effect of a critical level of repeated loading was achieved by translating the yield surface as a function of ϵ_a as well as reducing the size of the consolidation surface. The resultant p'-q diagram (Figure 4.3.4(b)) is similar to that of Sangrey et al (1969). The pore pressure vs number of cycles in Figure 4.3.4(c) and the deviator stress vs strain in Figure 4.3.4(d) show the same trends as the experimental data from Sangrey et al (1969) including hystesis loops in the stress strain diagram.

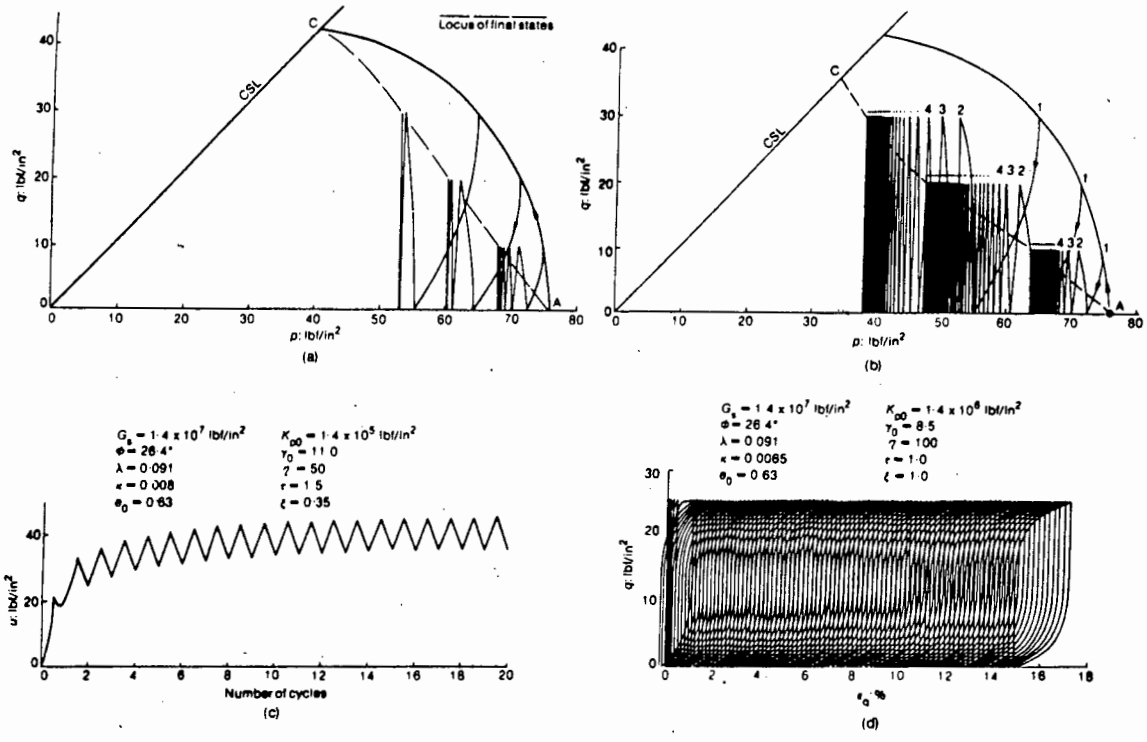

Figure 4.3.4 Prediction of one-way stress controlled loading using ins model (Mroz, Norris and Zienkiewicz, 1981)

The second method requires the introduction of an intermediate surface in the two-surface model which divides the consolidation surface into two regions. The intermediate surface, $F_1 = F_1(\underset{\sim}{\sigma}, e^p, \epsilon_a)$, shrinks away from the consolidation surface as cycling continues. The hardening modulus is defined by the intermediate surface for points inside the surface, and by the consolidation surface for points outside the surface.

The new surface causes the effective stress point to either always translate to failure on the critical state line, or to stabilize, depending on the function of ϵ_a chosen. The stabilization occurs on the minor axis of the intermediate surface and is independent of the stress ratio, in contradiction to the results of Sangrey et al (1969). No hysteresis is predicted in the stress-strain behaviour as shown in Figure 4.3.5 .

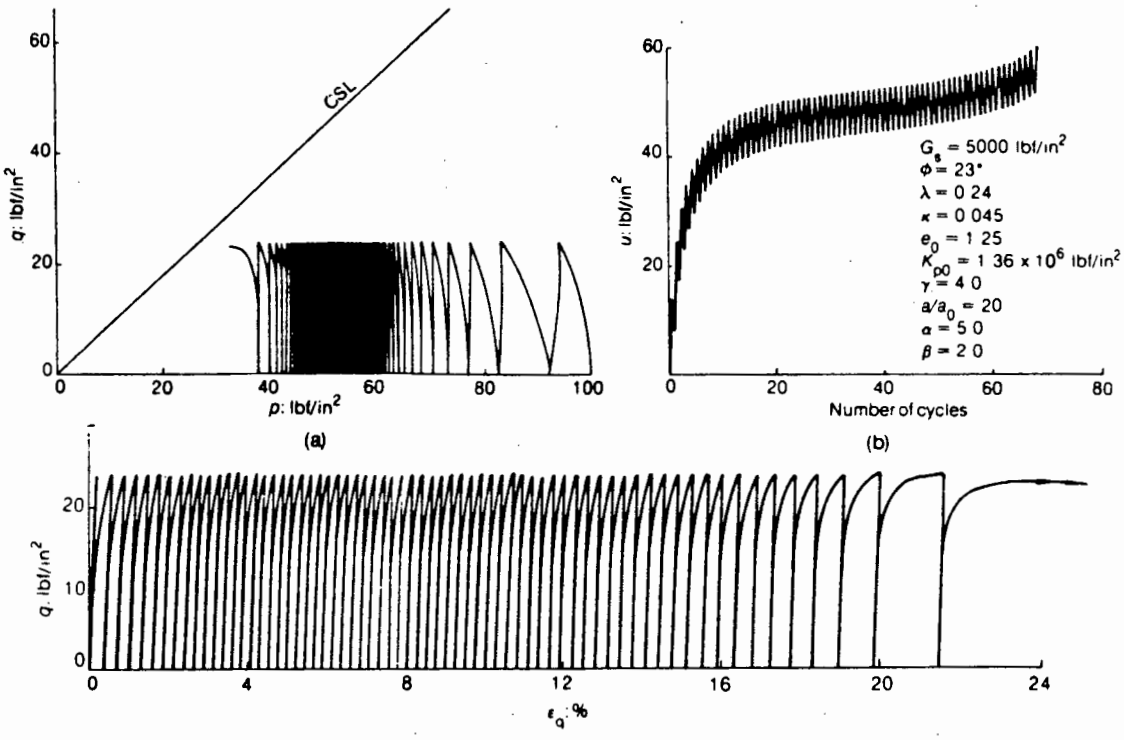

Figure 4.3.5 : Predictions of model with an intermediate surface (Mroz, Norris and Zienkiewicz, 1981)

At this stage, the testing of nested yield surface models has concentrated on stress controlled cyclic loading, Pietruszczak and Pooroorshasb (1985) consider that the predictions would not be as good under strain controlled conditions because of the sensitivity to the magnitude of the elastic shear modulus. The dependence of the yield surfaces on volumetric strain only is a problem of all critical state based models and results in poor prediction of hysteresis loops, shear modulus and shear strain (Pande and Pietruszczak, 1986).

4.4 MODELS BASED ON NESTED YIELD SURFACE CONCEPT

4.4.1 Bounding surface model

Dafalias (1982) had used the bounding surface concept to describe the cyclic behaviour of metals. The bounding surface formulation differs from that of Mroz and Norris (1982), but the concept of a bounding surface that describes the 'bounds' of material behaviour and a function of plastic hardening that describes the behaviour within the bounding surface remains the same. (Dafalias, 1982). The model has been generalised (Dafalias, 1986) to include viscoplastic as well as elastic plastic behaviour. The model is shown in Figure 4.4.1 .

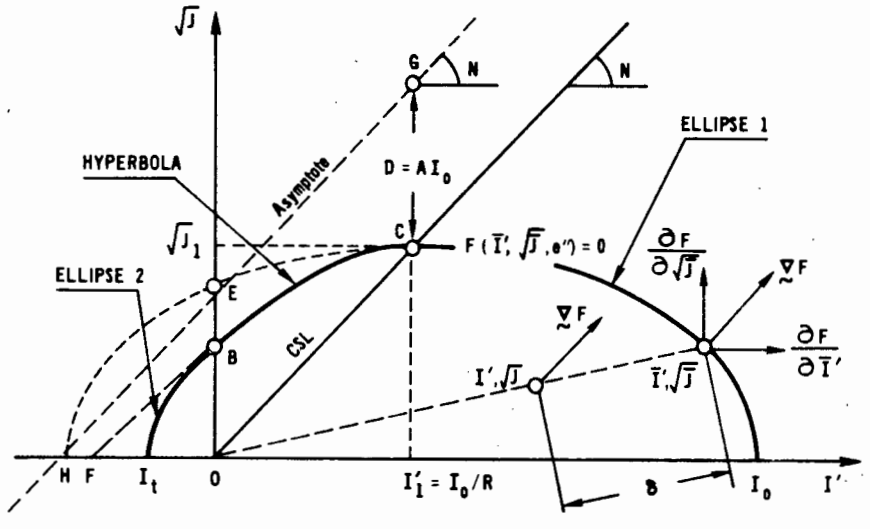

Figure 4.4.1 : Bounding surface model (Dafalias, 1986).

The elastic-plastic behaviour describes instantaneous deformation due to particle rearrangement. The viscoplastic effects are used to model the delayed deformation that occurs as clay particles shear with respect to each other. The strain tensor can be decomposed as :

$$\epsilon_{ij} = \epsilon_{ij}^{e} + \epsilon_{ij}^{p} + \epsilon_{ij}^{v} \qquad (7.3.7)$$

where the ϵ_{ij}^{v} are viscoplastic time dependent strains. The bounding surface consists of a hyperbola and two partial ellipses as shown in

Figure 4.4.1. This complex form allows a better prediction of the coefficient of lateral stress , K_o and of the deviatoric strain whilst retaining an associated flow rule.

Under cyclic loading, the effective stress path always translates to the critical state line. An "elastic nucleus" was incorporated into the model to account for the stabilization of the effective stress path at low stress ratios. A cyclic stress path moving entirely into the elastic nucleus will stablize, but a path outside or partially inside the elastic nucleus will tend to failure on the critical state (Dafalias, 1986). Cyclic degradation in strength is accounted for by reducing the bounding surface as a function of accumulated deviatoric strain, in the same way it was incorporated by Mroz, Norris and Zienkewicz (1981) in their infinite number of surfaces model.

The complete model becomes very sophisticated, but some flexibility was obtained by modularizing, so certain effects can be removed by setting parameters to zero if not required. The models are most often employed for monotonic loading with rate effects and anisotropy (Dafalias, 1986; Dafalias and Hermann, 1986). The results of the appliation of the model to verify the response of a few load applications on Kaolin as reported by Wroth and Loudon (1967) are shown in Figure 4.4.2 (Dafalias, 1982)

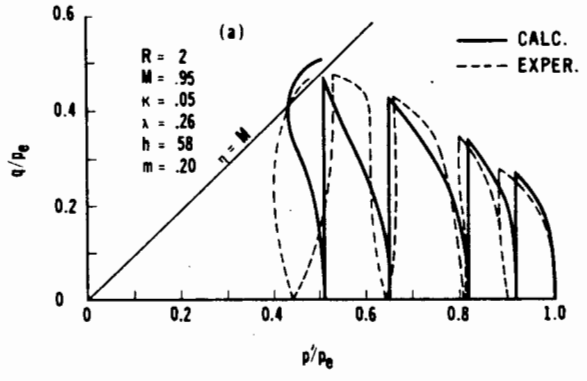

Figure 4.4.2 : Bounding surface model prediction of cyclic behaviour (Dafalias, 1982)

4.4.2 Multi laminate reflecting surface model

This model was proposed by Pande (1985) and is an elastic-visco-plastic modification to Modified Cam-clay. The principle involved is that a reversal of load implies that the current yield surface is reflected to cause plastic straining in the new direction. The model needs four yield surfaces to cause plastic strain in any direction and a fifth bounding surface to which the hardening is related as shown in Figure 4.4.3.

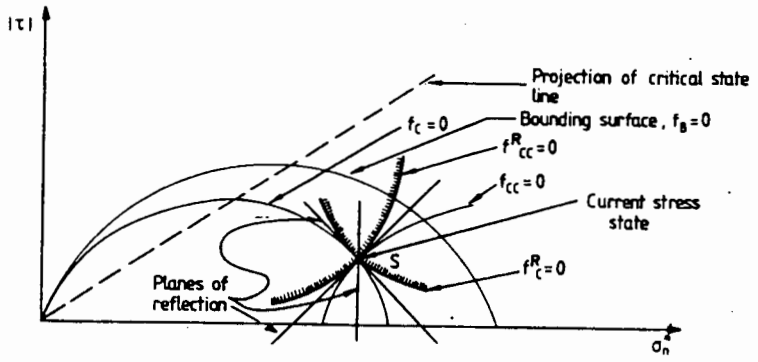

Figure 4.4.3 : Multi laminate reflecting surfaces model (Pande, 1985)

4.4.3 Geotechnical stress variables model

Hueckel and Nova (1979) and Nova (1982) present a model in which the parameters are related back to the critical state parameters M, λ, κ and hence is named the "geotechnical stress variables" model. The objective of the model is to predict behaviour below the yield surface. This is based on "para-elastic strain", namely strain that may or may not be recovered during a closed stress path, depending on the magnitude and direction of the path.

The change in material behaviour is concentrated at stress reversal points and the behaviour is a function of a hierarchical system of nested surfaces radiating from each stress reversal point. The hardening behaviour is controlled by the field of surfaces radiating from the current stress reversal point (Figure 4.4.4), until the stress path passes outside the stress reversal surface where hardening is controlled by a previous field of nested surfaces.

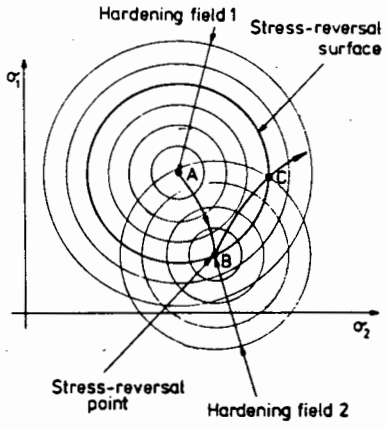

Figure 4.4.4 : Geotechnical stress variable model (Norris, 1982).

The model is complex and requires 10 parameters. However, Nova (1982) presents some analytical solutions for certain stress paths. These include the solution for the unloading-reloading cycles from Wroth and Loudon (Figure 4.4.5) which is in good agreement to the bounding surface model predictions of Dafalias (1982) (Figure 4.4.2). No predictions are given for steady cyclic loading with constant q_c.

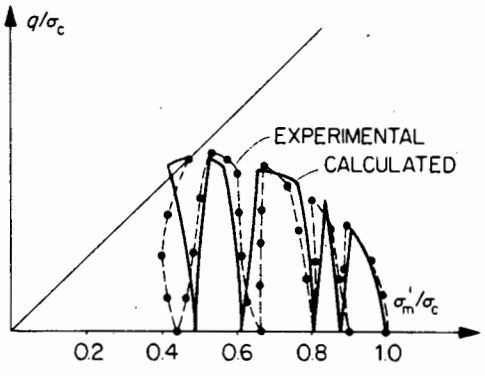

Figure 4.4.5 : Predicted and experimental behaviour of undrained cyclic loading of Kaolin (Nova, 1982)

4.5 EMPIRICALLY MODIFIED PLASTICITY MODELS

4.5.1 Pender model

Pender (1978, 1982) uses a critical state concept for modelling overconsolidated clay and dense sand under cyclic loading. The basis of the model is a function for the undrained stress path under triaxial conditions which Pender considers to be as reasonable an assumption as the thermodynamic assumptions on which conventional critical state models are based. Hypothetical functions for the yield surface, plastic potential and hardening were developed.

To model cyclic loading, a cyclic hardening function is postulated that depends on the change in deviatoric stress and on the number of half cycles. This implies that the soil has the ability to memorise half cycles. Functions for the shear modulus and damping based on available data are built into the model.

The model backpredicts the data well, but as pointed out by Pande and Pietruszczak (1986), the model is specific to triaxial conditions for which the functions were derived. Although the model was developed for overconsolidated soils, it is also used to predict the behaviour of normally consolidated clay (Pender, 1982).

4.5.2 Carter, Booker, Wroth model

In response to the increasing complexity demanded by nested yield surface models and other proposed models, Carter Booker and Wroth (1982) proposed a simplified model based on Modified Cam-clay that required only one additional parameter. This model is able to qualitatively predict the trends of soil behaviour, but not necessarily the exact response along the entire stress or strain paths. The aim was to predict the generation of pore pressure and the failure of the soil under undrained cyclic loading using parameters that can be directly chosen from triaxial test results.

The model is based on the experimental observations that the position and possibly the shape of the yield surface are changed by elastic

unloading. On reloading the stress point meets the yield surface sooner than predicted by Modified Cam-clay. The intrinsic assumption of the model is that the size of the yield surface is isotropically reduced on unloading though the shape remains the same implying that the hardening parameter is reduced. The parameter (θ) introduced controls the amount of reduction that occurs.

The parameter θ may theoretically be chosen from one cycle of unloading and reloading in an isotropic consolidation test. The preferred method is to choose θ from a plot of θ against the logarithm of the number of cycles to failure (log N_f) for various cyclic stress ratios (see Figure 4.5.1) and then find the value of θ that best fits the number of cycles to failure in the laboratory tests.

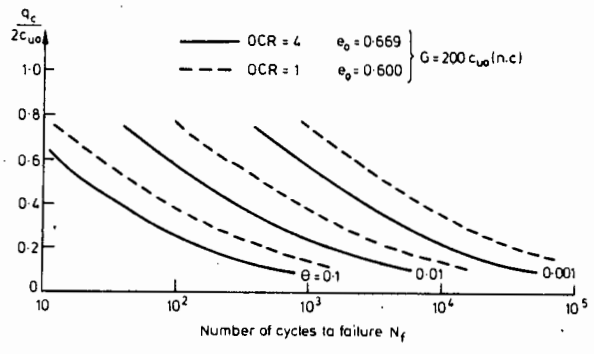

Figure 4.5.1 : Determination of θ using graph of θ versus log(N_f). (Carter, Booker, and Wroth, 1982)

Under undrained triaxial conditions with cyclic stress controlled loading, the number of cycles to failure increases with decreasing θ and decreasing cyclic stress q_c and is independent of shear modulus G. The model predicts the strength degradation, migration of the effective stress path and increase in pore pressure associated with cyclic loading, but no hysteresis effects are produced under one-way stress controlled loading.

In the undrained strain controlled situation, the effective stress path migrates with decreasing maximum stress in accordance with the observed behaviour. The deviator stress, however, tends to zero at failure and the material flows at zero shear stress. This is a phenomenon known as "liquefaction" and is more a characteristic of loose sand than clay, which always retains some residual shear stress. The migration is sensitive to the shear modulus chosen.

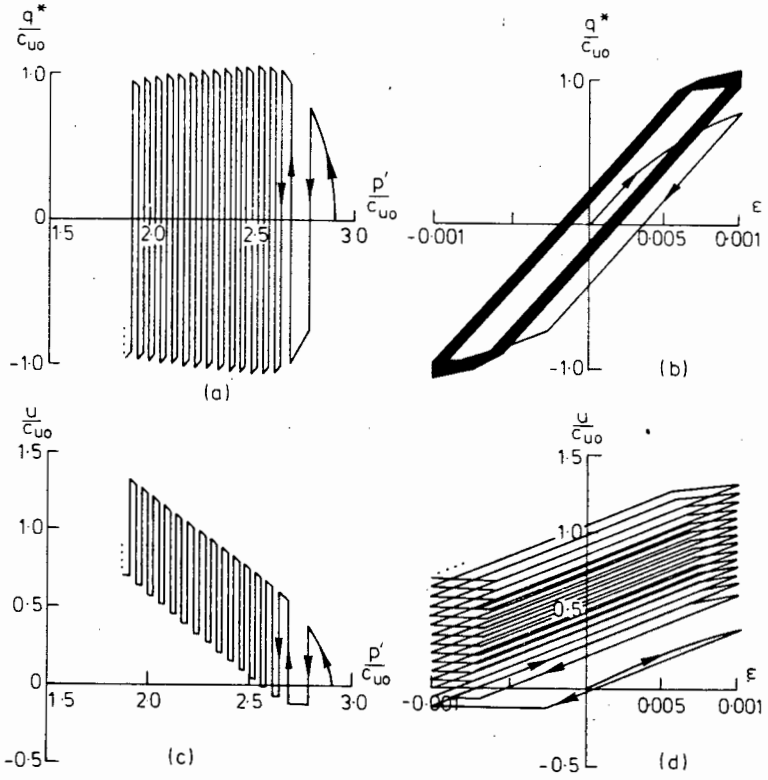

Figure 4.5.2 Undrained, two-way strain controlled loading. (Carter, Booker and Wroth, 1982)

A comparison with results from Taylor and Bacchus (1969) in Figure 4.5.3, shows that the shear strain is underpredicted and volumetric strain overpredicted. This is a consequence of the Modified Cam-clay yield surface and Carter, Booker and Wroth (1982) suggest that a surface similar to Cam-clay may be more appropriate.

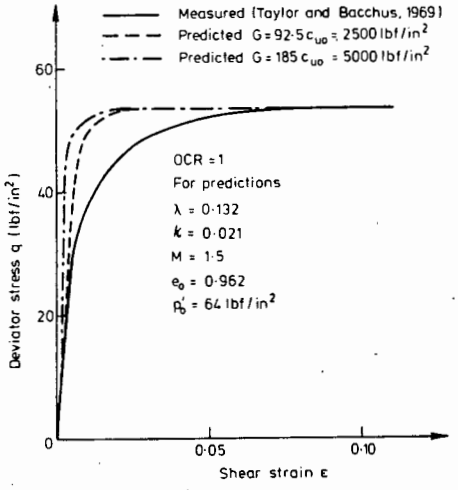

Figure 4.5.3 : Comparison of model predictions and experimental results (Carter, Booker and Wroth, 1982)

The increase in pore pressure is overpredicted especially in the later stages of the test. This leads to failure in fewer cycles than predicted. This model has the advantage of using few parameters, but retains the ability qualitively predict soil response to cyclic loading and will be considered in more detail in Chapter 6.

CHAPTER 5

NUMERICAL IMPLEMENTATION OF CONSTITUTIVE MODELS USING CRISP

5.1 FINITE ELEMENT SOLUTION OF BOUNDARY VALUE PROBLEMS

The creation of a boundary value problem results in a set of differential equations as shown in Section 2.2 . The exact solution to these equations cannot be determined analytically because of the nonlinear constitutive laws, varying loads and the nature of the boundary conditions. A numerical solution technique is required.

The exact solution will be continuous over the whole body. However, in the numerical procedure the continuous solution is represented by a finite set of functions. An error is therefore introduced into the numerical solution which is thus an approximation to the exact solution. The numerical solution converges to the exact solution as the number of terms in the set of approximating functions increases. (Reddy, 1984).

The solution technique used in this thesis is the finite element method (FEM). In engineering, the FEM is used in preference to conventional variational methods because it allows the solution of problems that have complex geometry, discontinuous loading and contain different types of material, all of which are likely to occur in a situation where soil is subjected to cyclic loading.

The problem is divided into subdomains called finite elements of simple geometric shapes. The solution is approximated by interpolation polynomials which are associated with the element in the element formulation. The solution process is therefore independent of the problem, unlike conventional Ritz or Galerkin methods and can be formalised in a computer program.

The interpolation functions are formulated in the local co-ordinates of the element and then are transformed into the global co-ordinates of the problem and assembled into the equilibrium equation.

For each element, the displacements at all points within the element, $\underset{\sim}{u}$ are expressed as functions of the element nodal displacements $\underset{\sim}{a}^{(e)}$

$$\underset{\sim}{u} = \underset{\approx}{N}^{(e)}\underset{\sim}{a}^{(e)} \qquad (5.1.1)$$

where $\underset{\approx}{N}$ is the matrix of the polynomial shape functions, and the superscript (e) denotes element. The derivation is considered standard (Zienkiewicz, 1977; Bathe and Wilson, 1976; Reddy, 1984; Britto and Gunn, 1987) and will not be repeated here.

The compatibility condition (2.2.1) can be written as

$$\underset{\sim}{\epsilon}^{(e)} = \underset{\approx}{B}^{(e)}\underset{\sim}{a}^{(e)} \qquad (5.1.2)$$

The compatibility matrix, $\underset{\approx}{B}$, is also known as the "strain matrix".

The constitutive relation for the element can be defined as :

$$\underset{\sim}{\sigma}^{(e)} = \underset{\approx}{D}^{(e)}\,\underset{\sim}{\epsilon}^{(e)} \qquad (5.1.3)$$

where $\underset{\approx}{D}$ is the constitutive matrix containing appropriate material properties of the element.

Application of the principle of virtual work (Bathe and Wilson, 1977) or a variational formulation based on the Ritz-Galerkin method (Reddy, 1984) then gives the finite element equilibrium equations :

$$\underset{\sim}{Q}(\underset{\sim}{a}) = \underset{\sim}{P} \qquad (5.1.4)$$

where $\underset{\sim}{a}$ is the vector of all global noded displacements and $\underset{\sim}{P}$ the vector of external nodal forces. $\underset{\sim}{Q}(\underset{\sim}{a})$ is thus a vector of internal nodal forces expressed as a function of the nodal displacements. This

equation can be written as the sum of the integrals over the volume ($\int_{vol^{(e)}}$) and surface area ($\int_{area^{(e)}}$) of the contributions of m elements such that :

$$\left\{\sum_{m} \int_{vol^{(e)}} \underset{\approx}{B}^{(e)T}\, \underset{\approx}{D}^{(e)}\, \underset{\approx}{B}^{(e)}\, dvol^{(e)}\right\} \underset{\sim}{a} = \left\{\sum_{m} \int_{vol^{(e)}} \underset{\approx}{N}^{(e)T}\, f^{(e)}\, dvol^{(e)}\right\} + \left\{\sum_{m} \int_{area^{(e)}} \underset{\approx}{N}^{(e)T}\, t^{(e)}\, darea^{(e)}\right\} - \left\{\sum_{m} \int_{vol^{(e)}} \underset{\approx}{B}^{(e)T}\, s^{(e)}\, dvol^{(e)}\right\} \tag{5.1.5}$$

where $\underset{\sim}{f}^{(e)}$ is the element body force vector,

$\underset{\sim}{t}^{(e)}$ is the element surface traction vector,

$\underset{\approx}{s}^{(e)}$ is the vector of initial stresses in the element.

The integration is performed using Gaussian quadrature at specified integration points. The position of the integration points depends on the element type and the interpolation functions.

For a linear elastic material and static loading conditions the equation 5.1.4 is linear and therefore

$$\underset{\sim}{Q}(\underset{\sim}{a}) = \underset{\approx}{K}\, \underset{\sim}{a} = \underset{\sim}{P} \tag{5.1.6}$$

where $\underset{\approx}{K}$ is the global stiffness matrix; i.e. formally,

$$\underset{\approx}{K} = \sum_{m} \int_{vol^{(e)}} \underset{\approx}{B}^{(e)T}\, \underset{\approx e}{D}^{(e)}\, \underset{\approx}{B}^{(e)}\, dvol \tag{5.1.7}$$

with $\underset{\approx e}{D}^{(e)}$ denoting the elastic constitutive matrix for the element.

If the material is elastic-plastic, the equation 5.1.4 is nonlinear and path dependent. The cyclic loading is considered to be a

continuously varying sequence of static loading and therefore $\underset{\sim}{P} = \underset{\sim}{P}(t)$. Although the material is assumed to be time independent, it is convenient to consider equation 5.1.4 as a function of time and use an iterative solution scheme. The equilibrium equation becomes :

$$\underset{\sim}{Q}(\underset{\sim}{a}(t)) = \underset{\sim}{P}(t) \qquad (5.1.8)$$

This is a nonlinear vector equation which can be either solved using a Newton-Raphson technique (Owen and Hinton 1986; Perrego, 1987) or by applying the method of successive approximation (Owen and Hinton, 1986).

Little information is provided in the published literature of constitutive modelling of soils on the numerical implementation of the models. Both Newton-Raphson and successive approximation methods are considered in detail for a bounding surface model by Hermann, Dafalias and De Natale (1982). Further applications of the FEM to soil mechanics are given by Naylor et al (1981).

5.2 NUMERICAL SOLUTION OF NONLINEAR EQUILIBRIUM EQUATIONS

5.2.1 Predictor phase

In the Newton-Raphson procedure, which is the most frequently used iterative scheme, the solution is obtained by dividing the load history into discrete time steps. The equation 5.1.8 for the (n+1)th step with a displacement change $\Delta\underset{\sim}{a}$ and load increment $\Delta\underset{\sim}{P}$, can be expressed as :

$$\underset{\sim}{Q}(\underset{\sim}{a}^n + \Delta\underset{\sim}{a}) - \underset{\sim}{P}^n - \Delta\underset{\sim}{P} = \underset{\sim}{0} \quad . \qquad (5.2.1)$$

This solution technique approximates the solution over the discrete interval and therefore out of balance force $\underset{\sim}{R}^n$ will exist which is the vector of residual loads by which the solution differs from equilibrium at the end of the n-th step. An iteration scheme is necessary which continues until the residual loads are reduced almost to zero for

each increment, hence converging to the exact solution. The (i+1)th iteration of the (n+1)th increment can be shown (Perrego, 1987) to have the form :

$$\left[\frac{\partial \underset{\sim}{Q}}{\partial \underset{\sim}{a}}\right]_{\underset{\sim}{a}^n + {}^{i}\underset{\sim}{\Delta a}} {}^{i+1}\underset{\sim}{\Delta a} = \underset{\sim}{R}^{n+1} \qquad (5.2.2)$$

$$= -\underset{\sim}{Q}(\underset{\sim}{a}^n + {}^{i}\underset{\sim}{\Delta a}) + \underset{\sim}{P}^n + \Delta\underset{\sim}{P} - \underset{\sim}{R}^n$$

This is a linear equation which can be solved using the conventional techniques for linear finite elements (Bathe and Wilson, 1976), which gives the (i+1)th estimate of the displacement increment ${}^{i+1}\underset{\sim}{\Delta a}$.

The matrix $\left[\partial \underset{\sim}{Q} / \partial \underset{\sim}{a}\right]$ is the global tangent stiffness matrix $\underset{\approx}{K}_T$ where :

$$\frac{\partial \underset{\sim}{Q}}{\partial \underset{\sim}{a}} = \underset{\approx}{K}_T = \int_{vol} \underset{\approx}{B}^T \underset{\approx}{D}_{ep} \underset{\approx}{B} \; dvol \qquad (5.2.3)$$

and $\underset{\approx}{D}_{ep}$ is the global elastic-plastic constitutive matrix given by equation (2.3.16) and is thus dependent on the yield surface, plastic strains and hardening parameters. This process of defining the tangent stiffness matrix and solving for the incremental displacement is known as the "predictor stage".

The Newton-Raphson method requires that the stiffness matrix is updated for each iteration. This is expensive in solution time, but results in quadratic convergence. A uniaxial representation of this scheme is given in Figure 5.2.1 .

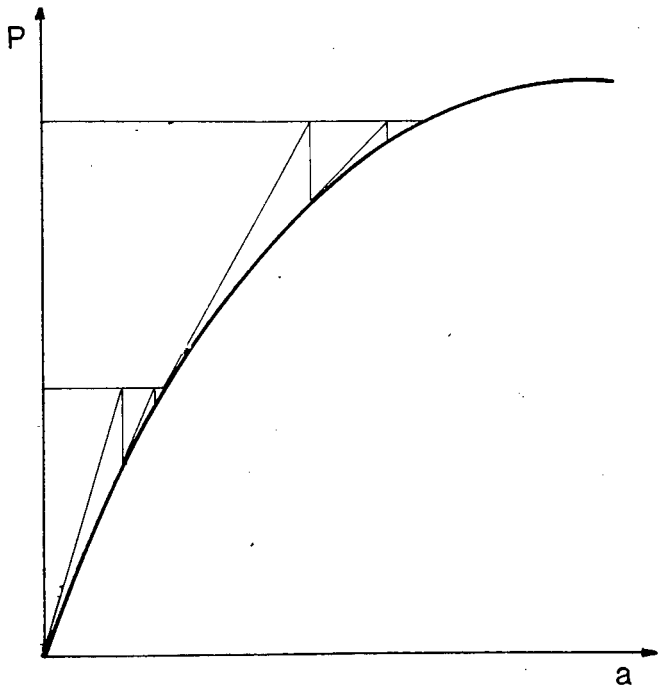

Figure 5.2.1 : Newton-Raphson method for uniaxial stress state.

A saving in solution time can be achieved using the modified Newton-Raphson scheme by only updating the tangent stiffness at the start of each increment and not during the iterations to reduce the residuals (as shown in Figure 5.2.2). The stiffness is only assembled once per increment and resolution schemes are used to solve the equations without reassembling the stiffness matrix. In the above methods the tangent stiffness changes during the solution and they are thus called variable stiffness methods.

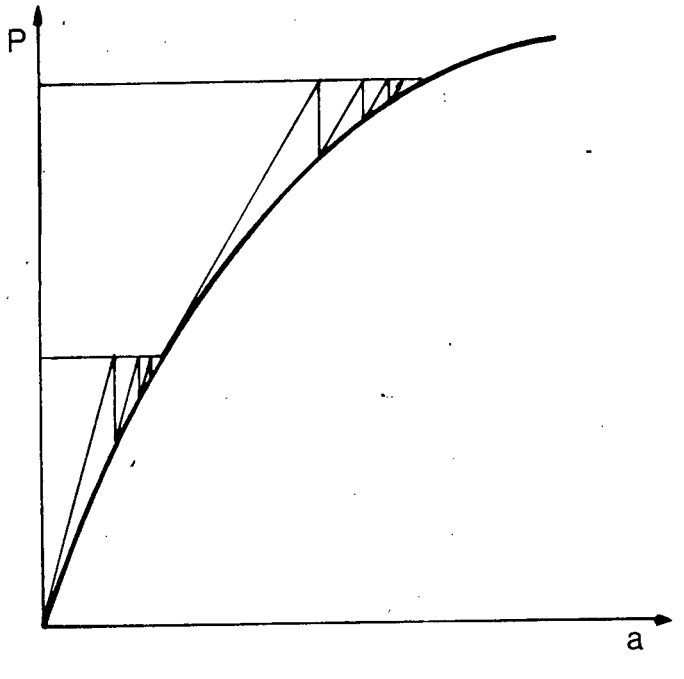

Figure 5.2.2 : Uniaxial representation of modified Newton-Raphson scheme.

In an initial stiffness approach, the stiffness is assembled once, at the beginning of the load history (see Figure 5.2.3). The resolution facility is used for all further increments. This reduces the time per iteration, but increases the convergence time.

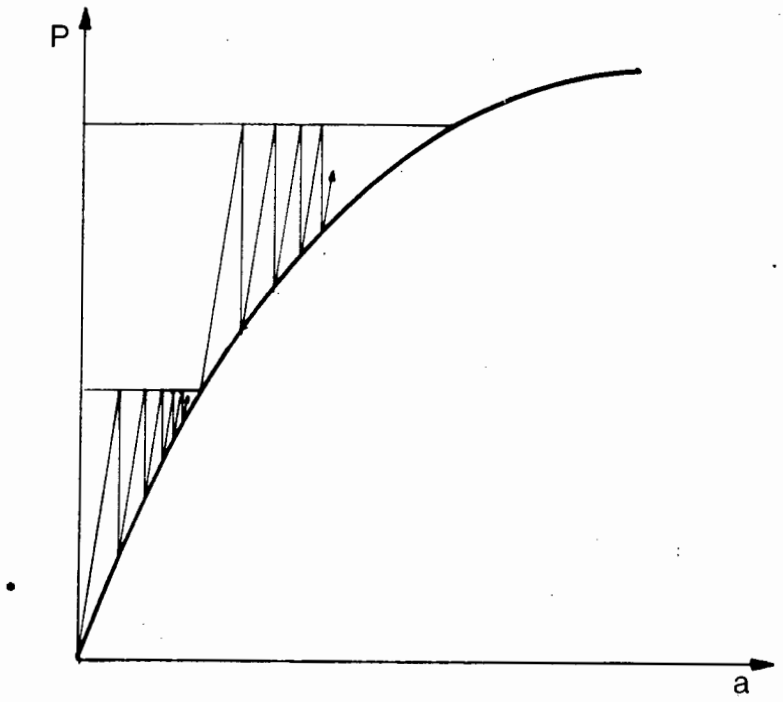

Figure 5.2.3 : Uniaxial representation of initial stiffness approach.

The initial stiffness method is stable and will always converge to the solution. The variable stiffness methods, however, are unstable for unloading, where there is a large change in the stiffness, and for softening behaviour, where the stiffness becomes negative. (Naylor, 1981). Combinations of these techniques where the initial modulus is used for the first iteration following which a new modulus is calculated at the end of the first or second iteration can over-come these problems. (Owen and Hinton, 1986).

5.2.2 Corrector phase

The evaluation of the residual forces $^{i}\underset{\sim}{R}^{n+1}$ in equation (5.1.10) requires the calculation of the internal forces $\underset{\sim}{Q}(\underset{\sim}{a}^{n} + \Delta\underset{\sim}{a})$. This involves the integration of the constitutive law (equation 2.3.15 to give updated values of stress, the hardening parameters and the plastic strains. (Ortiz and Popov, 1985), The iteration scheme therefore alternates between the predictor phase where displacement and total strain increments are calculated and corrector phase where the integration of the constitutive equation is performed. The assumptions

made about the choice of the predictor scheme only affect the convergence of the iterative procedure whereas the integration of the constitutive law affects the accuracy of the solution (Perrego, 1987).

The corrector phase is discussed by Ortiz and Popov (1985), Ortiz and Simo (1986), Perrego (1987) and Ortiz and Martin (1988). During yielding, the predicted values of stress will in general be outside yield surface and must be brought back to the yield surface. The surface is, however, changing as a result of hardening due to the new state and an iterative process is necessary to determine the final stress state. This is known as a return mapping algorithm and is equivalent to integrating the constitutive equation using the midpoint or trapezoidal rules depending on the manner in which the stress is returned to the yield surface (Krieg and Krieg, 1977; Owen and Hinton, 1980; Ortiz and Popov, 1985). However, Ortiz and Simo (1986) note that they are usually restricted to simple models such as the linear hardening von Mises surface with constant elastic moduli for which the yield surfaces change concentrically and a radial return can be applied.

For more complex yield surfaces and nonlinear elastic behaviour the return path must be calculated numerically. Most plasticity models for cyclic loading fall in this category. In particular the critical state based models are complex in terms of plasticity theory and exhibit nonlinear elastic behaviour and harden as a function of the mean pressure rather than the deviatoric plastic strain.

Ortiz and Simo (1986) present a corrector scheme for a Modified Cam-clay type of behaviour with nonlinear elastic, but volumetric response and linear elastic shear behaviour for finite strain analyses.

5.2.3 Determination of pore pressures

Soil is a two phase material and a further complication in the numerical solution is the coupling of the soil and water response in terms of stress governed by the effective stress principle. The development of pore water pressure depends on the drainage conditions in the soil.

For drained situations, the pore pressure is considered to be zero and the total stress equal to the effective stress. The boundary value problem is thus formulated in terms of effective stress, as if the soil were a single phase material.

In undrained conditions, the soil does not experience volume change and thus can be considered as incompressible. A separate, pressure insensitive formulation can be used for undrained conditions which will give the total stress response, but not allow evaluation of pore pressures.

The alternative method of modelling the soil in undrained conditions is to consider the soil as slightly compressible, apply a constraint of no volume change, formulate the constitutive behaviour in effective stress terms and hence calculate the pore pressure by means of the penalty function approach (Zienkiewicz, 1977).

The principle of the penalty method is that the equilibrium equation 5.1.8 is altered to :

$$(\underset{\approx}{K}_1 + \underset{\approx}{K}_2)\ \underset{\sim}{a}(t) \quad = \quad \underset{\sim}{P}(t) \qquad (5.2.4)$$

where $\underset{\approx}{K}_1$ is the stiffness matrix derived from the effective stress constitutive law and the matrix $\underset{\approx}{K}_2$ is defined by the constraint conditions. The components of $\underset{\approx}{K}_2$ in the undrained analysis of soil are the effective bulk modulus K' .

The combined bulk modulus of the soil and water phases, K_u , is represented by the product of the penalty number α and K' . This is a measure of the volumetric stiffness of the pore water the pore water pressure, u , can then be determined using :

$$u \quad = \quad K_u\ \epsilon_{kk} \quad , \qquad (5.2.5)$$

stresses are then computed for each integration point using linear interpolation. An equilibrium check is then performed to determine whether the stresses are in equilibrium with the external loads.

Each change of loading is then specified in an "increment block" which consists of a specified number of increments. This allows for the addition or removal of elements to simulate construction or excavation. The element stiffnesses are removed in the first increment and the resultant load is then spread over the increment block.

The loading can be applied as equivalent nodal loads or as actual pressures and the boundary conditions can be prescribed displacement increments or excess pore pressures.

A large amount of output is produced, including critical state variables when critical state models are used though the amount of data can be controlled to a certain extent using the input options. A personal computer can therefore only be used for very simple analyses because of the limited storage space. No graphical output is provided which makes the data difficult to intepret. The coding for a mesh plot routine is available.

CRISP is written in Fortran 77 with a top down design and pseudo dynamic dimensioning. This, combined with the extensive documentation (Britto and Gunn 1987), allows implementation of new elements, material models and numerical schemes. Fortran 77 is compiler dependent, but no problems were experienced in implementing the program on a PC-xt with Watfor-77 or on the DEC VAX/VMS 6230 with VAX Fortran.

In a finite element analysis, the size of the stiffness matrix, and the nodal displacement and load vectors are problem dependent. The technique of pseudo dynamic dimensioning is used to define all variables and arrays consecutively in a global array. The size of the global array can be changed to fit the computer memory, which becomes the limiting factor in the size of the analysis. Any additional arrays that are required by subsequent programmers can be defined by increasing the size of the global array. A disadvantage of top down

design, however, is that each variable must be passed down to the relevant subroutine through all intermediate subroutines. This results in long argument lists and data structures which are not hidden and which can therefore be accidentally altered. Modifications to the program are simplified because of the strict structuring.

5.3.2 CRISP numerical scheme

CRISP is based on small strain theory though it can be modified to update displacements in an approximation of finite strain theory. The solution technique used is a tangent stiffness method, but without iteration to reduce the residual in the predictor stage and without a corrector phase. This is specifically implemented because of problems with erratic convergence when using iterative procedures with soil models. In geotechnical applications, plastic deformation occurs over large parts of the mesh, in contrast to many structural situations where deformation is localised. The large plastic areas, the highly nonlinear nature of the models, the abrupt changes in stiffness at yield, and the strain softening behaviour of critical state models all lead to numerical instability (Britto and Gunn 1987, Naylor 1981).

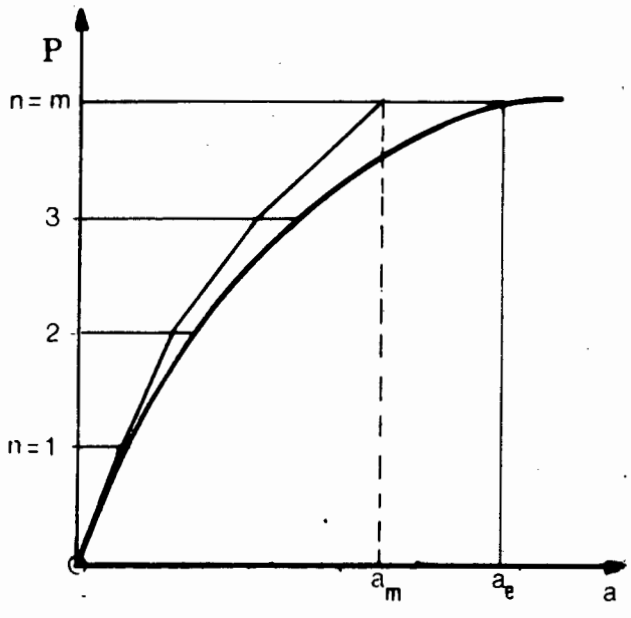

Figure 5.3.1 Schematic of tangent stiffness method without iteration

The solution found by this type of tangent stiffness method therefore always diverges from the exact solution. This can be seen in Figure 5.3.1 which also shows that the calculated solution results in stiffer response with an under-prediction of displacements. Thus, the calculated displacement a_m at iteration n = m is less than the exact displacement a_e. The divergence is measured by determining the residual forces which are the difference between the applied loads and the loads calculated from the stresses at the end of the increment. The percentage error is then found as :

$$[\%]\text{error} = \frac{\int_{\text{area}} \underset{\approx}{N}^{(e)T} \underset{\sim}{t}^{(e)} \overset{(e)}{\text{darea}} + \int_{\text{vol}^{(e)}} \underset{\approx}{N}^{(e)T} \underset{\sim}{f}^{(e)} \overset{(e)}{\text{dvol}} - \int_{\text{vol}^{(e)}} \underset{\sim}{B}^{T(e)} \underset{\sim}{\sigma}^{(e)} \overset{(e)}{\text{dvol}}}{\int_{\text{area}^{(e)}} \underset{\approx}{N}^{(e)T} \, t^{(e)} \overset{(e)}{\text{darea}} + \int_{\text{vol}^{(e)}} \underset{\approx}{N}^{(e)T} \overset{(e)}{\text{dvol}}}$$

The residual can be reduced by decreasing the size of the increments. The solution will converge to the exact solution as the increment size tends to zero. The residuals can be incorporated into the next increment if required. Each increment block that defines a change in load is divided into a number of increments. The increments can be equal or can be specified to have different sizes.

The method is numerically stable and the error in the solution can be controlled by the user. The method has the advantage that it corresponds to a forward Euler integration method in a coupled consolidation analysis.

The equations are solved using a frontal solver program based on Irons (1970). The solver has been modified to cope with varying numbers of degrees of freedom at nodes allowing for mixing of elements within a mesh. The solver assumes that the stiffness matrix is symmetric, which prevents the use of non-associated flow rules in the constitutive models.

The analysis procedure is given schematically in Figure 5.3.2

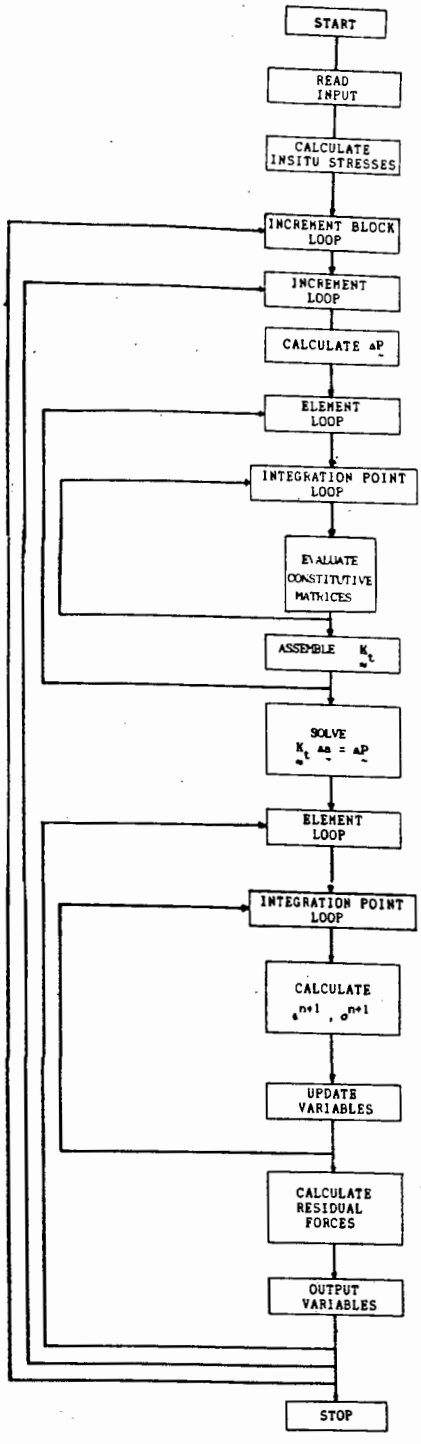

Figure 5.3.2 Nonlinear Finite Element Analysis Procedure in CRISP.

5.4 MODIFICATIONS TO CRISP

5.4.1 Pre-processing program

The specification of the input data for many cycles of loading is time consuming because each loading or unloading stage must be specified as an increment block with the incremental loads including the starting and finishing increment numbers. A pre-processing program was therefore written to save time and eliminate typing errors. This program requires that the mesh and in situ data for a given analysis are placed into a separate data file.

The pre-processor then interactively creates the data for the application of loading in a triangular wave form, either stress or strain controlled, between specified limits and for a specified number of cycles. The load data is appended to mesh data and placed in a word processing package to allow editing of the analysis, title or material parameters. On exiting the word processor, the data is written to the input file for the command procedure which runs the CRSIP program.

The complete analysis is performed in the following steps:

1. Set up mesh and in situ data using wordprocessing package
2. @PRECRISP (Command procedure for pre-processor)
3. @CRISPRUN (Command procedure for FE Package)
4. @POSTCRISP (Command procedure for post-processor)

5.4.2 Post-processing program

Mesh plotting routine

The commercially available version of CRISP produces no graphical output. Graphical output is especially useful in two situations. Firstly, when implementing a finite element mesh, the layout of the mesh with numbered elements and nodes can easily show any inconsistencies in the data input. Secondly, for the comparison of the

results of analyses, it is useful to have plots of the important variables which can easily be obtained graphically on the screen or plotter.

The program documentation (Britto and Gunn 1987) provides the coding for a mesh plotting routine is given, based on "GINO-F", a high level graphics library.

For this research work, the mesh plotting routine had to be re-written in SPOOLTEK, a lower level graphics package, and take account of the different normalization transformation (windowing) techniques of GINO-F and SPOOLTEK. The transformation ensures that an arbitrary sized mesh is transformed into the largest possible size for a laser printer hardcopy. An interactive display routine allows graphical output to be sent to the screen, a plot file or the laser printer.

Improvements to the original routine are that vertex node number internal node numbers and element number symbols are different sizes, but are proportional to the size of the finite element grid. The title of the analysis is read from the input data and plotted above the mesh plot.

Graphical output routine for critical state relationships

The aim of developing this post processing program was that the results of an analysis would be immediately available by specifing the appropriate filename only. The output would be presented diagrammatically with fixed axis dimensions to enable comparison of results and to avoid the need to respecify the axis dimensions. The choice of graph and output device could then be selected interactively.

The graphics are produced using NAG double precision high level graphics routine (NAG, 1985). This was used in preference to the SPOOLTEK graph routines which are less flexible and require that all character variables are stored as binary integers. The available NAG graphics implementation has the disadvantage of using double precision which doubles the memory requirement and hence halves the number of points that can be plotted.

The output from CRISP at the end of each increment, is directed to an ASCII output file. The variables output are:

- increment number (n),
- mean effective stress (p'),
- deviatoric stress (q),
- mean total stress (p),
- hardening parameter (p'_c),
- stress ratio (η), (η/M)
- the specific volume calculated from stress by critical state theory,
- the specific volume calculated from strain (v)
- natural logarithm of mean effective stress (ℓn p')
- the pore pressure (u),
- the axial strain (ϵ_a).

The use of an ASCII output file allows printing of the output file for a summary of the analysis results.

For simplicity, graphical output is produced for one integration point only. Numerical output may be selected at all integration points or at the centroid using the input options. Graphical output can be plotted for the centroid or the integration point closest to the third specified vertex node.

The program produced eight graphs showing the following relationships and are numbered as:

1.	stress plane	(q; p,p')
2.	stress - strain	(q; ϵ_a)
3.	pore pressure - strain	(u; ϵ_a)
4.	specific volume - pressure	(v; p')
5.	specific volume - ln(pressure)	(v; ln(p'))
6.	stress state ratio - strain	(n/m; ϵ_a)
7.	pressure - increment number	(p',p,p'_c,q;n)
8.	strain - increment number	(v, ϵ_a;n)

Using windowing facilities, these are output one per page or four per page as shown in Appendix B. An analysis title is requested interactively and is plotted at the top of each graph alongside the graph title.

In order to show the output within the critical state framework, the projections of the critical state lines and normal consolidation lines are plotted in graphs 1, 4 and 5. The CRISP program was modified to output the critical state parameters to a disk which is read by the graph plotting program. The critical state lines for the relevant model are then calculated and plotted with the finite element analysis output.

5.4.3 Modification of CRISP numerical scheme

To investigate the CRISP numerical scheme a Modified Cam-clay model was used to simulate a triaxial test. By increasing the deviator stress from an isotropic state, followed by loading steps, the stability of the algorithm can be determined.

As shown in Figure 5.4.1(a), at the point of unloading, the stress point followed the yield surface before moving into the elastic zone. When reloaded, the stress path passed through the loading stress path and yielding began at a value equal to the deviator stress prior to unloading. A further yielding then occurred before the next unloading. The correct behaviour where the stress path should be unchanged for elastic cycling is shown in Figure 5.4.1(b).

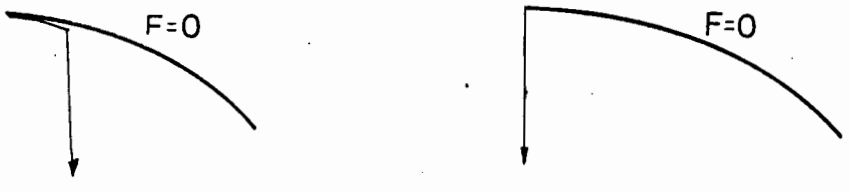

Figure 5.4.1 Unloading from the yield surface
(a) actual behaviour
(b) expected behaviour.

The behaviour results from the CRISP tangent stiffness algorithm. The tangent stiffness matrix is a function of the stress at the beginning of the increment and, therefore, when unloading from a plastic state, an elastic -plastic tangent stiffness matrix is calculated for the increment. At the end of the increment, the stress point is in an elastic state and therefore elastic unloading occurs subsequently.

These numerical difficulties can be solved by a combined stiffness algorithm (Owen and Hinton, 1986). An iteration for each increment is required and the stiffness in the initial iteration is always considered to be elastic and the stiffness in the following iterations is dependent on whether the stress state is elastic or plastic.

The procedure should be applied for every increment to account for random loading and unloading, but the increment block system in CRSIP implies that the direction of loading will only change at the beginning of an increment block. Thus, the first increment of the block is the only increment that requires a combined algorithm.

The algorithm is illustrated in the flowchart of Figure 5.4.2. The initial tangent stiffness is forced to be elastic. A loop at the integration point level determines whether the stress state at the end of the increment will be plastic or elastic. If the final state is elastic, the stresses will be updated and the analysis will proceed to the next increment. If, however, any of the integration points is in a plastic state, the stresses are not updated. The program will then return to the start of the increment block and the stiffness matrix will be recalculated, the relevant integration point being considered as in a plastic state of stress.

The check of the stress state at each integration point involves additional branches at element integration point and care must be taken to avoid inadvertently updating variables or prematurely branching out of a loop.

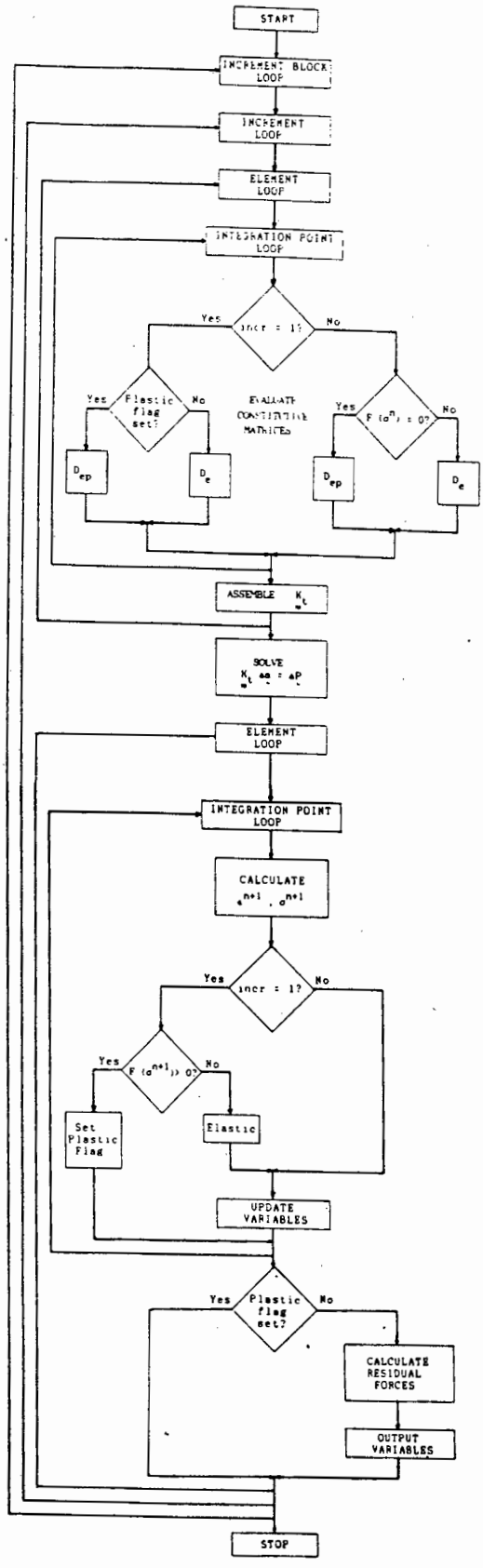

Figure 5.4.2 Flow chart of combined stiffness algorithm.

The results of the modified algorithm can be seen in Figure 5.4.3(a) where after 10 cycles of unloading and reloading there is no change in the stress path. This is confirmed in Figure 5.4.3(b) where it can be seen that no change in the hardening parameter has occurred due to the elastic cyclic loading in the elastic region.

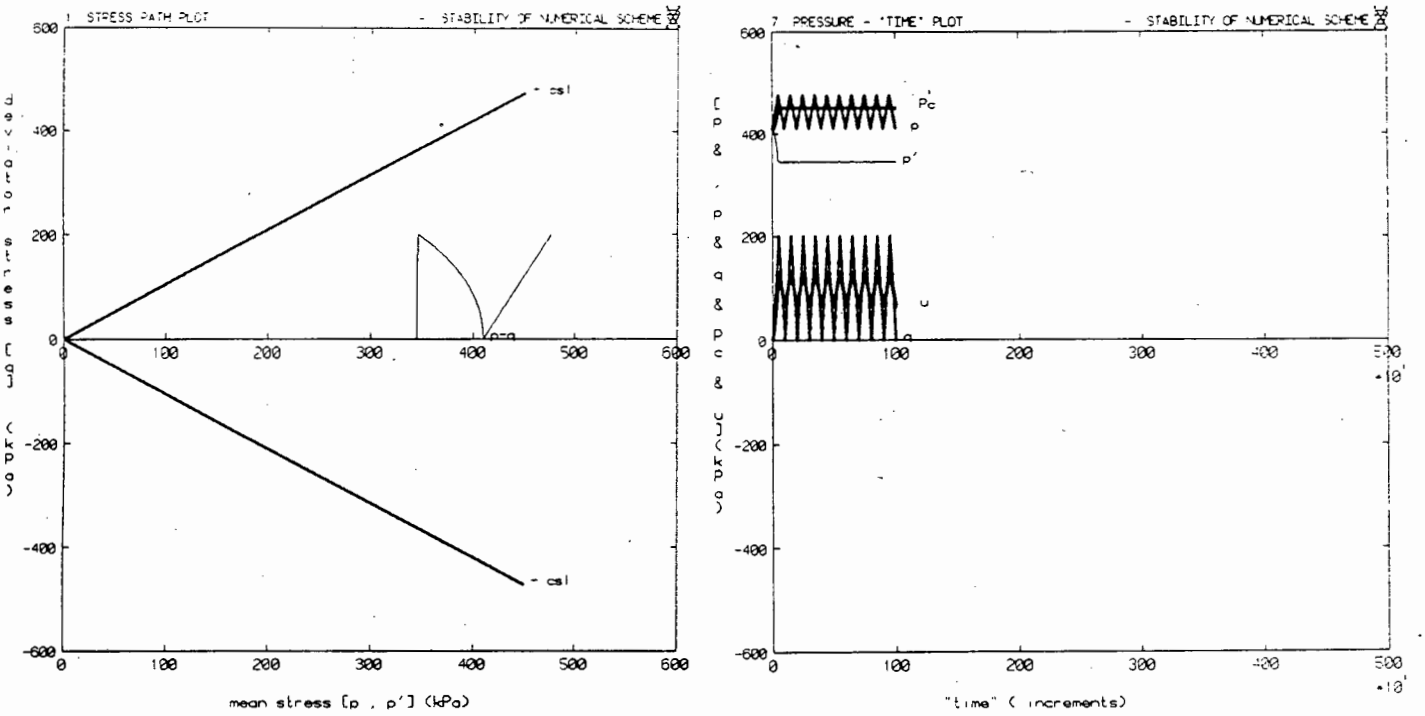

(a) (b)

Figure 5.4.3 Stability of combined algorithm for elastic unloading and reloading
(a) effective stress path
(b) hardening parameter.

Two further areas of concern are the convergence and the accuracy of the tangent stiffness algorithm. The use of a predictor phase without iterations to reduce the out-of-balance residuals affects the convergence and the lack of corrector phase to reduce the stress state to the yield surface.

The former problem can be solved in three ways. Firstly the most rigorous solution is to introduce a modified Newton Raphson algorithm (as described in Section 5.2.1). An attempt at introducing a resolution facility was made, but was not successful due to the lack of adequate documentation on the frontal solver routine in CRISP. Re-writing the solver was considered to be out of the scope of the thesis and the other two methods of reducing the out-of-balance residuals were investigated.

The second approach is to introduce the residuals into the next increment as an out-of-balance load (Naylor, 1981). The facility for this exists in CRISP, but, because the pore pressure is calculated using the penalty approach (see Section 5.2.3), the transferral of load from one increment to the next causes the pore pressure to be out of phase with the loading and large oscillations in the pore pressure and total stress response occur.

The third method is to reduce the increment size thus causing the numerical solutions to converge. The size of increment required is a function of the maximum applied load, the finite element mesh and the constitutive law.

The convergence is discussed in Section 6.3. A corrector was not implemented because of the problems caused by the nonlinear elasticity and the non-radial return method that would be required (as mentioned in Section 5.2.2). The reduction of the increment size decreases the inaccuracy. The finite element analyst should be aware of these limitations and approximations in the numerical scheme and take account for them in the evaluation of the results of the analysis.

CHAPTER 6

DEVELOPMENT AND IMPLEMENTATION OF THE MODEL FOR CYCLIC LOADING

6.1 DERIVATION OF MODEL

The constitutive model that was formulated is based on the empirical plasticity model of Carter, Booker and Wroth (1982) and was developed to include the Cam-clay as well as the Modified Cam-clay surfaces. Below the yield surface, the material behaviour was represented by a variable moduli form of elasticity.

The reasons for the choice of this constitutive law are that it is based on the critical state theory, which, as shown in the previous chapters, provides a sound basis for the representation of clay behaviour under static and cyclic loading, and has parameters that can be determined relatively easily. The modifications to account for cyclic behaviour require only a single additional parameter which can be determined using the available cyclic triaxial test device.

The physical interpretation of the parameter θ can be seen by considering the effect that the cyclic loading has on the stable state boundary surface (SSBS) and the critical state line. The material will unload from the yield surface into the elastic region, but on reloading the soil yields before the previous yield stress has been reached. In the context of plasticity theory, yielding can only occur when the stress point reaches a yield surface. The previous yield surface must therefore have been reduced as a consequence of the elastic unloading. In critical state theory, yielding may only occur along the stable state boundary surface and must occur at a constant specific volume in undrained conditions. This implies that the SSBS has, in fact, translated to allow the premature yielding to occur on reloading. The translated state surface intersects the isotropic plane on a line parallel to the normal consolidation line (NCL) as shown in Figure 6.1.1.

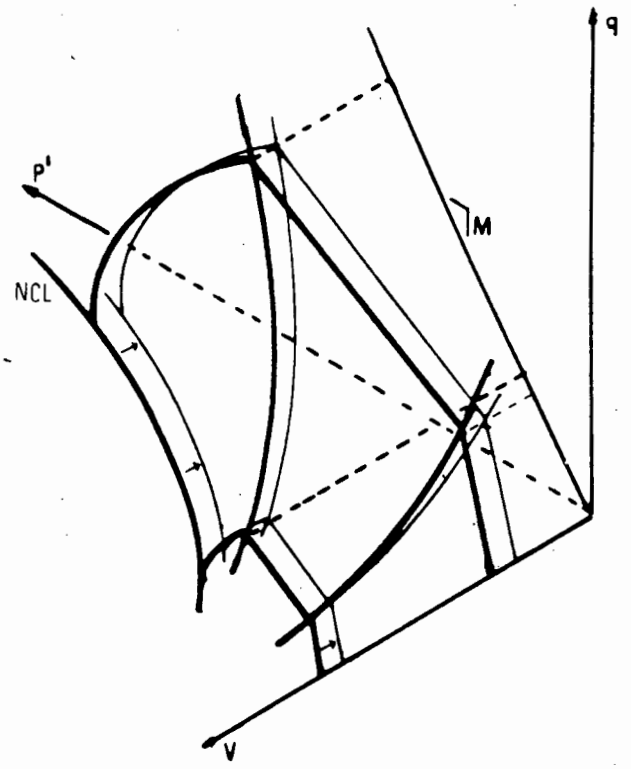

Figure 6.1.1 : Schematic of translation of state surface due to unloading (after Atkinson and Bransby, 1978).

As discussed in Section 4.1.2, this translation of the SSBS has been observed in laboratory tests, but does not affect the failure criterion which is the straight line projection of the critical state line in the p',q plane as shown in Figure 6.1.1. The parameter θ is a measure of the translation of the yield surface and will be defined explicitly later. Under continuous cyclic loading in undrained conditions, the constant translation of the yield surface will result in the stress state reaching the critical state line at a deviatoric stress much lower than the failure stress q_f. A degradation in the material strength has occured.

The derivation of the model is essentially the same for the Cam-clay and Modified Cam-clay yield surfaces. For monotonic loading, the conventional elastic-plastic constitutive laws apply. The elastic-plastic matrix D^{ep} is calculated from equation (2.3.16) and the normality rule is applied to the yield conditions (3.2.15) and (3.2.11). Thus the yield loci take the form :

for Cam-Clay :

$$F \equiv Q = M\, p' \ln\left(\frac{p_c'}{p'}\right) - q = 0 \qquad (6.1.1)$$

and for Modified Cam-clay :

$$F \equiv Q = M\, p'^2 - p' p_c' M^2 + q^2 = 0 \qquad (6.1.2)$$

where p_c' is the hardening parameter.

The current loading stress point is defined by a loading surface which is of similar shape to the yield surface. The loading surface intersects the isotropic axis at the point p_y' which is related to the yield surface hardening parameter p_c' as shown in Figure 6.1.2.

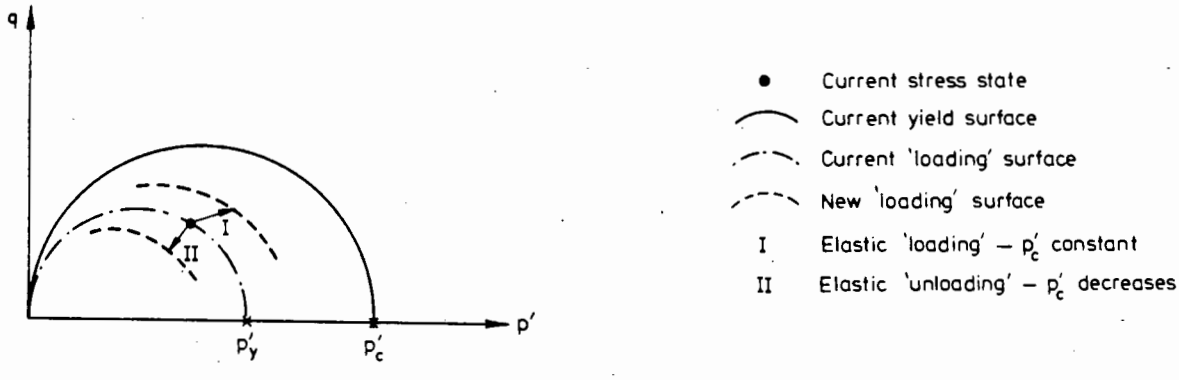

Figure 6.1.2 Schematic representation of yield and loading surfaces in p', q diagram.

The equation for p_y' can be obtained by rearranging the yield surface equations (6.1.1) and (6.1.2) and substituting p_y' for p_c'. The loading surface in terms of p_c' for Cam-clay is thus :

$$p_y' = p' \exp\left(\frac{q}{M\, p'}\right) \qquad (6.1.3)$$

and for Modified Cam-clay is :

$$p_y' = p' + \frac{q^2}{p' M^2} \qquad (6.1.4)$$

The difference between p_y' and p_c' defines the loading state of the soil.

For elastic loading :

$$p_y' < p_c' \quad \text{and} \quad dp_c' = 0 \quad , \quad dp_y' > 0 \qquad (6.1.5)$$

for hardening :

$$p_y' = p_c' \quad \text{and} \quad \frac{d\, p_c'}{p_c'} = \frac{d\, p_y'}{p_y'} \quad , dp_c' = dp_y' > 0 \qquad (6.1.6)$$

for softening :

$$p_y' = p_c' \quad \text{and} \quad \frac{d\, p_c'}{p_c'} = \frac{d\, p_y'}{p_y'} \quad , dp_c' = dp_y' < 0 \qquad (6.1.7)$$

for elastic unloading :

$$p_y' < p_c' \quad , \quad dp_c' = 0 \quad , \quad dp_y' < 0 \quad . \qquad (6.1.8)$$

The assumption that the yield surface is reduced on unloading implies a decrease in the hardening parameter p_c' .The actual mechanism is complex and cannot be determined until sufficient test data is available .The yield surface is assumed to decrease in proportion to the change in the loading surface thus :

$$\frac{dp_c'}{p_c'} = \theta \frac{dp_y'}{p_y'} \qquad (6.1.9)$$

where $0 \leq \theta \leq 1$. (6.1.10)

The degradation parameter θ is therefore a property of the soil which must be determined experimentally. For $\theta = 0$ no reduction in the yield surface occurs and for $\theta = 1$ the yield surface reduces along with the loading surface.

The modification is then introduced into the incremental solution scheme. At the n-th step, the hardening parameter $p_c'^{\,n}$ is known and the loading parameter $p_y'^{\,n}$ can be calculated from equations (6.1.3) and (6.1.4) for Cam-clay and Modified Cam-clay, respectively. Each of $p_c'^{\,n}$ and $p_y'^{\,n}$ are therefore a function of the stress $\underset{\sim}{\sigma}^n$ at the beginning of the increment, n. The numerical scheme (described in Section 5.3.2) provides updated stresses, $\underset{\sim}{\sigma}^{n+1}$ and strains, $\underset{\sim}{\epsilon}^{n+1}$ at the end of the n-th step, and hence updated values of the hardening parameter, $p_c'^{\,n+1}$ and loading parameter, $p_y'^{\,n+1}$ are calculated.

A sequence of conditional branches checks the conditions (of equations 6.1.5 to 6.1.8) to determine the change in the stress state over the increment. The condition (6.1.8) for unloading occurs when :

$$p_c'^{\,n+1} = p_c'^{\,n} \quad \text{and} \quad p_y'^{\,n+1} < p_y'^{\,n} \tag{6.1.11}$$

and therefore

$$dp_y' = p_y'^{\,n+1} - p_y'^{\,n} < 0 \tag{6.1.12}$$

By rearranging (6.1.9), the reduced value of the hardening parameter $p_c'^{\,n+1}$ is obtained as :

$$p_c'^{\,n+1} = p_c'^{\,n} + \frac{\theta \left(p_y'^{\,n+1} - p_y'^{\,n} \right) \cdot p_c'^{\,n}}{p_y'^{\,n}} \tag{6.1.13}$$

The values of the stresses, both $\underset{\sim}{\sigma}^{\,n}$ and $\underset{\sim}{\sigma}^{\,n+1}$, are needed at the end of the increment in contrast to conventional plasticity implementations.

On reloading, the stress point will meet the reduced yield surface and therefore yield at a deviator stress, lower than the unloading stress. The additional yielding that occurs due to the reduction in the yield surface results in an accumulation of plastic strain. This is an idealisation of the soil behaviour for which plastic strain will accumulate over the whole reloading section of the hysteresis curve. The translation of the state surface is therefore dependent on the amount of yielding that occurs and hence on the increment size of the incremental solution scheme. The convergence of the scheme is discussed in Chapter 8.

6.2 DETERMINATION OF THE DEGRADATION PARAMETER θ

Carter, Booker and Wroth (1982) give two methods of determining the parameter θ (as discussed in Section 4.5.2) - either from the observations of a cycle of isotropic consolidation and reloading or from a relationship between θ and the number of cycles to failure, N_f.

The first method has the problem that one cycle may not be representative of the behaviour of the soil over many cycles. In the second method, the number of cycles to failure, N_f is a function of the model parameters (λ, κ, M, Γ, θ), the initial state (p', q, v) and the applied cyclic stress q_c . To produce a graph of θ versus $\log(N_f)$ requires simulation of the cyclic triaxial test situation for the given parameters, varying the applied stress, the initial state and the degradation parameter, θ . The value θ relevant to the test situation can then be determined by simple interpolation between the magnitudes of θ used in the simulation as shown in Figure 6.2.1.

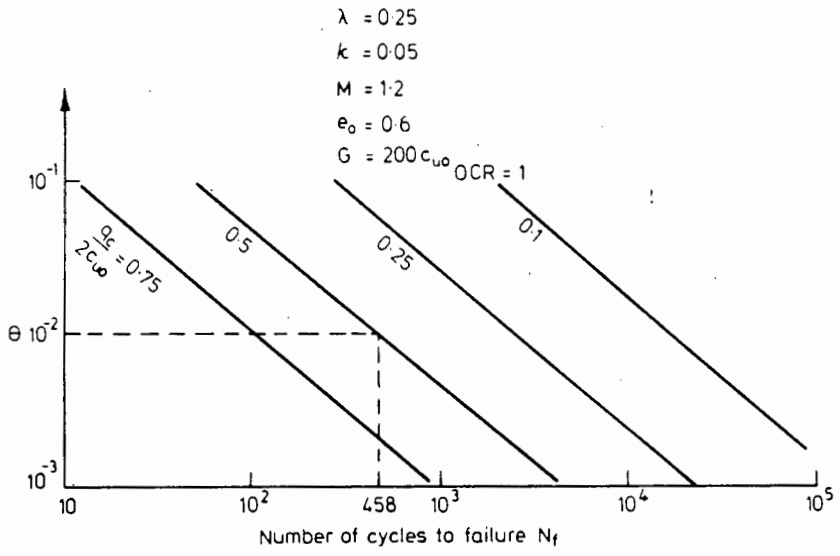

Figure 6.2.1 : Determination of parameter θ from graph of θ versus $\log(N_f)$ (Carter, Booker and Wroth, 1982)

The material parameters of a model should be obtained directly from the laboratory test data and thus the degradation parameter should not have to be evaluated from the results of many finite element back predictions of triaxial tests as required in the method described above.

As an alternative, a method for determining θ from cyclic triaxial tests was developed. This was achieved by considering the model behaviour in relation to the v_λ - η graph (Schofield and Wroth, 1969) from which the static critical state parameters (Γ, N and M) are derived (See Section 3.3).

In the v_λ - η diagram for the static case, the state surface can be transformed into a line interrupting the v_λ axis at N (the specific volume of the normal consolidation line for $p' = 1{,}0$) and ending at failure at the point ($v_\lambda = \Gamma$, $\eta = M$). This line defines yielding, and any point below the line is in an elastic state. A translated surface will therefore become a line parallel to the original static line with an intercept N' that defines the new consolidation line on the isotropic plane. This is shown in Figure 6.2.2(a) for Cam-clay which, applying equations, plots as a straight line with slope $M/(\lambda - \kappa)$. The appropriate Modified Cam-clay surface is transformed into a curve, obtained from equation 3.2.16 as indicated in Figure 6.2.2(b).

a)

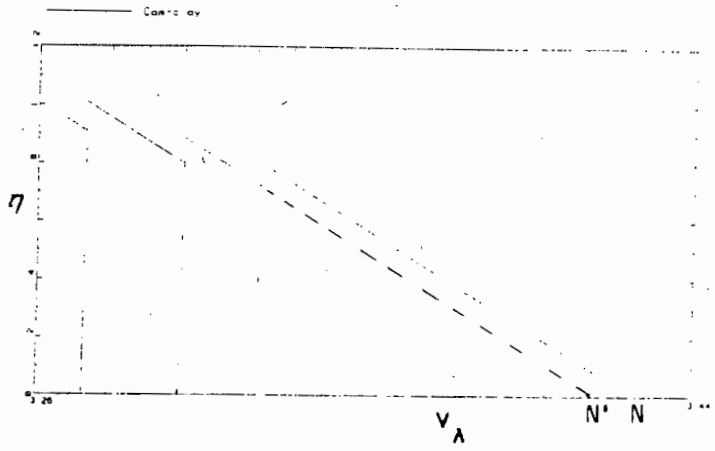

b)

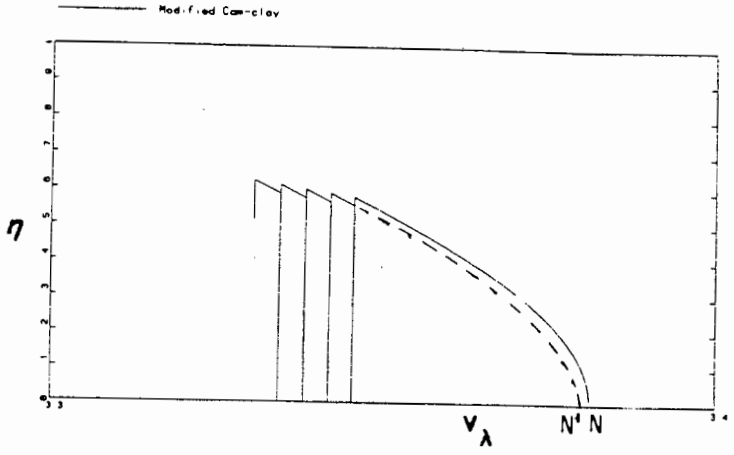

Figure 6.2.2 v_λ - η diagrams for cyclic loading
(a) Cam-clay model (b) Modified Cam-clay model

The change in v_λ for any cycle between consecutive unloading points i and i + 1, due to the unloading and reloading is the horizontal distance between the two lines, $\Delta v_\lambda^{\,i+1}$. (Note the distinctions between i - the cycle number, n - the increment number used in Section 6.1, and N_f - the cycle number at failure.). Thus for example :

$$\Delta v_\lambda^{\,1} = N - N^1 \qquad (6.2.1)$$

Since the gradient of the normal consolidation line is λ, ie

$$\frac{\Delta v_\lambda}{\Delta \ell n \; p_c'} = \lambda \qquad (6.2.2)$$

then $$(\Delta \ell n \; p_c') = \frac{\Delta v_\lambda^{\,i+1}}{\lambda} \qquad (6.2.3)$$

Note the change in hardening parameter, p'_c can be written as :

$$\ell n\, p'_c{}^{\,i+1} = p'_c - \frac{\Delta \hat{v}_\lambda{}^{i+1}}{\lambda} \qquad (6.2.4)$$

and thus :

$$\Delta p'_c = p'_c{}^{\,i} - \exp\left(\ell n\, p'_c{}^{\,i} - \frac{\Delta v_\lambda{}^{i+1}}{\lambda}\right) \qquad (6.2.5)$$

The stress states at the beginning of unloading (p'_a , q'_a) and the end of unloading are obtained from the test data as shown schematically in Figure 6.2.3. The values of $p'_c{}^{\,i}$ and $p'_y{}^{\,i}$ are equal since the unloading occurs from the yield surface. From the yield surface equations at (p'_a , q_a) :

For Cam-clay :

$$p'_c{}^{\,i} = p'_y{}^{\,i} = p'_a \exp\left(\frac{q_a}{M\, p'_a}\right) \qquad (6.2.6)$$

and at the end of unloading, the stress state is (p'_e , q_e) as in Figure 6.2.3 and therefore :

and $$p'_y{}^{\,i+1} = p'_e{}^{\,i} \exp\left(\frac{q_e}{M\, p'_e}\right) \qquad (6.2.7)$$

and for Modified Cam-clay :

$$p'_c{}^{\,i} = p'_y{}^{\,i} = p'_a + \left(\frac{q_a^2}{p'_a\, M^2}\right) \qquad (6.2.8)$$

and

$$p'_y{}^{\,i+1} = p'_e + \left(\frac{q_e^2}{p'_e\, M^2}\right) \qquad (6.2.9)$$

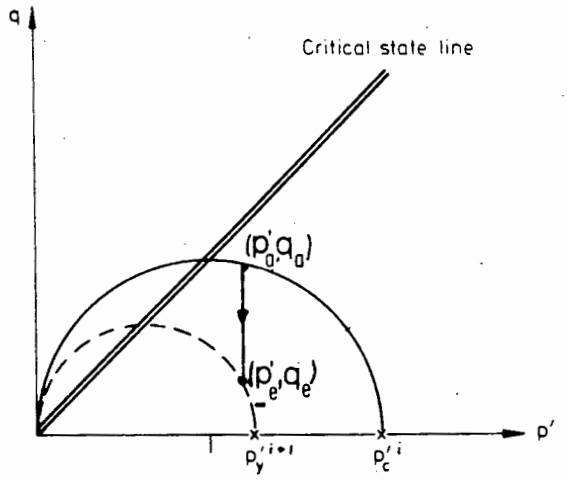

Figure 6.2.3 Loading and yield surfaces at the end of unloading.

The change in p'_y is thus

$$\Delta p'_y = p_y{}^{i+1} - p_y{}^{i} \qquad (6.2.10)$$

and from equations (6.2.5) and (6.2.10) and according to equation (6.1.9), the degradation parameter θ is obtained as :

$$\theta = \frac{\Delta\, p'_c}{\Delta\, p'_y} \quad .$$

The material will not in general exhibit purely elastic behaviour and as an idealisation of the hysteresis curve, it is convienient to consider the pressure at the end of unloading , p'_e to equal the pressure at the start of unloading, p'_a. This procedure can be easily programmed. The parameter θ is assumed to remain constant in the model implementation, but it is unlikely the test data will result in values of θ that are constant throughout the duration of the loading. The most appropriate magnitude of θ for a particular problem can be selected from a graph of θ versus the cycle number i.

6.3 APPLICATION OF THE CONSTITUTIVE MODEL FOR THE BACK PREDICTION OF TRIAXIAL TESTS

6.3.1 Finite element mesh

A conventional assessment of the effectiveness of a constitutive model is the simulation of the material behaviour in a standard laboratory test. In the following investigation, the finite element approach will be used to model the sample.

A finite element representation of a cylindrical triaxial test specimen was created using various mesh configurations which will be discussed later. The sample was modelled with an axisymmetric element formulation with height to diameter ratios of 1:1 and 2:1. The boundary conditions applied, constrain the centre line to be fixed in the horizontal (x) direction and free in the vertical (y) direction and the base was free in the x direction and fixed in the y direction. This is equivalent to a quarter of the sample with free end platens in the test apparatus. An initial confining pressure was applied to the two free sides. The top end of the sample was loaded in either stress or displacement increments and Figure 6.3.1 shows a schematic of the finite element representation of the triaxial test sample with the applied boundary conditions and loading.

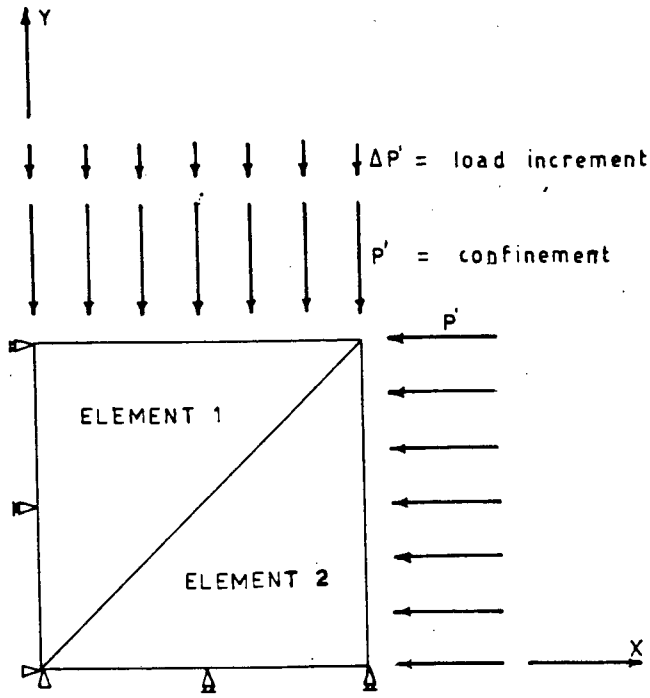

Figure 6.3.1 The Axisymmetric Finite Element Mesh for a Triaxial Sample.

As discussed in Chapter 5, the finite element analysis is a discretization of the equations of equilibrium and is therefore an approximation to the true solution. The finite element solution converges to the exact solution as the number of elements in the mesh and the order of the polynomial interpolation functions increase. The nonlinear solution technique will tend to converge as the increment size decreases. The convergence is a function of the mesh configuration and the constitutive model. The finite element analysis must preferably be benchmarked against a known solution, to compare the numerical solution with a known result.

The original critical state theory was formulated for an axisymmetric soil "element" and an analytical solution can be derived for the undrained effective stress path of a conventional triaxial compression test (Britto and Gunn, 1987). For Modified Cam-clay normally consolidated to a confining pressure p'_o , the equation is obtained from equations (3.1.10) and (3.2.16) and is thus

$$q^2 = (M\,p')^2 \left[\left(\frac{p'}{p'_o} \right)^{\left(\frac{-\lambda}{\lambda-\kappa} \right)} - 1 \right] \qquad (6.3.1)$$

which gives the value of q for a given p' or can be solved iteratively for p' given a value of q .

The finite element analysis of an undrained triaxial test was performed for both the Cam-clay and Modified Cam-clay models. Graphical output from the post-processing program is presented in Appendix B1 for the Cam-clay model and Appendix B2 for the Modified Cam-clay model. The following benchmarking study and discussion is based on the Modified Cam-clay model only. The convergence of the numerical scheme is observed by comparing the stress and strain magnitudes when the deviator stress reaches a selected level (200 kPa in the folllowing examples). The critical state parameters used in the benchmarking study were:

$$\lambda = 0{,}1 \quad , \quad \kappa = 0{,}04 \quad , \quad M = 1{,}05 \; .$$

These correspond approximately to the parameters for Kaolin derived in Section 8.1 The differences in magnitude do not affect the trends in the model predictions.

In Table 6.3.1 the results of the analysis to compare effects of different element types and configurations are listed, and plots of the meshes are given in Appendix A. The mesh configurations used were :

four cubic strain triangles (CuST),
two cubic strain triangles (CuST),
two linear strain triangles (LST).

The effect of increasing the number and order of the elements is negligible. The four element CuST mesh achieves a 0,1 kPa increase in the prediction of p' against the other two mesh arrangements, which show almost the same strain.

TABLE 6.3.1: Effect of mesh configuration on the effective stress path in undrained conditions.

Element type	No of elements	D.O.F. (-)	p' (kP_a)	q (kP_a)	ϵ_a (%)	CPU (s)	α [-]
CuST	4	90	340,09	200,00	1,0525	355	200
CuST	2	50	340,10	200,00	1,0521	193	200
LST	2	18	340,10	200,00	1,0518	65	200

A cyclic analysis can potentially involve thousands of cycles of loading and therefore minimising solution time is essential. Accuracy and solution time requirements are in contradiction and a compromise should be achieved between fewer lower order elements for the purpose of saving time and more higher order elements to increase the accuracy. In this analysis, it was decided to use the 2 LST element mesh because the negligible increase in accuracy did not warrant the substantial increase in computer time required (as listed in Table 6.3.1). Thus, approximately 100 cycles per hour CPU time can be analysed as opposed to 40 cycles per hour CPU time employing the for 2 CuST elements and 20 using 4 CuST elements,respectively.

The effect of changing the sample size in length and diameter and the aspect ratio was found to result in identical stresses p' and q, as well as strain ϵ_a as shown in Table 6.3.2.

TABLE 6.3.2: Effect of sample size - on the effective stress path in undrained conditions.

Length (mm)	Diameter (mm)	Aspect-ratio	P' (kP_a)	q (kP_a)	ε_a (%)	α (-)
75	35	2:1	340,77	200,00	1,0549	65
35	35	1:1	340,77	200,00	1,0549	65
200	100	2:1	340,77	200,00	1,0549	65

Once the mesh configuration has been chosen, the convergence of the numerical scheme can be evaluated. In CRISP, the tangent algorithm causes the numerical results to diverge from the exact solution as described in Section 5.3.2, but the numerical solutions converge as the increment size decreases.

In the analysis of an undrained test, the loading is specified in terms of total stress and the accuracy of the effective stress path is affected by two aspects. Firstly, the size of the deviator stress increment affects the solution as shown in Figure 6.3.1. The difference in mean effective stress p' between the analytical solution and the results of the finite element analysis increases as the deviator stresses and the step size increase. The magnitude of the variance, at a deviator stress of 200 kPa, can be seen in Table 6.3.3. The combination of the path dependence of the plasticity theory and the finite element formulation results in the decrease of strain with increasing step size, an underprediction of the strain results.

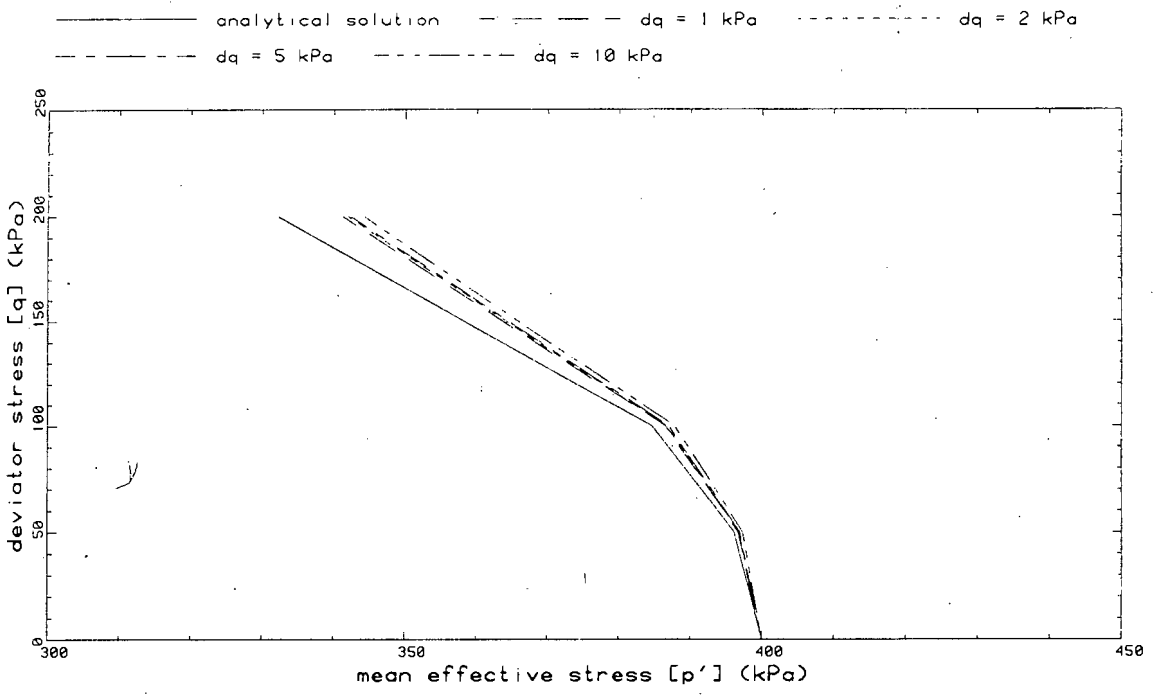

Figure 6.3.2 Effect of the increment size on the convergence of the numerical scheme

TABLE 6.3.3: Effect of increment size on effective stress path in undrained conditions.

Stress Increment dq (kPa)	q (kPa)	dq/q	p' (kPa)	p (kPa)	ϵ_a (%)	α (-)
1	200,00	200	340,77	466,67	1,0549	65
2	200,00	100	341,14	466,67	1,0504	65
4	200,00	50	341,89	466,67	1,0414	65
10	200,00	20	344,10	466,67	1,0162	65

Secondly, the pore pressure penalty function which is described in Section 5.2.3 controls the divergence from the analytical solution in similar manner. An increase in the penalty number, α ,which is the ratio of the undrained bulk modulus K_u to the effective bulk modulus K' , causes an increase in the pore pressure and a corresponding decrease in the divergence of the effective stress path obtained from the analytical solution. This effect is shown in Table 6.3.4 where an increase in α causes a decrease in p' which leads to the analytical value. As the value of α increased, the undrained soil becomes incompressible leading to the ill-conditioning of the finite element formulation (as explained in Section 5.3.2). This results in erroneous values for $\alpha > 1000$ where the sum of p' and u do not equal the total stress p . A value of $\alpha = 200$ was used in the analysis.

TABLE 6.3.4 Effect of Penalty Number α on the effective stress path stress path in undrained conditions.

Penalty No α	p' (kP_a)	q (kP_a)	p (kP_a)	u (kP_a)	ϵ_a (%)
65	340,77	200,00	466,66	125,90	1,0549
200	340,10	200,00	466,66	126,57	1,0518
500	339,91	200,00	466,66	126,77	1,0508
1000	338,85	200,00	466,66	126,84	1,0505
10000	339,94	200,00	466,57	127,31	1,0477
analytical solution	339,39	200,00	466,66	—	—

The cyclic behaviour of the model for normally consolidated clay was studied by representing the triaxial test specimen in a mesh with two linear strain elements. The confining pressure was set at 400 kPa and no backpressure was applied. Material parameters representative of a typical clay were derived from laboratory work by Wilson (1984). The loading and unloading of the sample was performed linearly, following a triangular waveform. The loading input data is created in the preprocessing program as described in Section 5.4.1.

The graphical output from the preprocessor is presented in Appendix B3. Two pages containing graphs numbered 1 to 8 are given for each analysis. A comparison of the predictions of the Cam-clay model (Appendix B3.1) and the Modified Cam-clay model (Appendix B3.2) proves that the trends in behaviour are similar, although the stress and strain magnitudes differ due to the alternative yield surface formulations. The effective stress paths show the characteristic log-spiral and elliptical shapes, respectively. The results of the analyses using Modified Cam-clay, for a single level of cyclic stress or strain are presented in the Appendices B3. Parameter studies carried out to determine the effect of changing the cyclic stress q_c and strain ϵ_c are discussed in the following sections.

6.3.2 Predictions for one-way stress controlled loading

The post-processor output for the case of one-way stress controlled loading of Modified Cam-clay, is shown in Appendix B3.2 for a cyclic stress application q_c of 200 kPa.

The first graph in Appendix B3.2 shows the migration in the effective stress path due to the cyclic loading. The initial decrease in p' is due to the initial monotonic loading to the cyclic stress level q_c. The elastic unloading and reloading shows a negligible change in mean effective stress p'. Modelling of the decrease in p' , associated with the migration of the effective stress path is achieved in the plastic reloading stage.

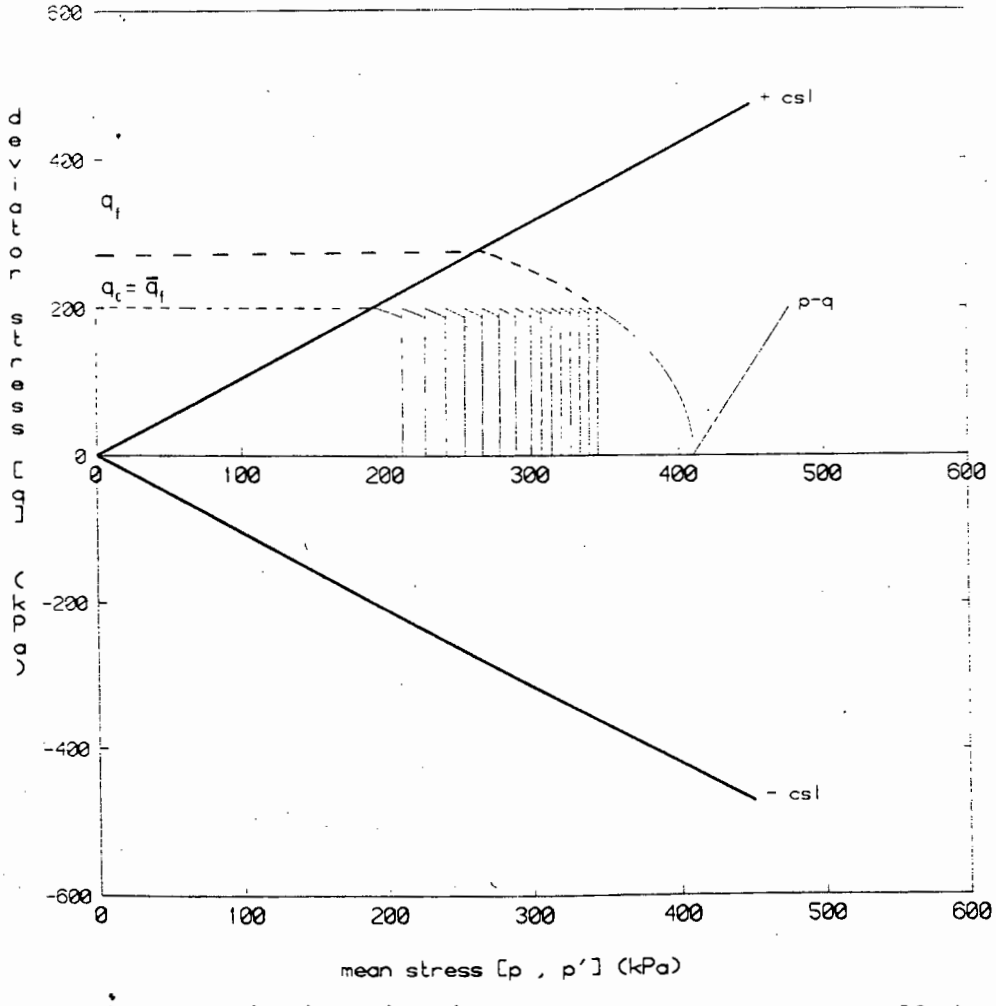

Figure 6.3.3 : Stress path migration due to one-way stress controlled loading.

The enlargement of the entire stress path to failure in Figure 6.3.3 shows that the magnitude of the change in p' increases as the stress path tends toward the projection of the critical state line and is a function of the parameter θ . The migration of the effective stress

path occurs for all values of cyclic stress with the number of cycles to failure decreasing with increasing cyclic stress level because of the resulting reduction in distance between the initial unloading point and the critical state line. The amount of plastic reloading is dependent on the time step.

The soil sample will fail when the effective stress path reaches the critical state at a value of deviatoric stress $\bar{q}_f$ equal to the cyclic stress q_c and the stress ratio reaches M (ie when $\eta/M = 1$ as shown in graph 5, Appendix B3.2) . The undrained strength continually decreases due to the cyclic loading from the initial (static) value of $c_{uo} = q_f/2$ to the final value $c_{uf} = \bar{q}_f/2 = q_c/2$ (see Figure 6.3.3). This is representative of the behaviour that would be expected to occur above the critical level of repeated loading (CLRL) described in Section 4.1.2 . The model therefore exhibts no CLRL and is only suitable for modelling behaviour above the CLRL . Modelling of the response below the CLRL could be possible by changing the degradation parameter during the cyclic loading.

An understanding of the mechanism that results in the different ultimate states is necessary. The response is dependent on the material history and could be related to a function of accumulated strain as in the nested yield surface models discussed in Section 4.3.2. Until sufficient testing (ie for a variety of material types, confining pressures p', cyclic stress levels q_c, and frequencies) has been performed to investigate the phenomonen, it was decided that there is no point in implementing an arbitrary function merely to "tune" the model to a specific set of laboratory data.

The deviator stress - strain behaviour represented in graph 2 (Appendix B3.2) is also given in Figure 6.3.4(a) which shows the entire behaviour until failure at the critical state. The elastic unloading and reloading causes no hysteresis and the accumulation of plastic strain occurs entirely in the plastic reloading stage. The strain vs. increments graph in Figure 6.3.4(b) depicts the initial increase in strain due to the monotonic loading, the gradual increase in accumulated strain due to the plastic reloading and the sudden increase

at failure. The magnitude of the strain is affected by the choice of shear modulus G. Two types of variable moduli elasticity were implemented by choosing the Poisson's ratio constant and allowing the shear modulus to vary as a function of p' or p_c'. However, little difference in behaviour was observed because of the small variation in p' over an unloading and reloading cycle.

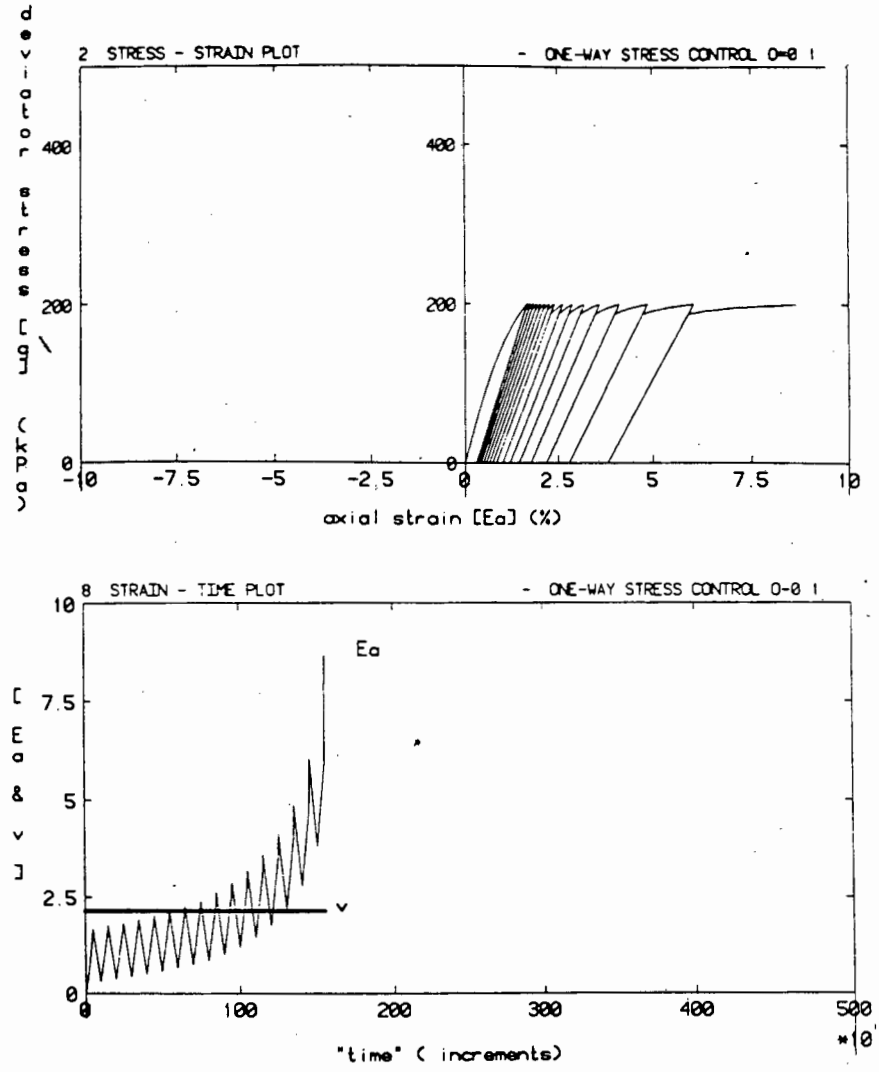

Figure 6.3.4 : Deviator stress and strain behaviour for one-way stress controlled loading. a) stress - strain, b) strain - increments

The pore pressure varies in phase with the loading (as shown in graphs 3 and 7) and gradually increases due to the plastic strain increase. The graphs of v-p' and v-ℓnp' (graphs 4,5, Appendix B3.2) show the negligible change in the specific volume (approximately 0,0002) as would be expected in undrained loading. The v-p' line passes through

the projection of the initial critical state line as a result of the translation of the state surface. The final projection of the critical state line is not represented in the graph.

6.3.3 Predictions for two-way stress controlled loading

The effective stress path in two-way stress controlled loading shown in Appendix B3.3 migrates toward the critical state line, but with a decrease in mean pressure due to reloading in both tension and compression. The deviator stress - strain relationship shows hysteresis loops, but these do not cycle about the origin as generally observed for laboratory tests (see also Section 4.1.4). Modelling of hysteresis loops cycling around the origin would require a kinematic hardening model such as a nested yield surface formulation with the resulting increase in complexity and the number of parameters.

6.3.4 Predictions for one-way strain controlled loading

The model response to one-way strain controlled loading is plotted in the graphs provided in Appendix B3.4 . Of interest in one-way strain controlled loading is that whilst the strain remains positive, the deviator stress varies between compression and extension. In practice, a lift off of the loading ram might occur in the place of the extension phase.The lack of laboratory test data in the literature prevents any comparison with the response of real soil from tests.

6.3.5 Predictions of two-way strain controlled loading

Graph 1 of Appendix B3.5 demonstrates the variation in the effective stress state with a decreasing peak deviator stress due to the cyclic two-way strain controlled loading. This behaviour compares well to that found by Taylor and Bacchus (1969), described in Section 4.1.4.

The model deviator stress-axial strain response (graph 2, Appendix B3.5) shows the hysteresis loops that cycle about the origin with decreasing apparant shear modulus. This compares favourably with the behaviour presented in Section 4.1.4 , but the initial increase in apparant shear modulus does not occur in the laboratory data. The shape of the hysteresis loops and the magnitude of the peak deviator

stress that is attained are highly dependent on the magnitude of the shear modulus G and the cyclic strain ϵ_c . The hysteresis curves for ϵ_c = 1% and ϵ_c = 4% from Figures 6.3.5 show that the higher value of cyclic strain results in the stress in the stress state approaching the critical state (see Figure 6.3.5(b)) with an accompanying increase in the amount of plastic strain that occurs during the plastic part of the reloading as well as an increase in the amount of hysteresis.

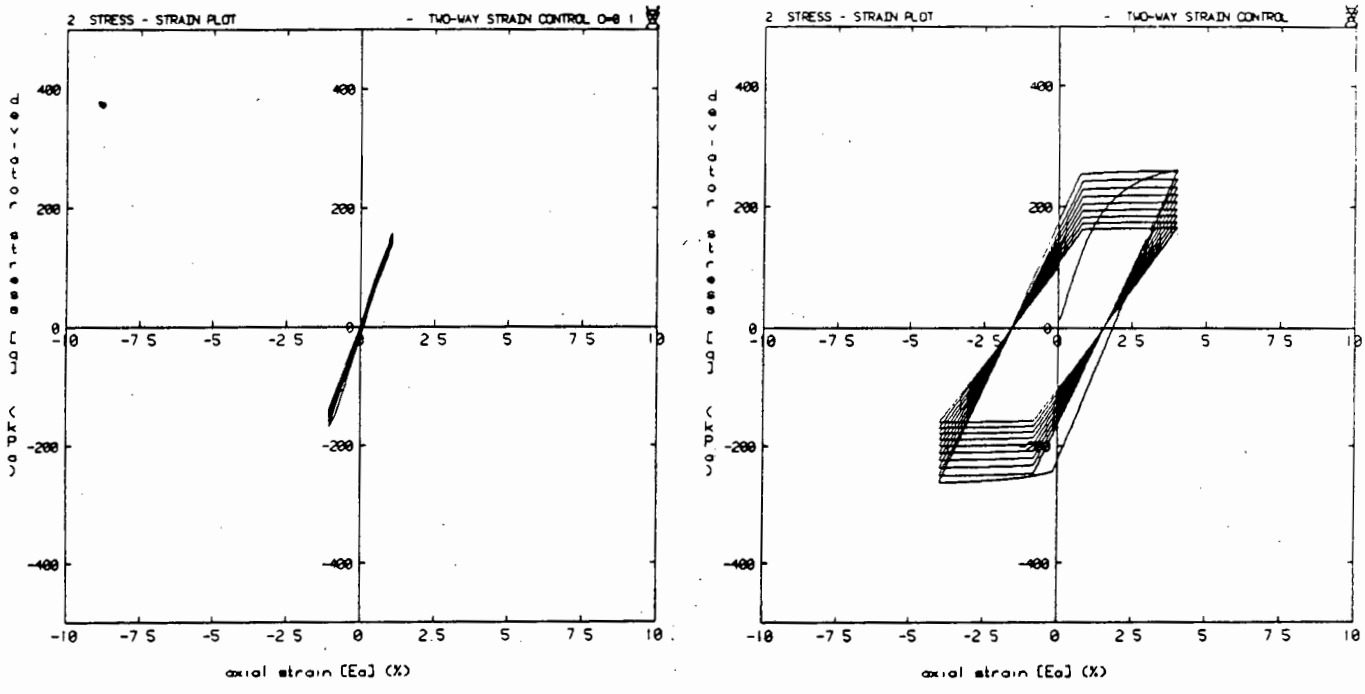

Figure 6.3.5 : Hysteresis curves for two-way strain controlled loading.
a) ϵ_c = 1% , b) ϵ_c = 4%.

Two type of variable elasticity were applied , relating the shear modulus G, and the Poisson's ratio ν. One parameter is kept constant and the other varies as a function of the mean effective stress p', or hardening parameter p'_c. The effect of increasing the shear modulus G is to increase the peak deviator stress attained in any one cycle. This is shown in Figure 6.3.6 for ϵ_c = 0,3% where the higher modulus (for example G = 20 000 kPa) results in higher stress levels and increased hysteresis compared to the response with G = 2000 kPa which shows no hysteresis at all. The peak strain is lower than the applied cyclic strain of ϵ_c = 0.3% due to the finite element solution technique applied in this research work. The use of variable shear moduli has

little effect and the difference between formulations with $G = G(p'_c)$ and $G = G(p')$ is negligible. Both plot as the same line (a,d in Figure 6.3.6). The effect of different values of shear modulus reduces as the cyclic strain increases.

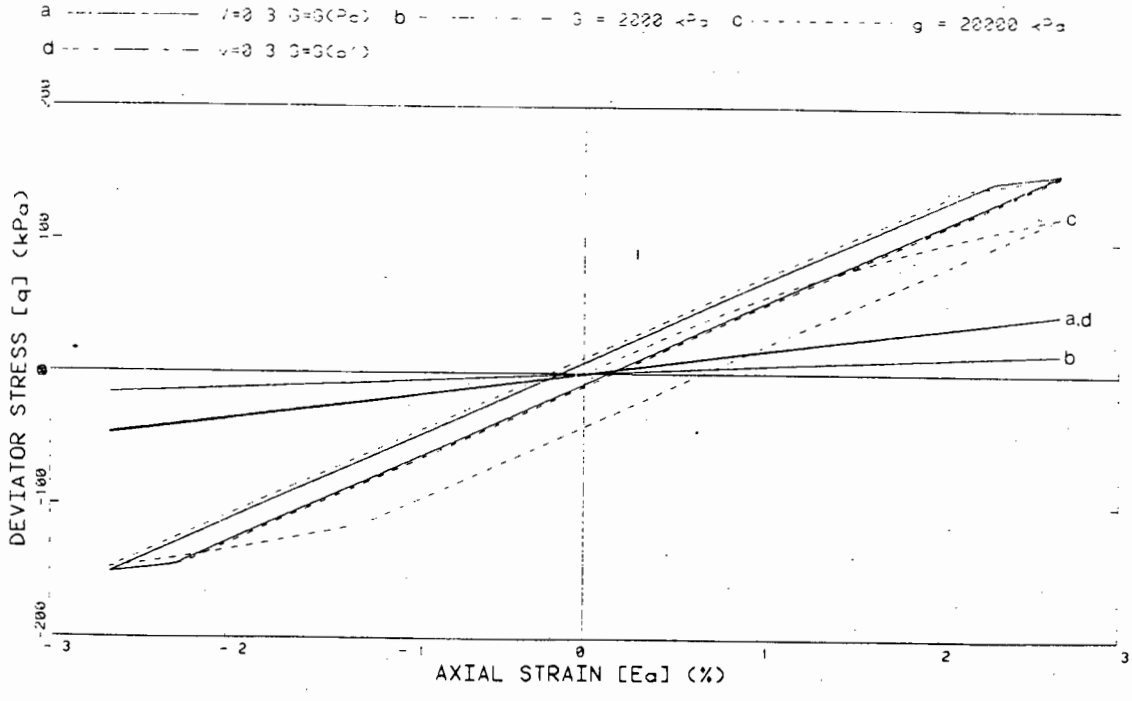

Figure 6.3.6 : Effect of constant and variable shear moduli

The pore pressure varies in phase with the loading (see graph 3, Appendix B3.5) and increases as the number of cycles resulting in the effective stress path migration. The effective stress path crosses the total stress path in extention resulting in negative pore pressures which is to be expected. This could be avoided by applying a back pressure. The plot of specific volume against mean effective stress (see graph 4, Appendix B3.5) shows that the volume is essentially constant during the undrained cyclic loading.

The evaluation of the model given above is essentially qualitative, and a series of laboratory tests were performed to determine the behavior

of a local clay under cyclic loading, and compare the model predictions and test results. The experimental procedures and results are discussed in the following chapter and the comparison for one-way stress controlled loading of the clay is given in Chapter 8.

CHAPTER 7

LABORATORY TESTING OF KAOLIN

7.1 MATERIAL DESCRIPTION AND TEST PROGRAM

A constitutive model must be based on a sound understanding of the material behaviour and it was for this reason that an attempt was made to test a clay under cyclic conditions. The laboratory tests would also provide the data required to determine the model parameters for the soil.

The clay used for all tests was a Kaolin, locally available from Serina Quarry in Noordhoek. Testing of a similar Kaolin was undertaken in previous research work (Wilson, 1984) which involved consolidometer and static triaxial tests and provides a basis for comparison.

The material was purchased in a dry powder form, its clay content (particle sizes less than 0.002 mm) is 52%. The Atterberg limits were determined to be :

Liquid limit	=	61 %
Plastic limit	=	42 %
Plasticity index	=	19 %
Shrinkage limit	=	8 %

The grading curves, plasticity chart and mineralogical analysis are shown in Appendix C1.

The testing program consisted of consolidometer tests and conventional static triaxial tests to determine the critical state parameters, and a series of cyclic triaxial tests to investigate the response of the clay to one-way stress controlled loading. From these results, the degradation parameter θ will be derived in Chapter 8.

The consolidometer tests were performed in the University of Cape Town laboratory and the triaxial tests were undertaken at Ninham Shand Materials Testing Laboratory in Cape Town. Computer controlled equipment with electronic data logging is essential for cyclic triaxial testing because of the long test durations and the rapidly changing test conditions. The only available device is the GDS Triaxial Testing System (GDSTTS) at the Ninham Shand laboratory which is a fully computer controlled triaxial device for static and cyclic load application and will be described in more detail in Section 7.4. The demands on the machine for commercial testing placed limitations on the amount and duration of tests that could be performed.

7.2 CONSOLIDOMETER TESTS

Four consolidation tests were performed on the kaolin to simulate one dimensional compresssion and hence determine the gradients of the normal consolidation line, λ and swelling line, κ form the load - displacement relationships. The parameter κ should in fact be determined from isotropic consolidation tests, to avoid the variation in lateral stress that occurs during unloading in the consolidometer. The triaxial test facilities needed for isotropic consolidation tests were not available for these time consuming tests, and the approximation of κ evaluated from the consolidation tests was considered to be sufficiently accurate.

The first consolidation test was not successful because of an error in the electronic mass balance and the results were discarded. The following three tests (A, B, C) were run simultaneously using Kaolin that had been mixed with water from powder to a paste with a moisture content slightly wet of the liquid limit and allowed to settle for 48 hours in a humid environment.

Sample A was loaded in increments to 600 kPa and then unloaded to 25 kPa . The first test had shown that 24 hours were necessary for the consolidation curve to level off and this was chosen as the time increment for loading. The sample was removed so that the parameters λ and κ could be found for use in the finite element analyses. The

samples B and C initially followed the same path as A. In test B, the specimen was reloaded to 800 kPa , then removed as a check on the results of test A. The third sample C was reloaded to 1200 kPa and then unloaded to determine the effect of multiple unloading cycles. The analysis of the data was done on a spread sheet package, the results are presented in Appendix C2, and the consolidation curves in an e-log(σ'_v) diagram are shown in Figure 7.2.1.

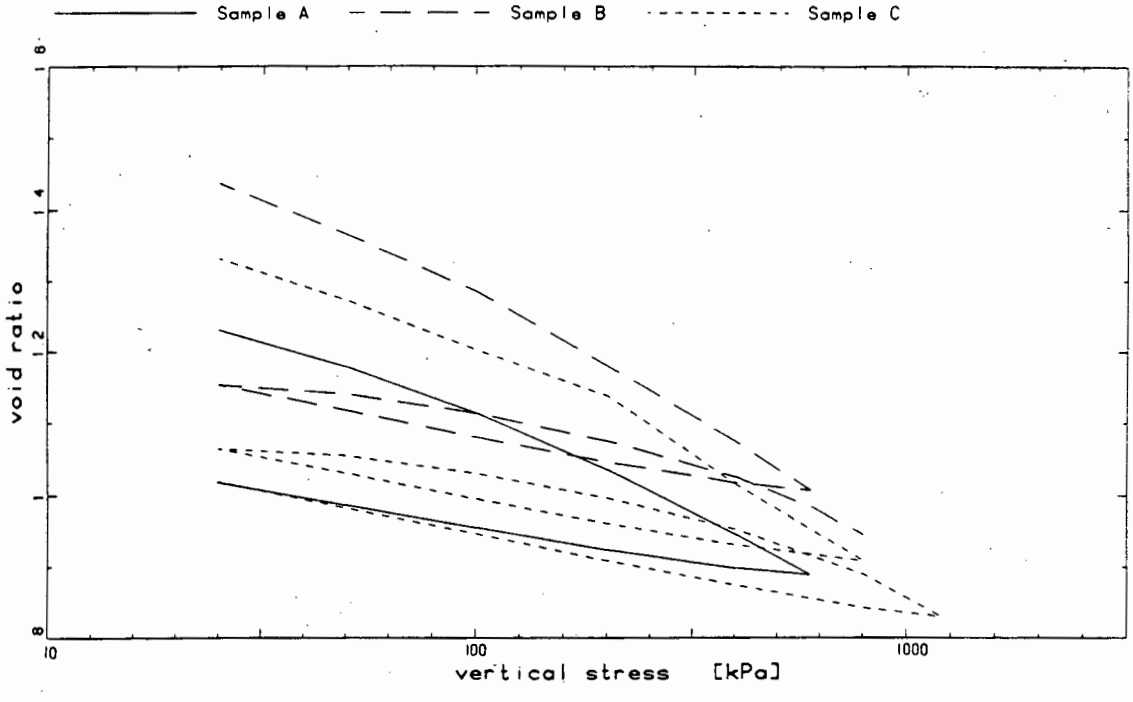

Figure 7.2.1 : Consolidation curves for Kaolin.

The requirements of 24 hours for consolidation implies long test durations. Allowing for two days sample preparation and one day for sample removal and drying, the test durations were as follows :

discarded test	:	11 days
test A	:	15 days
test B	:	20 days
test C	:	26 days.

The slope of the consolidation curves are found in the void ratio - log of vertical stress (e-log(σ'_v)) plane and converted to λ by dividing by 2,303 as discussed in Section 3.3. The calculated values of λ are given in Table 7.2.1. Similarly, the gradients, κ were calculated from the average slope of the swelling lines and are given in Table 7.2.2.

Table 7.2.1 : Values of λ determined from consolidation tests

test	A	B	C
Average λ	0,130	0,154	0,158

Table 7.2.2 : Values of κ determined from consolidation tests

test	A	B	C
Average κ	0,043	0,049	0,046

These values are much lower than those obtained by Wilson (1984),namely λ = 0,206 and κ = 0,07 . The difference in magnitude can be attributed to the higher clay content (62%) of the other test material. As shown in Casagrande's (1948) plasticity chart (see Appendix C1), the clay used in this test program is far below the A-line, indicating a relatively inactive clay material. The material is therefore expected to have the silt characteristics evident in the flatter consolidation and swelling curves.

The variation in the void ratios is approximately 0,02 which is a result of different degrees of saturation at preparation and variations in the water content.

The results of test B and C show the hysteresis expected in an unloading and reloading cycle and the translation of the normal consolidation line. On reloading, both samples reach the unloading stress with a lower specific volume and then follow lines approximately parallel to the initial consolidation line.

7.3 STATIC TRIAXIAL TESTING

The Kaolin was tested in saturated, consolidated undrained (CU) conditions to determine the critical state parameters M, N, Γ . The test device used is a conventional Wyekam Farrance, strain rate controlled, triaxial testing machine. The reason for the use of the conventional static device was to gain experience in the preparation and testing of the Kaolin without the additional complications due to the electronic data aquisition and control presented by the GDS system. No comparative studies were undertaken on the influence of the two different test machines and procedures involved.

The clay, originally in dry powder form, had to be reconstituted for testing. Reconstitution of the soil by mixing the powder into a slurry, removing entrapped air by vacuum and consolidating the slurry was not possible due to a lack of the necessary vacuum and consolidation apparatus. The material was therefore prepared by mixing with deaired water and was allowed to stabilize for 24 hours to obtain a more homogeneous sample. The clay was then compacted into a split mould of 50 mm diameter and 100 mm length.

The first sample was prepared just wet of the liquid limit, but proved to be too wet and could not be extruded. Subsequent samples were mixed dry of the liquid limit and could then be successfully extruded. The high liquid limit and low plasticity index meant that the clay absorbed large amounts of water, but that the difference between the plastic and liquid states was small and a small addition of water could cause the sample to become too wet to extrude.

Two samples were saturated simultaneously with three cell pressure increments of 50 kPa, followed by three 100 kPa increments to 350 kPa over 18 hours in total. The back pressure was kept at 20 kPa below the cell pressure. Skempton's B parameter check was performed and both samples registered B = 1,00 $\pm$ 0,02, which was considered within the resolution of the limits of the cell pressure gauge and pore pressure transducer.

The samples were isotropically consolidated to 400 kPa mean effective pressure with a cell response of 780 kPa and backpressure of 380 kPa.

A cell leak during the consolidation of the first sample resulted in an error in the measurement of the volume change and the test was discarded, but the following test was successful. The volume change was measured on the backpressure line and the resulting moisture content of 36% corresponds to a specific volume of 1.9758, using a specific gravity of 2.71 (Wilson,1984) The theoretical time to failure t_f was calculated (Head, 1982) from

$$t_f = 0{,}51\ t_{100} \qquad (7.\ 3.1)$$

and was found to be 184 minutes (t_{100} is the theoretical time to 100% consolidation from the volume change versus square root time graph). Using t_f = 240 minutes , and an estimated failure strain ϵ_f of 10%, the strain rate was determined as 0,0016 in/min ≈ 0,04 mm/minute.

The sample failed in a combination of barrelling and slip plane modes. The results of the loading were calculated on an HP-86 computer and the area corrections for barrelling based on elasticity theory were applied, but no area corrections were made for the slip plane failure because it was not certain at which stage slip failure began.

A linear stress correction of 0 kPa to 4 kPa over the strain range of 0 to 10% was applied to correct for the radial strength of the membrane. No correction was applied to account for the effect of the membrane on the slip plane failure. The membrane penetration effect on pore pressure and volume change is negligible for clays (Head, 1982).

An overview of the results is presented graphically in Figure 7.3.1 . On the stress path plot (Figure 7.3.1(a)) unusual increase in mean effective pressure p' as the soil tends toward failure at maximum deviator stress q . This is could be due to the change in sample shape resulting in failure before the average stress state in the sample reaches the critical state (Schofield and Wroth, 1969). The same effect is noticeable in the test results of Wilson (1984), and Sangrey et al (1969). Barden (1971) suggests that the reorientation of clay

particles results in a structure with slip planes interspaced with zones of simple shear which cause a deviation from the uniform triaxial conditions that are assumed to exist.

(a)

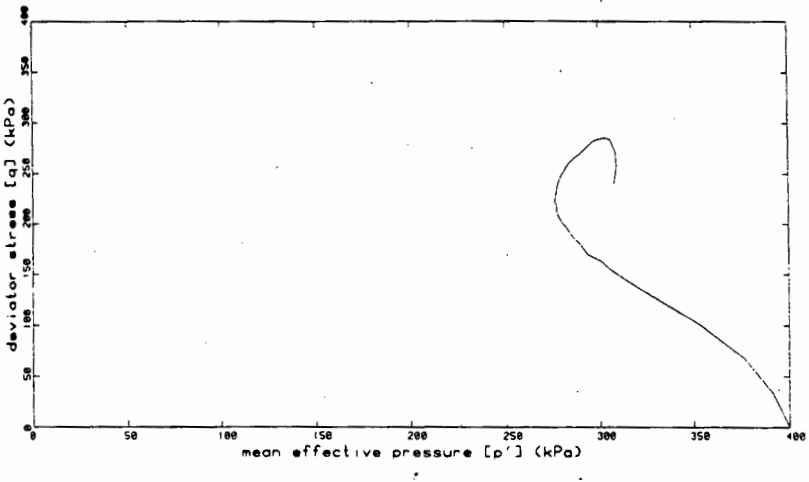

(b)

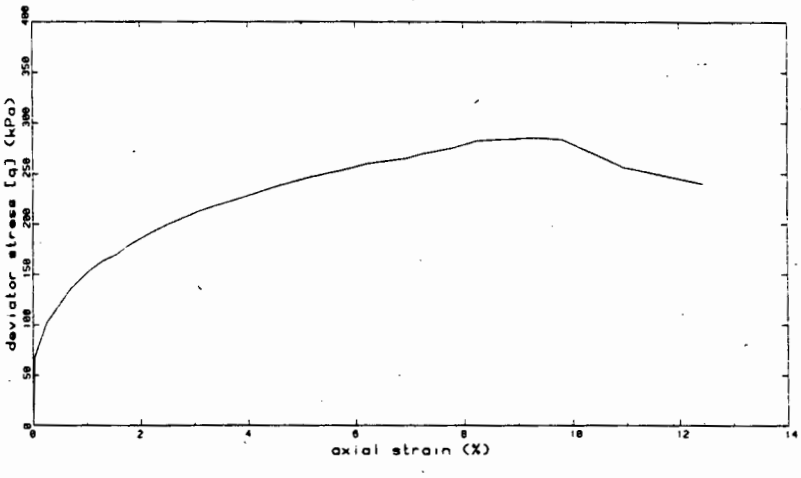

(c)

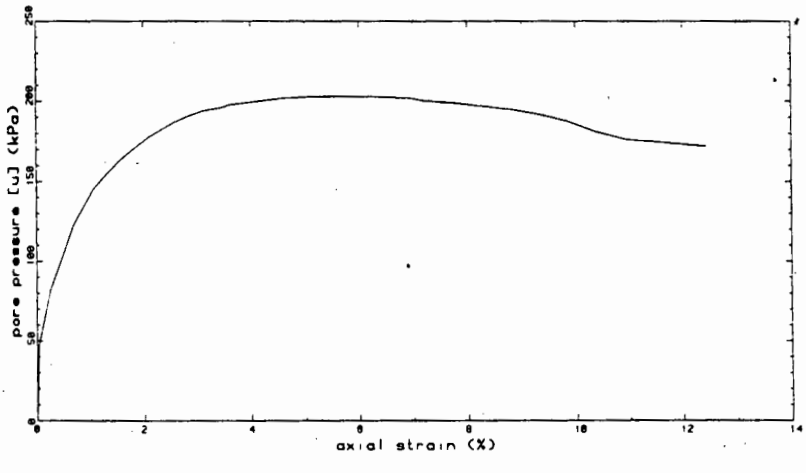

Figure 7.3.1 : Results of static triaxial test on Kaolin.
a) stress path, b) stress - strain,
c) pore pressure - strain.

As shown in Figures 7.3.1(b) and 7.3.1(c), the deviatoric stress and pore pressure both increase sharply with increasing strain, then tend to a constant value as expected for a normally consolidated specimen, but the decrease of pore pressure prior to failure and the decrease in deviator stress after failure are considered to be a result of inhomogeneous sample structure shortly before and at failure, as discussed above.

7.4 CYCLIC TRIAXIAL TESTS

7.4.1 Equipment

The GDS triaxial testing system consists of a Bishop-Wesley stress path cell which allows a variety of stress paths to be applied to the sample using hydraulic pressures which are electronically controlled. The tests that can be performed include unconsolidated undrained, consolidated undrained, drained, K_o- consolidation and swelling, linear stress paths and one-way stress controlled cyclic loading. The cell can accommodate 50 or 100 mm samples by changing the cell pedestal. A schematic diagram of a Bishop-Wesley cell is given in Figure 7.4.1 and Plate 7.4.1 shows the GDS system.

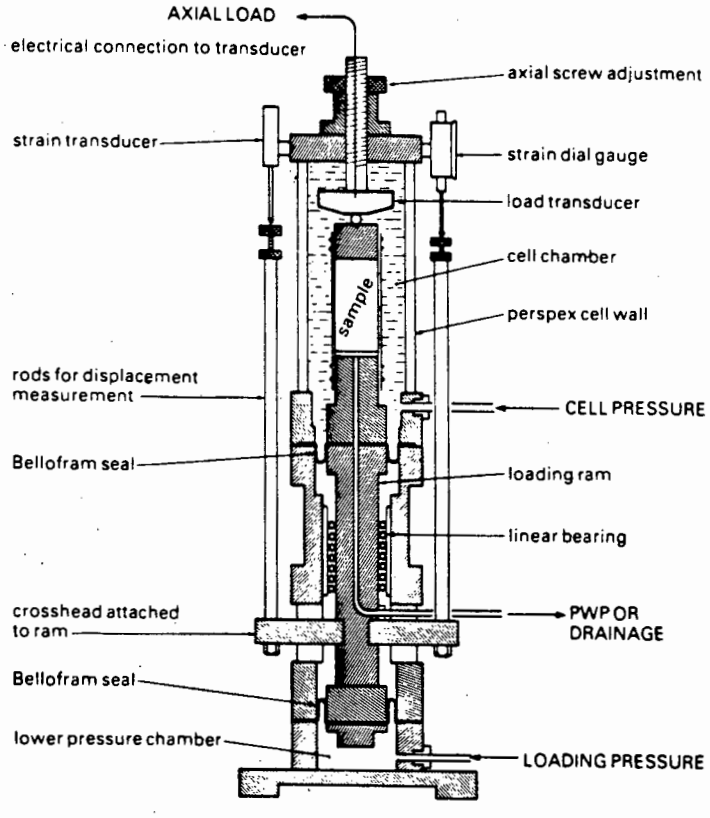

Figure 7.4.1 : Diagram of Bishop-Wesley triaxial cell. (after Head, 1986)

The cell body is similar to that of a conventional cell, but the axial load is applied by a ram which is hydraulically driven by pressurising water in a chamber below the ram. The ram is guided in a set of rolling bearings. The fluids in the cell and the lower chamber are separated by Bellofram rolling diaphragms. The pressure required in the lower chamber to cause a given load on the sample is thus a function of the cell pressure. The applied axial load is calculated from the pressure in the lower chamber, and then corrected for the friction in the guide bearings and rolling diaphragms (GDS 1986).

The cell, lower chamber and back pressures are each controlled by a separate, motor driven digital controller. Each GDS controller consists of a piston moving horizontally in a cylinder. The piston is actuated by a stepping motor and gearbox moving on a slide.

Plate 7.4.1 : GDS Triaxial Testing System

The drained water in the cylinder is pressurised and displaced by the piston allowing the controller to apply a target pressure or target volume. The pressure is measured by an integral solid state pressure transducer accurate to 0,1 % of the pressure change. The volume change is measured by counting the steps of the stepping motor and is accurate to 0,25 % . The resolution of the pressure and volume displays are 1 kPa and 1 mm^3, respectively though the resolution for controlling and logging the pressure is 1/4096 kPa (0,244 x 10^{-3} kPa) and the corresponding volume resolution is 1 mm^3.

The pore pressures are measured by a "digital pressure interface" - a pore pressure transducer at the cell exit and connected into the back pressure supply line.

Each digital controller may operate in "stand alone" mode to control the pressures and volumes, or may be controlled by computer through an IEEE-interface. The system at the Ninham Shand laboratories makes use of a Hewlett Packard 86B computer which is programmed to perform the test control, data logging and data presentation. The program is

provided by GDS and is not accessible to users. The data is logged into the memory at discrete intervals and may only be saved to disc at the completion of a test sequence. This is a serious disadvantage since the HP 86B memory can only accommodate 350 data sets which is equivalent to the data taken in about 15 load cycles. The cycles for which data is to be stored must be selected manually. A further problem with storage in memory is that all data will be lost if the power fails or if an incorrect key is pressed accidentally.

The system records the volume and pressure movements from each of the digital controllers and the stresses and strains are calculated from these. The axial strain is calculated from the change in volume of the lower chamber. Graphs and tables of 27 variables can be plotted using a separate program on completion of the test. The time interval between each reading can allow important data to be missed and it becomes difficult to interpret data, especially trends in peak values.

The consolidation is controlled by the GDS system and the back pressure controller accommodates the expelled water and hence measures the volume change. The back pressure controller has a total volume of 500 mℓ of water, but a portion of this is used to achieve the back pressure which limits the amount of consolidation that can occur. The controllers have limit settings on both the pressure and volume measurements and if an upper or lower limit is reached, the controller corrects by emptying or filling the cylinder.

The GDS system can only perform one-way stress controlled cyclic loading and therefore the other types of cyclic loading could not be investigated. The loading is specified as a datum in terms of total stress, a cyclic stress amplitude and a period in minutes. The wave shape can be either triangular, sinusoidal, or square. The system applies an estimate of the stress increment and then checks the response and corrects the value in the following stress increment.

The wave form is therefore dependent on the soil response. A loading period that is too short will result in a flattening of the wave form and the desired cyclic stress will not be attained. The determination of the appropriate period is a trial and error process for each soil type and cyclic stress level.

7.4.2 Results

The first sample tested was a 50 mm diameter sample, but a leak in the pore pressure system caused the cell pressure and back pressures to equalise and the sample was removed and discarded.

Subsequent samples were 100 mm in diameter and 200 mm long as used in the commercial test program. Leakage and de-airing problems associated with frequent changes of the sample platen were eliminated. The different sample sizes introduced a further approximation into the comparison of the static and cyclic tests.

The first few tests were not successful due to inexperience with the system and also because of misinterpretation of the manual which is ambiguous at times.

The saturation of the sample is achieved using the controllers in "stand alone" mode. A cell pressure of 50 kPa was applied, the sample allowed to consolidate, and then a back pressure of 30 kPa was applied. The cell presssure was ramped to a chosen value using the pressure ramp function of the controllers, with the back pressure ramp constantly remaining 20 kPa less. The B parameter check was performed by applying a cell pressure increment and measuring the pore pressure change on the digital pressure interface.

The clay has a high water content, and the samples were therefore consolidated in two steps, at the same effective stress of 400 kPa, to avoid reaching the controller limits. The backpressure controller was emptied after the first step and consolidation proceeded in the second step. The GDS program recorded the sample volume change and the sample size calculated in the first step was used in the second procedure.

When the cyclic loading was applied to the first sample, a decrease in cell pressure occurred in drained conditions, the sample would have therefore expanded and was discarded. One test was used to attempt to determine a suitable load period. Cyclic loading of periods from 3 minutes to 25 minutes were applied. The minimum period that was needed was 10 minutes and only at 25 minutes was the wave form properly

defined and relatively smooth. The following sample was tested at a period of 10 minutes to maximise the number of cycles that could be applied in the available two days. The cyclic deviator stress used was 125 kPa with a stress amplitude of 50 kPa. The deviator stress q_c therefore ranges between 25 kPa and 125 kPa.

A susequent sample was tested at a period of 60 minutes to ensure a pore pressure equalization and to investigate rate effects. Unfortunately an increase in back pressure was trapped into the back pressure line during the change from the consolidation stage to the cyclic stage which affected the measured effective stress state though the recorded total stress behaviour seems correct. The peak axial strain in each cycle is larger than the strain that occurred in the test with a 10 min load period. This indicates that the material is not rate independent as discussed in Section 4.1.5.

Cyclic triaxial testing of clay is very time consuming and many tests must be performed to evaluate the response of the material and investigate rate effects, and the influence of mean effective stress, deviator stress and overconsolidation ratio. The discussion of results that follows is limited by the incomplete nature of the data logging, but serves to illustrate the trends of the material behaviour and highlights further problems with the test equipment.

Total stress path (p - q) :

The slope of the mean normal total stress, deviator stress line in the tests 4 and 6 is 3:1 . This is expected since the loading is specified in terms of total stress. There were no deviations and thus the stress paths were constant over the entire test duration.

Effective stress path (p' - q) :

The initial stress path cannot be obtained because data logging begins when datum has been reached. The translation of the effective stress path due to the cyclic loading is evident in Figure 7.4.2. The unloading and reloading stress paths are concave to the origin. The reason for this response is unclear, but could be a result of the apparatus compliance.

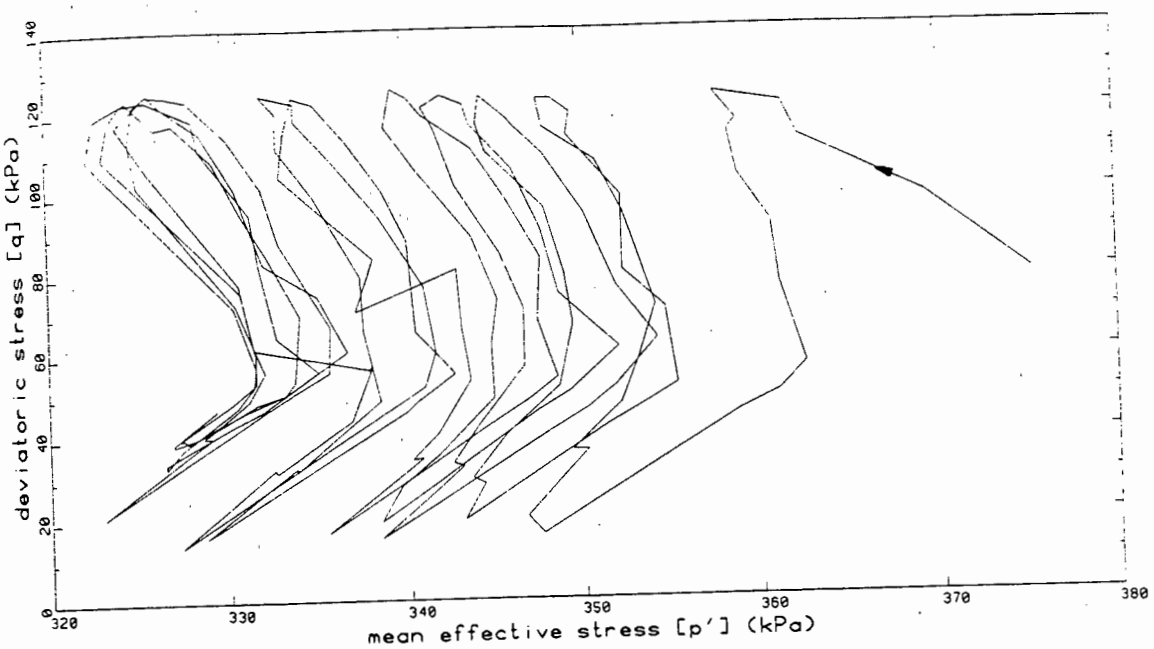

Figure 7.4.2 Stress path diagram for cyclic test

The apparent stabilization of the effective stress path would suggest that the cyclic deviator stress is below the critical level of repeated loading. For confirmation of this behaviour, the application of many more cycles of loading are needed (Sangrey et al (1969) applied at least 100 cycles after stabilization). Due to the limited time available for each test period, the additional continuous cyclic loading of up to four days was out of the question.

Deviator stress - axial strain ($q - \epsilon_a$)

The deviator stress - axial strain graphs (see Figure 7.4.3) show a characteristic S-shaped loop. The loading curve shows a sudden decrease followed by a gradual increase in slope. The unloading modulus is greater than the loading modulus, but shows a similar decrease and then an increase in magnitude.

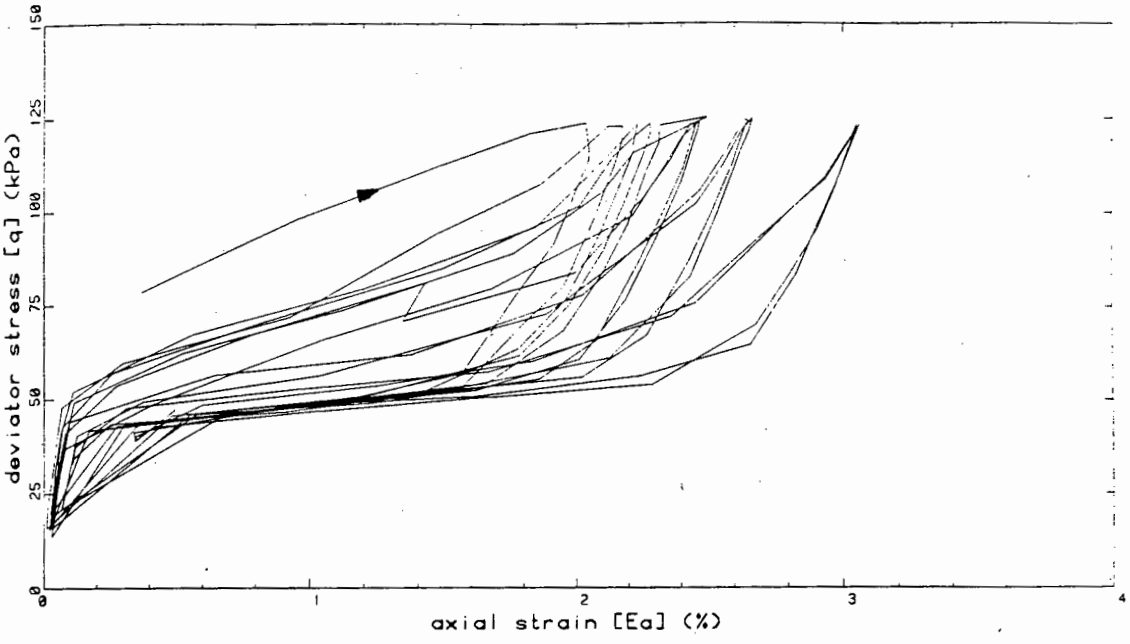

Figure 7.4.3 : Deviator stress-axial strain graph for cyclic triaxial test.

The amount of accumulation of strain decreases with increasing numbers of cycles. This is consistent with the behaviour of a clay below the critical level of repeated loading. The flattening of the central portion of the hysteresis loops was initially thought to be a rate effect, but cycles at 6 minutes, 16 minutes and 60 minute periods showed similar shapes.

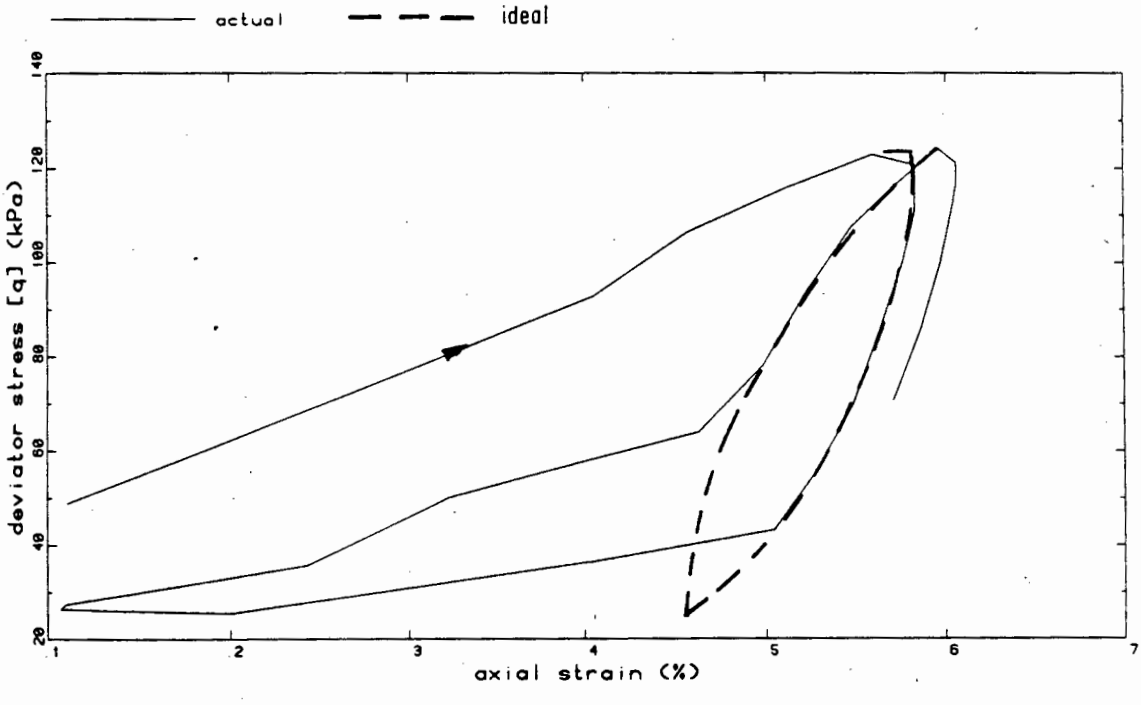

Figure 7.4.4 : Schematic comparison of actual and expected stress-

The strain values, however, always reduce almost to zero on unloading which is inconsistent with the expected accumulation of plastic strain. This suggests that there is a problem with the measurement of axial strain. A schematic diagram showing a corrected stress - strain curve is given in Figure 7.4.4. In the cyclic tests, the height calculated by the GDS program after consolidation and cyclic loading was always of the order of 10 mm greater than the measured height and the calculated diameter was about 2 mm less than that measured. The measured height and diameter of the static test, however, corresponded to the calculated value within 1 mm.

The validity of the calculation of the axial strain by applying equations based on elastic theory to assign values to the change in length and diameter from a measured value of volume change in the lower chamber is questioned. The purpose of the test is to determine the amount of plastic deformation that will occur which can only be determined by an external deformation measurement. The independent measurement of displacement could be achieved using a dial gauge or transducer to measure the ram displacement. Any incorrect assumption about the axial strain affects the calculated stress which is based on the area of the sample. For more exact results, the radial strain could be measured using a lateral strain measuring device (Head, 1982).

Pore pressure - time :

A consideration of the pore pressure - time graph (Figure 7.4.4)also shows a decrease in the accumulation of pore pressure which therefore tends to a constant value. This confirms the conclusion that the soil tended to a stable non-failure condition and hence indicating that the trends in the strain are correct, even though the magnitudes are incorrect.

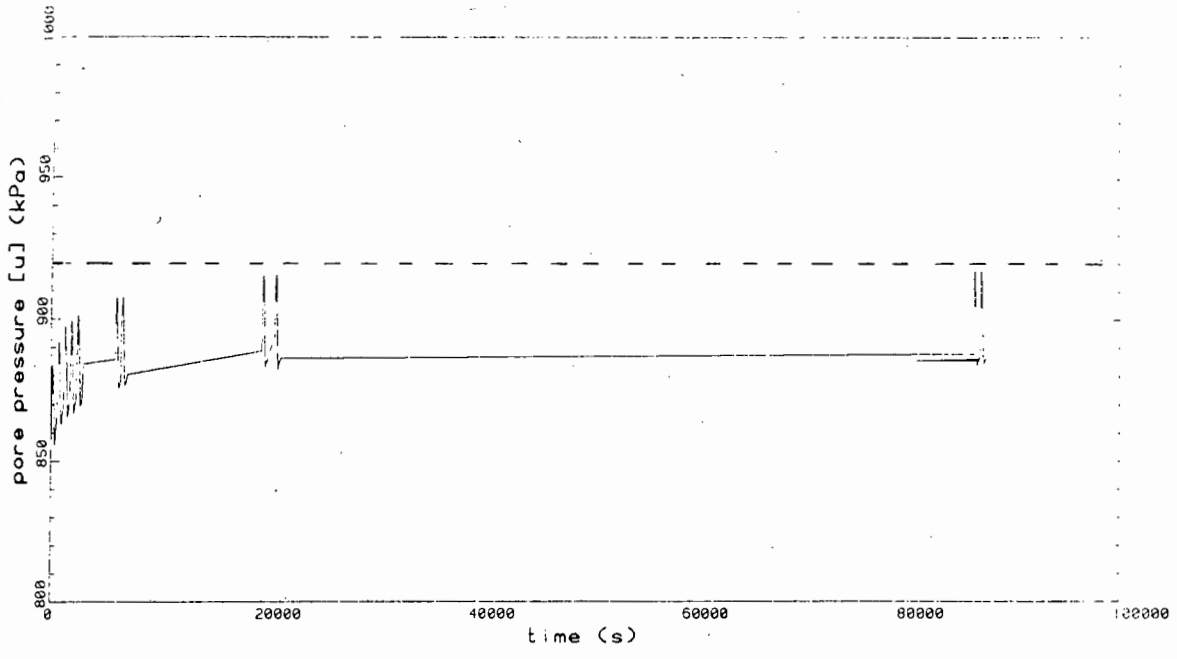

Figure 7.4.5 : Pore pressure - time graph

The problems of incorrect strain and stress measurement invalidate the cyclic test procedure. The program code is secured and cannot be modified to include independent deformation measurement facilities. The development of an improved version of the test program was considered to be beyond the scope of this research work.

CHAPTER 8

COMPARISON OF MODEL PREDICTIONS AND LABORATORY TEST RESULTS

8.1 DETERMINATION OF PARAMETERS FOR KAOLIN

In Chapter 6, it was shown that the constitutive relation implemented could achieve a qualitative prediction of the behaviour of one-way stress controlled cyclically loaded clay. The constitutive law for soil should also provide quantitative predictions of the effective stress-strain behaviour and the pore pressure response, using parameters chosen from a series of laboratory tests.

The most convenient method for verifying the model behaviour is to backpredict a variety of laboratory test stress paths, and in particular, the tests that were used to evaluate the material parameters. In this research work the static triaxial test path and one-way stress controlled cyclic loading situations will be considered.

The parameters that are required for the static analysis are the gradients of the normal consolidation and swelling lines (λ and κ, respectively), the slope of the critical state line in the $p' - q$ diagram (M) and the specific volume at $p' = 1$, of either the normal consolidation line (N), or the critical state line (Γ). The cyclic triaxial simulation requires the additional degradation parameter, θ.

The consolidometer tests resulted in magnitudes of the parameter λ ranging from 0,130 to 0,158 as discussed in Section 7.2. The gradient of the swelling lines κ, varied between 0,043 and 0,049 and therefore the average values of λ and κ for the Kaolin were determined as 0,15 and 0,046, respectively. The parameters M and N (or Γ) could then be evaluated from the static triaxial test results using the method of transforming the stress path into the v_λ (specific volume at unit stress p') and η, (stress ratio q/p') plane.

The results of the static triaxial test path in the $v_\lambda - \eta$ diagram are given in Figure 8.1.1, using the equation 3.3.3 with the initial specific volume of 1,975 obtained from the sample moisture content (as described in section 7.3.). The Cam-clay model idealises this curve as a straight line and the Modified Cam-clay stress path would plot as a curve. The test path is straight over the central section of the load path. The deviation at the beginning is due to initial stresses caused by inhomogeneous sample preparation and the final variation is due to the change in specimen shape at failure. The difference between the soil behaviour and the straight line could also indicate a difference between the soil behaviour and the Cam-clay idealisation, i.e. another yield surface may be more appropriate.

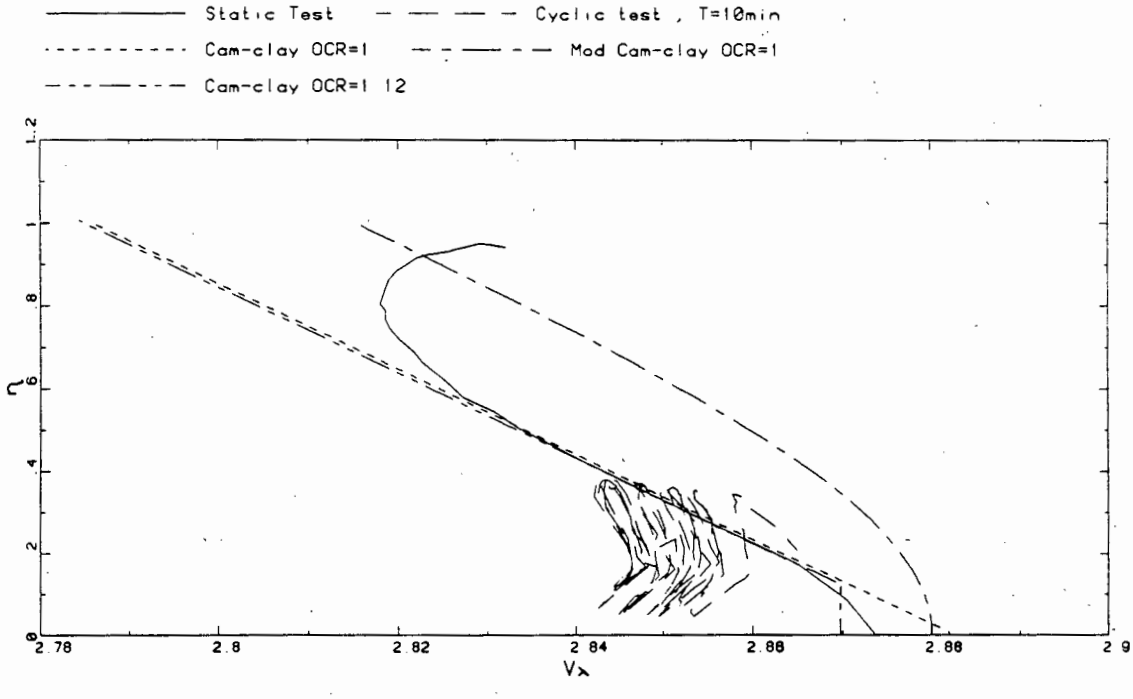

Figure 8.1.1 : $v_\lambda - \eta$ diagram for triaxial tests and model predictions.

The fitted straight line intercepts the v_λ-axis at a specific volume of 2,882, which is therefore the parameter N (see Section 3.3). A Modified Cam-clay yield surface and a Cam-clay yield surface were

applied to determine the most appropriate surface. The parameter N positions the normal consolidation line in the v - p' plane and therefore, to ensure that the initial specific volume remains similar for the analyses using either Cam-clay or Modified Cam-clay models. Since the relationship between N and Γ depends on the shape of the yield surface, the value of Γ (which determines the position of the critical state line in the v - p' plane) will differ for the two models.For Cam-clay, with λ = 0,15 and κ = 0,046, the parameter Γ is 2,778 and therefore M was calculated to be 1,07 Equation (3.2.17) for Modified Cam-clay implies that Γ is 2,809 with the same value for M.

8.2 BACKPREDICTION OF STATIC TRIAXIAL TEST

A series of Finite Element back predictions of the static triaxial test were performed to choose the best fitting yield surface for the cyclic analyses. The material parameters that were determined are similar to those used in the benchmarking analyses in Section 6.3.1 which showed that the convergence and accuracy depended on the choice of stress increment (Δq) and penalty number (α). Thus, Δq = 1.0 kPa and α = 200 were considered to be appropriate for this analysis. The mesh with two linear strain triangles was used.

The v_λ - η graph of Figure 8.1.1 and the graphs presented in Figure 8.2.1 indicate that the results of the experiments lie between the Cam-clay and the Modified Cam-clay response and that the best fit is provided by Cam-clay with an overconsolidation ratio of 1,12 i.e. an initial preconsolidation pressure of 450 kPa. The preconsolidation pressure must be greater than the confining pressure to obtain an overconsolidated clay with the same initial specific volume.

The stress path plot in Figure 8.2.1(a) shows that the Modified Cam-clay overestimates the soil strength and the Cam-clay model results in an underestimate. Figure 8.2.1(b) confirms the criticism that Modified Cam-clay underpredicts strain and Cam-clay overpredicts strain as expressed in Section 3.4. The best fit is again given by the Cam-clay with OCR = 1,12 because of the initial elastic loading. The magnitude of the shear modulus within the range of 2 MPa to 150 MPa does not noticeably affect the magnitude of the strain.

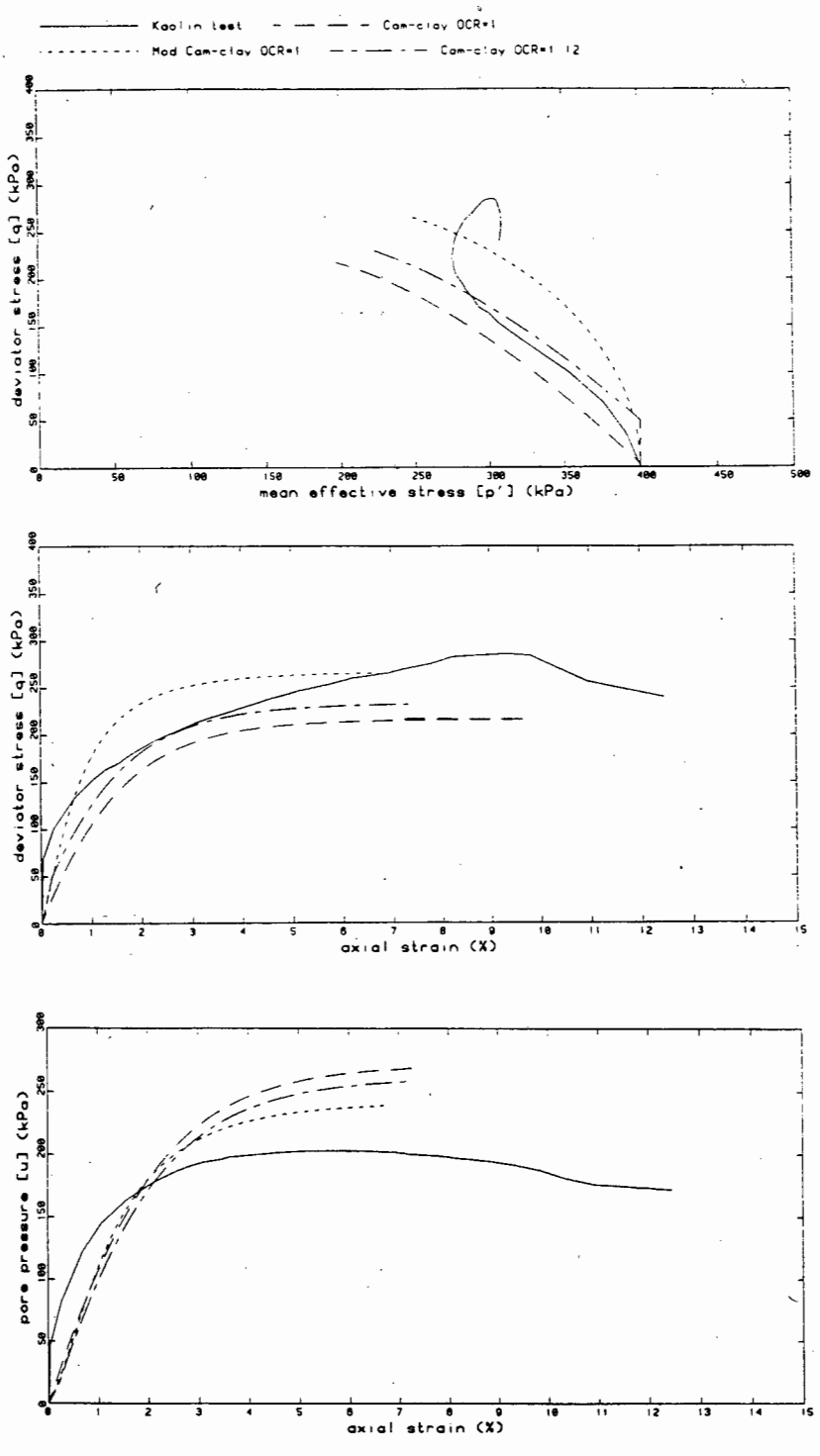

Figure 8.2.1 Back predictions and experimental results of static triaxial test on Kaolin .

a) stress path diagram

b) stress - strain diagram

c) pore pressure - strain diagram.

The pore pressure predictions are less successful (see Figure 8.2.1(c)) and all three models result in similar behaviour which initially underpredicts, then overpredicts the pore pressure for a given strain.

8.3 BACKPREDICTION OF CYCLIC TRIAXIAL TESTS

The final parameter required for the prediction of the cyclic triaxial tests is the degradation parameter θ. Since the test did not reach failure, the evaluation of θ from a graph of θ against the log of the number of cycles to failure (see Section 7.4) is impossible. The number of cycles to failure is extremely sensitive to the increment size in the numerical scheme. A decrease in step size from 10 kPa to 1kPa can cause a significant reduction in N_f for a particular situation due to the increased plastic deformation that occurs in reloading. As shown in Figure 8.3.1 for $\theta = 0,1$. For θ below about 0,05 too large a step size may prevent plastic reloading and the model will cycle elastically with no migration in the effective stress state.

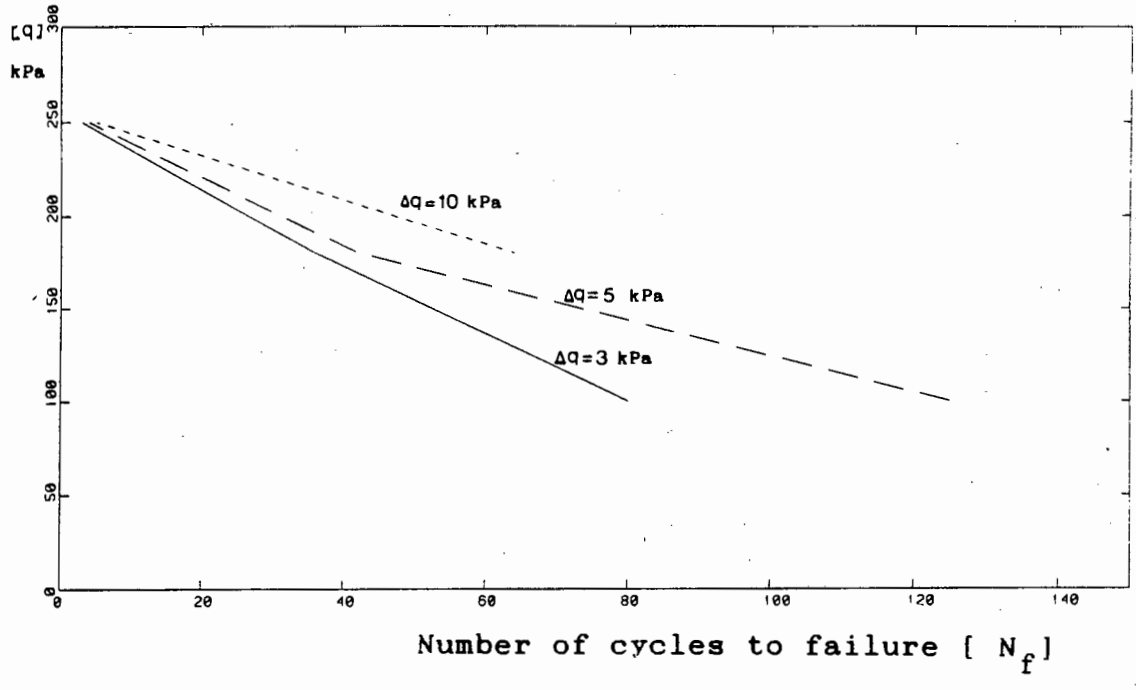

Figure 8.3.1 : Convergence of q versus log N_f relationship.
($\theta = 0.1$)

The values of θ for a one-way stress controlled cyclic triaxial test were calculated using the procedure of Section 6.2 for Cam-clay and are given in Table 8.3.1.

Table 8.3.1 Values of degradation parameter θ for cyclic triaxial test on Kaolin.

cycle number i	1	2	3	4	5	11	35
degradation parameter θ	0,1141	0,0370	0,0286	0,0283	0,0283	0,01781	-

There is thus a decrease of nearly one order of magnitude in the first cycle and then a slow decrease to cycle number 35 where it becomes impossible to determine the parameter which can be seen in Figure 8.3.2.

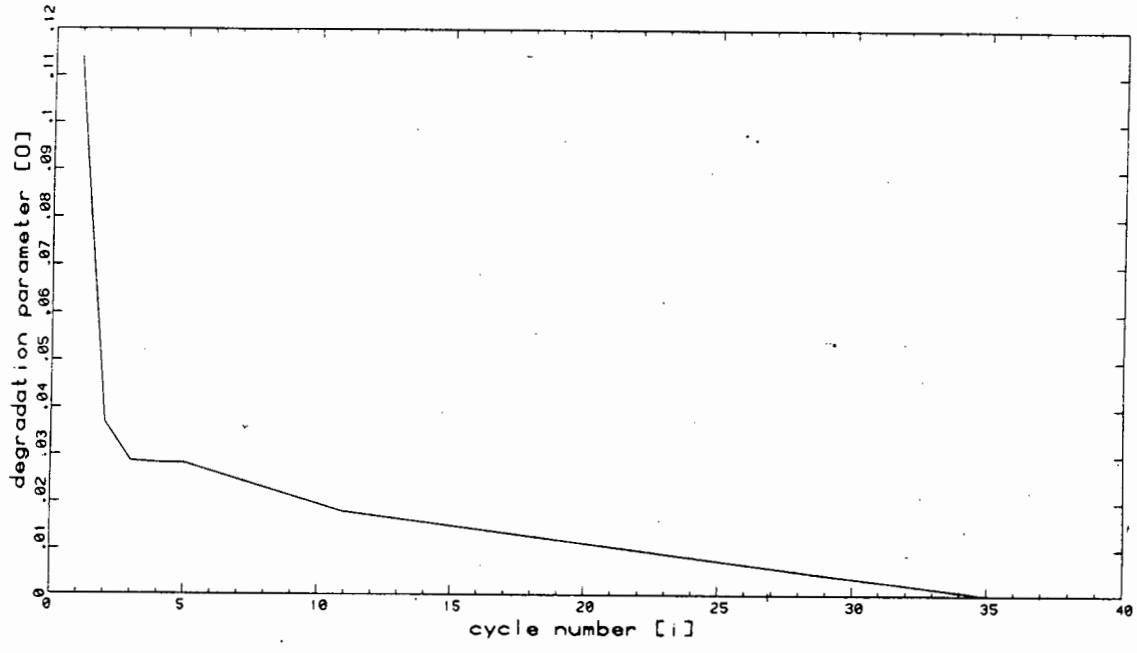

Figure 8.3.2 : Degradation parameter for cyclic triaxial test

It is evident that the assumption of a constant θ for all load cycles is invalid for this load situation and that θ is a function of the number of cycles and possibly the accumulated plastic strain. No improvement on the evaluation of θ can be made until sufficient laboratory test data is available.

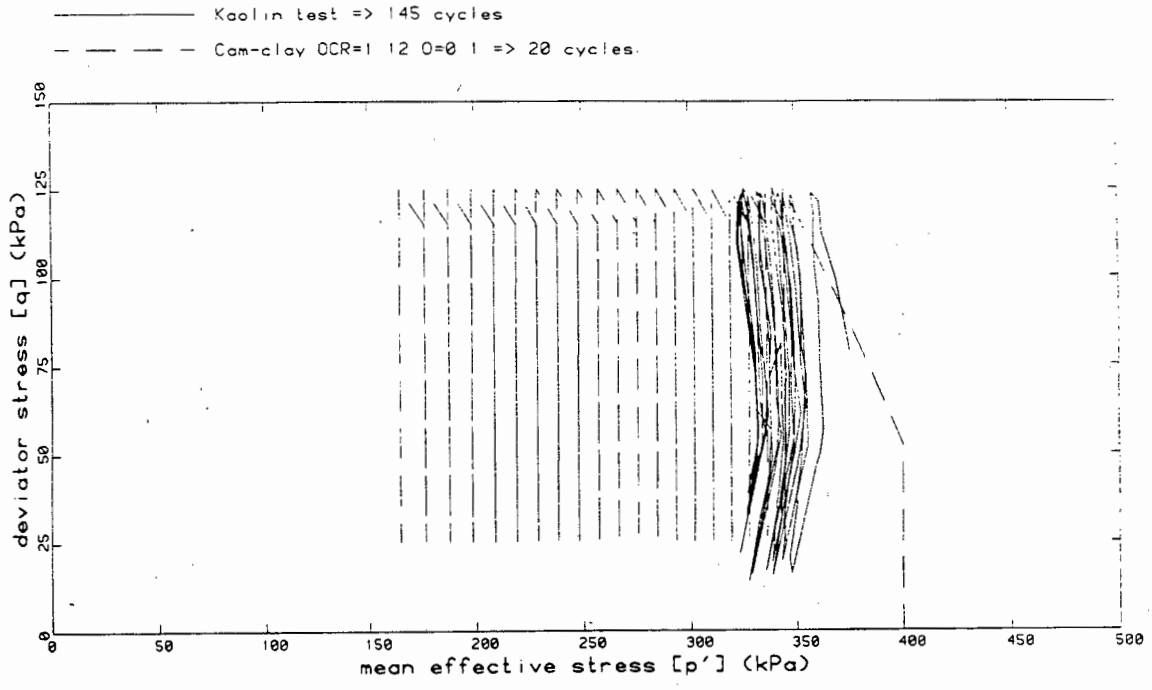

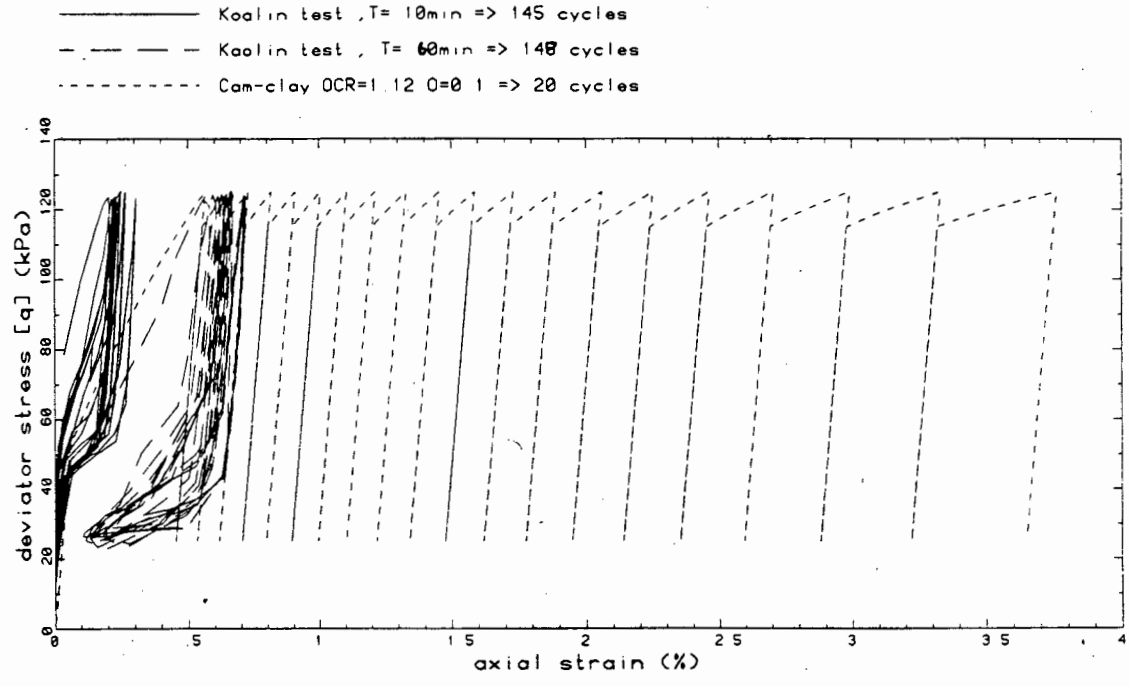

Figure 8.3.3 : Backpredictions and experimental results of cyclic triaxial tests on Kaolin, (a) stress path diagram,
(b) stress-strain diagram

A comparison of the laboratory test data and the results of a finite element analysis with θ = 0,1 is given in Figure 8.3.3. The migration of the effective stress path in Figure 8.3.3(a) is overestimated by the model, which does not show the stabilization that occurs in the laboratory test data. The model cannot, therefore, be used to predict clay response at cyclic stress levels below the critical level of repeated loading (CLRL). It is suggested that the predictions above the CLRL may be more correct, but this cannot be verified due to the lack of data.

There is, however, no consistent method for determining the CLRL and this mechanism should be researched in future, because the ability to distinguish between cyclic stress levels that lead to failure and those that lead to stabilization of the material is of great significance to design practice.

The deviator stress - strain predictions and the results of laboratory tests with load periods of T = 10 min and T = 60 min is given in Figure 8.3.3(b). For the slower test, the model predicts the strain values of the initial cycle reasonably well. This may well be a coincidence because the magnitude of the axial strain is in question due to the inadequate deformation measurement facilities of the testing system (see Section 7.4.2).

At this stage, it becomes obvious that no further research into the response to cyclic loading is feasible until the triaxial testing system is improved to include more frequent data logging, data storage to disk, and independent deformation measurement.

CHAPTER 9

CONCLUSIONS

The objective of this research was the development of a constitutive model for the behaviour of clay under cyclic loading, on the basis of a sound understanding of the material response to load. The development process would then provide an awareness of the concepts involved in the formulation of constitutive relations, and more specifically, in the implementation and application of a constitutive model for soil under cyclic loading.

A review of the roles of constitutive modelling in mechanics, showed that the need to specify the loading and unloading criteria limited the usefulness of elastic theories in the modelling of cyclic loading. The application of the constitutive models to clays can be achieved with the critical state concept. Critical state theory provides a framework for the understanding of soil behaviour from a consideration of the initial stress state and the load path. The conceptual model can then be developed into a constitutive model using plasticity theory. This method has the advantage that the parameters have physical meaning and can also be determined from standard laboratory tests.

Constitutive laws for cyclic loading of clay were reviewed in order to find a model that could accurately predict the behaviour of clay under cyclic loading, but still have parameters that could be determined from available laboratory tests. Many models have been proposed, but very few published papers provide predictions for a significant number of cycles. Two approaches to modelling emerged, generalised models with many parameters, as opposed to simpler, empirical modifications of the critical state theory.

The model that was developed in this research work, is an extension to the isotropic hardening plasticity model, employing the Modified Cam-clay yield surface formulated by Carter, Booker and Wroth (1982). The Cam-clay yield surface was applied in addition to the Modified Cam-clay surface and four parameters are needed for the prediction

of static loading. The modelling of the cyclic loading is derived from the translation of the failure surface during unloading, for which an additional parameter θ is required. The model assumes that the yield surface is reduced on unloading, in an isotropic manner, in proportion to the change in the current stress state due to the unloading. This change in the yield surface is expressed by the degradation parameter θ.

The model was implemented into a finite element program so that the model could be used in the solution of boundary value problems. The program that was selected for this purpose is the Critical State Program, CRISP, which was developed specially for clay materials and other geotechnical engineering applications. No graphical output is provided, and therefore a post-processing program was written to graphically relate the critical state parameters for each analysis. A pre-processor was written to produce input data consisting of a triangular wave form, with a choice of stress or strain control, and either one-way or two-way loading.

Solution techniques for the nonlinear equilibrium equations are seldom mentioned in the literature on constitutive modelling of soils under cyclic loading. A study of nonlinear finite element techniques showed that the predictor phase of the Newton Raphson solution scheme influences the convergence of the solution, and the corrector phase affects the accuracy. In addition, convergence of the solution is affected by the penalty function method used to model the two phase behaviour of the soil.

The tangent predictor implemented in CRISP was modified for cyclic loading by introducing a combined stiffness algorithm. This method was found to ensure the stability of the numerical solution by forcing the tangent stiffness at unloading to be elastic. Major modifications of the program were required, resulting in substantial supplementary programming.

The model was evaluated by comparing backpredictions from a finite element analysis and observations of cyclic triaxial tests on clay, obtained from literature. The comparison showed that the model was

most appropriate for one-way, stress controlled loading and two-way, strain controlled loading. The predictions under one-way strain controlled loading could not be evaluated because of the lack of literature for these tests. The model does not show the hysteresis loops that occur in two-way stress controlled tests, which would require a kinematic hardening plasticity approach. Hysteresis is not observed in the stress - strain curves for one-way stress controlled loading, but does occur for two-way strain control.

The major achievement of the model is the ability to predict the accumulation in permanent strain that results from the cyclic loading. In undrained conditions, the resulting pore pressure increase causes a migration of the effective stress path. The model can therefore show the experimentally observed degradation in ultimate strength due to the cyclic loading. In two-way strain controlled conditions, the peak deviator stress decreases as the stress path migrates toward failure, in good accordance with laboratory test results.

The experimental part of this research consisted of cyclic triaxial tests performed on a local Kaolin. A GDS Triaxial Testing System was available which could only perform one way stress controlled tests. The tests were performed to determine the model input parameters and provide data for further evaluation of the model predictions.

The results showed that the trends in the stress, strain and pore pressure response of the Kaolin corresponded well to the behaviour of similar materials observed from literature. The stress state being below the critical level of repeated loading, the pore pressure and strain reach a stable state where no additional change occurs. The stress - strain curves show a characteristic S - shape, with the strain always returning to zero at the end of unloading. The test program was limited by the time constraints of the research work and the commercial demands on the machine.

The output from the control system consistently underestimated the deformation of the sample because of the deformation measurement technique programmed into the system. The system must be modified to

include independent deformation measurements for reliable results, but this was considered to be outside of the scope of this research.

The model with a Cam-clay yield surface, consolidated with an overconsolidation ratio of 1,12, was found to provide the best prediction of the soil behaviour in the static triaxial tests and this was employed for the backprediction of cyclic triaxial tests. An analytical approach for determining the model parameter directly from laboratory tests was developed. The method is based on the transformation of the laboratory data in the $v_\lambda - \eta$ coordinates which were used to determine the critical state parameters. The application of the method to the cyclic triaxial test results on Kaolin showed that the degradation parameter θ was not constant with the number of cycles, as assumed in the model. There is, however, insufficient data available to substantiate any relationship between degradation parameter θ and either the number of cycles, or the accumulated plastic strain.

Modelling of clays under cyclic loading cannot advance until a substantial effort is made to provide enough laboratory testing to fully understand the mechanisms of the soil response. This should distinguish between the general behaviour of the clay material and the specific nature of each particular clay type. Further research should also investigate the effect of the interaction of the soil mass with structural elements, both of which are important for design practice.

The experimental research should not proceed in isolation from the constitutive modelling because the subjects are complementary. Developments in one field will result in advancement in the other, and can thus achieve the ultimate aim of a generalised constitutive model.

This research work has shown that the results are dependent on the assumptions made in the formulation and solution of the constitutive laws and in the computer programs selected but these assumptions are

not always evident. Specifically, the application of a constitutive model requires understanding of the expected material response to obtain a meaningful analysis. The model that has been developed has limitations. It is not valid for certain load paths, but achieves a coherent means of qualitatively predicting the response of clay to cyclic loading with a minimum of parameters. However, used with judgement, the model provides the ability to predict the behaviour of clays under cyclic loading until more generalised models are available.

LIST OF REFERENCES

ANDERSON, K.H., BROWN, S., FOSS, I., POOL, J.H., ROSENBRAND, W.F. (1976). "Effect of cyclic loading in clay behaviour", Design and Construction of Offshore Structures; ICE, London, pp 75 - 79.

ATKINSON, J.H. (1981). "Foundations and Slopes: An introduction to applications of critical state soil mechanics"; McGraw-Hill, London.

ATKINSON, J.H., BRANSBY, P.L. (1978). "The Mechanics of Soils; An introduction to critical state soil mechanics"; McGraw-Hill, London.

ATKINSON, J.H., RICHARDSON, D. (1985). "Elasticity and Normality in Soil-Experimental Examinations"; Geotechnique, 35, No 4, 443 - 449.

BANERJEE, P.K., BUTTERFIELD, R.(Eds) (1985)."Developments in Soil Mechanics and Foundation Engineering - 2; Stress and strain modelling of soils"; Elsevier, NY.

BATHE, K., WILSON, E.L. (1976). "Numerical Methods in Finite Element Analysis"; Prentice - Hall, New Jersey.

BARDEN, L. (1971). "Examples of Clay Structure and Its Influence on Engineering Behaviour"; Stress-Strain Behaviour of Soils, Parry, R.G.H Ed); Proc. Roscoe Memorial Symposium, Foulis and Co. pp 195-205.

BRITTO, A.M., GUNN, M.J. (1987). "Critical State Soil Mechanics via Finite Elements"; Ellis Horwood, Chichester.

BUTTERFIELD, R.E. (1979), "A Natural Compression Law for Soils (An advance on e-log p')"; Geotechnique, 29, pp 469-480.

CAKMAK, A.S. (Ed) (1987). "Soil Dynamics and Liquefaction"; Elsevier, N Y.

CALLADINE, C.R. (1963). Correspondence: "The Yielding of Clay", Geotechnique, 13, pp 250-255.

CARTER, J.P., BOOKER, J.R., WROTH, C.P. (1982). "A Critical State Soil Model for Cyclic Loading"; Soil Mechanics - Transient and Cyclic Loads, (Pande, G.N. and Zienkiewicz, O.C., Eds.); John Wiley and Sons Ltd., pp 219-252.

CASAGRANDE, A. (1948). "Classification and Identification of Soils"; Transactions of the American Society of Civil Engineers, Vol. 113, p 901.

CHEN, W.F., BALÁDI, G.Y. (1985). "Soil Plasticity - Theory and Implementation"; Elsevier, N Y.

CHEN, W.F.,SALEEB, A.F. (1982). "Constitutive Equations for Engineering Materials; Vol.1 - Elasticity and Modelling"; Wiley - Interscience, New York.

DAFALIAS, Y.F. (1986). "Bounding Surface Plasticity; I: Mathematical Foundation and Hypoplasticity"; ASCE, J of Engineering Mechanics, Vol 112, No EM 9, Sept., pp 966-987.

DAFALIAS, Y.F. (1986). "On Elastoplastic Viscoplastic Constitutive Modelling of Cohesive Soils"; Geomechanical Modelling in Engineering Practice, (Dungar, R., Studer, J.A., Eds), A.A. Balkema, Rotterdam, pp 313 - 330.

DAFALIAS, Y.F., HERMANN, L.R. (1986), "Bounding Surface Plasticity, II: Application to Isotropic Cohesive Soils"; ASCE, J. of Engineering Mechanics, Vol. 112, No. EM 12, Dec.,pp 1263-1292.

DAFALIAS, Y.F., HERMANN, L.R.(1982). "Bounding Surface Formultion of Soil Plasticity"; Soil Mechanics - Cyclic Transient Loads, (Pande, G.N., Zienkiewicz, O.C., Eds); John Wiley and Sons Ltd. , pp 253 - 282.

DEC (1988),"Vax Fortran, User Manual, Version 5.0"; Digital Equipment Corp., Massachusetts.

DESAI, C.S., SIRIWARDANE, H.J. (1984), "Constitutive Laws for Engineering Materials: with Emphasis on Geologic Materials"; Prentice - Hall, New Jersey.

Di MAGGIO, F.L., SANDLER, I.S. (1971). "Material Model for Granular Soils"; Journal of the Engineering Mechanics Division, ASCE, Vol 97, No EM3, June , pp 935 - 950.

DRUCKER, D.C., GIBSON, R.E., HENKEL, D.J. (1957). "Soil Mechanics and Work-Hardening Theories of Plasticity"; Transactions of the American Society of Civil Engineers; Vol. 122, Paper No. 2864, pp 338-346.

DRUCKER, D.C., PRAGER, W. (1952), "Soil Mechanics and Plastic Analysis on Limit Design"; Quarterly of Applied Mathematics, Vol 10, 1952, pp 157 -165.

DUNCAN, J.M., CHANG, C-Y, (1970). "Nonlinear Analysis of Stress and Strain in Soils"; ASCE, J. Soil Mechanics and Foundations Division, Vol. 96, No SM5, Sept. pp 1629-1653.

DUNGAR, R., STUDER, J.A. (Eds),(1986). "Geomechanical Modelling in Engineering Practice"; A.A. Balkema, Rotterdam.

G D S (1986). "GDS Triaxial Testing System (Version 5): Users Handbook"; GDS Instruments, Surrey, England.

HARDIN, B.O., DRENEVICH, V.P. (1972). "Shear Modulus and Damping in Soils: Measurements and Parameters"; ASCE, J. Soil Mechanics and Foundations Division, Vol. 98, No. SM 6, June, pp 603-624.

HEAD, K.H. (1982). "Manual of Soil Laboratory Testing; Vol. 2: Permeability, Shear Strength and Compressibility Tests"; Pentech Press, London.

HEAD, K.H. (1986). "Manual of Soil Laboratory Testing; Vol. 3: Effective Stress Tests"; Pentech Press, London.

HERMANN, L.R., DAFALIAS, Y.F., De NATALE, J.S. (1982). "Numerical Implementation of a Bounding Surface Soil Plasticity Model"; Int. Symp. on Numerical Models in Geomechanics, ZÜrich, Sept , A.A. Balkema, Rotterdam. pp 334-343.

HILL, R. (1950). "The Mathematical Theory of Plasticity"; Oxford University Press, 1950.

HOLTZ, R.D.,KOVACS, W.D. (1981). "An Introduction to Geotechnical Engineering"; Prentice-Hall, New Jersey.

HUEKEL, T., NOVA, R. (1979). "Some Hysteresis Effects of the Behaviour of Geologic Media"; Int. J. Solids Structures, Vol. 15, pp 625 - 642.

IRONS, B.M. (1970). "A Frontal Solution Program for Finite Element Analysis"; Int. J. Num. Meth. in Engineering, Vol. 2, pp 5 - 32.

JAIN, S.K. (1980). "Fundamental Aspects of the Normailty Rule and their Role in Deriving Constitutive Laws of Soils"; Engineering Publications, Blacksburg.

JAUNZEMIS, W. (1067). "Continuum Mechanics"; MacMillan, New York.

KO, H-Y., STURE, S. (1981). "State of the Art: Data Reduction and Application for Analytical Modeling"; Laboratory Strength of Soils, ASTM, Special Technical Publication 740, (Yong, R.N., Townsend, T.C. Eds), pp 329-386.

KONDNER, R.L. (1963). "Hyperbolic Stress-Strain Response: Cohesive Soils"; ASCE, J. of Soil Mechanics and Foundations Division, Vol. 89, No. SM1, pp 115-143

KRIEG, R.D., KRIEG, D.B. (1977). "Accuracies of Numerical Solution Methods for the Elastic-Perfectly Plastic Model"; Transactions of the ASME, J. of Pressure Vessel Technology, Nov., pp 510-515.

LUONG, M.P. (1980). "Stress-Strain Aspects of Cohesionless Soils under Cyclic and Transient Loading"; Proc. Int. Symp. on Soils Under Cyclic and Transient Loading, (Pande, G.N.,Zienkiewicz, O.C., Eds.); A.A. Balkema, Rotterdam, pp 315-324.

MARTIN, J.B. (1975). "Plasticity: Fundamentals and General Results"; M I T Press, Cambridge, Mass.

MATSUI, T., OHARA, H., ITO, T. (1980)."Cyclic Stress - Strain, History and Shear Characteristics of Clay"; ASCE, J. of Geotechnical Engineering; Vol.106, No. GT 10, Oct., pp 1101-1119.

MEIMON, Y., HITCHER, P.Y. (1980). "Mechanical Behavior of Clays Under Cyclic Loading"; Int. Symp. on Soils under Cyclic and Transient Loading, Swansea, (Pande G.N. and Zienkiewicz O.C. Eds); A. A. Balkema, Rotterdam, pp 77-88.

MROZ, Z. (1980). " On hypoelasticity and plasticity approaches to constitutive modelling of inelastic behaviour of soils"; Int. J. for Numerical and Analytical Methods in Geomechanics, Vol. 4, pp 45-55.

MROZ, Z., NORRIS, V. A. (1982)."Elastoplastic and Viscoplastic Constitutive Models for Soils with Application to Cyclic Loading"; Soil Mechanics - Transient Cyclic Loads, (Pande G. N., Zienkiewicz O.C. Eds), John Wiley and Sons Ltd.,N Y, pp 173-219.

MROZ, Z., NORRIS, V.A., ZIENKIEWICZ, O.C. (1981). "An Anisotropic, Critical State Model for Soils Subject to Cyclic Loading"; Geotechnique 31, No 4, pp 451-469.

N A G (1985). "N A G Graphical Supplement"; Numerical Algorithms Group, Oxford.

NAYLOR, D. J., PANDE, G. N., SIMPSON, B., TABB, R. (1981). "Finite Elements in Geotechnical Engineering"; Pineridge Press, Swansea.

NELSON, I. (1977). "Constitutive Models for use in Numerical Computations"; Proceedings of DMSR, Karlsruhe, Sept., Vol.2, A. A. Balkema, Rotterdam. p 45.

NORRIS, V. A., (1986). "Numerical modelling of soil response to cyclic loading using 'stress -reversal surfaces'"; Geomechanical Modelling in Engineering Practice, (Dungar, R., Studer, J.A. Eds), A.A. Balkema, Rotterdam, pp 351-367.

NOVA, R. (1982). "A Constitutive Model for Soil Under Monotonic and Cyclic Loading"; Soil Mechanics - Cyclic and Transient Loads, (Pande, G. N., Zienkiewicz O.C., (Eds), John Wiley and Sons Ltd.,N Y, pp 343-374.

ORTIZ, M., MARTIN, J.B. (1987). "Symmetry - Preserving Return Mapping Algorithms and Incrementally Extremal Paths: A Unification of Concepts"; Report No.14, Applied Mechanics Research Unit, UCT.

ORTIZ, M., POPOV, E.P., (1985). "Accuracy and Stability of Integration Algorithms for Elastoplastic Constitutive Relations"; Int. J. Numerical Methods in Engineering, Vol. 21, pp 1501-1576.

ORTIZ, M., SIMO, J. C. (1986). "An Analysis of a New Class of Integration Algorithms for Elastoplastic Constitutive Relations"; Int. J. Numerical Methods in Engineering, Vol. 23, pp 353-366.

OWEN, D.R.J., HINTON, E. (1986). "Finite Elements in Plasticity, Theory and Practice"; Pineridge Press, Swansea.

PANDE, G. N. (1985). "Multilaminate Reflecting Surface Model and its Applications"; Developments in Soil Mechanics and Foundation Engineering, (Banerjee P.K. and Butterfield R. Eds); Elsevier Applied Science, Vol. 2, pp 69-104.

PANDE, G.N., PIETRUSZCZAK, S. (1986). "A critical look at constitutive models for soils"; Geomechanical modelling in engineering practice, (Dungar, R., Studer, J.A. Eds); A.A. Balkema, Rotterdam, pp 369-395.

PEACOCK, W.H.,SEED, H.B. (1968). "Sand Liquefaction Under Simple Shear Conditions"; ASCE, J. of Soil Mechanics and Foundations Division, Vol. 94, No.3, Mar., pp 689-708.

PENDER, M.J. (1977). Discussion: " Generalized Cap Model for Geological Materials"; ASCE, Journal of the Geotechnical Engineering Division, Vol. 103, No. GT7, July, pp 821-822.

PENDER, M.J. (1978). "A Model for the Behaviour of Overconsolidated Soil"; Geotechnique, 28, pp 1-25.

PENDER, M.J. (1982)."A model for the cyclic loading of over consolidated soil"; Soil Mechanics - Cyclic and Transient Loads, (Pande, G.N., Zienkiewicz, O.C. Eds), John Wiley and Sons Ltd., pp 283-312.

PEREGO, U. (1987). "Explicit Backward Difference Operators and Consistent Predictors for Linear Hardening Elastic-Plastic Constitutive Laws"; UCT/CSIR Applied Mechanics Research Unit, Technical Report, No.91.

PIETRUSZCZAK, S., POOROOSHASB, H.B. (1985). "On Modelling of Cyclic Behaviour of Soils"; Developments in Soil Mechanics and Foundation Engineering, (Banerjee, P.K. and Butterfield, R. Eds); Vol 2, Elsevier Applied Science, pp 139-184.

POTTS, D.M. (1985). "Behaviour of Clay During Cyclic Loading"; Developments in Soil Mechanics and Foundation Engineering, (Banerjee, P.K. and Butterfield, R. Eds), Vol. 2, Elsevier Applied Science, pp 105-138.

PRATER, E.G., STUDER, J.A. (1986). "Material Testing Procedures and Equipment"; Geomechanical Modelling in Engineering Practice, (Dungar, R., Studer, J.A. Eds); A.A. Balkema, Rotterdam, pp 99-134.

PREVOST, J.H.(1986). "Constitutive Equations for Pressure-Sensitive Soils: Theory, Numerical Implementation, and Examples" Geomechanical Modelling in Engineering Practice. (Dungar, R., Studer, J.A. Eds); A.A. Balkema, Rotterdam, pp 331-349.

PREVOST, J.H., HOEG, K. (1975). Soil Mechanics and Plasticity Analysis of Strain Softening"; Geotechnique, 25, No 2, pp 279-297.

PROCTER, D.C., KHAFFEF, J.H. (1984). "Cyclic Triaxial Tests on Remoulded Clays", ASCE, J. of Geotechnical Engineering. Vol. 110, No. GT10; Oct., pp 1431-1445.

PYKE, R. (1986). "The Use of Linear Elastic and Piecewise Linear Models in Finite Element Analysis"; Geomechanical Modelling in Engineering Practice, (Dungar, R.,Studer, J.A. Eds), A.A. Balkema, Rotterdam, pp 167-188.

REDDY, J.N. (1984). "Energy and Variational Methods in Applied Mechanics with an Introduction to the Finite Element Method"; John Wiley and Sons Ltd., New York.

RESENDE, L., MARTIN, J.B. (1985). "Formulation of Drucker-Prager Cap Model"; ASCE, J. of Engineering Mechanics Division, Vol. 111, No. EM7, pp 855-881.

RICHARD, R.M.,ABBOTT, B.J. (1975). "Versatile Elastic-Plastic Stress-Strain Formula"; ASCE, J.of Geotechnical Engineering Division, Vol. 101, No.4, Aug., pp 511-515.

ROSCOE, K.H., BURLAND, J.B. (1968). "On the Generalized Stress-Strain Behaviour of 'Wet' Clay"; In Engineering Plasticity, (Heyma, J., Leckie, F. Eds); Cambridge University Press.

ROSCOE, K.H., POOROORSHASB, H.B. (1963). "A Theoretical and Experimental Study of Strains in Triaxial Compression Tests on Normally Consolidated Clays"; Geotechnique, Vol 13. pp 211-240.

ROSCOE, K.H., SCHOFIELD, A.N., THURAIRAJAH, A. (1963). "Yielding of clays in states wetter than critical"; Geotechnique, 13, pp 211-240.

SANDLER, I.S., Di MAGGIO F.L., BALADI, G.Y. (1976). "Generalized Cap Model for Geological Materials"; ASCE, Journal of the Geotechnical Engineering Division, Vol.102, No GT7, July , pp 683-699.

SANGREY, D.A., FRANCE, J.W. (1980). "Peak Strength of Clays After Residual Loading". Int. Symp. on Soils Under Cyclic and Transient Loading, (Pande, G.N., Zienkiewicz, O.C. Eds); A.A. Balkema, Rotterdam, pp 421-430.

SANGREY, D.A.,HENKEL, D.J., ESRIG, M.I. (1969)."The Effective Stress Response of a Saturated Clay to Repeated Loading"; Canadian Geotechnical Journal, 6, pp 241-252.

SCHOFIELD, W., WROTH, P. (1968). "Critical State Soil Mechanics"; McGraw-Hill, London.

SCOTT, R.F. (1984). "Plasticity and Constitutive Relations in Soil Mechanics"; ASCE, J. of Geotechnical Engineering Division, Vol.111, No.3, May, pp 563-605.

SELLERS, E.J. (1987). "Constitutive Modelling of Cyclic Behaviour of Soil"; BSc-Thesis, University of Cape Town.

SHEU, W.Y., CHANG, N.Y. (1987). "Cyclic Behaviour of a Clay: Experiment and Modelling"; Soil Dynamics and Liquefaction, A.S.Cakmak (Ed); Elsevier, Amsterdam.

SILVER, M.L., SEED, H.B. (1971). "Deformation Characteristics of Sand Under Cyclic Loading"; ASCE, J. Soil Mechanics and Foundations Division, Vol. 97, No.SM8, Aug., pp 1081-1098.

SIMO, J.C., TAYLOR, R.L. (1985). "Consistent Tangent Operators for Rate Independent Elastoplasticity"; Comput. Meth. Appl. Mech. Eng., Vol.48, pp 101-118.

TAKAHASHI, M., HIGHT, D.W., VAUGHN, P.R. (1980). "Effective Stress Changes Observed During Undrained Cyclic Material Tests on Clay"; Int. Symp. on Soils Under Cyclic and Transient Loading, (Pande, G.N., Ziekiewicz O.C. Eds); A.A. Balkema, Rotterdam, pp 201-210.

TAYLOR, P. W., BACCHUS, D.R. (1969). "Dynamic Cyclic Tests on a Clay". Proc., VII International Symposium Soil Mechanics and Foundation Engineering, Mexico, pp 401-409.

VAID, V.P.,CHERN, J.C. (1985). "Cyclic and Monotonic Undrained Response to saturated Sands"; Advances in the Art of Testing Soils Under Cyclic Conditions, (Khoshla, V. Ed), ASCE, New York.

VALANIS, K.C., READ, H.E. (1982). "A New Endochronic Plasticity Model for Soils"; Soil Mechanics - Cyclic Transient Loads, (Pande, G.N., Ziekiewicz, O.C. Eds); John Wiley and Sons Ltd., N Y, pp 375-438.

VAN EEKELEN, H.A.M., POTTS, D.M. (1978). "The Behaviour of Drammen Clay Under Cyclic Loading"; Geotechnique, 28, pp 173-196.

VAN EEKELEN, H.A.M. (1977)."Single Parameter Models for Progressive Weakening of Soils by Cyclic Loading". Geotechnique, 27, No 3, pp 357-368.

VAN EEKELEN, H.A.M. (1982). "Fatigue Models for Cyclic Loading"; Soil Mechanics - Transient and Cyclic Loads, (Pande, G.N., Ziekiewicz, O.C. Eds); John Wiley and Sons Ltd.,N.Y, pp 459-468.

VARDOULAKIS, I., DRESCHER, A. (1985). "Behaviour of Granular Soil Specimens in the Triaxial Compression Test", Developments in Soil Mechanics and Foundation Engineering, (Baneriee, P. K., Butterfield, R. Eds): Elsevier Applied Science, Vol.2, pp 215-252.

WILSON, B.P. (1984). "Practical Aspects of the Critical State Model in Soil Mechanics"; MSc-Thesis, University of Cape Town.

WONG, R.T.,SEED, H.B.,CHAN, C.K. (1975). "Cyclic Loading Liquefaction of Gravelly Sands"; ASCE, J. Geotechnical Engineering Division, Vol. 101, No.GT6, June, pp 571-583.

WOOD, D.M. (1982). "Laboratory Investigations of the Behaviour of Soils Under Cyclic Loading: A Review", Soil Mechanics - Cyclic and Transient Loads, (Pande G.N., Zienkiewicz, O.C. Eds); John Wiley and Sons Ltd, N Y, pp 513-582.

WOOD, D.M. (1984). "On Stress Parameters"; Geotechnique, Vol. 34, No 2, pp 282-287.

ZIENKIEWICZ, O.C., HUMPHESON, C., LEWIS, R.W. (1975). "Associated and Non-Associated Visco-Plasticity in Soil Mechanics", Geotechnique, 25, No 4, pp 671-689.

ZIENKIEWICZ, O.C. (1977). "The Finite Element Method"; 3rd Ed., McGraw-Hill, U.K.

ZYTYNSKI, M., RANDOLPH, M.F., NOVA, R., WROTH, C.P.(1978) Short Communications: "On modelling the unloading - reloading behaviour of soils"; International Journal for Numerical and Analytical Methods in Geomechanics, Vol 2, pp 87-94.

Appendix A1 : Mesh plot, four, cubic strain, triangular elements

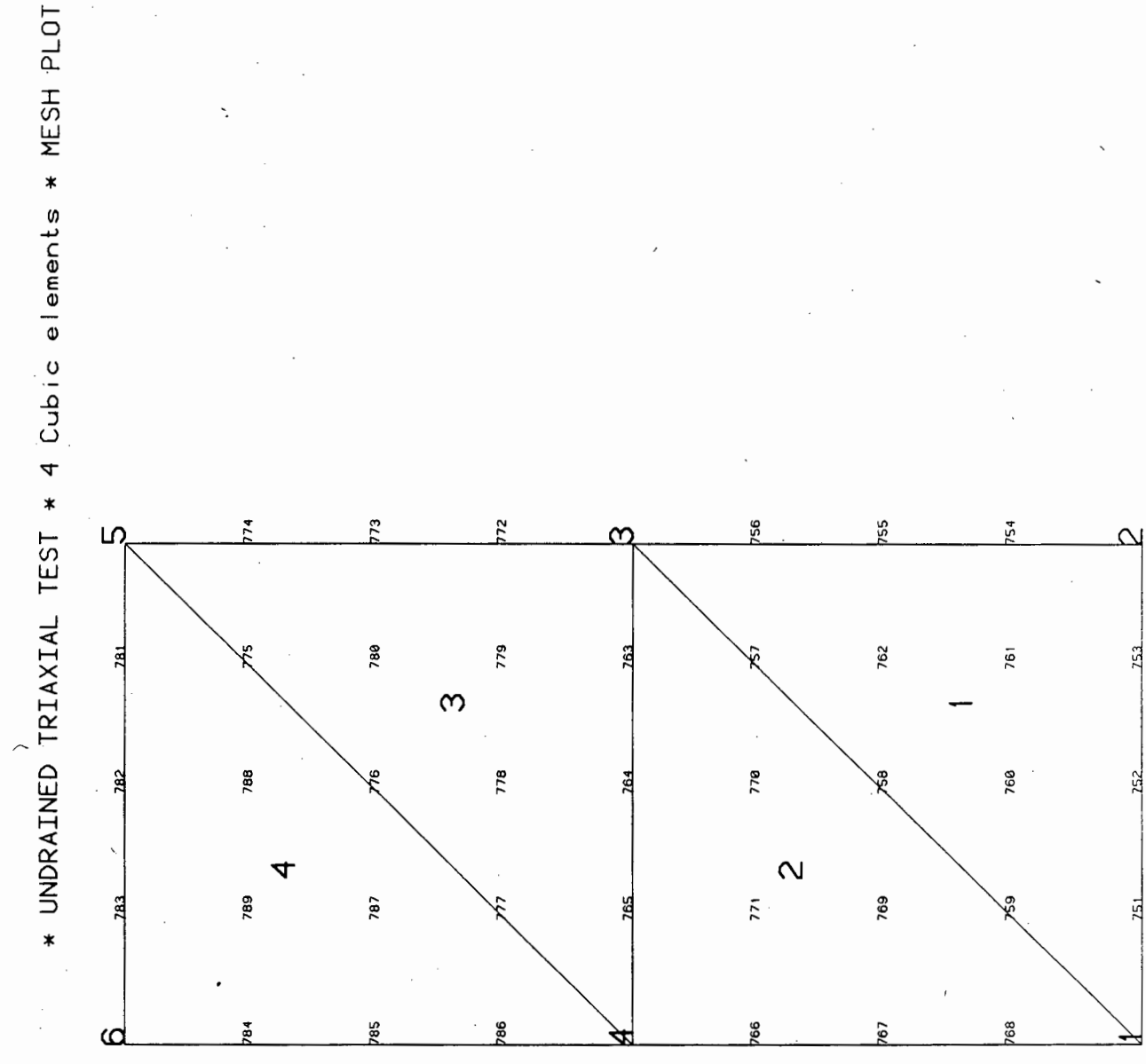

Appendix A2 : Mesh plot, two, cubic strain, triangular elements

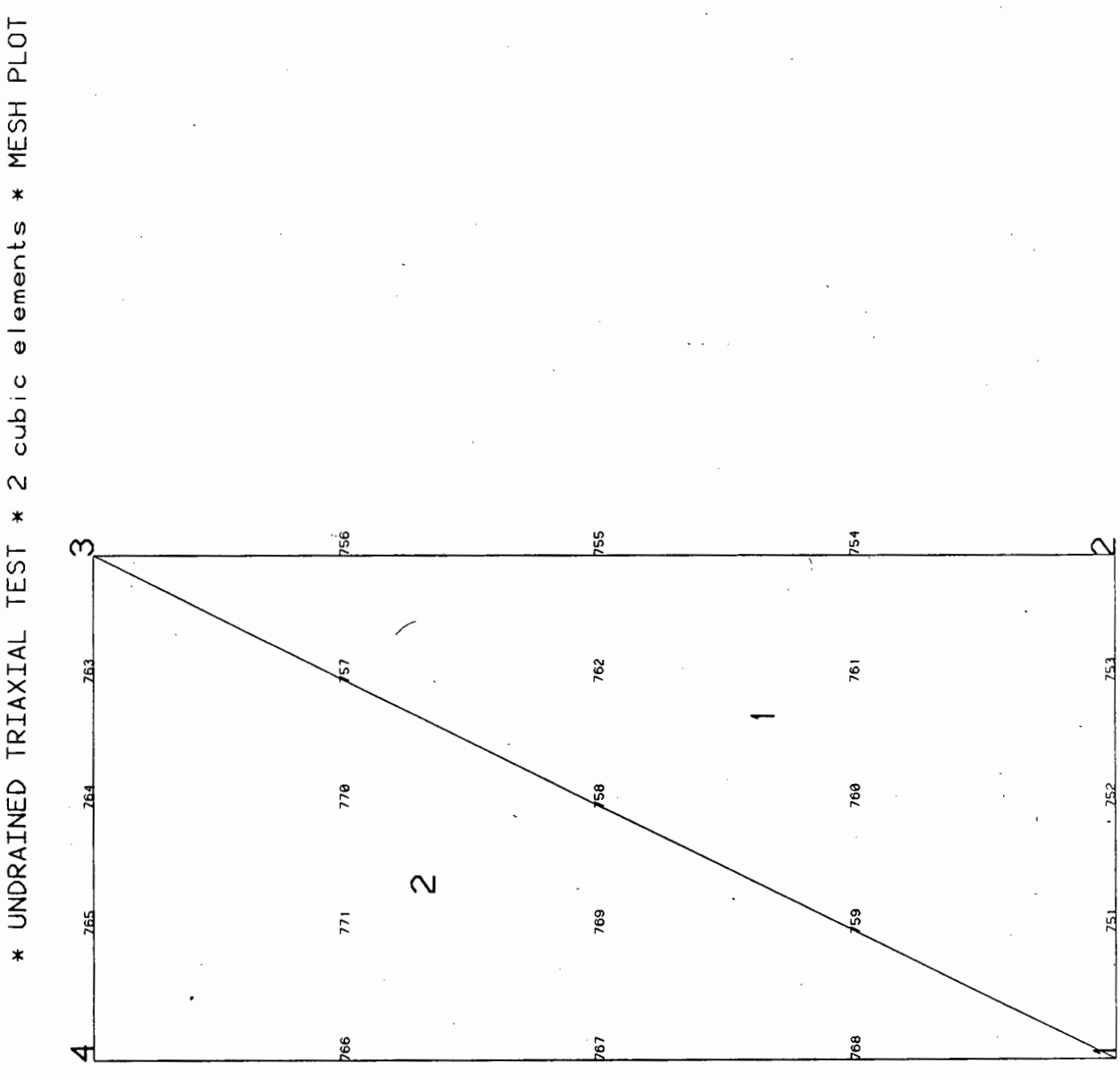

Appendix A3 : Mesh plot, two, linear strain, triangular elements

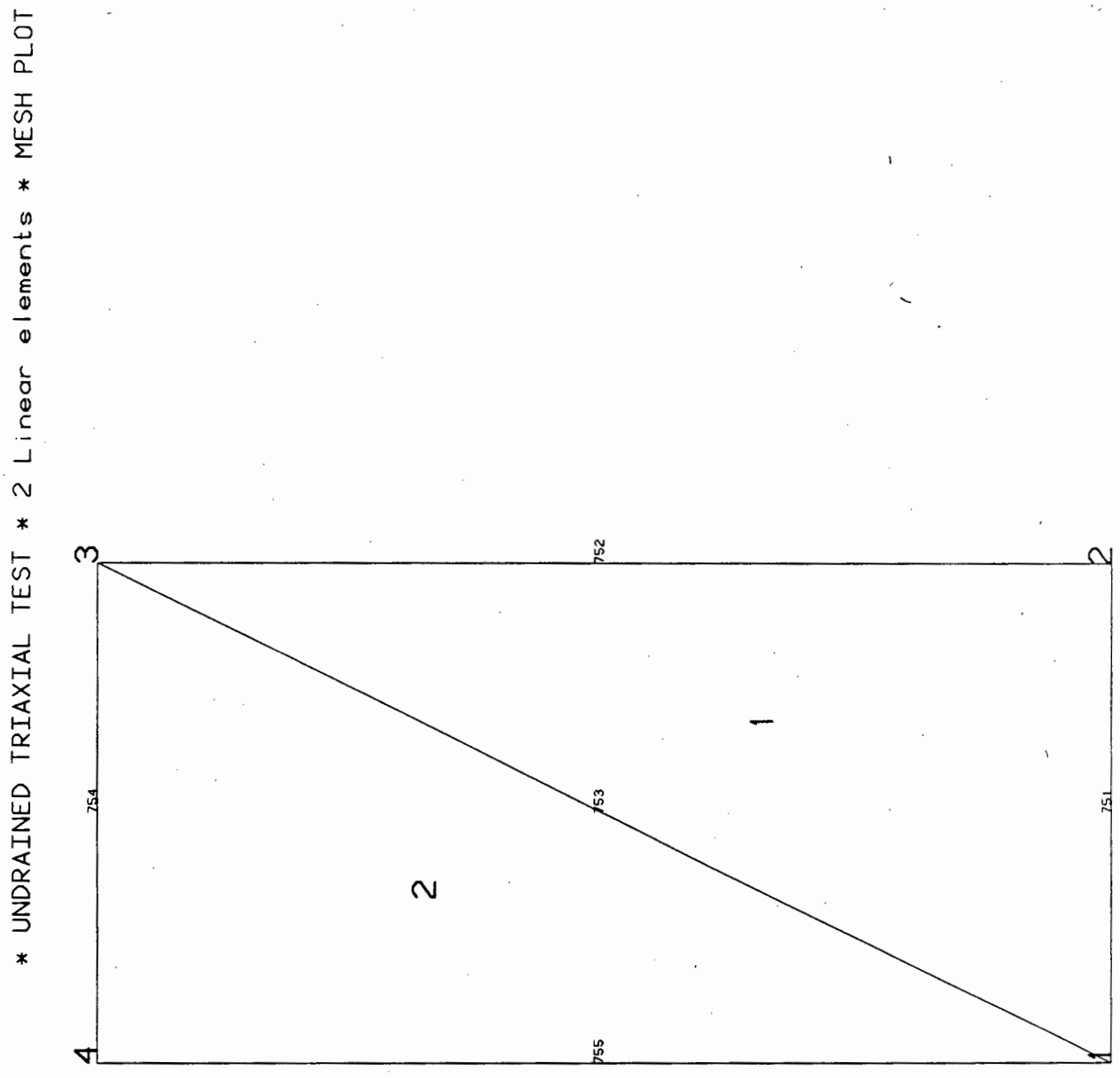

Appendix B1 : Static triaxial test back prediction
(Cam-clay model)

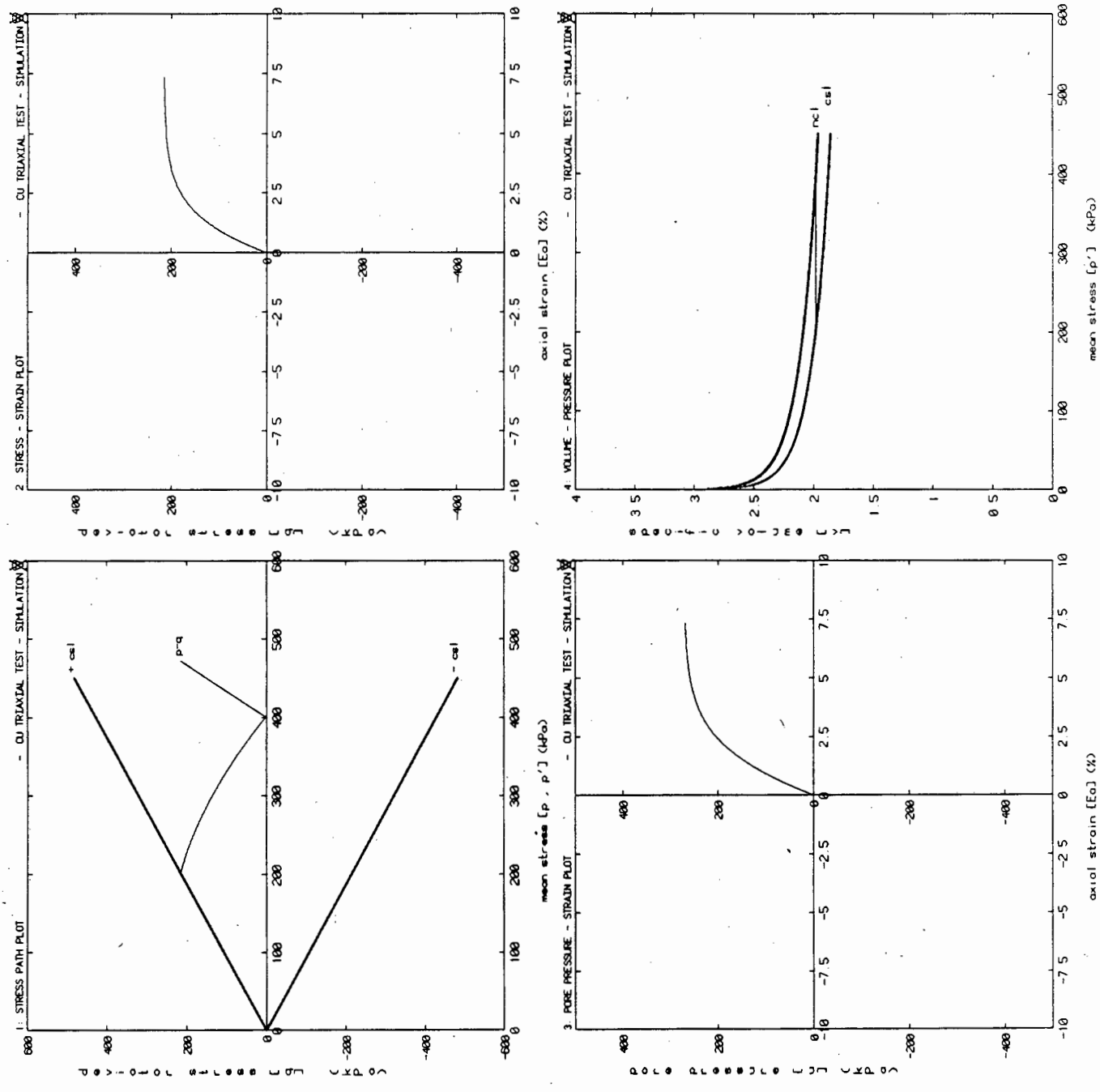

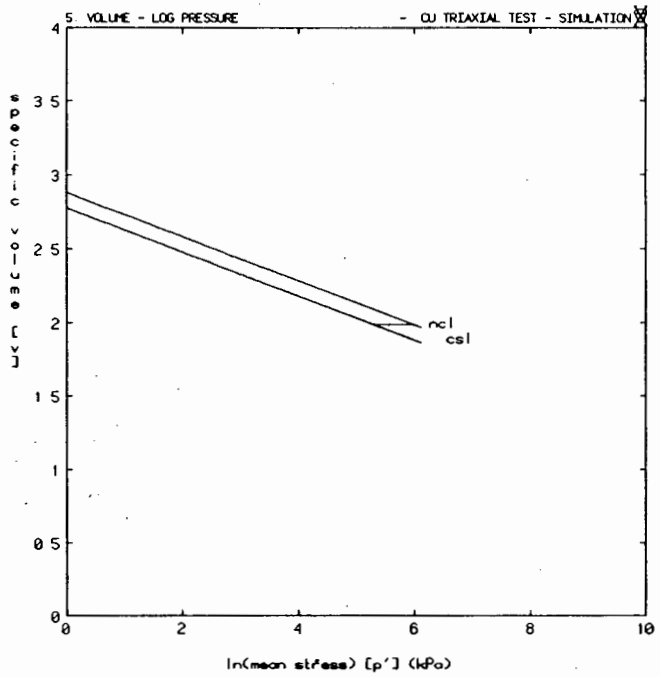
5: VOLUME - LOG PRESSURE - CU TRIAXIAL TEST - SIMULATION
specific volume [v]
ln(mean stress) [p'] (kPa)
ncl
csl

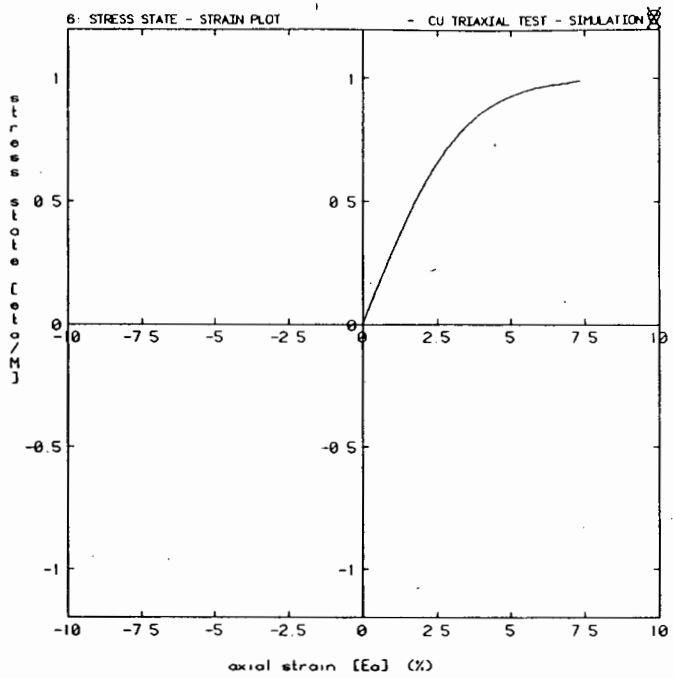
6: STRESS STATE - STRAIN PLOT - CU TRIAXIAL TEST - SIMULATION
stress state [eta/M]
axial strain [Ea] (%)

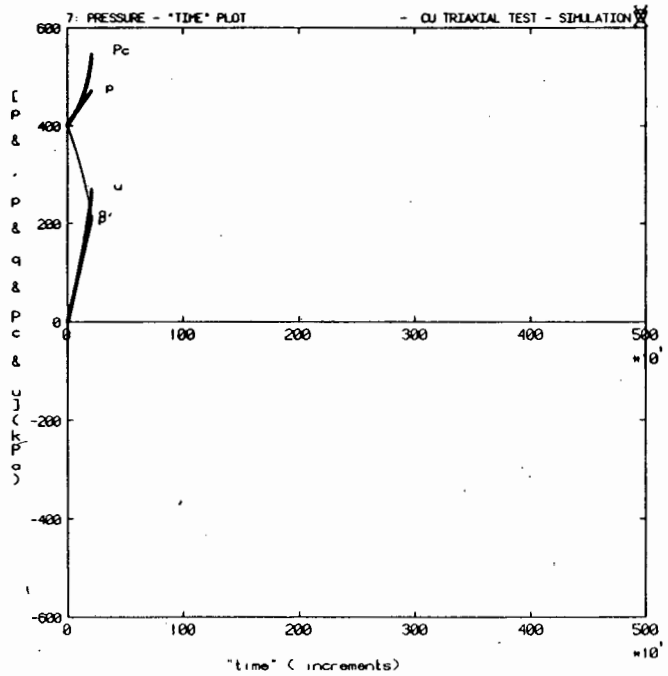
7: PRESSURE - "TIME" PLOT - CU TRIAXIAL TEST - SIMULATION
[p&,p&q&pc&u](kPa)
"time" (increments)
Pc
p
q
β'
u

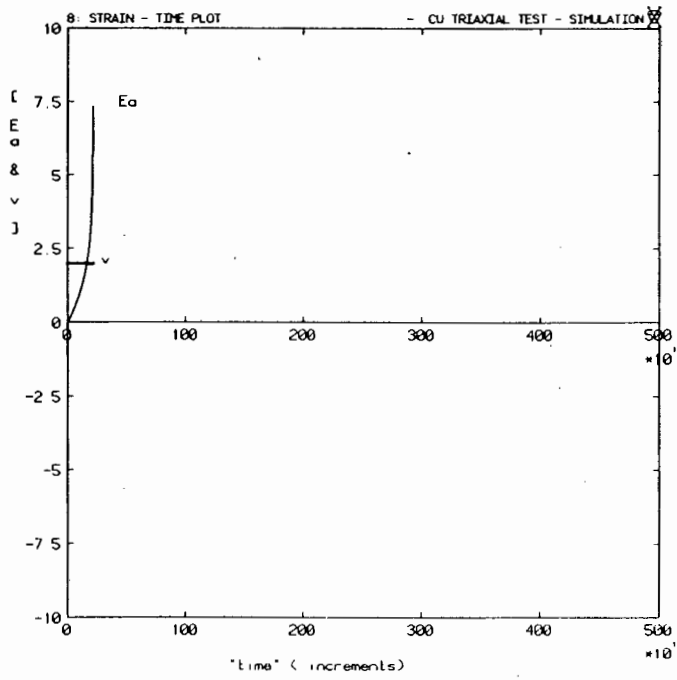
8: STRAIN - TIME PLOT - CU TRIAXIAL TEST - SIMULATION
[Ea&v]
"time" (increments)
Ea
v

Appendix B2 : Static triaxial test back prediction
(Modified Cam-clay model)

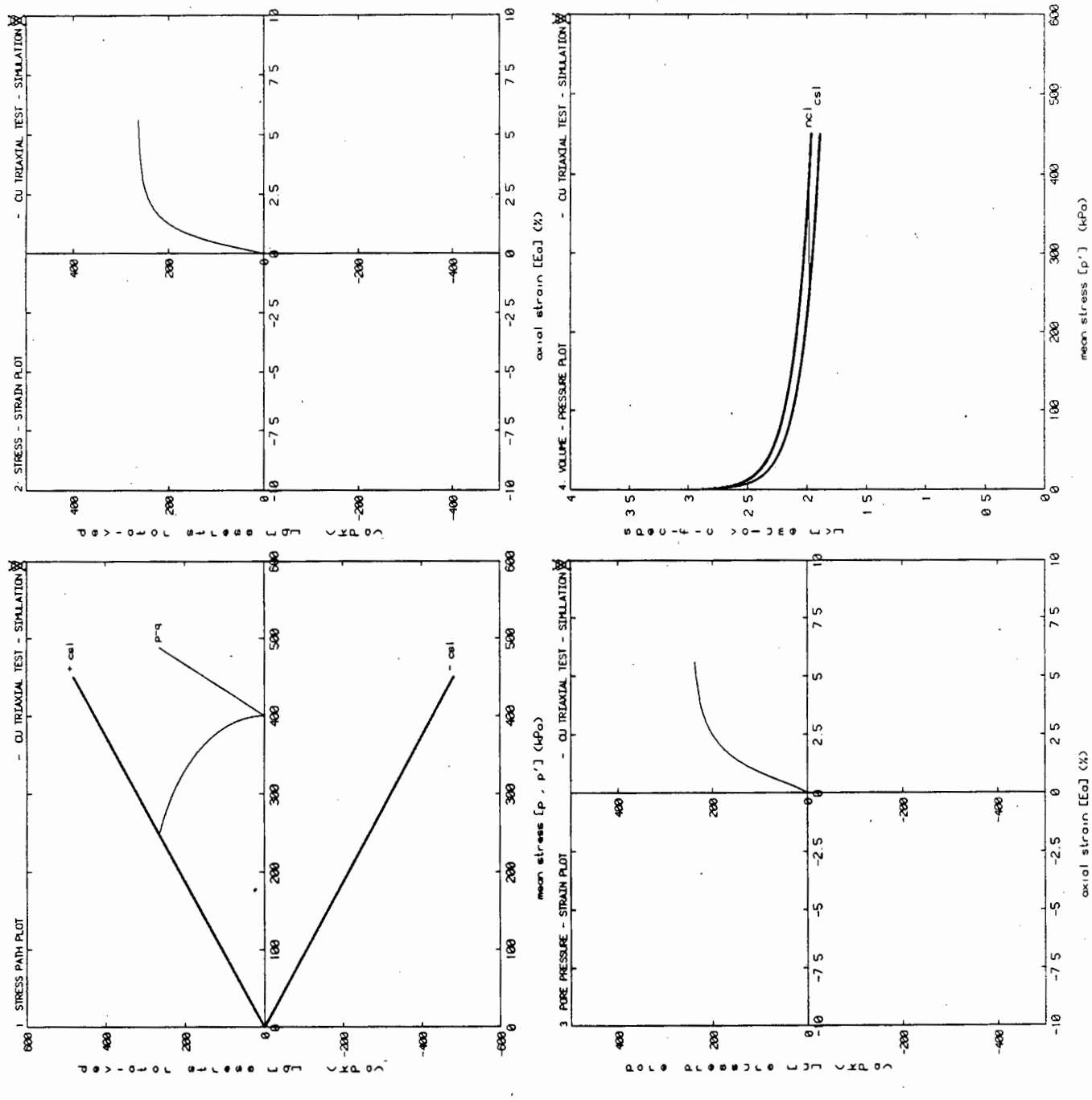

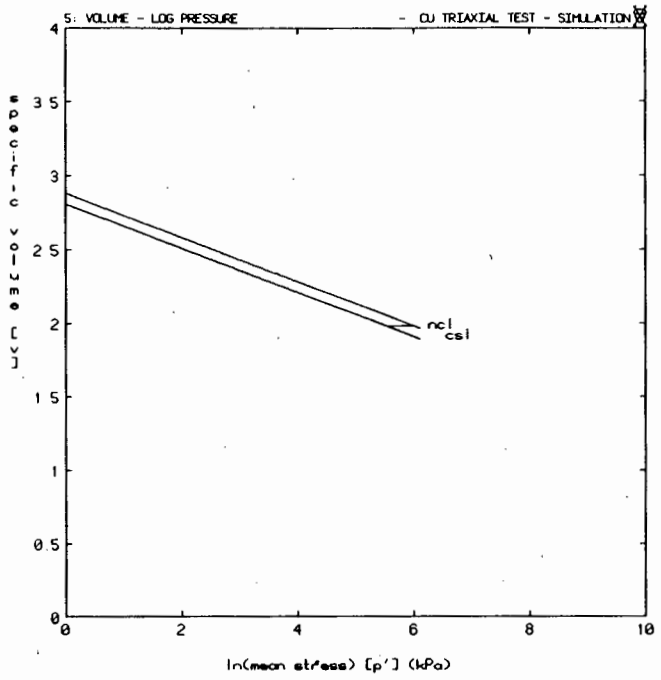
5: VOLUME - LOG PRESSURE - CU TRIAXIAL TEST - SIMULATION
specific volume [v]
ln(mean stress) [p'] (kPa)
ncl
csl

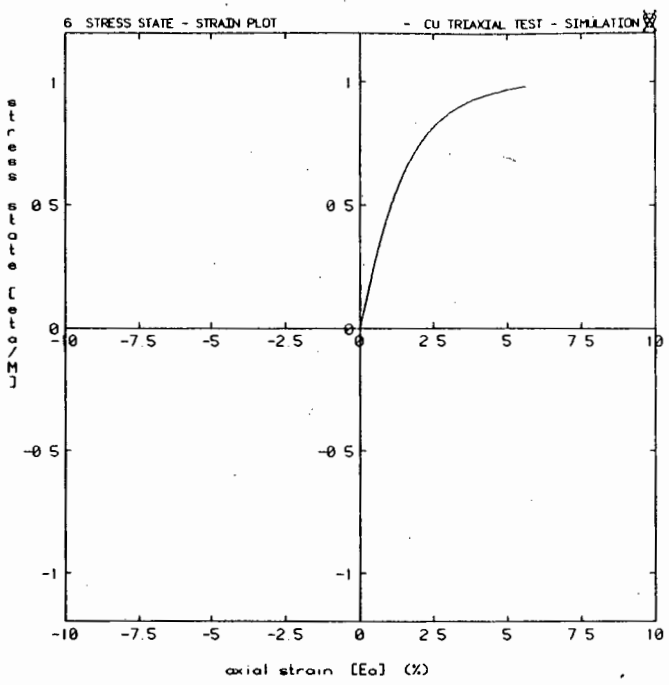
6 STRESS STATE - STRAIN PLOT - CU TRIAXIAL TEST - SIMULATION
stress state [eta/M]
axial strain [Ea] (%)

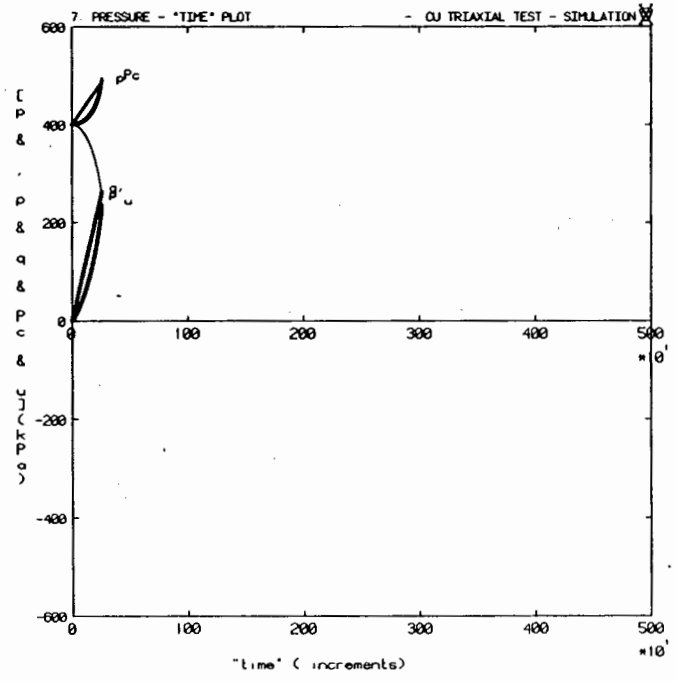
7 PRESSURE - "TIME" PLOT - CU TRIAXIAL TEST - SIMULATION
[p & p & q & Pc & U] (kPa)
pPc
p'c
"time" (increments)
*10'

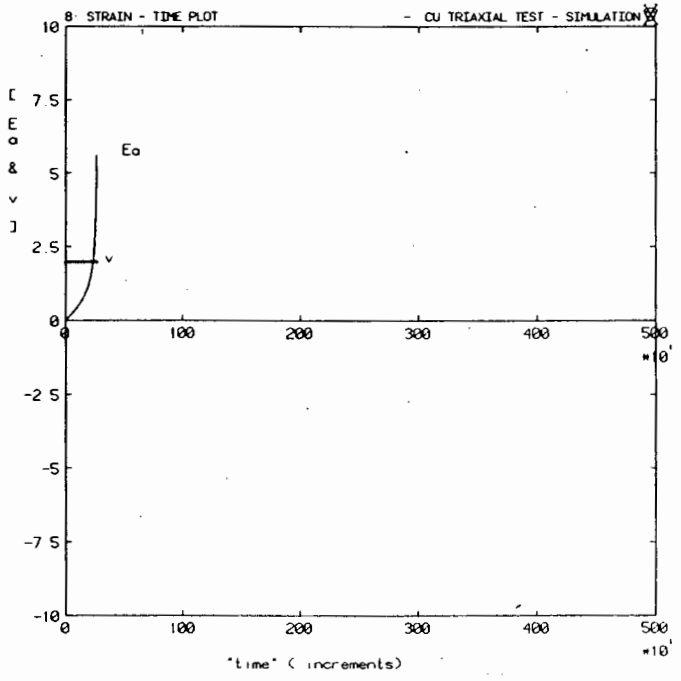
8 STRAIN - TIME PLOT - CU TRIAXIAL TEST - SIMULATION
[Ea & v]
Ea
v
"time" (increments)
*10'

Appendix B3.1: Cyclic triaxial test back prediction
One-way stress control
(Cam-clay model)

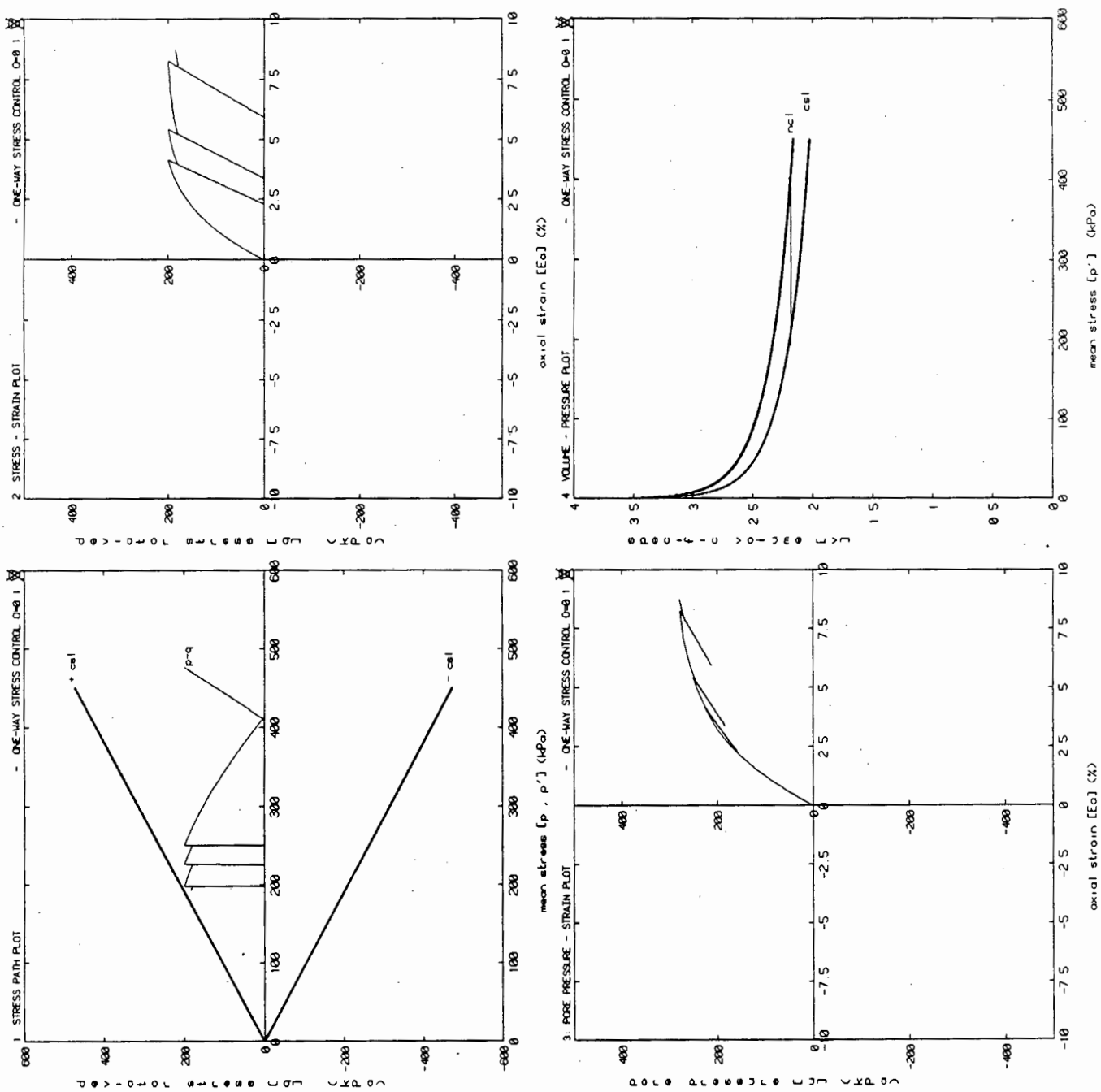

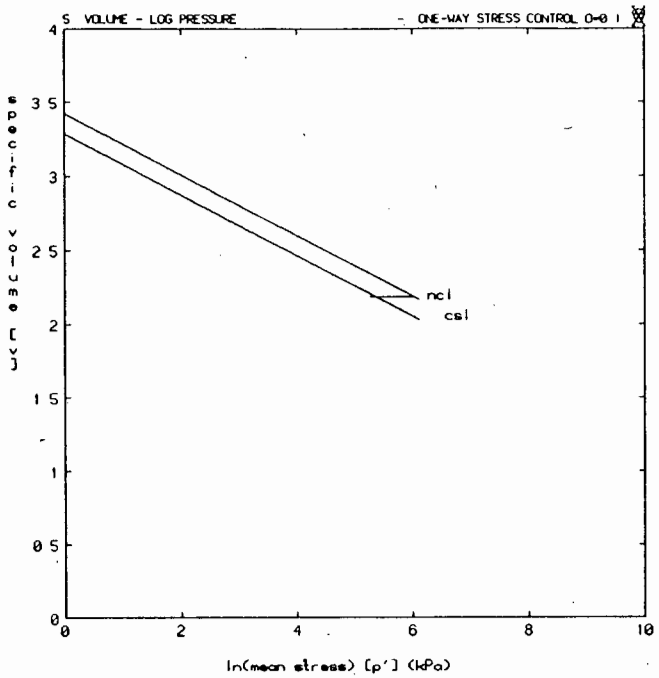
5 VOLUME - LOG PRESSURE
- ONE-WAY STRESS CONTROL O=0 1
specific volume [v]
ncl
csl
ln(mean stress) [p'] (kPa)

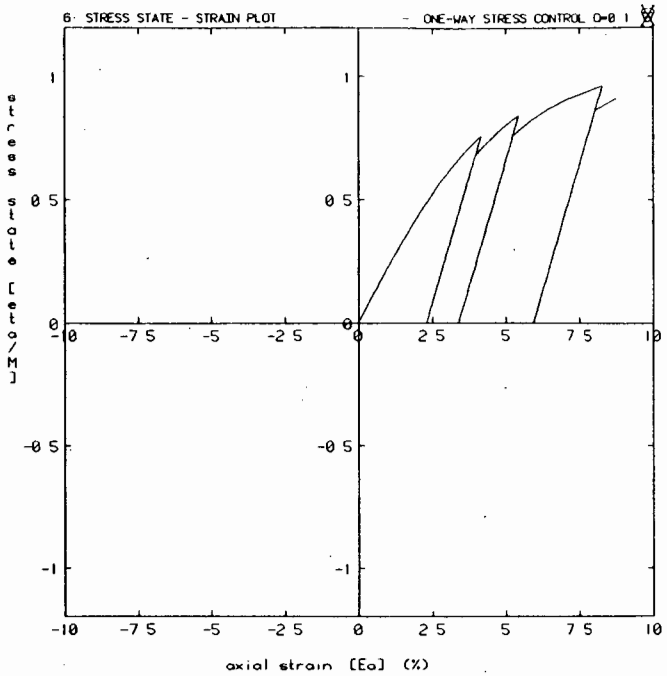
6: STRESS STATE - STRAIN PLOT
- ONE-WAY STRESS CONTROL O=0 1
stress state [eta/M]
axial strain [Ea] (%)

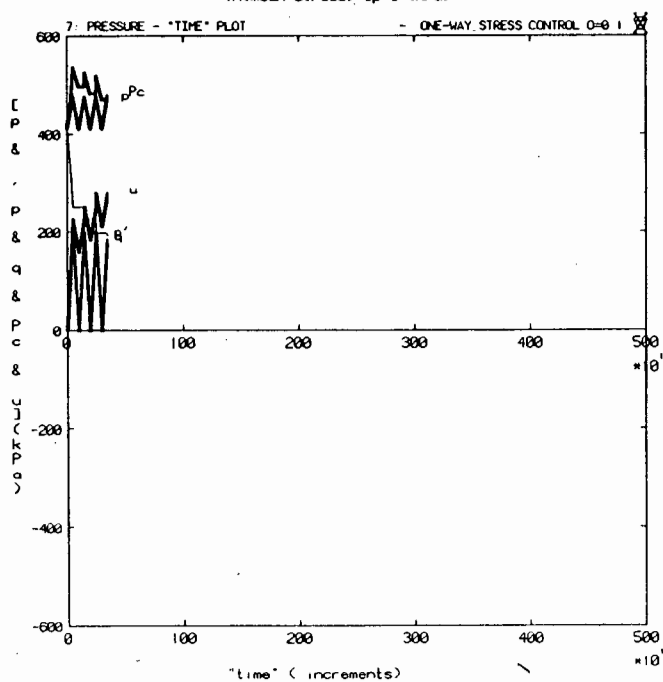
7: PRESSURE - "TIME" PLOT
- ONE-WAY STRESS CONTROL O=0 1
[p&,p&q&pc&u](kPa)
pPc
u
p'
"time" (increments)
*10'

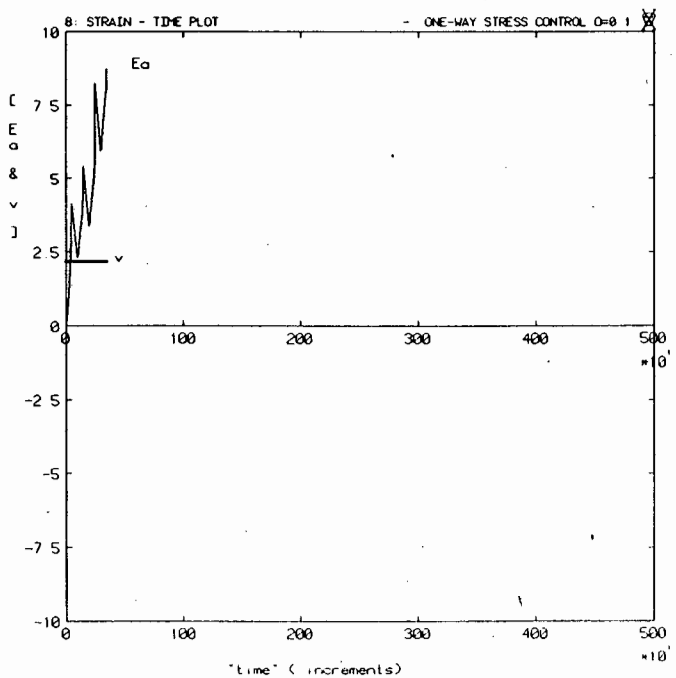
8: STRAIN - TIME PLOT
- ONE-WAY STRESS CONTROL O=0 1
[Ea&v]
Ea
v
"time" (increments)
*10'

Appendix B3.2: Cyclic triaxial test back prediction
One-way stress controlled loading
(Modified Cam-clay model)

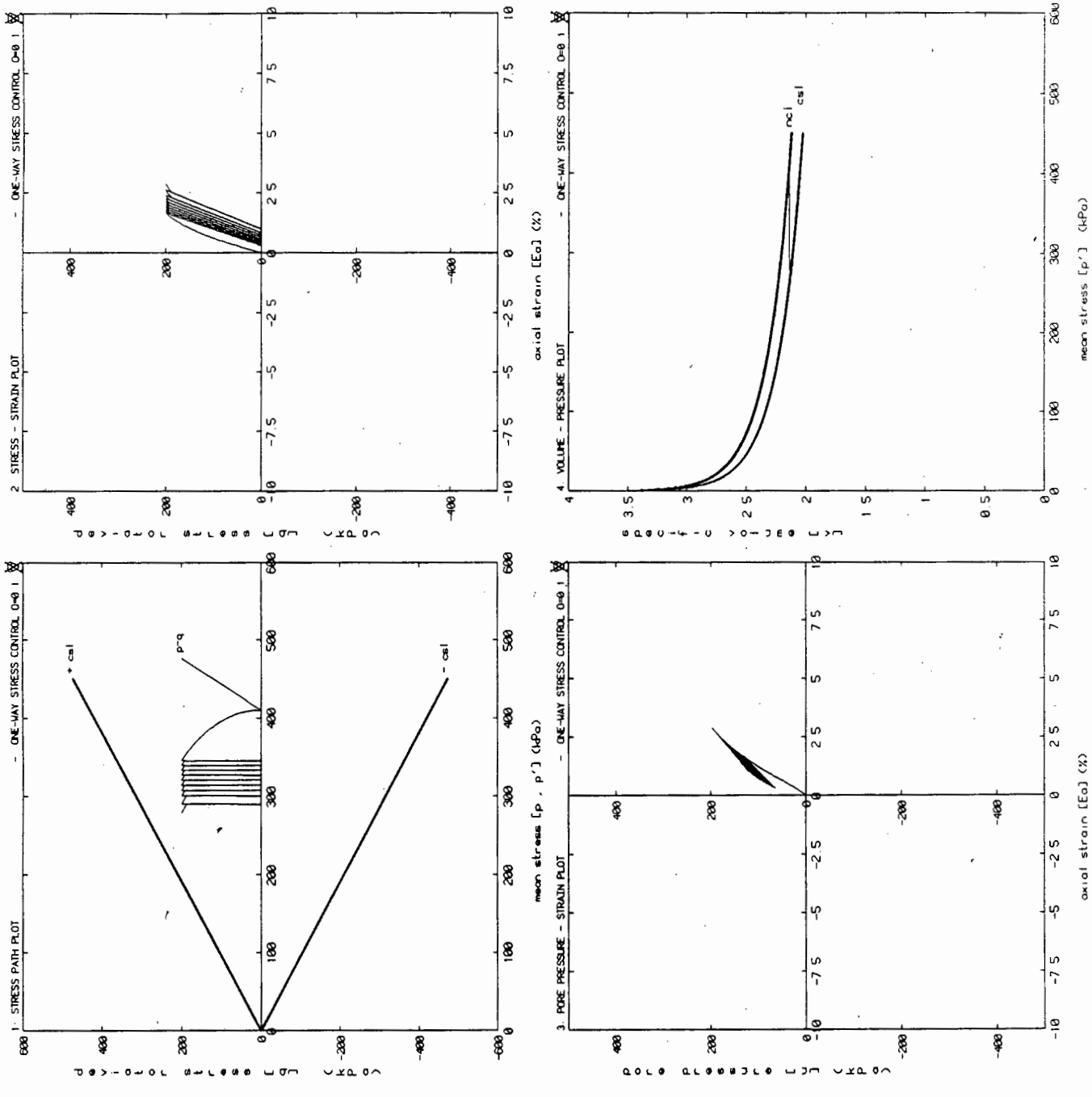

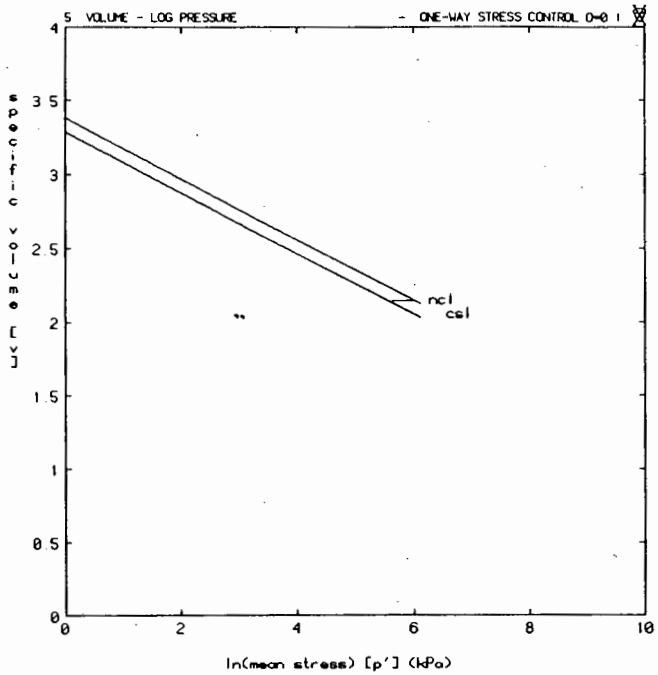
5 VOLUME - LOG PRESSURE
- ONE-WAY STRESS CONTROL O=0 1
specific volume [v]
ln(mean stress) [p'] (kPa)
ncl
csl

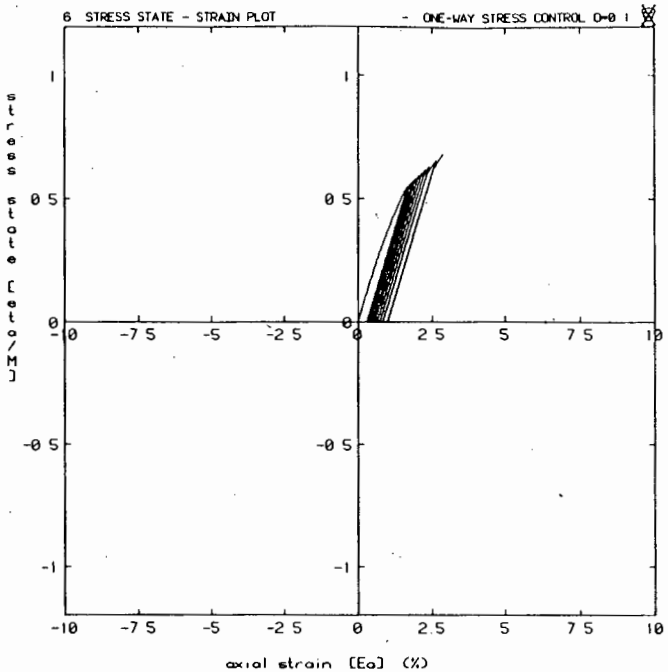
6 STRESS STATE - STRAIN PLOT
- ONE-WAY STRESS CONTROL O=0 1
stress state [eta/M]
axial strain [Ea] (%)

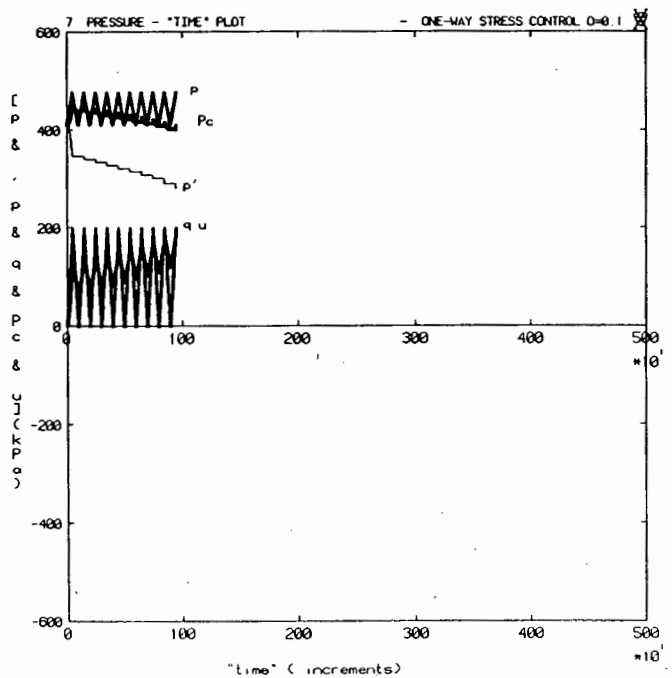
7 PRESSURE - "TIME" PLOT
- ONE-WAY STRESS CONTROL O=0 1
[p & p & q & Pc & U](kPa)
"time" (increments)
P
Pc
p'
q u

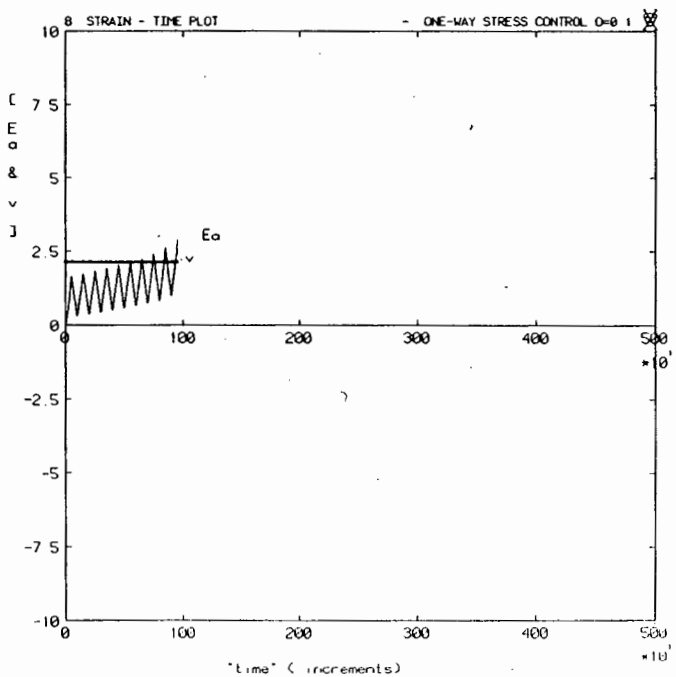
8 STRAIN - TIME PLOT
- ONE-WAY STRESS CONTROL O=0 1
[Ea & v]
"time" (increments)
Ea
v

Appendix B3.3: Cyclic triaxial test back prediction
Two-way stress controlled loading
(Modified Cam-clay model)

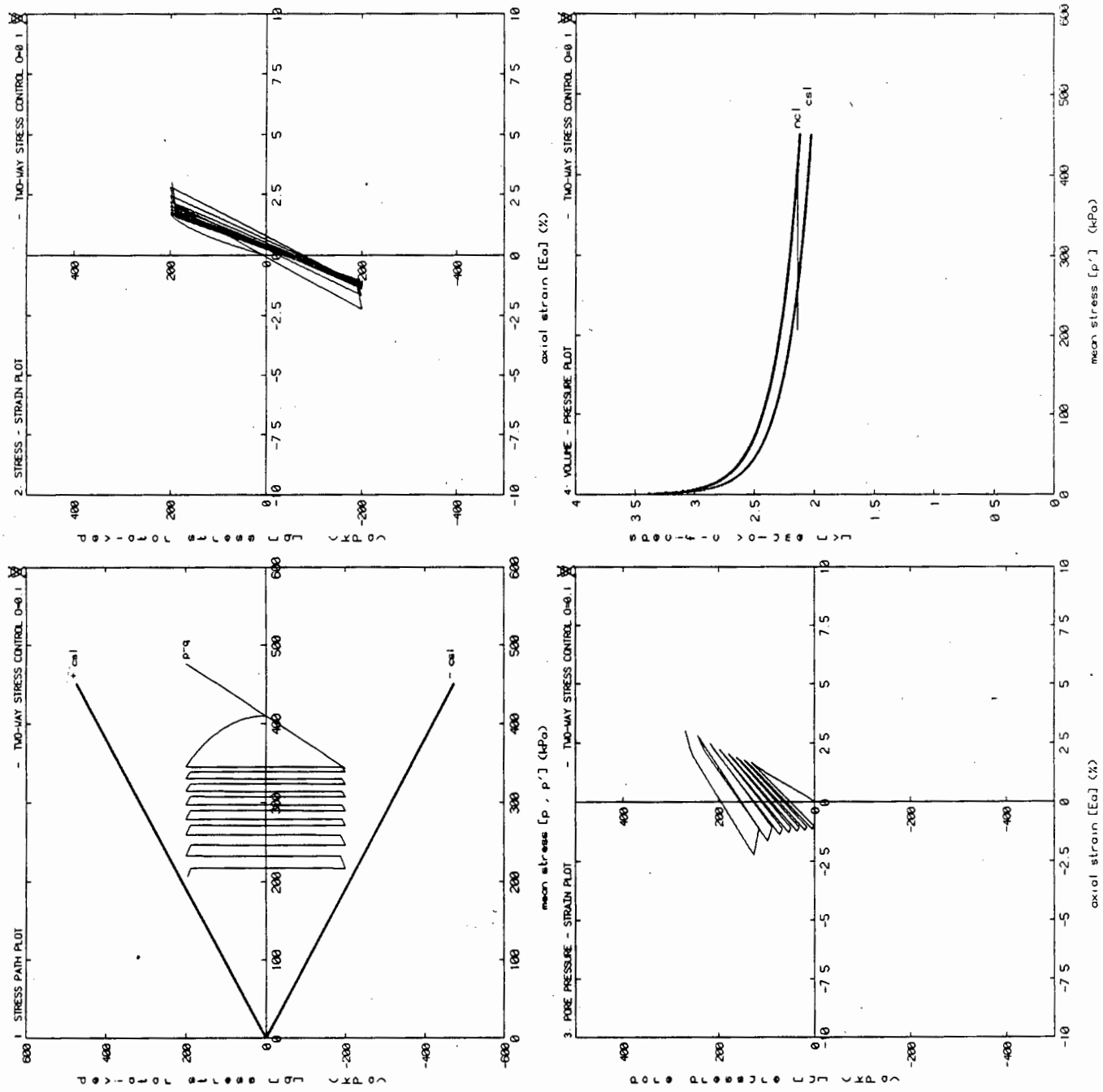

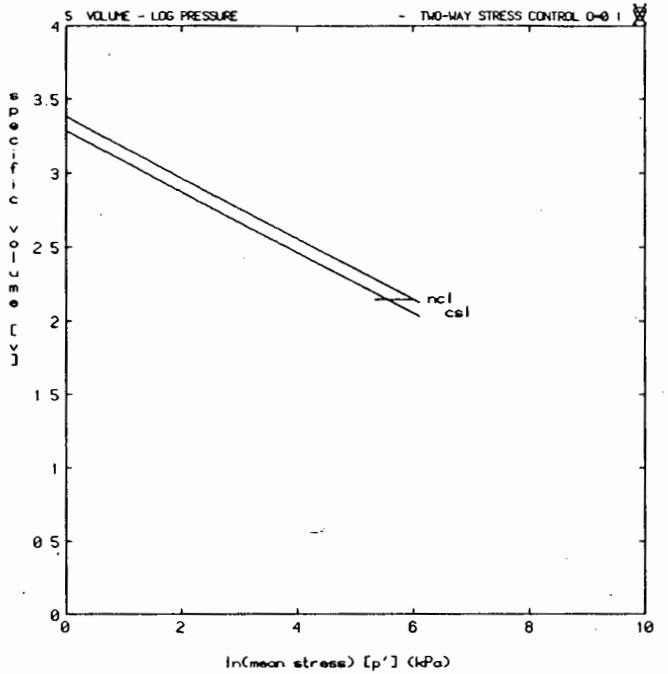
5. VOLUME - LOG PRESSURE - TWO-WAY STRESS CONTROL O=0.1
specific volume [v]
ln(mean stress) [p'] (kPa)
ncl
csl

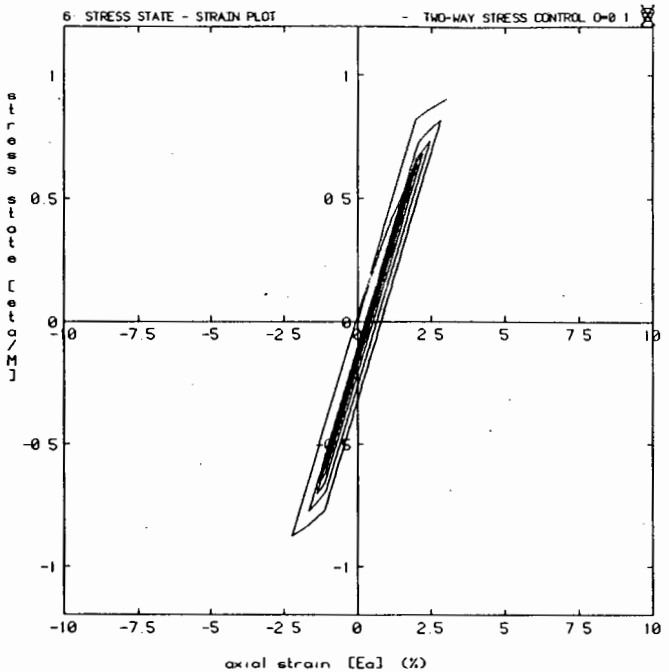
6. STRESS STATE - STRAIN PLOT - TWO-WAY STRESS CONTROL O=0.1
stress state [eta/M]
axial strain [Ea] (%)

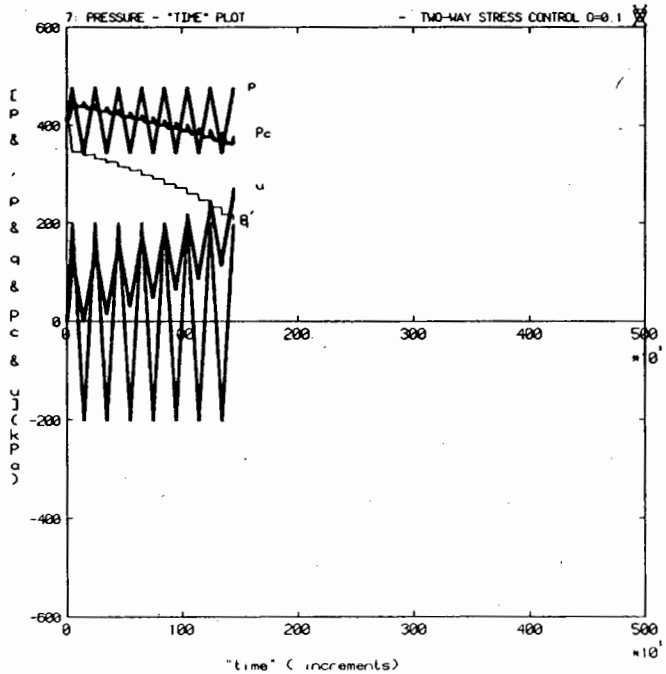
7. PRESSURE - "TIME" PLOT - TWO-WAY STRESS CONTROL O=0.1
[p & p & q & pc & u] (kPa)
"time" (increments)
p
Pc
u
q'

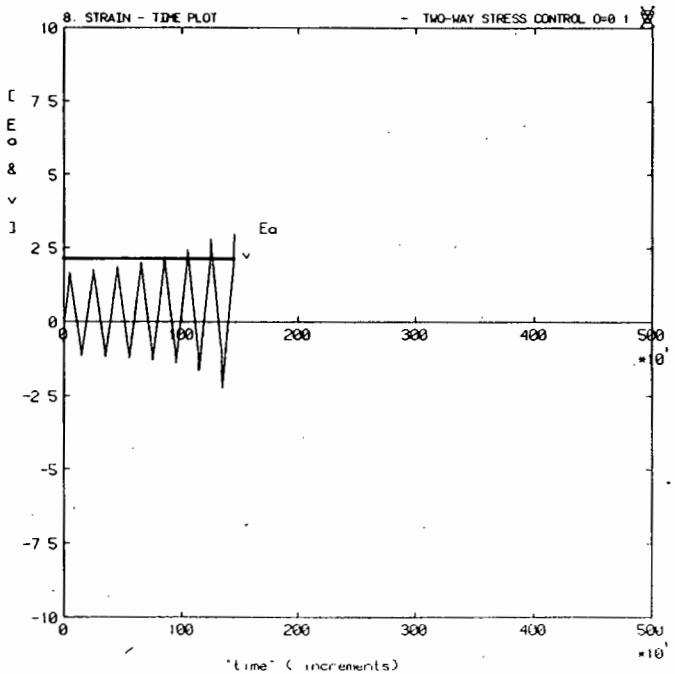
8. STRAIN - TIME PLOT - TWO-WAY STRESS CONTROL O=0.1
[Ea & v]
"time" (increments)
Ea
v

Appendix B3.4: Cyclic triaxial test back prediction
One-way strain controlled loading
(Modified Cam-clay model)

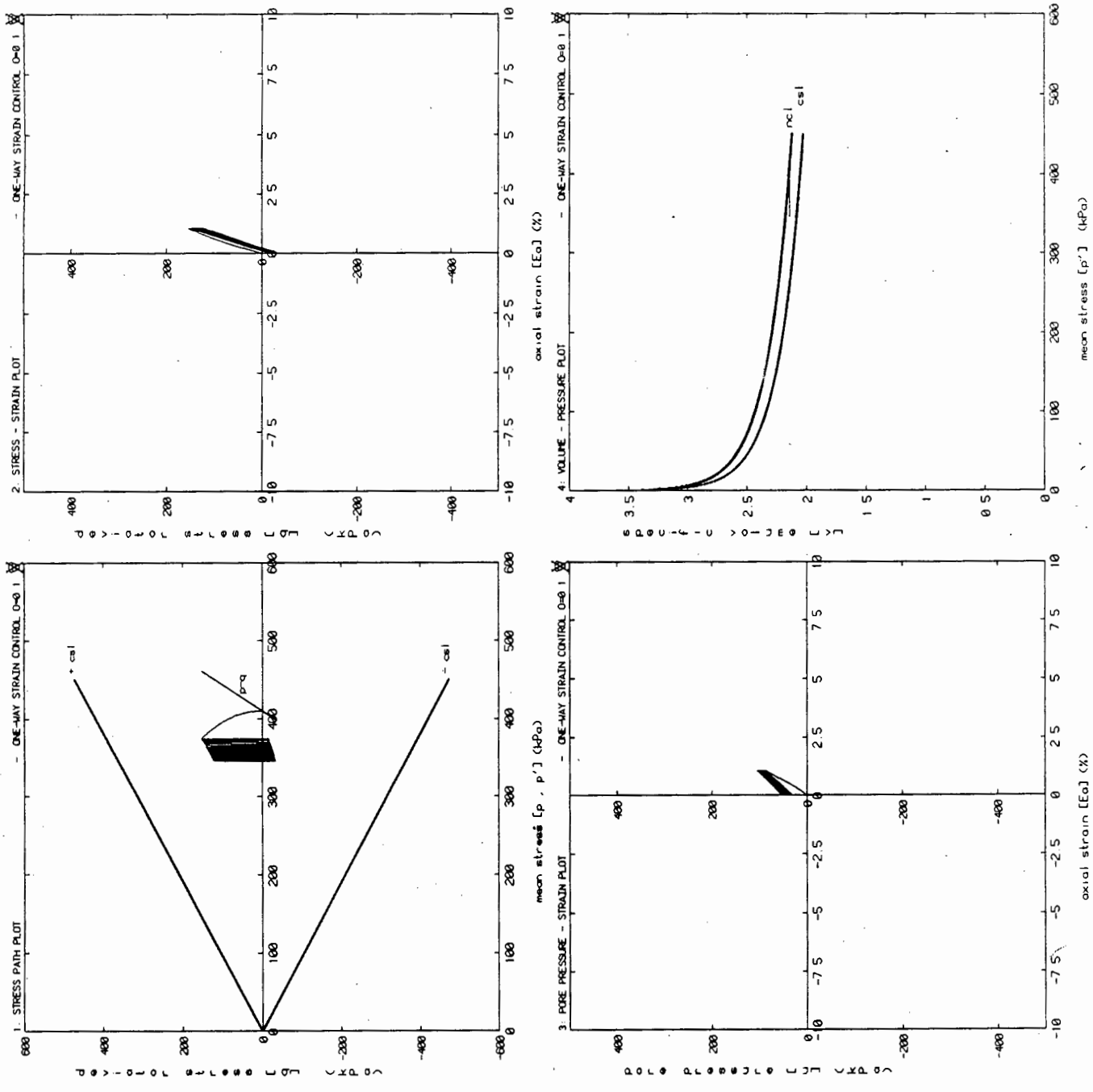

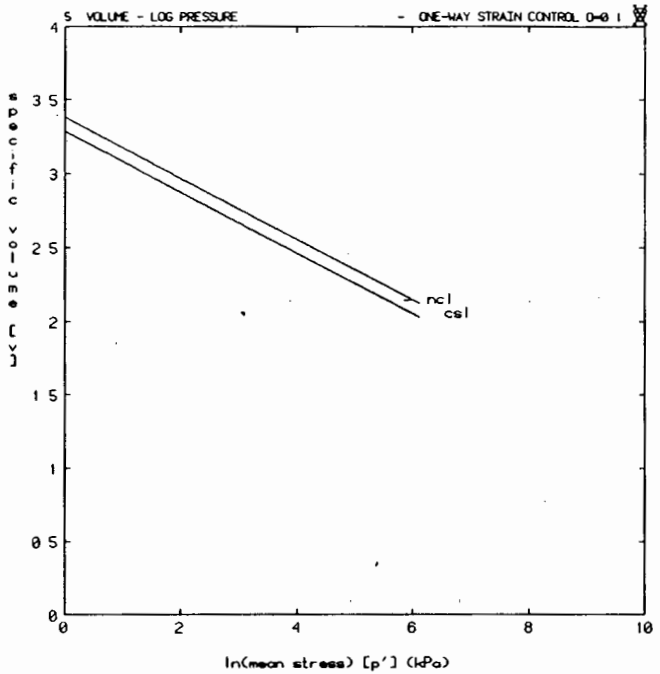
5 VOLUME - LOG PRESSURE
- ONE-WAY STRAIN CONTROL O=0.1
specific volume [v]
ln(mean stress) [p'] (kPa)
ncl
csl

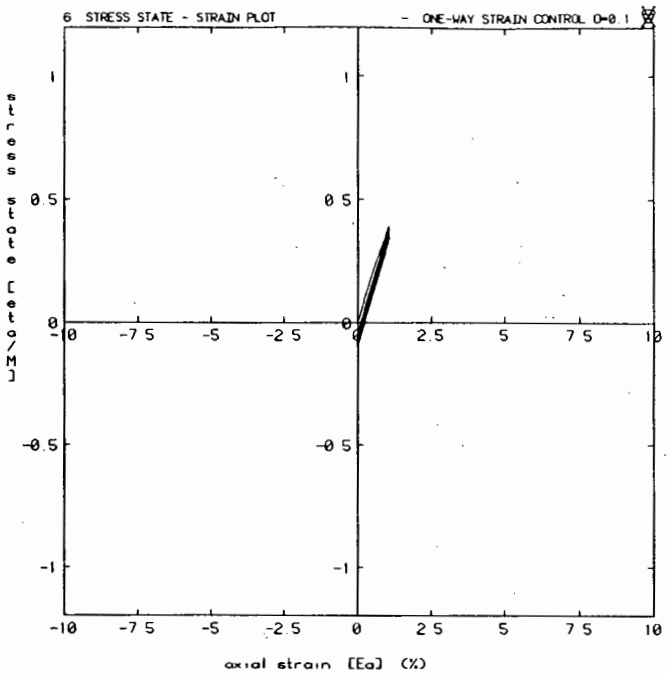
6 STRESS STATE - STRAIN PLOT
- ONE-WAY STRAIN CONTROL O=0.1
stress state [eta/M]
axial strain [Ea] (%)

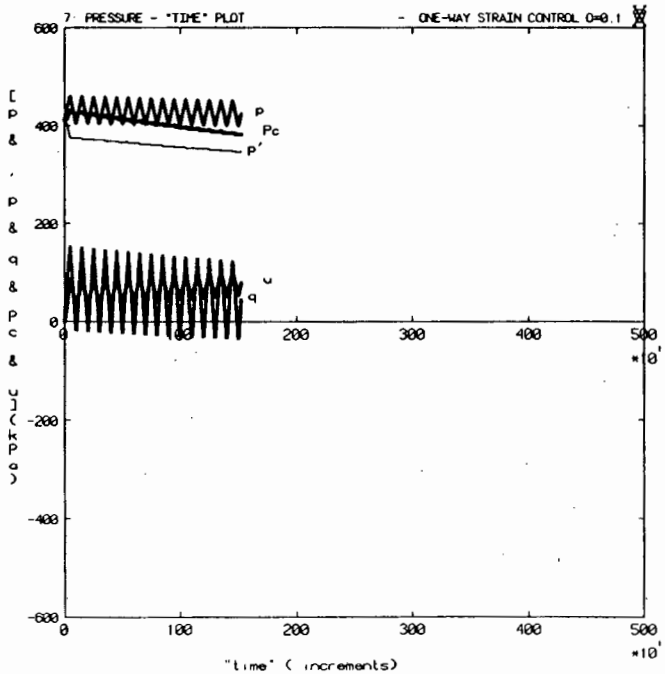
7 PRESSURE - "TIME" PLOT
- ONE-WAY STRAIN CONTROL O=0.1
[p&.p&q&pc&u](kPa)
"time" (increments)
p
Pc
p'
q
u
*10'

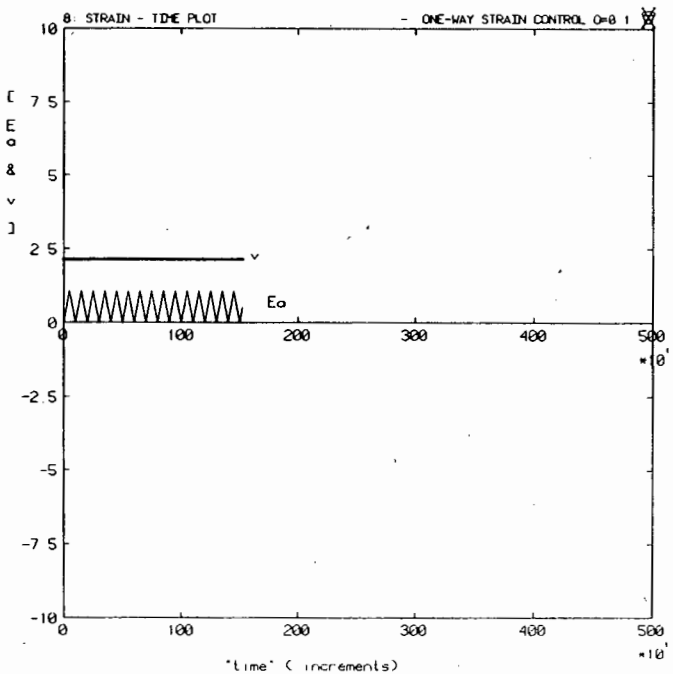
8 STRAIN - TIME PLOT
- ONE-WAY STRAIN CONTROL O=0.1
[Ea&v]
"time" (increments)
v
Ea
*10'

Appendix B3.5: Cyclic triaxial test back prediction
Two-way strain controlled loading
(Modified Cam-clay model)

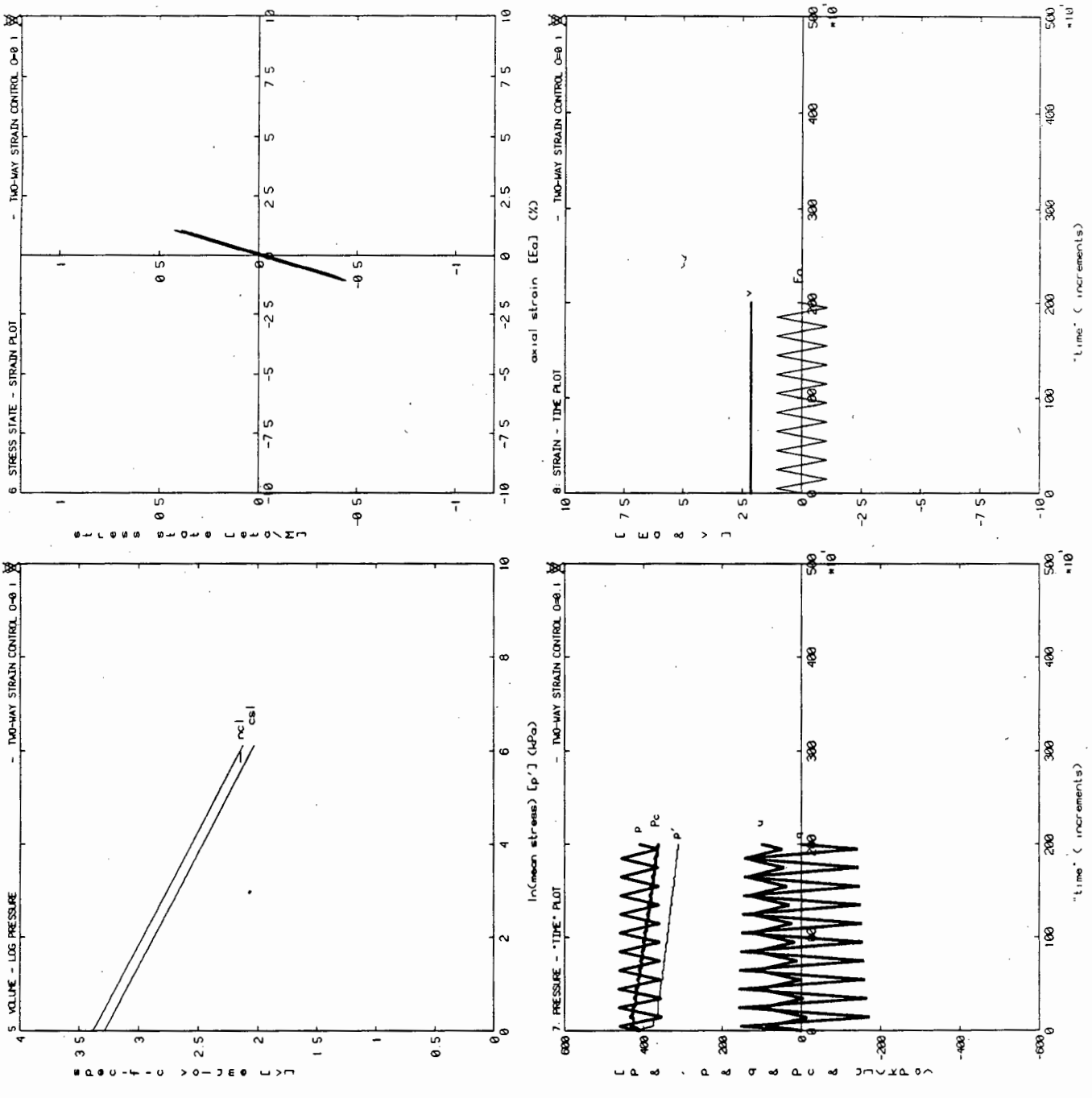

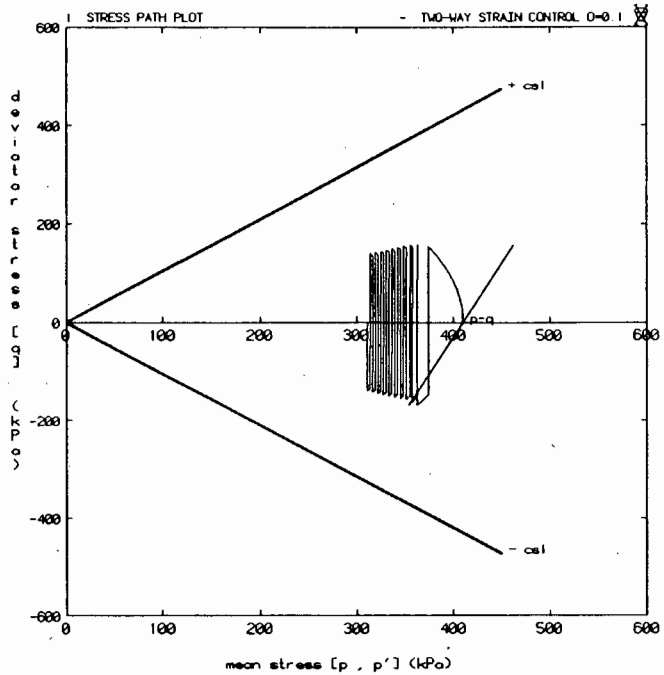
1 STRESS PATH PLOT - TWO-WAY STRAIN CONTROL O=0.1
deviator stress [q] (kPa)
mean stress [p , p'] (kPa)
+ csl
- csl
p=q

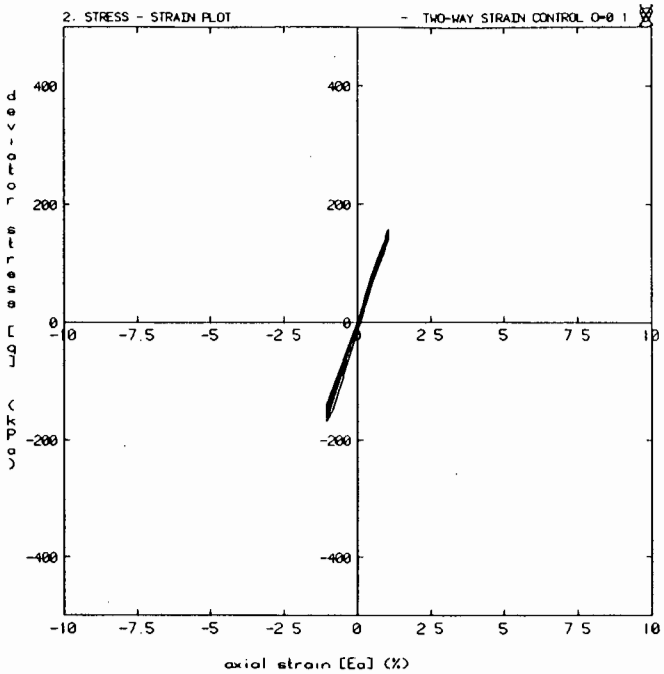
2. STRESS - STRAIN PLOT - TWO-WAY STRAIN CONTROL O=0.1
deviator stress [q] (kPa)
axial strain [Ea] (%)

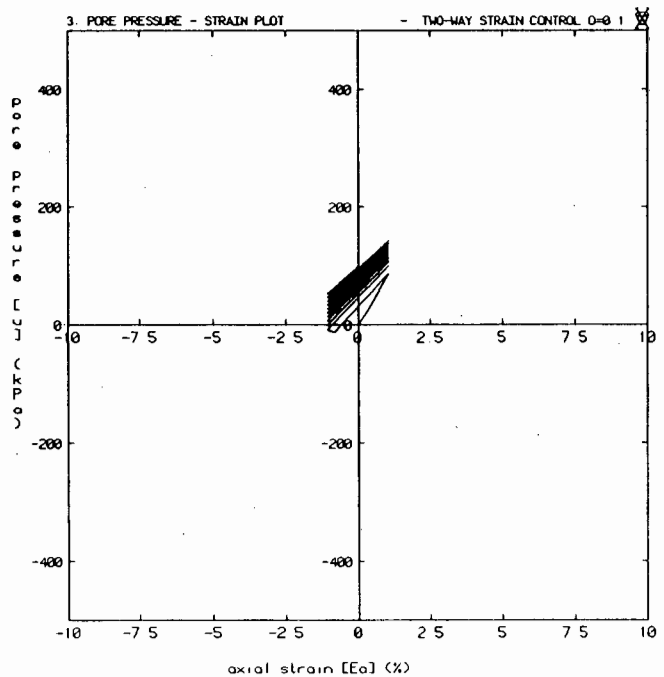
3. PORE PRESSURE - STRAIN PLOT - TWO-WAY STRAIN CONTROL O=0.1
pore pressure [u] (kPa)
axial strain [Ea] (%)

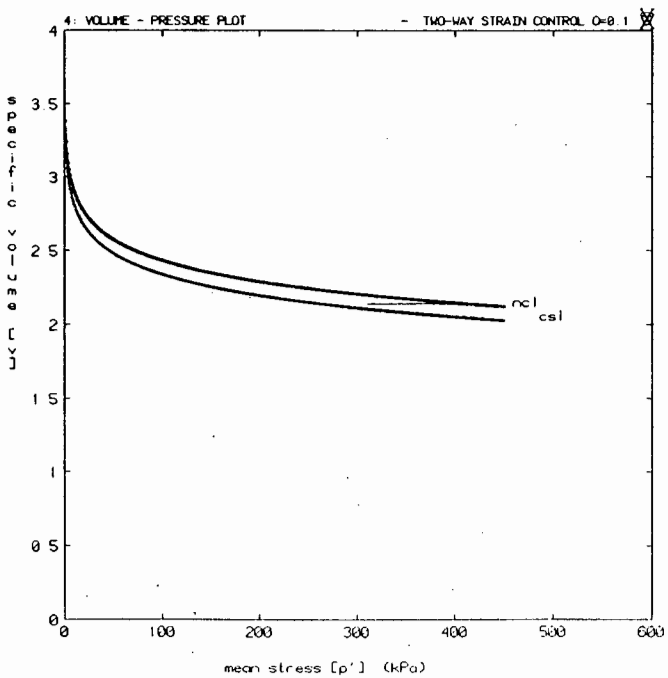
4. VOLUME - PRESSURE PLOT - TWO-WAY STRAIN CONTROL O=0.1
specific volume [v]
mean stress [p'] (kPa)
ncl
csl

Appendix C1 : Properties of Serina Kaolin.

Material : Dry Kaolin powder

Grading :

μm	% passing
20	100
12	95
10	93
6	83
4	71
3	63
2	52

Chemical analysis

	% oxide
SiO_2	46
Al_2O_3	38
K_2O	1.0
Fe_2O_3	0.65
TiO_2	0.58
CaO	0.10
MgO	0.18
Na_{2O}	0.20

Plasticity chart

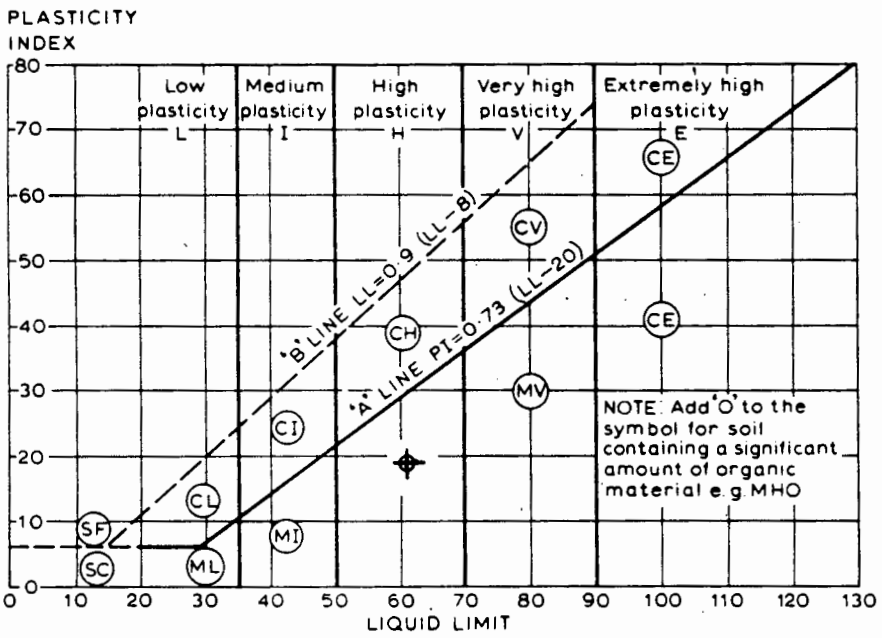

Appendix C2: Consolidation test results

CONSOLIDATION TEST RESULTS

SAMPLE :	Kaolin A
Mass - Wet+ring (g) :	245.85
Mass - Dry+ring (g) :	195.20
Mass - Ring (g) :	95.37
Moisture content (%) :	50.74
Sample Height (mm) :	20.00
Sample Diam (mm) :	76.12
Mass of solids (g) :	99.83
Specific Gravity Gs :	2.71
Rel Density of water:	1.00
Height of Solids Hs (mm) :	8.09
Height of Voids Hv (mm) :	11.91

Pressure	Dial	Dial change	dH	Hv	e	log(p)
0	0	0	0.0000	11.9052	1.4707	
25	970	970	1.9400	9.9652	1.2311	1.3979
50	1182	1182	2.3640	9.5412	1.1787	1.6990
100	1441	1441	2.8820	9.0232	1.1147	2.0000
200	1761	1761	3.5220	8.3832	1.0356	2.3010
400	2124	2124	4.2480	7.6572	0.9459	2.6021
800	2353	2353	4.7060	7.1992	0.8894	2.9031
400	2316	2316	4.6320	7.2732	0.8985	2.6021
200	2212	2212	4.4240	7.4812	0.9242	2.3010
100	2087	2087	4.1740	7.7312	0.9551	2.0000
50	1959	1959	3.9180	7.9872	0.9867	1.6990
25	1833	1833	3.6660	8.2392	1.0178	1.3979
(kPa)	(readings)		(mm)	(mm)	()	(kPa)

CONSOLIDATION TEST RESULTS

SAMPLE : Kaolin B

Mass - Wet+ring (g) :	239.69
Mass - Dry+ring (g) :	188.45
Mass - Ring (g) :	96.66
Moisture content (%) :	55.82
Sample Height (mm) :	19.08
Sample Diam (mm) :	76.11
Mass of solids (g) :	91.79
Specific Gravity Gs :	2.71
Rel Density of water:	1.00
Height of Solids Hs (mm) :	7.44
Height of Voids Hv (mm) :	11.64

Pressure	Dial	Dial change	dH	Hv	e	log(p)
0	2512	0	0.0000	11.6352	1.5629	
25	2044	-468	0.9360	10.6992	1.4371	1.3979
50	1780	-732	1.4640	10.1712	1.3662	1.6990
100	1480	-1032	2.0640	9.5712	1.2856	2.0000
200	1090	-1422	2.8440	8.7912	1.1809	2.3010
400	693	-1819	3.6380	7.9972	1.0742	2.6021
800	443	-2069	4.1380	7.4972	1.0070	2.9031
400	483	-2029	4.0580	7.5772	1.0178	2.6021
200	590	-1922	3.8440	7.7912	1.0465	2.3010
100	718	-1794	3.5880	8.0472	1.0809	2.0000
50	857	-1655	3.3100	8.3252	1.1183	1.6990
25	987	-1525	3.0500	8.5852	1.1532	1.3979
50	941	-1571	3.1420	8.4932	1.1408	1.6990
100	842	-1670	3.3400	8.2952	1.1142	2.0000
200	698	-1814	3.6280	8.0072	1.0755	2.3010
400	512	-2000	4.0000	7.6352	1.0256	2.6021
800	360	-2152	4.3040	7.3312	0.9847	2.9031
1600	212	-2300	4.6000	7.0352	0.9450	3.2041
(kPa)	(readings)		(mm)	(mm)	()	(kPa)

CONSOLIDATION TEST RESULTS

SAMPLE : Kaolin C

Mass - Wet+ring (g) :	210.59
Mass - Dry+ring (g) :	166.25
Mass - Ring (g) :	83.00
Moisture content (%) :	0.53
Sample Height (mm) :	19.30
Sample Diam (mm) :	70.04
Mass of solids (g) :	83.25
Specific Gravity Gs :	2.71
Rel Density of water:	1.00
Height of Solids Hs (mm) :	7.97
Height of Voids Hv (mm) :	11.33

Pressure	Dial	Dial change	dH	Hv	e	log(p)
			==	==	===	======
0	3710	0	0.0000	11.3268	1.4206	
25	3355	-355	0.7100	10.6168	1.3316	1.3979
50	3122	-588	1.1760	10.1508	1.2731	1.6990
100	2842	-868	1.7360	9.5908	1.2029	2.0000
200	2584	-1126	2.2520	9.0748	1.1382	2.3010
400	2095	-1615	3.2300	8.0968	1.0155	2.6021
800	1669	-2041	4.0820	7.2448	0.9086	2.9031
400	1758	-1952	3.9040	7.4228	0.9310	2.6021
200	1878	-1832	3.6640	7.6628	0.9611	2.3010
100	2015	-1695	3.3900	7.9368	0.9954	2.0000
50	2157	-1553	3.1060	8.2208	1.0311	1.6990
25	2290	-1420	2.8400	8.4868	1.0644	1.3979
50	2253	-1457	2.9140	8.4128	1.0551	1.6990
100	2156	-1554	3.1080	8.2188	1.0308	2.0000
200	2019	-1691	3.3820	7.9448	0.9964	2.3010
400	1846	-1864	3.7280	7.5988	0.9530	2.6021
800	1593	-2117	4.2340	7.0928	0.8896	2.9031
1600	1357	-2353	4.7060	6.6208	0.8304	3.2041
800	1406	-2304	4.6080	6.7188	0.8427	2.9031
400	1533	-2177	4.3540	6.9728	0.8745	2.6021
200	1670	-2040	4.0800	7.2468	0.9089	2.3010
100	1821	-1889	3.7780	7.5488	0.9468	2.0000
50	1965	-1745	3.4900	7.8368	0.9829	1.6990
25	2108	-1602	3.2040	8.1228	1.0188	1.3979
(kPa)	(readings)		(mm)	(mm)	()	(kPa)

APPENDIX D

EXAMINATIONS WRITTEN BY THE AUTHOR TO COMPLETE THE REQUIREMENTS OF THE DEGREE

Course Number		Result	Credit Rating
CIV588F	Applied mechanics I	2-	3
CIV592F	Project Management in Civil Engineering	2+	3
AMA363F	Numerical Analysis	1	3
AMA367F	Continuum Mechanics	3	3
CIV525S	Contract Law	1	3
CIV 544S	Constitutive modelling of soils	1	3
CIV589S	Applied Mechanics II	1	3
CIV504S	Structural Dynamics	1	3
CIV593S	Engineering Software Design	1	3
CIV500Z	"Constitutive modelling of the behaviour of clays under cyclic loading."		20
			47
	Credit requirements for Degree		40